MODELLING, CHARACTERISATION AND OPTIMISATION OF DEEP GEOTHERMAL ENERGY IN THE CHESHIRE BASIN

by

CHRISTOPHER SIMON BROWN

A thesis submitted to the University of Birmingham for the degree of DOCTOR OF PHILOSOPHY

Department of Civil Engineering

University of Birmingham

October 2019

UNIVERSITYOF
BIRMINGHAM

University of Birmingham Research Archive

e-theses repository

Abstract

Despite the significant geothermal resource in the UK, only one small scale scheme in Southampton is presently operating. Few wells have been drilled to target deep resources, particularly in the Cheshire Basin where only two wells have penetrated depths approaching 3 km. As a result, the knowledge of aquifer quality in the more central parts of the basin is limited, meaning there is a high geological risk associated to any geothermal development. To investigate this, a single well model was designed to simulate the extraction of fluid from the Collyhurst Sandstone Formation. Simulations of a range of geological and engineering parameters highlighted hydraulic conductivity could be the most significant obstacle to production, however, it could be minimised by altering engineering parameters (i.e., production rate, length and position of the well screen). A key issue with conventional extraction only methods is the disposal of waste water. To circumvent this issue, innovative deep borehole heat exchangers and standing column wells were modelled. Results indicated that both methods can produce heat loads up to 3.7 MW for short periods. Further analysis was also undertaken on heat exchangers, highlighting significant savings could be made from switching to a geothermal run heat network (>£49 million).

Dedication

To my parents and grandparents: Rachel, Andrew, Pam, Betty and the two Alans. Without whom

none of this would have been possible.

'Audere est Facere'

Acknowledgments

Contents

LIST OF FIGURES

LIST OF TABLES:

LIST OF ABBREVIATIONS

HSA = Hot sedimentary aquifer

BHE = Borehole heat exchanger

SCW = Standing column well

HDR = Hot dry rock

EGS= Enhanced geothermal system

TVDSS = Total vertical depth sub sea level

SSG = Sherwood Sandstone Group

WRRF = Wem Red Rock Fault

NOMENCLATURE FOR NUMERICAL MODELLING

Symbol	Parameter	Units
t	Time	seconds
λ	Thermal conductivity	W/m/°C
T	Temperature	°C
q	Heat flow	W·m^{-2}
C	Specific heat capacity	J/kg °C
ρ	Density	kg /m^3
$\emptyset$	Porosity	%
α	Thermal diffusivity	m^2/s
R_d	Retardation factor	-
K	Hydraulic conductivity	m/s
v	Darcy velocity	m^3/s
Ss	Storage coefficient	-
h	Hydraulic head	m
Pr	Penetration ratio	-
PC	Pricketts penetration constant for additional drawdown	-
A	Area	m
u	Fluid velocity in the pipe	m/s
b_{pg}	Reciprocal of thermal resistance between pipe and grout	W/m^2 °C
Q	Production rate	m^3/s
W	Source or sink	m/s
rw	Radius of the well in the reservoir (screened interval)	m
re	Extrapolated radius	m
Subscripts		
b	Bulk	-
s	Solid phase	-
f	Fluid phase	-
p	Pipe	-
g	Grout	-
$prod$	Production temperature	-
rej	Rejection temperature	-
i	Inlet pipe	-
o	Outlet pipe	-

CHAPTER 1 - INTRODUCTION

This chapter outlines the key aims and objectives of the thesis, as well as summarising each chapter.

1.1 Introduction

Globally, the renewable energy market is growing with the utilisation and development of geothermal energy considered as a clean, efficient alternative to fossil fuels. Fossil fuels are a limited resource with approximately one-third of reserves being depleted due to a sharp increase in their use since the 1950s (Ringrose, 2017). Therefore, it is important that in order to meet the growing demand for energy a suitable alternative resource is found. Heat energy within the Earth's crust can be produced as geothermal energy. Typically, this is exploited by shallow ground source heat pumps within 100 m of ground level where the Earth's surface is heated by the sun, or through deep geothermal wells extracting fluid that has been heated by the Earth's geothermal gradient. Deep geothermal schemes (>1 km) are currently being used to produce energy around the world, as both power and heat, usually focusing on high-enthalpy resources where temperatures exceed 150 °C (e.g., Iceland (Elders et al. 2014)). Low-enthalpy systems, such as the deep, Mesozoic sedimentary Wessex and Cheshire Basins in the UK, could generate useable geothermal energy; however, they typically cannot produce the +125 °C temperatures required for economic electricity generation and would be better suited to district heating schemes (+75 °C) (Arup, 2013).

Deep geothermal resources can be classified as (DiPippo, 2012):

- **Hydrothermal** – the most commonly developed geothermal resource where brines are extracted from permeable formations. This includes hot sedimentary aquifers (HSA);

- **Hot Dry Rock (HDR)** – where low permeability, high temperature systems are stimulated creating an artificial reservoir allowing fluid to be injected and extracted in a multi-well system;

- **Geopressured** – where reservoirs have very high pressure, high temperature and dissolved methane; and,

- **Magma energy** – where cold fluid is injected at high pressure into high temperature magma and then circulated back to the surface.

In the UK, deep geothermal resources include hydrothermal and hot dry rock (Downing and Gray, 1986a,b) with hot sedimentary aquifers (HSAs) being the focus of this thesis's research. There are four major Mesozoic sedimentary basins in England and Wales which have the potential to yield low-enthalpy geothermal resources from HSAs. These include the Worcester, East England, Wessex and Cheshire Basins (Busby, 2010, 2014) (Fig. 1.1). The Cheshire Basin is the focus of this thesis; however, analysis was also undertaken for the Wessex Basin, which currently has the only commercial scheme presently operating in the UK (Lund et al., 2005, 2011). The Cheshire Basin is located in the northwest of England and contains high-quality, Permo-Triassic sandstones, whilst the Wessex Basin is located in the south of England and contains high-quality Triassic sandstones.

Regional map of the UK highlighting the key geothermal prospects

Figure 1.1*: Map of the UK highlighting key Mesozoic basins and granitic intrusions (after Downing and Gray, 1986b; Busby, 2010; Pasquali et al., 2010). Low-enthalpy HSAs are confined to Mesozoic basins, whilst hot dry rock prospects are related to high heat flow igneous intrusions. Brown Mesozoic basins highlight other minor basins in the UK.*

Deep geothermal Mesozoic basins in the UK are estimated to hold between 201 and 327 x 10^{18}J of energy as low-enthalpy resources (Downing and Gray, 1986b; Rollin et al., 1995; Pasquali et al., 2010; Jackson, 2012; Busby, 2014). Around 23 % (75 x 10^{18} J) of this is estimated to be contained in the Cheshire Basin (Table 1.1) (Rollin et el., 1995). This is the equivalent of nearly 3 billion barrels of oil (Hirst et al., 2015) or 4.6 million GWh of energy (Busby, 2010). Most of the low-enthalpy resources in the UK are untapped, although there has been some exploitation from a single well scheme in Southampton (Wessex Basin) (Price and Allen, 1984; Gluyas et al., 2018). In contrast to countries with more developed district heating schemes supplied by deep geothermal energy, such as Paris, France (Busby et al., 2014), many of the major cities in the UK do not overlie Mesozoic basins (Fig. 1.2). This has led to a lack of deep geothermal exploration in the UK. Despite this, there is still a large supply of energy but the risk of investment in such schemes is perceived as being relatively high, both financially and geologically. With the aim of de-risking prospects and reducing uncertainty in the geological and engineering characteristics of target reservoirs in UK Mesozoic basins, a modelling approach has been adopted that utilises a low-cost single well strategy that can potentially match low-enthalpy geothermal resources (<100 °C) to nearby, smaller towns and cities with high heat demand (Fig. 1.2).

Basin	Total geothermal resources (x 10^{18} J)	
	Triassic	Permian
East England	122.2	x
Wessex	27.2	x
Worcester	8.2	60.3
Cheshire	36.2	38.5
Northern Ireland	35	x

Table 1.1: *Identified resources of low-enthalpy schemes across the UK (Downing and Gray, 1986b; Rollin et al., 1995). Where x denotes that there is no Permian strata.*

a. Outline of Mesozoic basins in England and Wales

b. Heat demand in the UK

Figure 1.2: *(a) Outline of major Mesozoic basins and granite batholiths in England and Wales. (b) Heat demand in England and Wales (red - high heat demand (up to 46 KWh/m²), blue – low heat demand (down to 0 KWh/m²)). Images modified after NHP (2017), Downing and Gray (1986b) and Busby (2010).*

To reduce the financial and geological risk associated with deep geothermal wells in the UK, both closed and open loop borehole heat exchangers have been proposed as alternative methods of heat extraction (Law et al., 2015). Borehole heat exchangers operate by circulating fluid within a borehole. The fluid is injected at the surface at a cool temperature which heats with depth before being returned to the surface. Closed loop boreholes are sealed from the surface to the base with no fluid flux out of the borehole (Fig. 1.3b). This significantly reduces the geological risk (e.g., from poor hydraulic properties). Open loop borehole heat exchangers, often referred to as standing column wells (Fig. 1.3c), have an open (lined or perforated) section allowing fluid fluxes with the surrounding rocks. Although both closed loop borehole heat exchangers and standing column wells are not a new or novel idea, they are usually used to exploit shallow geothermal energy. Thus by using them at depth, the temperature will be higher and more heat and energy can be extracted. Both configurations are explored in this thesis as alternatives to conventional extracting only wells (Fig.

1.3a), such as the 'Marchwood' and 'Western Esplanade' geothermal wells in Southampton which exploit the HSAs in the Wessex Basin (chapter 4).

Standing column wells are usually used in shallow surroundings with much of the borehole interval perforated or lined. In contrast, heat extraction from deep geothermal systems using this method must be based on near fully-sealed boreholes (i.e., not perforated) with a small screened or perforated interval present at the target aquifer depth (Fig. 1.3c). This is to prevent potentially saline water contaminating the fresh shallow aquifers. This method has been referred to as a 'deep geothermal single well' in current UK literature (Collins and Law, 2017; Westaway, 2018). This terminology is ambiguous and to avoid confusion will be referred to as a standing column well (SCW).
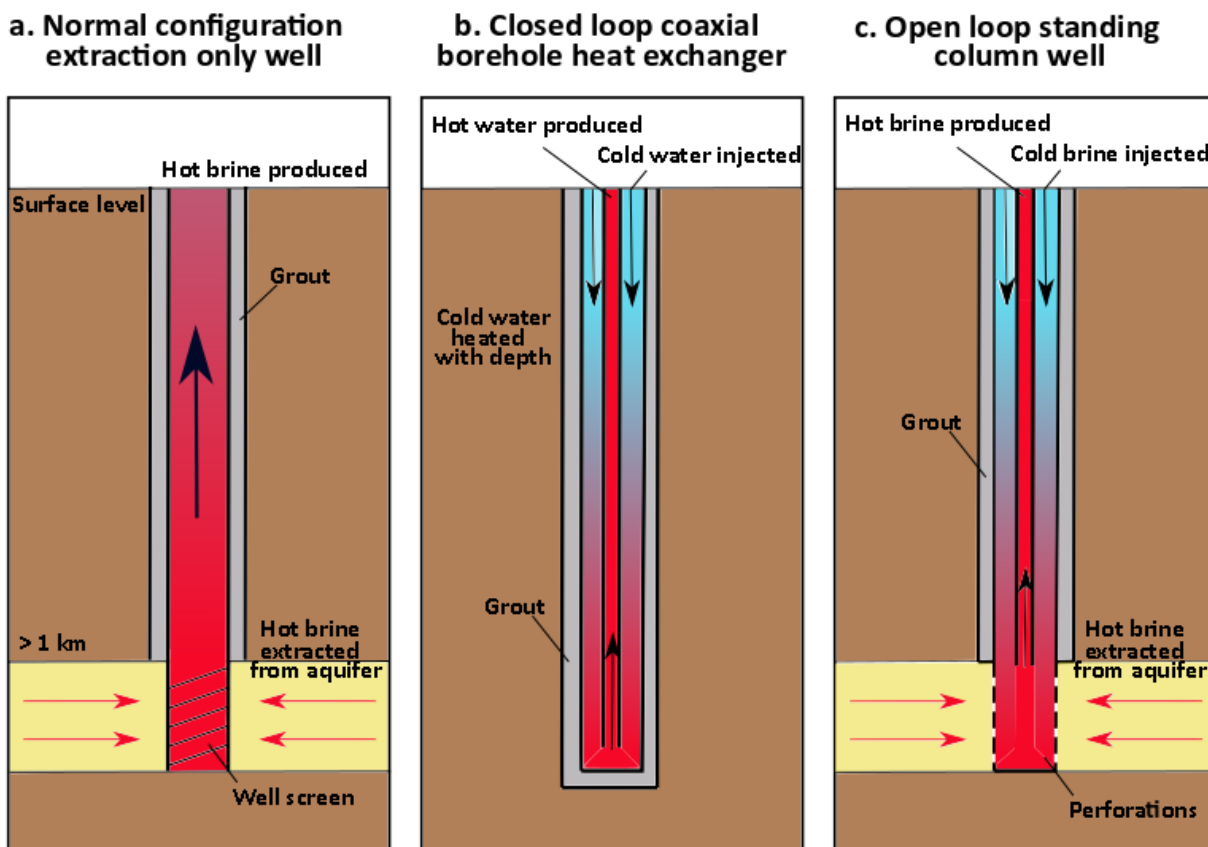
Figure 1.3: *Different forms of single well geothermal schemes: (a) normal configuration, extraction only geothermal well, (b) closed loop coaxial borehole heat exchanger (e.g., Law et al., 2015) and (c) standing column well or deep geothermal single well configuration (e.g., Collins and Law, 2017).*

1.2 Aims and Objectives

The overall aim of this thesis is to investigate the impacts of geothermal extraction from a single well scheme in the Crewe area of the Cheshire Basin, UK. Although a significant amount of research has been undertaken to quantify the total energy resource in the basin, minimal attention has been given to the exploitation of this resource. This thesis bridges that gap by modelling a range of geological and engineering scenarios for a geothermal well in the Crewe area.

The first objective of the research was to develop a numerical simulation model using existing methods from the literature which can replicate a range of borehole configurations of a single well. This model is intended for practical use by the PhD sponsor, Cheshire East Council, who wish to develop a district heat network in the Crewe area of the Cheshire basin supplied by a deep geothermal well. As such, it should capable of being run on a standard computer with modest to low computational performance.

Currently, the geology underlying the Cheshire Basin is lacking hydro-physical data from deep boreholes, with only two boreholes penetrating depths of ~3 km (Prees-1 and Knutsford) (Plant et al., 1999; Hirst et al., 2015; UKOGL, 2019). Therefore, the second key objective was, to identify any potential geological and engineering risks for the Cheshire Basin and to evaluate their impacts on well performance (i.e., lifetime, energy production, drawdown and production temperature).

The third objective was to investigate new novel methods of production aiming to minimise geological and engineering risks. Different wellbore configurations (Fig. 1.3) were modelled with the goal of reducing the risk associated with geothermal development and reducing the amount of waste water requiring disposal. The different well configurations modelled include injection-extraction single wells, deep borehole heat exchangers and standing column wells.

The final key objective was to investigate heat exchanger performance and the economic benefits of using a geothermal fuelled district heat network in comparison to a fossil fuelled boiler fed network. This involved analysing the effectiveness and costs of heat exchangers.

These objectives were met through a series of modelling studies using data from literature for the Cheshire Basin and UK. Models were developed on MATLAB using both numerical and analytical solutions (chapters 4-7). Geological and engineering risks were identified by undertaking a parametric study (chapter 5), whilst the new novel methods of extraction were investigated by testing the performance of different wellbore configurations (chapter 6). The performance of a heat exchanger and heat network was evaluated by modelling a range of potential production temperatures and economic conditions (chapter 7).

1.3 Thesis overview

Chapter 2 and 3 present a review and evaluation of the published research on the geology of the Cheshire Basin, geothermal resources in the UK and modelling techniques. **Chapter 3** also outlines the key governing equations for the models, whilst discussing the rationale for their use.

Chapter 4 presents a modelling study using the techniques developed in the previous chapters including error analysis and a comparison to analytical solutions and case studies. The model is used to forecast production in the Wessex Basin, Southampton, under different borehole configurations, including: an extraction only well, standing column wells and deep borehole heat exchangers.

Chapter 5 investigates the extraction of fluid and heat from the Crewe area of the Cheshire Basin from a single extraction well. A parametric study is undertaken to highlight the key parameters that influence well performance. These are determined by evaluating the energy extracted, production temperatures and drawdown. The most significant parameters that inhibit production are

also modelled under further scenarios to investigate mitigation strategies. The impact of seasonal effects is also considered.

Chapter 6 models a range of extraction scenarios aiming to limit the amount of waste water produced during development of deep geothermal resources in the Cheshire Basin. This includes the modelling of standing column wells and borehole heat exchangers, whilst also considering a single well injection-extraction method which is modelled as an aquifer thermal energy storage scheme.

Chapter 7 provides an outline of heat loss in heat exchangers and considers the economic benefits of using a geothermal energy fed district heat network, rather than the use of conventional fossil fuel boilers. The optimal surface area and maximum net profit for counter-current flow heat exchangers is identified for a range of temperatures.

Chapter 8 discusses the impacts and limitations to the development of geothermal resources in the Cheshire Basin. The limitations include, but are not restricted to; waste water disposal from single well schemes, public perception and the protection of the resource.

Finally, **chapter 9** concludes the main findings of the thesis and highlights the scope for further research.

CHAPTER 2 - AN OVERVIEW OF THE GEOTHERMAL DEVELOPMENTS IN THE UK AND THE GEOLOGY OF THE CHESHIRE BASIN

This chapter provides an outline of the types of deep geothermal energy in the UK, outlining extraction methods and current developments. A review of the geology of the Cheshire Basin is then discussed.

2.1 Introduction

The Cheshire Basin is one of a series of Permo-Triassic basins located across England which formed during the collapse of part of the Variscan Orogenic belt. It is located in the northwest of England and is one of three major basins in the area, the others being the Carlisle and East Irish Sea Basins (Abdoh et al., 1990). It covers an aerial extent of 3,500 km^2 and is estimated to reach a maximum length and width of 100 km and 55 km, respectively (Hirst et al., 2015). The basin is dominated by clastic sediments with a thick succession of mudstone overlying Permo-Triassic aeolian- to fluvial- sandstones. The underlying basement is considered to be either Carboniferous sandstones (e.g., Hirst et al., 2015) or meta-sedimentary Palaeozoic strata (Abdoh et al., 1990; Mikkelsen and Floodpage, 1997).

In the 1970s the Arabian oil embargo triggered national research into alternative energy sources (Dunham, 1974; Downing and Gray, 1986a). The Cheshire Basin was investigated as a low-enthalpy hydrothermal resource since it has a thick succession of sandstones that retain favourable hydraulic characteristics at depth. It is widely acknowledged that the heat flow underpinning the basin is similar to that of the national average of 52 - 55 mW/m^2 (Burley et al., 1980; Downing and Gray, 1986a, 1986b; Busby, 2014). Although this is relatively low, the combination of low-moderate heat flow combined with the thick succession of high-quality aquifers could prove the basin to be suitable for deep geothermal energy exploitation. Variations in heat flow are also expected to occur due to groundwater movement in aquifers which could result in areas of higher heat flow (Downing and Gray, 1986b). At present, geothermal exploitation focus remains on Mesozoic sandstones with

little consideration of deeper Palaeozoic geothermal aquifers. The quality and thickness of the Palaeozoic rocks underlying the Cheshire Basin are unknown, untested and deemed to have a high level of geological risk for exploration. In this chapter the geothermal resources in the UK are outlined, followed by the geology of the Cheshire Basin, including basin infill and underlying basement.

2.2 Geothermal developments in the UK

2.2.1 Types of deep geothermal resources in the UK

Heat energy is transferred from the high temperature core of the Earth, and radiogenic elements in the crust, toward the cooler surface of the Earth. Within the crust, heat flow is driven by conduction within solid rocks and advection within fluids. Deep geothermal energy schemes aim to extract water from deep, permeable rock at temperatures where energy extraction is economic (Burley et al., 1980). To determine the viability of the system, the enthalpy or total heat in place must be defined, which is done so using the classification scheme utilised by other authors when investigating UK geothermal resources (Muffler and Cataldi, 1978). Low-enthalpy systems are generally considered at temperatures below 100 °C, whilst high-enthalpy schemes are over 150 °C (Adams et al., 2010). The total heat in place can be estimated by calculating the geothermal resource. Thorough investigatory work has been undertaken in the UK to determine the geothermal resource in Mesozoic basins. In the UK, it is estimated that a total of 327 x 10^{18} J is stored in place (Rollin et al., 1995), with 23 % of this located in the Cheshire Basin (Table 1.1).

Low-enthalpy schemes involve wells penetrating hot sedimentary aquifers (HSA) heated by conductive and convective heat flow (Fig. 2.1). In the UK, most low-enthalpy geothermal schemes being explored aim to target HSA's in Mesozoic basins. This however, is not always the case, as the Slitt Vein targeted by the Weardale borehole aimed to explore natural fractures in a hydrothermal vein (discussed further in section 2.2.2) (Manning et al., 2007; Busby, 2010). In the UK, high-enthalpy

schemes targeting temperatures over 150 °C are being investigated in granitic batholiths and are generally referred to as hot dry rock (HDR) schemes or enhanced geothermal systems (EGS) (Fig. 2.1) (Downing and Gray, 1986b; DiPippo, 2012 etc). HDR schemes refer to rocks at high temperatures that are impermeable and contain no water. They are hydraulically stimulated un-naturally or 'fracked' with water pumped down boreholes and heated by the rock material, then pumped back to the surface. An EGS refers to the stimulation and fracturing of rock to artificially create a reservoir. The main Mesozoic basins in the UK include the Wessex, Cheshire, Worcester, East England, Lough Neagh, Rathlin and Larne (Fig. 1.1). The main HDR prospects include the Cornubian, Lake District, Weardale and Eastern Highlands Batholiths.
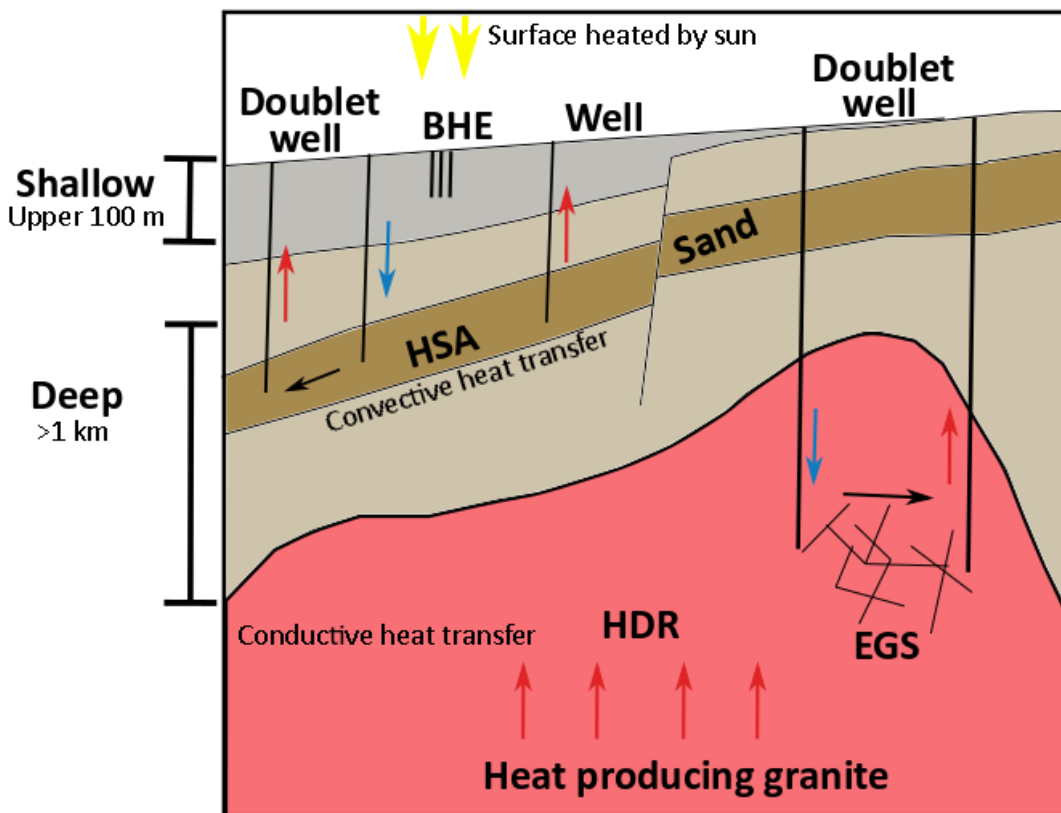
Figure 2.1: *Schematic of potential deep and shallow geothermal schemes in the UK, including: hot dry rock (HDR), enhanced geothermal systems (EGS), hot sedimentary aquifer (HSA) extraction via doublet or single well schemes and shallow heat extraction via borehole heat exchangers (BHEs).*

Shallow geothermal schemes are also utilised; these can involve the extraction of heat through either closed or open borehole heat exchangers (BHEs) (Fig. 2.1). Shallow systems operate in the upper 100 m of the subsurface and can be made up of a BHE array to meet a given demand predefined by a ground source heat pump.

Deep geothermal energy in the UK will be used for two primary applications – electricity and spatial heating. Three types of geothermal power plants are used to produce electricity: dry steam, flash and binary power plants (Feili et al., 2013). Binary power plants could be used for HSAs, as they target low-temperature systems, whilst dry steam and flash plants target higher temperature systems. A binary power plant produces energy by heating a fluid with a lower boiling point which evaporates, expands, condenses and returns to the evaporator through a feed pump (Fig. 2.2) (DiPippo, 2012). The efficiency of current power plants is ~10 % (Huddlestone-Holmes and Hayward, 2011). Basal temperatures for Permo-Triassic sandstones in the Cheshire Basin (<100 °C) would be uneconomic to convert to electricity, as it is estimated that the geothermal fluid needs to be in excess of 125 °C for economic electricity conversion (Arup, 2013). At present, it is expected that heat energy extracted from the Cheshire Basin will be utilised directly, with district heating being the primary use. A district heating scheme distributes heat from a central location (i.e., the geothermal extraction borehole) and, dependent on the temperature, the heat may be increased using a heat pump or additional boiler. The geothermal fluid passes through a heat exchanger and is then distributed using a heating grid to substations. A cascade system, where the heat of the geothermal fluid is utilised sequentially at different temperatures, can increase the application of the energy (Rubio-Maya et al., 2015). A typical system may include electricity generation (if possible), then subsequent uses of direct heat via district heating and balneology (therapeutic thermal spas) (Fig. 2.3).

Processes of a binary power plant
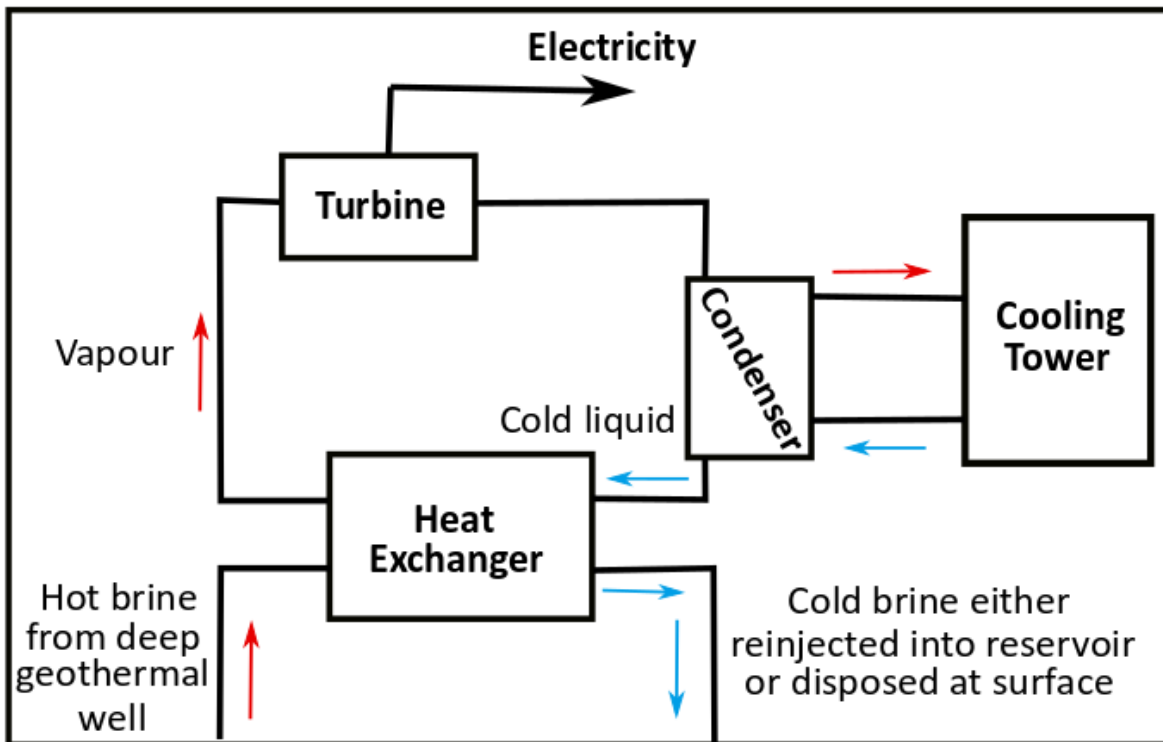
Figure 2.2: *Schematic of the processes in a binary power plant (after Clauser, 2006).*

Example of a cascade scheme for the Cheshire Basin
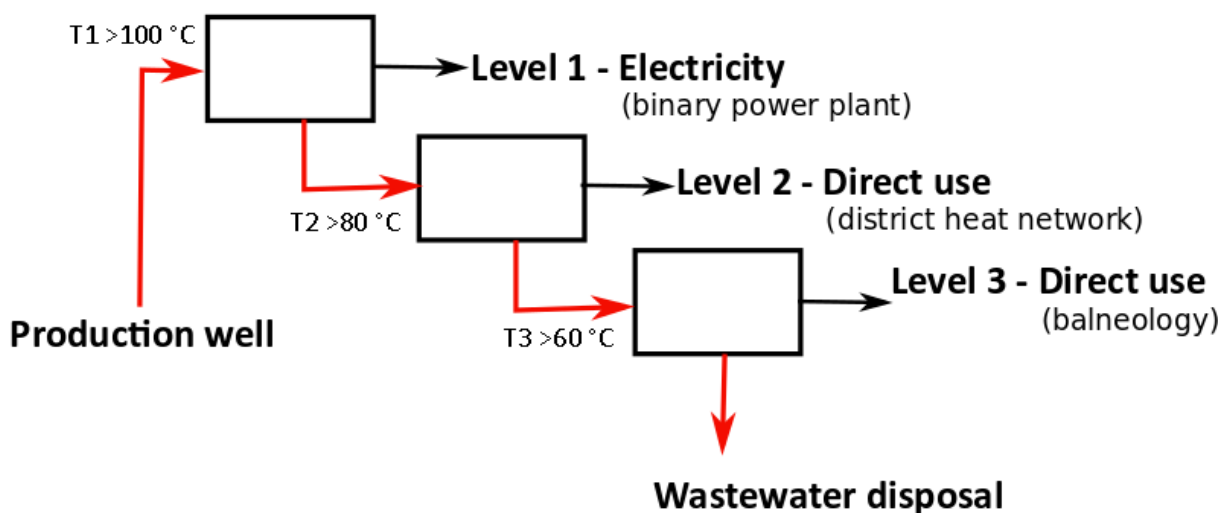
Figure 2.3: *Schematic of a potential cascade scheme for the Cheshire Basin (modified from Rubio-Maya et al. 2015).*

2.2.2 Overview of current UK schemes

Currently, the only deep geothermal energy scheme is in the Wessex Basin, Southampton, where it contributes to district heating. Two wells were drilled for exploration, the Western Esplanade and Marchwood Wells, both targeting the Sherwood Sandstone Group as a low-enthalpy resource. The Marchwood Well targeted sandstone at a depth of 1,660 m finding the sandstone to be 59 m thick, whilst the Western Esplanade Well targeted sandstone at a depth of 1,725 m (Knox et al., 1984; Downing and Gray, 1986b). Southampton Council have been utilising the resource from the Wessex Basin for a small-scale district heating scheme for over 25 years.

In recent years, potential geothermal prospects have been investigated in the UK focusing on the Weardale and Cornwall Granites. The Eastgate-1 borehole (Durham), drilled in 2004, targeted a low-enthalpy system focusing on natural fractures filled with water (Busby, 2010). The borehole penetrated the Slitt Vein (Fig. 2.4) reaching a depth of 995 m with a bottom-hole temperature of 46 °C (Manning et al., 2007). Water infiltration into the borehole was recorded at a series of intervals. Further investigation at a second borehole drilled 700 m away in 2010 identified the high permeability in the fractures was unique to the 2004 borehole (Younger et al., 2012). A third exploratory well targeting the Fell Sandstone Formation has also been drilled recording an elevated heat flow associated with the Weardale Granite. The well was drilled to a depth of 1,821 m in the Newcastle region proving a geothermal gradient of 37 °C/km and 300 m thickness of sandstone (Younger et al., 2015)

Mid- to high-enthalpy projects are being pursued in Cornish granites by EGS Energy Ltd and Geothermal Engineering Ltd. Both schemes plan to exploit granite at temperatures of 190 °C at 4.5 km depth and can be used for direct heat use or electricity generation. The United-Downs project led by Geothermal Engineering Ltd has just finished drilling (mid 2019), whilst drilling at the Eden Project (EGS energy Ltd) is yet to begin, with funding still to be secured (as of mid-2019). Geothermal

Engineering Ltd (GEL) has also conducted investigations into low-enthalpy resources from closed and open sources (Law et al., 2014, 2015). This novel method aims to extract heat from a deep closed loop BHEs or standing column well (Fig. 1.3), where fluid is circulated within a well. Simple preliminary modelling has been undertaken on this concept providing positive results (e.g., Law et al., 2015).

Schematic of the Slitt Vein prospect
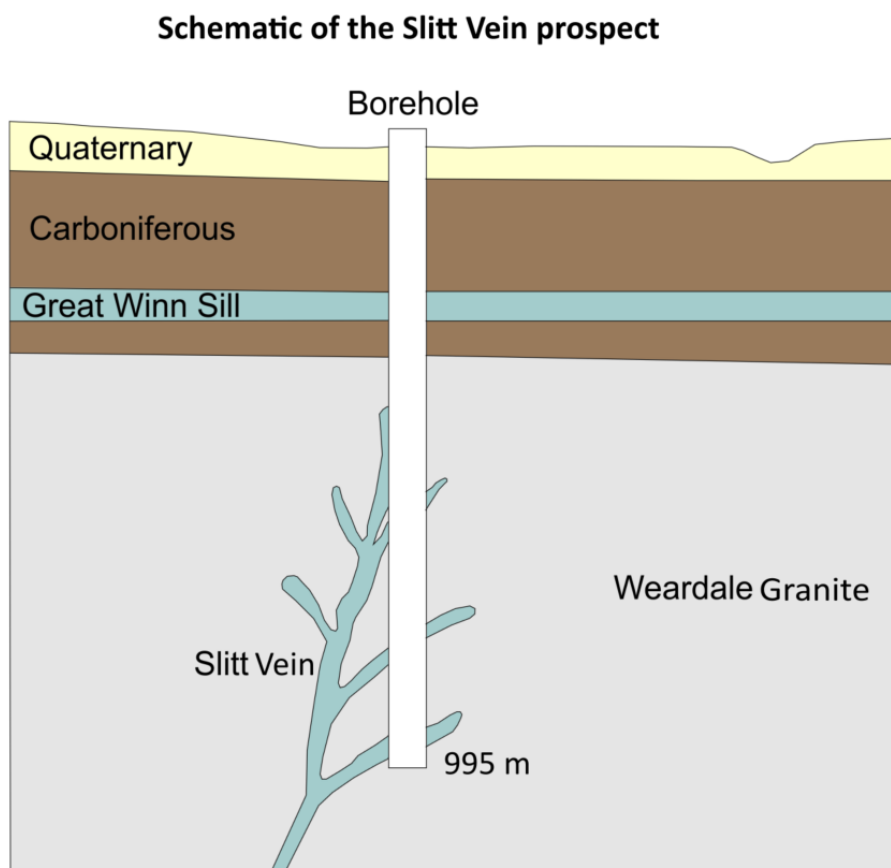
Figure 2.4: *Schematic of the Slitt Vein through the Eastgate-1 borehole (after Manning et al., 2007).*

A smaller project in Cornwall has been undertaken by GEL to supply 35 °C heat to a swimming pool (Jubilee pool, 2019). Geothermal drilling has been completed (Fig. 2.5), however, well failure at 0.4 km due to high fluid velocities likely from intercepting fractures has limited the project (BBC, 2019) – such that additional heating is likely to be required. The resource will be exploited using the deep standing column well method (Collins and Law, 2017).

Figure 2.5: *Example drilling rig for the Jubilee Pools project (Arup, 2018a).*

Shallow ground source heat pumps are also using energy from the subsurface (3000 – 5000 installations per year in the UK) (Lund et al., 2016), but are commonly associated to small-scale use and application (e.g., domestic, retail, public buildings).

2.2.3 Heat flow of the UK

Heat flow in the UK is relatively low due to much of the land area being covered by low thermal conductivity sedimentary rocks of Palaeozoic to Mesozoic age. Thermal anomalies are identified in the UK and tend to be constrained to areas where high heat-flow (HHF) granites have been identified (Fig. 2.6). The arithmetic average of heat flows calculated for the UK is 68±26 mWm^{-2}, which is skewed due to the inclusion of HHF granites (~15 % of heat flow measurements) (Rollin,

1995). The exclusion of HHF granites gives a mean value of 52 – 55 mWm^{-2} (Burley et al., 1980; Downing and Gray, 1986a, 1986b; Busby, 2014).

Heat flow in the UK
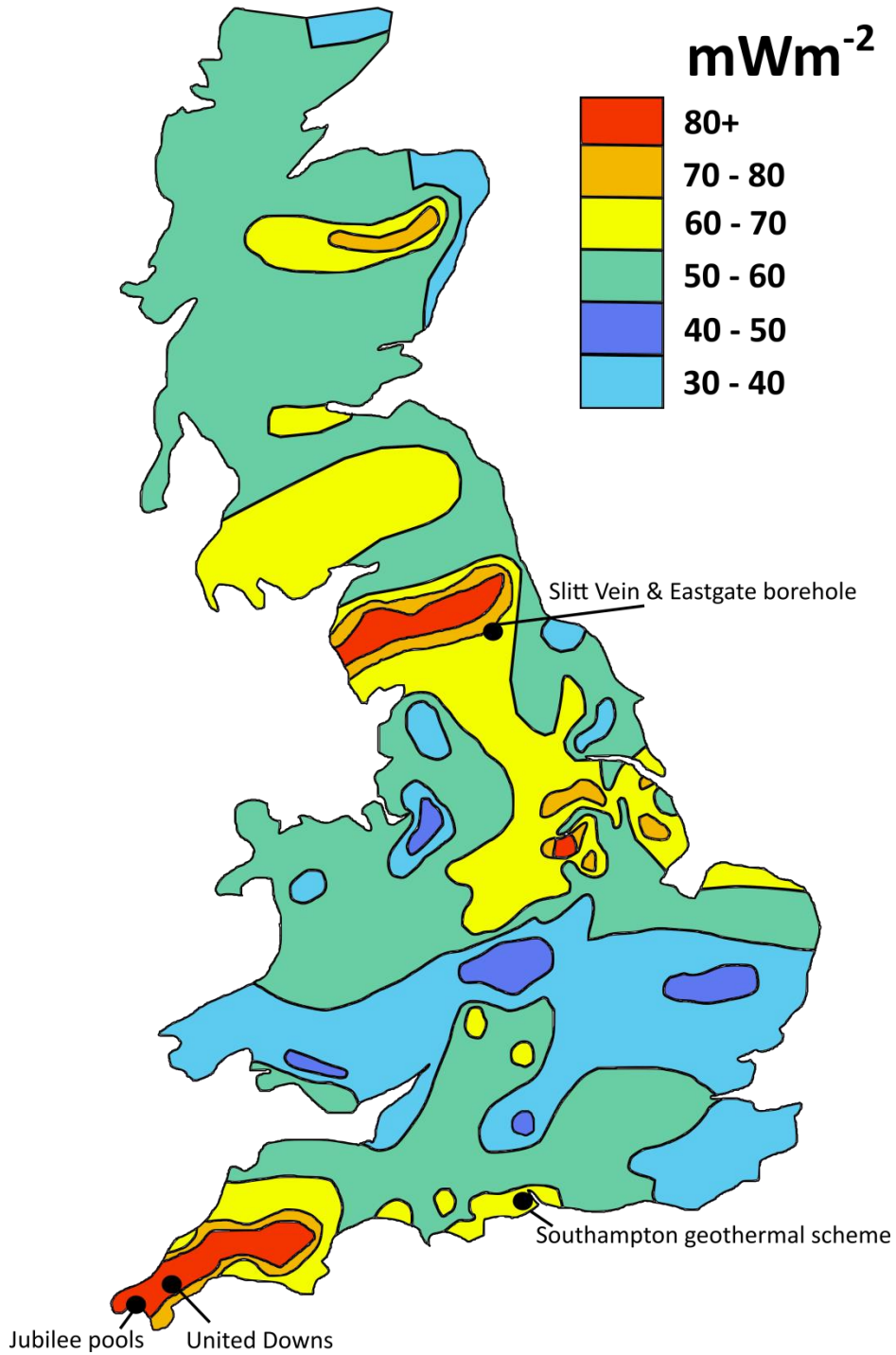
Figure 2.6: *Heat flow map of the UK (modified after Busby, 2010).*

Heat flow (Q) is calculated using Fouriers law (Allen et al., 1985; Busby, 2010, 2014 etc):

$$Q = -\lambda \frac{\delta T}{\delta z} \qquad\qquad\qquad 2.1$$

where λ is the thermal conductivity and $\frac{\delta T}{\delta z}$ is the thermal gradient. The value is always negative to represent the transfer of heat from high to low temperatures.

Thermal conductivities of sedimentary rocks vary across the country ranging from 0.31 to 5.4 W/m °C (Downing and Gray, 1986a). The higher conductivities are within salt deposits, limestones and sandstones, whilst the lower conductivities are found in mudstones and coals. HDR prospects tend to have a higher heat flow as granitic rocks have higher thermal conductivities and radiogenic heat production than sedimentary rocks.

Busby et al. (2011a) modelled temperature distribution across the UK. They identified an average geothermal gradient of 28 °C/km for the upper 1 km of crust over the whole country, which is higher than that proposed by previous authors (e.g., Downing and Gray, 1986a). Cooler temperature gradients are associated with Mesozoic sedimentary basins, whilst hotter temperatures are constrained to areas of HHF granites. The buried Weardale, Carnmenellis and Scottish Granites all have elevated geothermal gradients and high heat production, with a geothermal gradient closer to 40 °C/km (Downing and Gray, 1986a; Busby et al., 2011a). The sedimentary rocks overlying the granites have lower thermal conductivities and insulate the granites causing a geothermal anomaly. This ambiguity in thermal gradients, and thus heat flow, must be considered when modelling as it can lead to over- or under-estimations of temperatures.

There are eight major deep sedimentary basins in the UK, four in England and Wales, and four in Northern Ireland. The four Mesozoic basins in England and Wales considered to have potential for geothermal development include the Cheshire, Wessex, Worcester and East England Basins (Busby, 2010), whilst Northern Ireland has three basins of Permo-Triassic age and one of

Carboniferous age: Lough Neagh, Larne, Rathlin and North West Basins, respectively (Fig. 1.1) (Pasquali et al., 2010). The basins identified have: high to moderate heat flows, significant reservoir thickness, high transmissivities and are buried to sufficient depths to exceed 40 °C (Jackson, 2012).

The Wessex, Worcester and East England Basins have relatively high gradients of 30 °C/km, 20 – 25 °C/km and 26 – 30 °C/km, respectively (Allen et al., 1985). The basins in Northern Ireland have far higher geothermal gradients up to 38 °C/km (Jackson, 2012). The Cheshire Basin has a low heat flow (52 mWm^{-2}) and geothermal gradient (20 °C/km) compared to the average of the UK (Burley et al., 1980; Downing and Gray, 1986a). Recent further analysis, aiming to correct the thermal gradients of uncorrected wells, has suggested the geothermal gradient in the Cheshire Basin could be closer to 27 °C/km (Busby, 2014).

2.2.4 Data from existing deep boreholes in the Cheshire Basin

Two boreholes have been drilled to depths exceeding 3 km in the Cheshire Basin; these include Prees-1 and Knutsford which were drilled in excess of 3.73 km TVDSS (True vertical depth subsea) and 3 km TVDSS, respectively (UKOGL, 2019). The Knutsford borehole was drilled to the north of the Cheshire Basin, whilst the Prees-1 borehole was drilled to the southwest of the basin. The Prees-1 and Knutsford boreholes have a significant thickness of sandstones, 1,623.1 m TVDSS and 1,921.3 m TVDSS, respectively (UKOGL, 2019). Boreholes in the central part of the basin rarely exceed 1 km depth (e.g., Burford and Elworth), with ~95 % of wells being either confidential or drilled to depths of less than 50 m (Hirst, 2017). Uncorrected temperature plots from the deepest wells indicate thermal gradients exceeding 20 °C/km (Fig. 2.7, Table 2.1 and 2.2) (Hirst et al., 2015).

Prees-1	
Temperature (° C)	Depth (m)
53	1731
56	1932
59	2164
62	2396
66	2750
70	2889

Table 2.1: *Uncorrected temperatures for the Prees-1 Well (Plant et al., 1999; Hirst et al., 2015). For well*

locations see figure 2.8.

Knutsford	
Temperature (° C)	Depth (m)
27	715
31	909
39	1500
43	1803
45	2000
51	2230

Table 2.2: *Uncorrected temperatures for the Knutsford Well (Plant et al., 1999; Hirst et al., 2015). For well*

locations see figure 2.8.
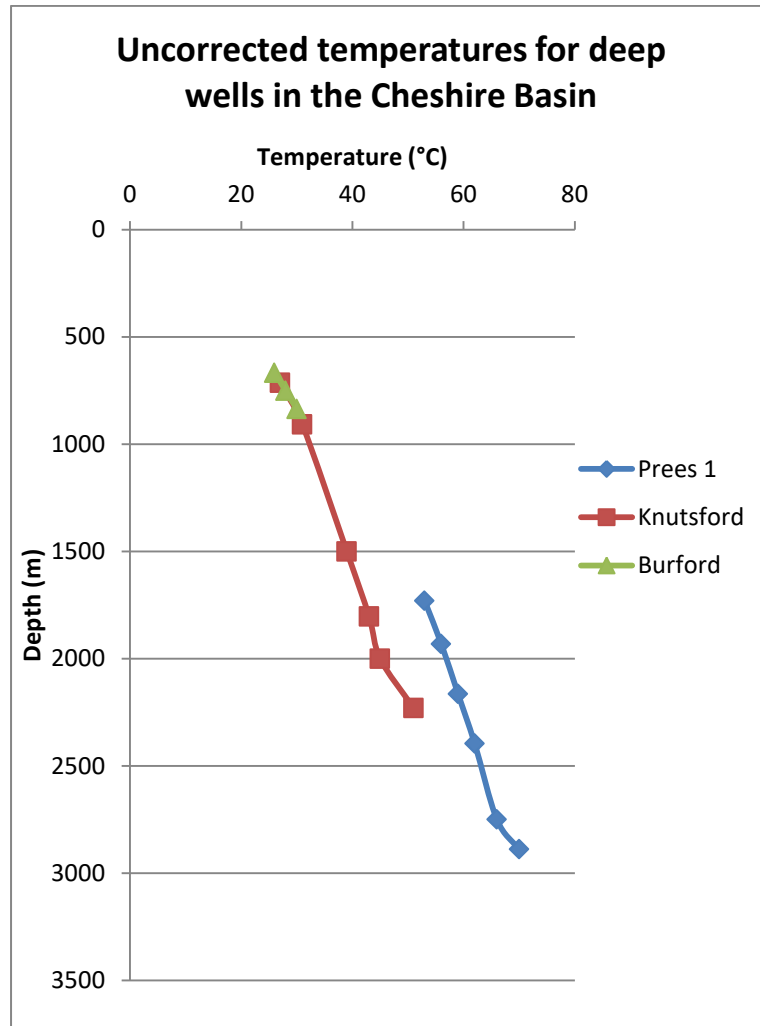
Figure 2.7: *Graph showing uncorrected temperature variation with depth for a selection of deep wells.*

Limited thermal modelling has been undertaken for the Cheshire Basin; however, the modelling which has been undertaken focuses on static models at the base of the Permo-Triassic infill and highlights an increase in temperature towards the basin depocentre (Fig. 2.8) (Downing and Gray, 1986; Plant et al., 1999; Busby, 2011b). Initial modelling depicted an increase in temperature to the northeast (Downing and Gray, 1986b), whilst Plant et al. (1999) suggested an increase to the southwest. The most recent thermal modelling by Busby (2011b) shares similarities between the two, however, estimates higher temperatures. This could be due to it being based on further work correcting thermal gradients that has predicted gradients of up to 27 °C/km (Busby, 2014).

Temperatures at the base of Permo-Triassic rocks after:

a. Downing and Gray, 1986

80°C +
60 - 80°C
40 - 60°C
20 - 40°C

KW

PW

20 km

b. Plant et al. 1999

KW

67°C+
57 - 67°C
48 - 57°C
38 - 48°C
29 - 38°C
19 - 29°C

PW

c. Busby, 2011

KW

80°C+
70 - 80°C
60 - 70°C
50 - 60°C
30 - 50°C
<30°C

PW
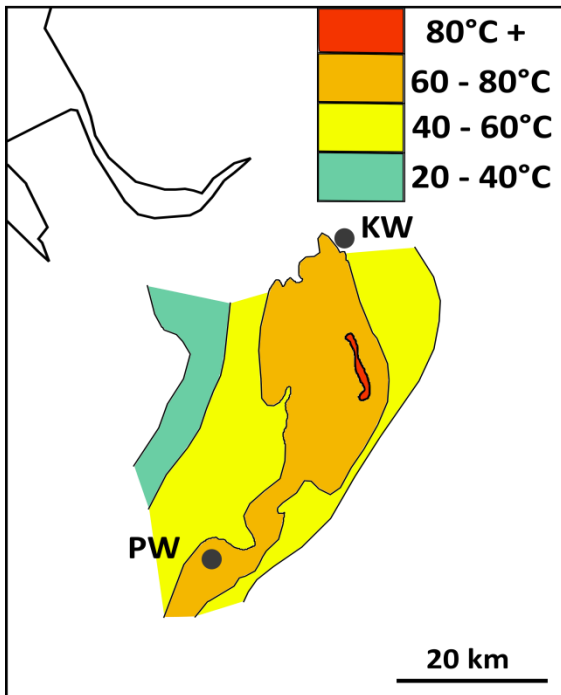
Figure 2.8: *Temperature variations at the base of the Permo-Triassic within the Cheshire Basin (images modified from (a) Plant et al., 1999, (b) Downing and Gray, 1986 and (c) Busby, 2011b). PW = Prees-1 Well, KW = Knutsford Well.*

Hydro-physical data for Permo-Triassic sandstones shows that in large diameter borehole flow rates for the Sherwood Sandstone Group of 100 l/s and up to 30 l/s for the Collyhurst Sandstone Formation can be attained (Plant et al., 1999; Griffiths et al., 2003; Hirst et al., 2015). In core plug studies, porosity ranges from 13 to 30 % for the Sherwood Sandstone Group and 20 to 24 % for the Collyhurst Sandstone Formation, whilst hydraulic conductivities can be found from 0.006 to 10 m/day and from 3.7×10^{-5} to 10 m/day respectively (Allen et al., 1997). It is also worth noting that analogous data can be used from the East Irish Sea, with a detailed study undertaken by Hirst (2017). The large variations in the range of data are likely to be due to different facies within the rock being tested.

The lack of physical data in the centre of the Cheshire Basin makes it difficult to constrain the geology. Seismic data is available and has been analysed, giving structural maps for lithological formations (Downing and Gray, 1986b; Plant et al., 1999). Seismic data is of poor quality at depth in areas due to dissolved halites in the Mercia Mudstone Group causing collapse of the overlying strata (Evans et al., 1993).

2.3 Geological history of the Cheshire Basin

The Cheshire Basin consists of a sequence of sedimentary clastic rocks dating from the Permian to the Jurassic, with minor Quaternary superficial deposits. The Mesozoic sandstones are the focus of this study; however, the Permo-Triassic infill is underlain by Palaeozoic rocks which were deformed during the Caledonian and Variscan Orogenies. Both tectonic events are described here as they are responsible for the formation of structural and sedimentological controls within the basin, and are also responsible for much of the basin development across the whole of Northwest Europe (Butler, 1990).

2.3.1 Caledonian Orogeny

The earliest sediments encountered in the deep wellbores within the Cheshire Basin are from the Silurian (Prees-1 borehole) (UKOGL, 2019). In addition, the major structures in the Cheshire Basin are believed to have first formed during the Caledonian and Variscan Orogenies (Smith, 1999; Hirst et al., 2015), before later reactivation during Permo-Triassic extension. The Caledonian Orogeny occurred from the Cambrian to the Devonian (540 - 400 Ma) and is related to the closure of the Iapetus Ocean between Laurentia, Baltica and Avalonia (Fig. 2.9) as a sequence of 5 orogenic events; the Penobscotian, Grampian, Shelveian, Scandian and Acadian (Rast and Crimes, 1969; Fitches and Campbell, 1987; Hutton and Murphy, 1987; Dewey and Mange, 1999; McKerrow et al., 2000; Mendum, 2012).

Figure 2.9: *Positions of the UK and major continental terranes prior to the Caledonian Orogeny (after McKerrow et al., 2000).*

Although the Caledonian Orogeny is not directly associated with the creation of the Cheshire Basin, it does have significant local implications. During the closure of the Iapetus Ocean the position

of the UK was spread between Laurentia and Avalonia, with the Cheshire Basin located on the northern margin of Avalonia in a continental shelf area (Fig. 2.9). As a result, Silurian age sediments underlying the Cheshire Basin are expected to consist of deep marine deposits (shales) evolving into shallow marine tropical limestones when Avalonia drifted to lower latitudes (Cocks, 1989).

After the collapse of the Caledonian Orogeny, the Devonian 'Old Red Sandstone' Formation was deposited in extensional basins across much of the UK (McClay et al., 1986; McKerrow et al., 2000). However, the lateral continuity of these Devonian sediments across the UK is unpredictable, particularly in the Cheshire Basin where there are no wells penetrating rocks of this age. Some authors suggest that the Cheshire Basin was located on a regional high at this time with no regional sedimentation (Mikkelsen and Floodpage, 1997), whilst others suggest sediment was removed during transtension during Devonian extension (Soper and Woodcock, 2003).

2.3.2 Variscan Orogeny

The Variscan Orogeny occurred during the late Carboniferous, when Gondwana moved northward colliding with Laurasia, forming the supercontinent Pangaea (Fig. 2.10a). The collision was continuous at an oblique angle between the two continents, causing rotation and major structures across the UK (Waters and Davies, 2006; McCann, 2008). The Variscan Front stretched from Pembroke to Kent (Fig. 2.10b) (Leveridge and Hartley, 2006) and the Cheshire Basin was located to the north of this in the Variscan Foreland. Faults in the region are oblique to the Variscan Front, with an orientation of WNW – ESE, due to reactivation of Caledonian basement faults (Smith, 1999).
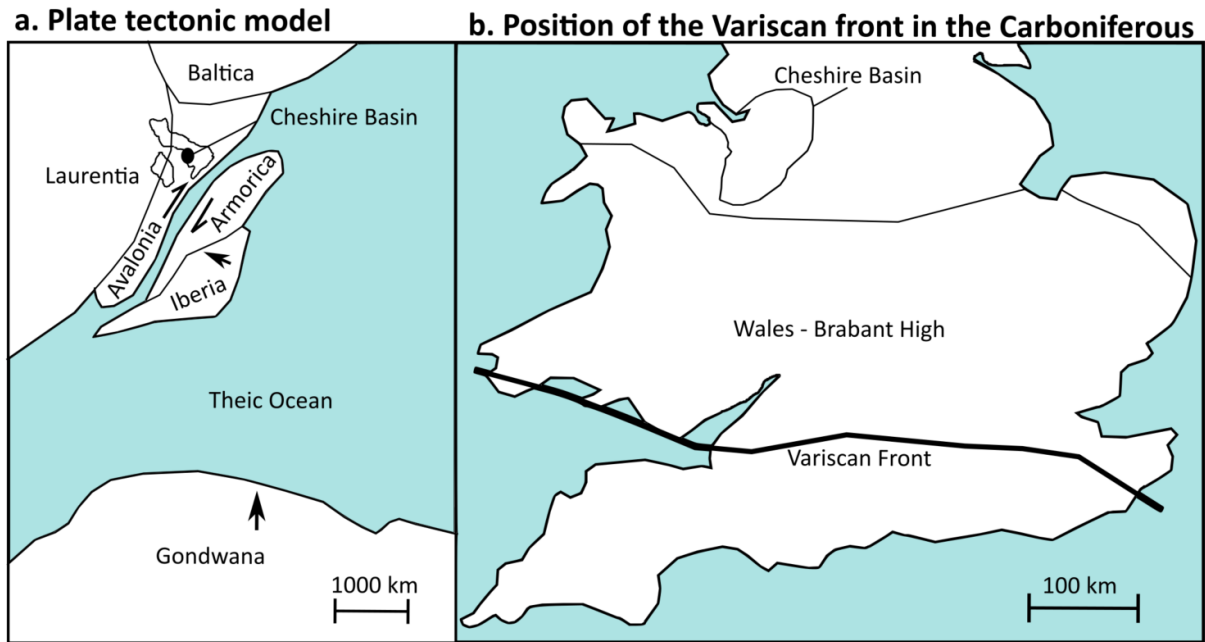
Figure 2.10: *(a) Plate tectonic reconstruction for the Carboniferous showing the position of the UK (after Waters and Davies, 2006) and (b) the position of the Variscan Front in the UK during the Carboniferous (Rippon et al. 2006).*

Two late phases of uplift occur in Westphalian strata; the first at the end of Westphalian A – C strata (identified by an unconformity) and the second during Westphalian C – D strata (identified by structural features) (Smith, 1999), leading to the erosion of Carboniferous strata (Fig. 2.11). To the end of the Carboniferous fold thrust structures are associated with crustal shortening due to the Variscan Orogeny. East to west compression occurred late in the Variscan Orogeny, with the event being restricted to Britain, accounting for block rotations within the foreland (Peace and Besly, 1997; Smith, 1999).

2.3.3 Permo-Triassic extension

The Variscan compression in the late Carboniferous was followed by the extensional collapse of the orogeny in the early Permian (Fig. 2.11) (Woodcock and Strachan, 2009). Due to the instability of Pangaea, rifting and separation of continents occurred soon after the formation, with the North Atlantic forming in the Early Cretaceous (Glennie, 1995). From the Carboniferous to Jurassic, rifting

occurred across Europe associated with the breakup of Laurasia (Rowley and White, 1998). The East Irish Basin, West Lancashire Basin and Cheshire Basin make up a larger basin system with similar stratigraphy and basinal settings. Two dominant rifting periods have been documented in the Dinantian to Westphalian and then further rifting throughout the Permian to Triassic (Rowley and White, 1998).
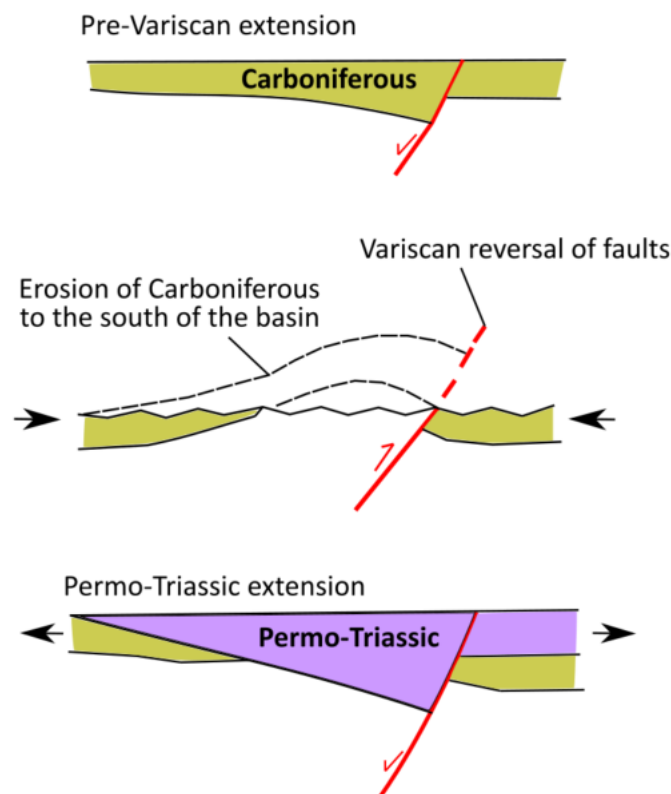
Figure 2.11: *Schematic of the tectonic history of the Cheshire Basin (after Plant et al., 1999).*

Permian extension after the Variscan Orogeny created tilted fault blocks and initiated the extensional sedimentary basins seen across the UK, with major extension in the mid-late Triassic followed by further thermal subsidence (Ruffell and Shelton, 1999). It has also been stated that most Triassic extension occurred early in the Triassic (Evans et al., 1993). East to west extension resulted in reactivation of Caledonian NW-SE and NE-SW structures in the Cheshire Basin (Hirst et al., 2017).

Sediments deposited in the Permian extensional sequence are initially of terrestrial origin, with fluvial and aeolian processes responsible for sedimentation. The late Triassic to Jurassic period represents a transgression from terrestrial to marine sediments (Rowley and White, 1998). The Triassic Sherwood Sandstone Group is sourced from remnants of the Variscan highlands, whilst the Mercia Mudstone Group comprises of sediment derived from reactivated footwall sides of Variscan faults (Ruffell and Shelton, 1999). Fault controlled subsidence on the eastern margin in the upper Triassic resulted in the Cheshire and Worcester Basins being connected as a single drainage basin, with upper Triassic sediment sourced from France (Naylor et al., 1989).

2.4 Present structure of the Cheshire Basin

The modern Cheshire Basin is an asymmetrical half graben, with Permo-Triassic fill, constrained to the east by the Wem Red Rock Fault (WRRF) and then to the west by onlapping strata onto basement (Fig. 2.12) (Bloomfield et al., 2006). The WRRF is a reactivated basement structure, and the major constraining fault in the west (East Delamere fault) is a reactivated structure (Brenchley, 2006). The basin stretches 100 km north to south and 55 km east to west, covering an area of 3,500 km^2 (Plant et al., 1999; Hirst et al., 2015), with up to 4.5 km in thickness sediment infill (Naylor et al., 1989).

a. Geological map of the Cheshire Basin

West Lancashire Basin

East Irish Sea

Manchester

b.

Cheshire Basin

Well site - Crewe

Key:
- Lias Group
- Mercia Mudstone Group
- Sherwood Sandstone Group
- Appleby Group
- Carboniferous
- Pre - Carboniferous
- Faults

N

12 miles

Worcester Basin
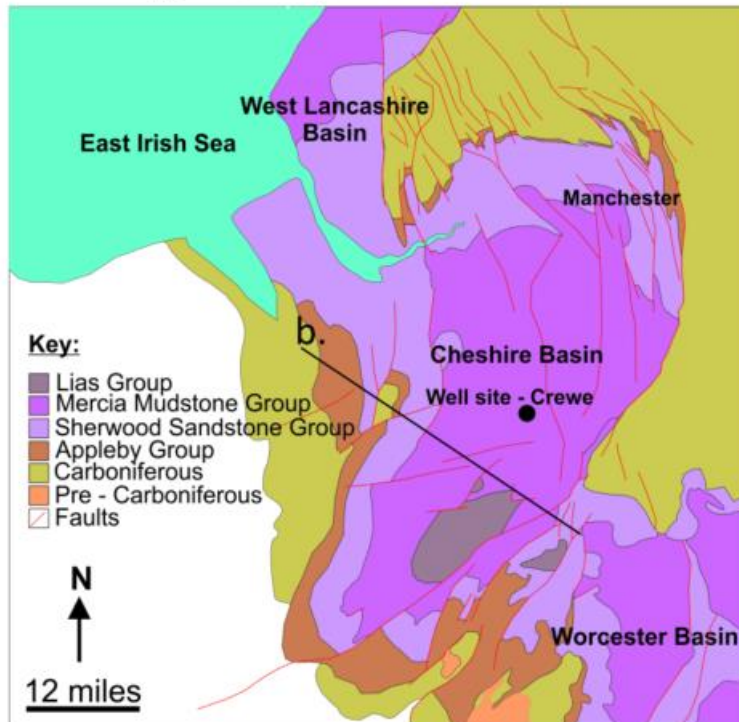
b. Cross section of the Cheshire Basin

NW

SE

0
1
2
3
4
5

km

0   5 km

Key:

MMG (U. Triassic) - Mercia Mudstone Group consists of mudstone and minor siltstone with halite bearing beds common.

SSG (L. Triassic) - Sherwood Sandstone Group consists of aeolian to fluvial sandstones deposited in an arid setting.

Permian - Aeolian to fluvial sandstones overlain by marl deposited during a marine incursion.

Carboniferous - Primary focus on the barren measures terrestrial to fluvial sandstone. Later stages dominated by marine carbonates.

Pre Carboniferous - Basement (age undifferentiated)

Figure 2.12: *(a) Geological outcrop map of the Cheshire Basin (after Plant et al., 1999; Hirst et al., 2015; UKOGL, 2019). Permo-Triassic sandstones are the dominant infill (Appleby and Sherwood Sandstone Groups), capped by a sequence of thick mudstones (Mercia Mudstone and Lias Groups). (b) Cross-section of the basin (after Plant et al., 1999), with the potential extent of Carboniferous strata in the subsurface.*

More than 600 faults have been identified from seismic data in the region with most of them being sub-planar, small and extensional, with dips ranging from 55 ° - 80 °, and throws ranging from 100 - 500 m (Chadwick, 1997; Plant et al., 1999). The authors of the studies also suggested larger, deeper faults, with throws ranging from 500 – 2,500 that, divide the basin into a series of tilted fault blocks and identified three principle fault orientations in the basin (faults intersecting through the base of the Permian):

1.) NE to SW – concentrated to the south of the basin with orientations parallel to the WRRF.

2.) N to S – dip-slip faults located in the central part of the basin, with fault orientation perpendicular to the major extensional direction in the Permian and Triassic. The larger faults are likely to be associated to pre-existing Caledonian and Variscan sutures.

3.) NW to SE – the dominant trend in the northeast of the basin and most likely to be associated with basement given that the Carboniferous rocks have a similar fault.

Permo-Triassic sedimentary infill is dominated by thick successions of fluvial and aeolian sandstones sourced from the Variscan Orogeny (Rayner, 1981; Naylor et al., 1989), with the Sherwood Sandstone Group (SSG) deposited following a brief marine incursion at the end of the Permian (Fig. 2.13). The SSG retains high porosity and is considered key to geothermal exploration due to favourable thermal and hydro-physical parameters. The late Triassic and Jurassic sediments of the Merica Mudstone, Penarth and Lias Groups represent a major marine transgression and change to fully marine setting (Naylor et al., 1989; Williams and Eaton, 1993; Wilson, 1993). Quaternary superficial deposits that formed during the last glacial period cap the top of the basin.

Figure 2.13: *Lithostratigraphic column of the Cheshire Basin (after Mikkelsen and Floodpage, 1997).*

2.5 Pre-Permian strata

Silurian aged rocks consisting of sandstone and shales (Fig. 2.13) (Jones, 1925, 1949; Dineley, 1960; Cocks et al., 1984; Brenchley, 2006; Howells, 2007) are the earliest encountered below the Cheshire Basin (Prees-1 borehole) (Mikkelsen and Floodpage, 1997). The extent and lateral continuity is unknown; however, they are overlain by an unconformable carbonate sequence of Dinantian limestones (Mikkelsen and Floodpage, 1997; Smith et al., 2005) and clastic Namurian sandstones and shales (Williams and Eaton, 1993; Smith, 1998). After the Caledonian Orogeny, extension in the Dinantian created a series of basins and platforms with mixed carbonate and clastic input, followed by subsidence in the Namurian and Westphalian, dominated by deltaic depositional environments (Fig. 2.14) (Waters et al., 2006; Andrews, 2013; Hirst, 2017). The thick deltaic sequence of Westphalian aged rocks comprises of 'coal' and 'barren' measures (Warwickshire Group) which make up the wider Pennine Basin (Gibson, 1901; Powel et al., 2000).

The succession of pre-Permian strata in the central parts of the basin (i.e., Crewe area) is heavily debated due to the absence of borehole data at depth, with some authors suggesting that the Coal Measures (and possibly Barren) were removed due to Variscan thrusting (Mikkelsen and Floodpage, 1997; Plant et al., 1999), such that Permian rocks rest unconformably on Lower Palaeozoic metamorphic rocks (Fig. 2.15). The implications on modelling of the equivocal nature of pre-Permian strata in the Crewe area is discussed further in chapter 5 (section 5.2).

Paleogeography during the Carboniferous
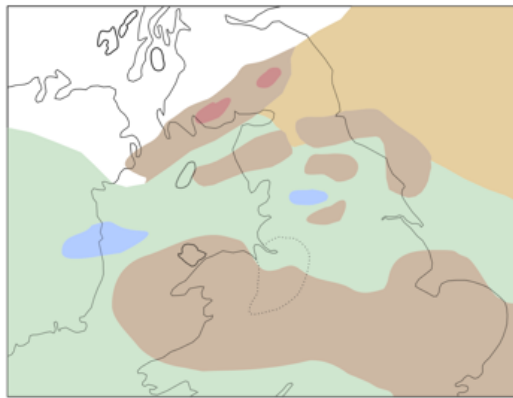
a. Early Visean
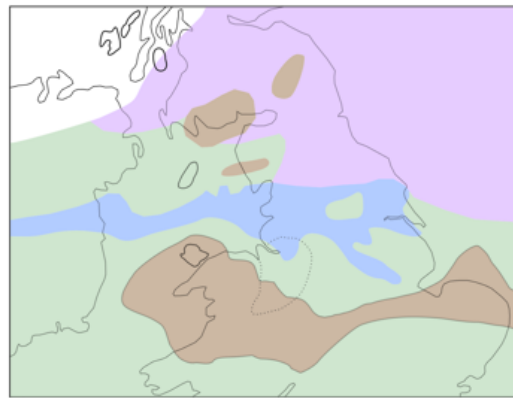
b. Late Visean
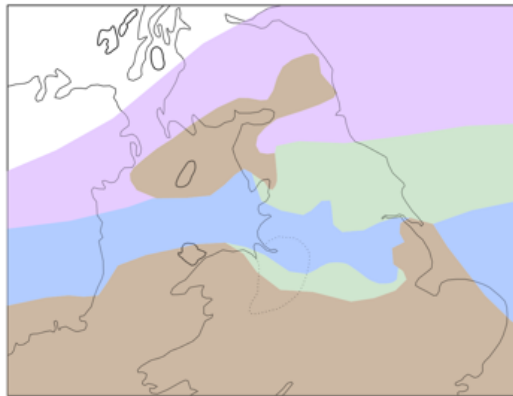
c. Early Namurian
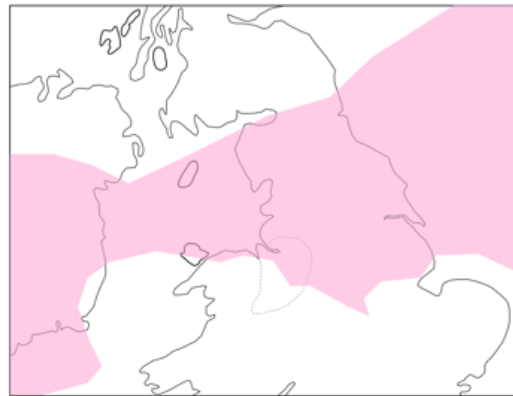
d. Early Westphalian
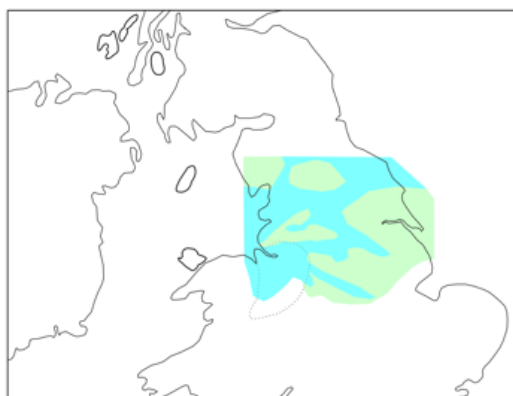
e. Carboniferous Basins and platforms across the UK

Key:
- Coastal facies
- Milstone Grit
- Topographic High
- Highlands
- Shallow Marine Carbonates dominant
- Basin
- Coal Measures
- Carbonate Platforms
- Basin

Figure 2.14: *Paleogeography throughout the Carboniferous (modified from Cope et al., 1992, Waters et al., 2009 and Andrews, 2013). (a) Depositional setting at the start of the Visean, (b) at the end of the Visean, (c) in the early Namurian, (d) in the early Westphalian and (e) an overview of basin and platform formation for the early Carboniferous (Mississipian).*

Figure 2.15: *(a) Map highlighting the extent of Coal Measures in the Cheshire Basin and (b) a cross-section highlighting the limits of Palaeozoic rocks underneath the Cheshire Basin (after Mikkelsen and Floodpage, 1997). PW = Prees-1 Well, BW = Burford Well, KW = Knutsford Well, MMG = Mercia Mudstone Group, SSG = Sherwood Sandstone Group, MMF = Manchester Marl Formation, CF = Collyhurst Sandstone Formation, CM = Coal Measures, BM = Barren Measures/Warwickshire Group, NA = Namurian, DI = Dinantian, LP = Lower Palaeozoic.*

2.6 Permo-Triassic stratigraphy of the Cheshire Basin

2.6.1 Permian Appleby and Cumbrian Coast Groups

Permian strata are considered as two formations, the Collyhurst Sandstone Formation and the Manchester Marl Formation. They are part of the Appleby and Cumbrian Coast Groups respectively. The previous formation names are listed in Table 2.3.

Formation/Group	Previous name(s)
Mercia Mudstone Group	Keuper Marl, Keuper Saliferous beds (split between different formations as upper and lower)
Helsby Sandstone Formation	Keuper Sandstone, Bulkeley Hill etc.
Wilmslow Sandstone Formation	Upper Mottled Sandstone
Chester Formation	Chester Pebble beds, Bunter etc.
Kinnerton Sandstone Formation	Lower Mottled Sandstone
Manchester Marl Formation	Manchester Marl
Collyhurst Sandstone Formation	Lower Mottled Sandstone, Permian Sandstone, Lower Permian Sandstone

Table 2.3: *Previous names typically used in the Cheshire Basin for current formations (after BGS, 2019).*

2.6.1.1 Collyhurst Sandstone Formation

The Collyhurst Sandstone Formation is an arenaceous sandstone that lies at an angular unconformity to Westphalian strata (Mikkelsen and Floodpage, 1997; Griffiths et al., 2003). The unconformity is overlain by discontinuous fluvial – alluvial fans, which are likely to be a result of mass flows into the subsiding basin (Macchi, 1981). The Collyhurst Sandstone Formation is similar in character and depositional environment (aeolian) to the Kinnerton Sandstone Formation, but shows occasional fluvial sediments (Hull, 1864; Evans et al., 1993). The formation varies in thickness

dramatically and often includes thin bands of breccia (Rayner, 1981). The formation consists of cross-bedded sandstone with minor siltstone inclusions. The sandstone is 'fine- to medium- grained, well-sorted and poorly cemented with high hydraulic conductivity' (Allen et al., 1997).

Not only does the Collyhurst Sandstone Formation have favourable intergranular features, but also has high-quality macroscale features. When the rock is silicified, cross-bedding splits along foresets, creating hydraulic pathways (Hull, 1864; Hughes, 2003). The distribution of cemented zones are, however, relatively unknown (Waugh, 1970; Arthurton and Wadge, 1981).

The Collyhurst Sandstone Formation forms the lowest stratigraphic unit within the basin and has porosities up to 33.6 % (Allen et al., 1997). Recorded permeabilities vary between 2 x 10^{-14} to 1.8 x 10^{-11} m^2 (Harvey and Gray, 2013) with the higher values likely to be caused by increased flow through fault or fracture intersection. The mean hydraulic conductivity of the Collyhurst Sandstone Formation (and Kinnerton Sandstone Formation) has been recorded as 0.4 m/day, with the majority of tested samples exceeding 0.1 m/day (Table 2.4). These high-quality properties were interpreted as being due to the aquifer having medium- to coarse- grains with limited cementation (Allen et al., 1997).

	Permeability (m^2)	Hydraulic conductivity (m/day)	Porosity
Helsby Sandstone Formation	8.3853E-12	20	2-35 %
Wilmslow Sandstone Formation	9.869E-13	2.353881595	6-35 %
Chester Formation	2.46725E-12	5.884703987	20-30 %
Kinnerton Sandstone Formation	1.9738E-12	4.707763189	9-17 %
Collyhurst Sandstone Formation	4.19265E-14	0.1	13-32 %

Table 2.4: *Typical hydraulic properties of aquifers (Downing and Gray,1986b; Allen et al., 1997; Gray and Harvey, 2006; Kinniburgh et al., 2006; Harvey and Gray, 2013). Converted assuming fluid is 80 °C.*

2.6.1.2 Manchester Marl Formation

The Manchester Marl Formation represents a minor marine incursion in the mid Permian (Naylor et al., 1989), with sediments thinning to the south, leaving the Collyhurst Sandstone and Kinnerton Sandstone Formations in hydraulic continuity (Fig. 2.16). It was identified in Manchester as the 'Upper Permian' Formation, consisting of marls interbedded with limestone and ironstone (Hull, 1864), with the formation becoming siltier to the south (Evans et al., 1993). Rare fossils are also found at the base of the formation such as marine bivalves and formanifera (Rayner, 1981).
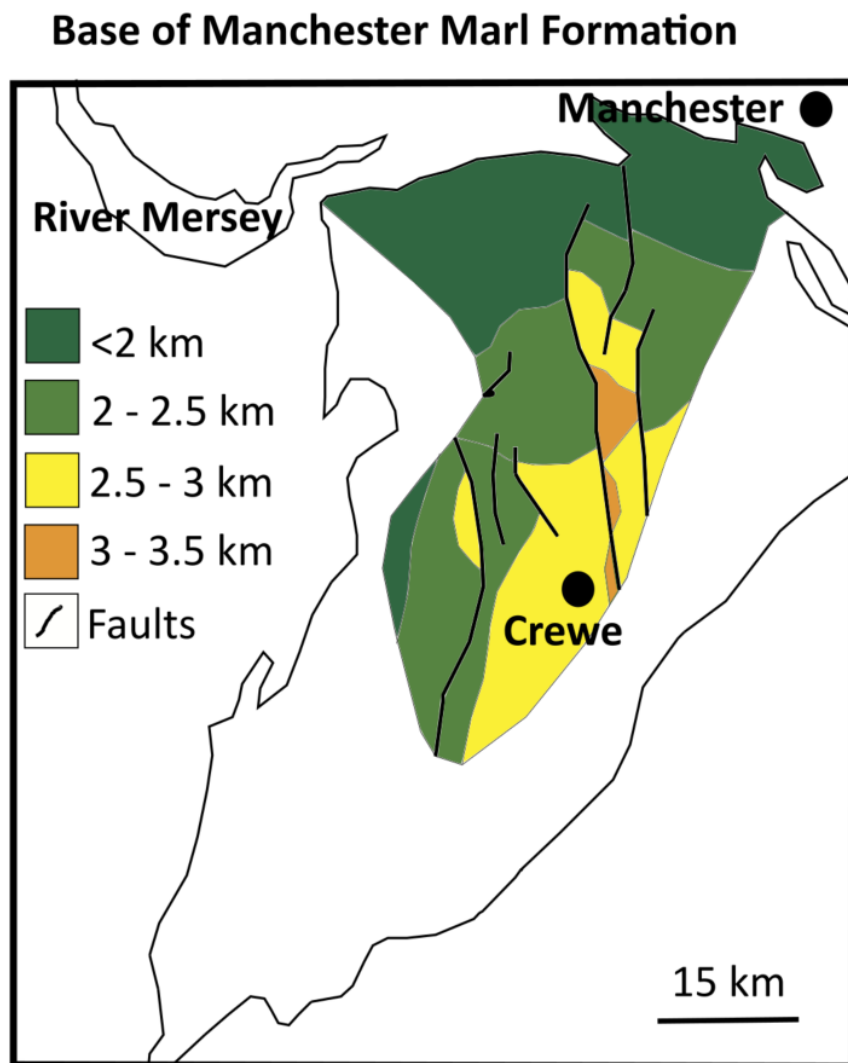
Figure 2.16: *Map of the extent of the Manchester Marl Formation in the Cheshire Basin (after Downing and Gray, 1986b).*

The Knutsford borehole indicates the thickness of the Manchester Marl Formation to be 148 m (Fig. 2.17) (Downing and Gray, 1986b), with thicknesses in the Crewe area reaching up to 500 m (from depth contours from Downing and Gray, 1986b and Plant et al. 1999).
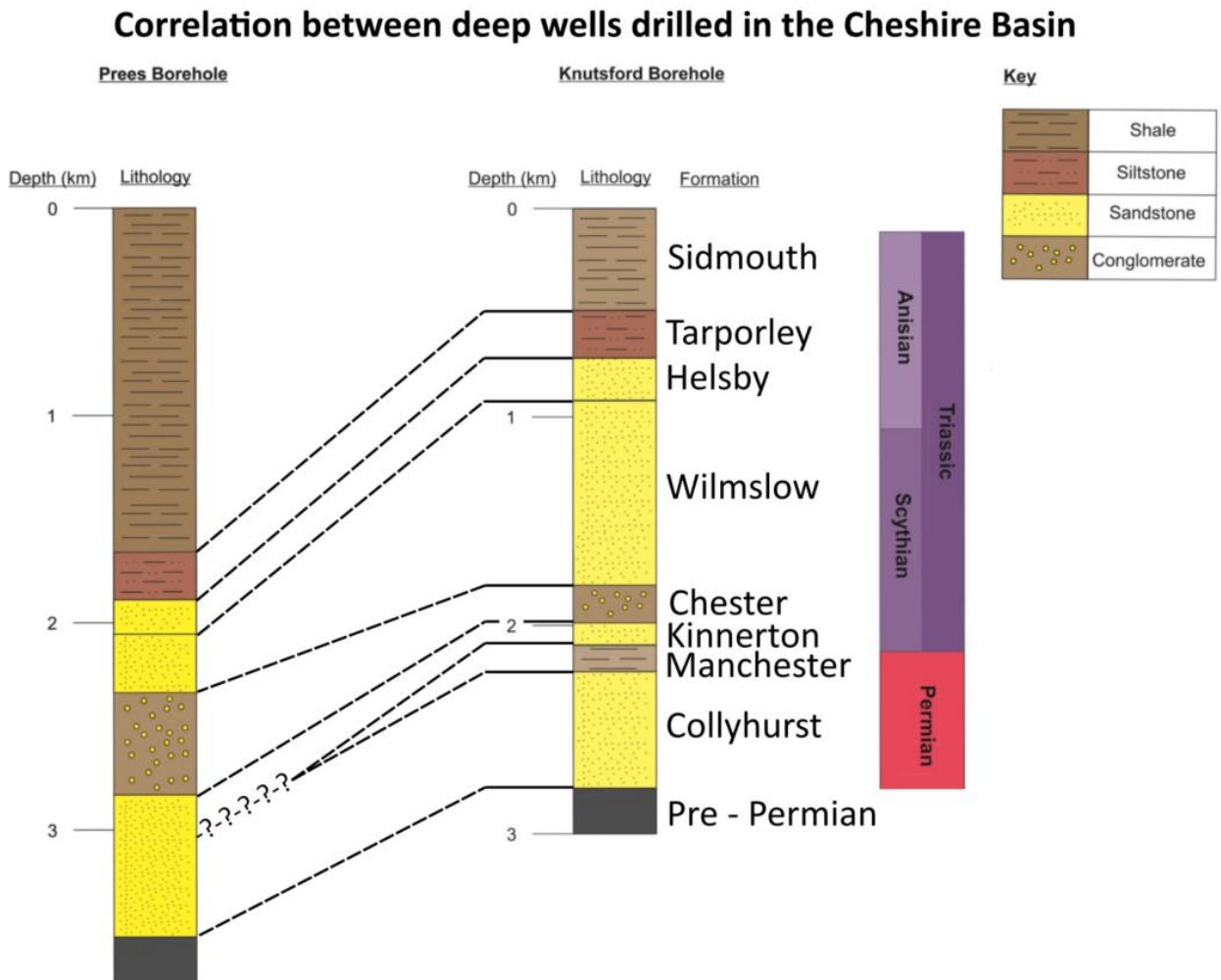
Figure 2.17: *Correlation between the Prees-1 and Knutsford boreholes after Mikkelsen and Floodpage, (1997). Various authors suggest the presence of Manchester Marl Formation at Prees-1 (Evans et al., 1993; Plant et al., 1999), whilst others suggest it does not reach that far south in the basin (Downing and Gray, 1986b; Mikkelsen and Floodpage, 1997). For locations of Prees-1 and Knutsford boreholes see figure 2.15.*

2.6.2 Triassic Sherwood Sandstone Group

2.6.2.1 Kinnerton Sandstone Formation

The Kinnerton Sandstone Formation is an arenaceous sandstone deposited in an aeolian environment, consisting of fine- to coarse- grained red bed sandstone with muddier, interdune lenses (Ambrose et al., 2014). It is largely pebble free, but does have a brecciated base and tends to thin to the north, pinching out before the Manchester region (Evans et al., 1993). Many consider the Kinnerton Sandstone and Collyhurst Sandstone Formations to be one entitiy due to the thinning of the Manchester Marl Formation southward, leaving the two in hydraulic continuity (Downing and Gray, 1986b). Shallow boreholes in the south have demonstrated high intergranular porosity, particularly in the upper stratigraphy (Lovelock, 1977; Downing and Gray, 1986b). Further analysis indicates horizontal permeabilities that exceed 2×10^{-12} m^2 (over 50 % of that analysed), whilst geophysical logs indicate porosity ranging from 9 - 17 % (Downing and Gray, 1986b).

2.6.2.2 Chester Formation

The Chester Formation consists of fluvial orthoquartzitic sandstones and conglomerates, previously called the Chester Pebble Bed Formation (Table 2.3) (Mikkelsen and Floodpage, 1997; Ambrose et al., 2014). Clast-supported, red, conglomerate and coarse-grained, cross-bedded sandstone lithofacies dominate (Fig. 2.18) (Downing and Gray, 1986b). The pebbles are sourced from the south of the basin with palaeocurrent data indicating flow was to the NNW (Smith, 1998). The conglomeratic unit is separated by laterally discontinuous 1 metre thick mudstone bands, which act as baffles to flow (Griffiths et al., 2003). Cross bedding, point bar migration and ripples are often identified in outcrop studies. The Chester Formation was deposited in the early Triassic and are believed to mark a fault-controlled period of subsidence within the basin, with deposition within braided river systems (Naylor et al., 1989). The formation lies conformably on the Permian strata (Mikkelsen and Floodpage, 1997).

Outcrops of the Chester Formation
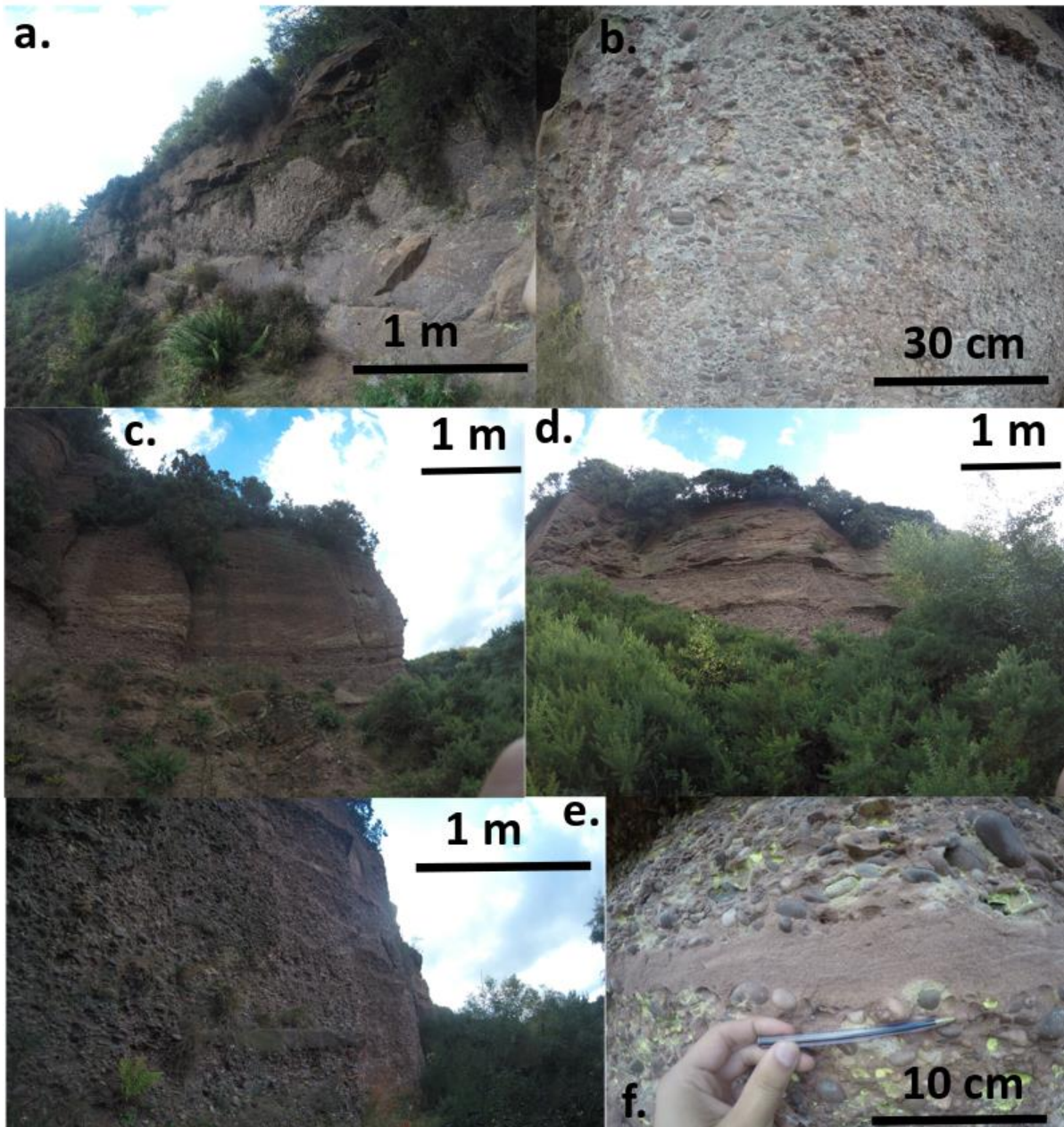
Figure 2.18: *Various images of the Chester Formation. (a) Channel highlighted with coarse pebbles bound by sandstone sheets, (b) clast supported conglomerate with rounded pebbles, (c) large cross bedding with smaller pebbles still seen, (d) 1 m foresets in sandstone lenses within the formation, (e) minor sandstone wedges in a thick conglomeratic sequence and (f) close in section of ripples in a sandstone lens. Photo from Hulme Quarry.*

The Chester Formation is observed to have 20 – 30 % porosity in the Cheshire Basin. Across the UK it is observed to be as low as 7 % (Gray and Harvey, 2006) and as high as 35.3 % (Allen et al.,

1997). Permeability is observed to be up to 2.5 x 10^{-12} m^2 (Harvey and Gray, 2013). The formation is also likely to yield high secondary porosity and permeability if cemented – leading to the rock having high strength and potentially open joints and fractures (Griffiths et al., 2003). Although this is good for the creation of hydraulic pathways, it may suppress primary porosity. The highly heterogeneous nature of the formation (Fig. 2.18) also leads to problems predicting fluid flow and the thermal regime.

2.6.2.3 Wilmslow Sandstone Formation

The Wilmslow Sandstone Formation lies conformably on the Chester Formation (Mikkelsen and Floodpage, 1997) and was deposited in an aeolian setting, thickening to the south east and centre of the basin (Ambrose et al., 2014). It is a red/orange coloured, fine- to medium- grained poor quality sandstone with high clay content, with argillaceous laminae (Downing and Gray, 1986b; Bloomfield et al., 2006). Originally the Wilmslow Sandstone Formation had been interpreted as sheet flood deposits in the East Irish Sea (Meadows and Beach, 1993), until further work by Mountney and Thompson (2002) proved the sandstone to be deposited in an aeolian sabkha environment.

The formation is poorly cemented (Barker and Tellam, 2006), but when cemented, it consists of 'authigenic quartz overgrowths enclosing iron sulphides', with fluids at the time of mineralisation predicted to be up to 150 °C, and with a high salinity derived from upper Triassic salt deposits (Naylor et al., 1989). The poorly cemented nature of the rock often causes fractures to be closed (Griffiths et al., 2003). Silicified layers dominate the lower parts of the formation (Evans et al. 1993), leading to greater porosity in the upper part (Downing and Gray, 1986b). The Wilmslow Sandstone Formation is of similar quality to the Helsby Sandstone Formation. The minimum and maximum values for porosity in literature are 6 – 35 % (Kinniburgh et al., 2006). The permeability is seen to be up to 9.9 x 10^{-13} m^2 (Gray and Harvey, 2006).

2.6.2.4 Helsby Sandstone Formation

The Helsby Sandstone Formation marks the top of the Sherwood Sandstone Group and overlies the Wilmslow Sandstone Formation on the Hardegson Unconformity. The Unconformity is regionally extensive (Downing and Gray, 1986b), with up to 900 m of erosion in the basin due to Triassic uplift (Evans et al., 1993). The Helsby Sandstone Formation formed under aeolian conditions with large outcrops seen to the north of the Cheshire basin. The formation is characterised by large, cross-bedded sandstone separated by fine-grained sandstone with high clay content / mudstone interdunes (Fig. 2.19) (Mountney and Thompson, 2002). Periodic fluvial sandstones are also seen with a high quantity of coarse, rounded pebbles included as matrix-supported conglomeratic layers. Ambrose et al. (2014) and Thompson (1970) described it as a brown, pebbly sandstone, identifying three members based on the concentration of aeolian and fluvial facies: Frodsham, Delamere and Thurston Members. The Frodsham and Thurston Members being aeolian in origin whilst the Delamere Member is fluvial (Mountney and Thompson, 2002).

The Delamere Member is composed of fluvial sandstone, conglomerate and intervals of aeolian dune strata (Thompson, 1969). Porosity and permeability are greatest in the mid Cheshire Basin where the Delamere Member is absent, leaving the more permeable aeolian members (Lovelock, 1977; Downing and Gray, 1986b). The late Frodsham Member represents an aeolian succession which ended as a consequence of the marine incursion of the Tarporley Formation. The early Thurston Member represents a period of aeolian deposition with minor, low sinuosity fluvial ephemeral channels (Thompson, 1970).

Outcrops of the Helsby Sandstone Formation

Figure 2.19: *Various images of the Helsby Sandstone Formation, Delamere Member. (a) Shows fractures along the foresets of cross beds and (b) showing highly weathered faces, whereas (c) is a close up section with rootlet.*

The Helsby Sandstone Formation has the best aquifer characteristics throughout the Cheshire Basin. Porosity ranges from 2 – 35 % (Allen et al., 1997). The large range in porosity is due to the variable quality of sediment through facies changes. High porosities represent clean fluvial sandstones or aeolian sandstones whereas the low porosities are indicative of interdune or flood plain deposits. Equivalent formations across the UK have even higher recorded porosities (up to 36.2 % in the Staffordshire Basin) (Allen et al., 1997). Hydraulic conductivity reaches up to 20 m/day (Allen et al., 1997). It is also worth noting that the Bulkeley Hill Formation is now classed as the Helsby Sandstone Formation (BGS, 2019).

2.6.3 Triassic Mercia Mudstone Group

2.6.3.1 Tarporley Formation

The Tarporley Formation represents a major marine transgression that is seen across Europe (Williams and Eaton, 1993; Wilson, 1993). In the Cheshire Basin, the formation 'consists of fine grained sand and silt deposited in intertidal conditions' (Naylor et al., 1989).

The Tarporley Formation was reclassified as the lower most unit of the Mercia Mudstone Group (Unit A) (Howard et al., 2008). The Tarporley Formation is sometimes described as the Malpas Sandstone. Mikkelsen and Floodpage (1997) suggested that the Malpas Sandstone was deposited in a lobe stretching from the southwest of the basin to just south of Boots Green borehole (Fig. 2.20). Local sandstone channel successions observed in the East Irish Sea could also occur in the Cheshire Basin (Colter and Ebburn, 1978; Downing and Gray, 1986a). In areas across the basin when the formation consists of sandstone, permeability and porosity are up to 4×10^{-13} m^2 and 21 %, respectively (Downing and Gray, 1986b). The Mercia Mudstone Group is predicted to reach a thickness of 1200 m in the Crewe area (Plant et al., 1999).

2.6.3.2 Sidmouth Formation

The Sidmouth Formation dominates the Upper Triassic and succeeds the Tarporley Formation. It consists of mudstones that were deposited as intertidal flats which were restricted from the sea and endured periodic incursions (Naylor et al., 1989). The Mercia Mudstone Group was reclassified by Howard et al. (2008), with the Wilkesley, Byley, Northwich and Bollin Formations now classified as the Sidmouth Formation (for previous descriptions see Evans, 1970; Evans et al., 1993; Hobbs et al., 2002; Howard et al., 2008).
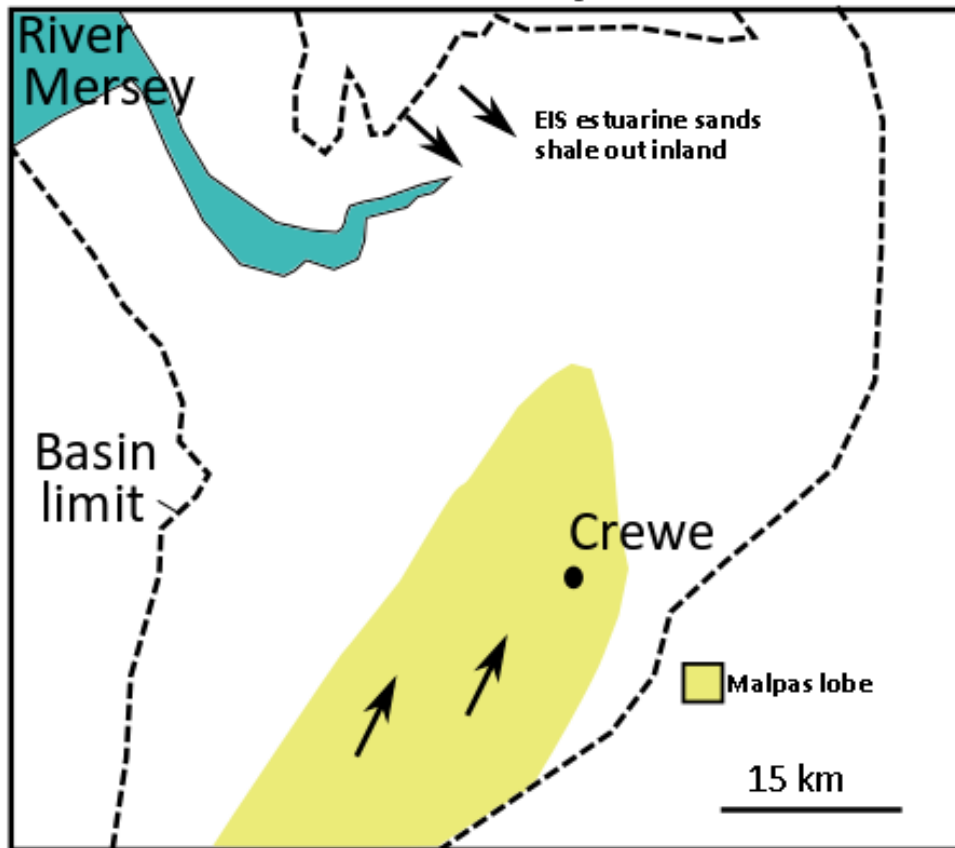
Figure 2.20: *Map showing the extent of the Malpas sandstone lobe in the Tarporley Formation in the Cheshire Basin (after Mikkelsen and Floodpage, 1997). EIS = East Irish Sea.*

2.6.4 Triassic Penarth and Jurassic Lias Groups

The Triassic Penarth and Jurassic Lias Groups are only found in outliers within the Cheshire Basin. The Penarth and Lias Groups overly the Mercia Mudstone Group and consist of marine mudstones interbedded with minor limestones and sandstones (Cox et al., 1999; BGS, 2019). The Penarth Group is situated on an erosional unconformity and is Rhaetian in age (Mikkelsen and Floodpage, 1997). Both the Penarth and Lias Groups form fault-controlled outliers at Firth Farm and Prees. The Firth Farm outlier is controlled by the west-southwest oriented Firth Fault and the Prees outlier by the Wem Red Rock Fault (Mikkelsen and Floodpage, 1997). Both the Penarth and Lias

Groups are only of importance locally to the southwest of Crewe. The maximum thickness observed is 500 m (Plant et al., 1999).

Summary

The Cheshire Basin is an extensional sedimentary basin with Permo-Triassic infill covering an area of 3,500 km^2 with burial depths of up to 4.5 km. The Manchester Marl Formation is an aquiclude that prevents the Permian Collyhurst Sandstone Formation and the Triassic Sherwood Sandstone Group from being in hydraulic continuity. The Sherwood Sandstone Group is succeeded by the Mercia Mudstone Group, Triassic-Jurassic outliers and Quaternary deposits. It is, however, debated which basement strata underlie the basin, with some suggesting it to be Carboniferous sandstones (e.g., Hirst et al., 2015), whilst others suggest meta-sedimentary Palaeozoic strata (Abdoh et al., 1990; Mikkelsen and Floodpage, 1997).

The moderate heat flow of 52 mWm^{-2} (Burley et al., 1980) combined with thick deposits of sandstone and high-quality hydraulic properties (up to 10 m/day hydraulic conductivities) (Allen et al., 1997) make the Cheshire Basin an area with significant potential for the development of deep hydrothermal resources. Recent corrections to bottom-hole temperatures indicate gradients may reach 27 °C/km (Busby, 2014); meaning the geothermal resource may be far greater than previously estimated. Thermal modelling also indicates that the highest temperature at the base of the Permo-Triassic is in the basin depocentre to the east of Crewe (Downing and Gray, 1986; Busby, 2011b).

Although there is a vast amount of data available for the Cheshire Basin, local conditions at depth to the Crewe area are uncertain, in terms of both the stratigraphy and the hydro-thermal parameters. Seismic data, outcrop studies and core plug analysis can help with correlation of stratigraphy in the subcrop and give good estimations of likely physical properties, including porosity, hydraulic conductivity etc.

CHAPTER 3 - NUMERICAL METHODS AND GOVERNING EQUATIONS

In this section the key governing equations and numerical methods are discussed, giving a rationale for the modelling technique used.

3.1 Introduction

Multiple analytical and numerical solutions can be found for the simulation of heat and fluid fluxes in the reservoir and wellbore of a geothermal system. Analytical solutions are usually simplified or constrained to 1D or 2D, focusing on either the wellbore or reservoir. For instance, in the commonly used doublet system, the time of thermal breakthrough in a hot sedimentary aquifer can be established using the well-known solution by Gringarten (1978), whilst pressure difference can also be identified (Muskat, 1946). In low-enthalpy single well systems, the change in head can be established by modelling fluid extraction using the Theis solution for fully penetrative wells (Theis, 1935) or the adapted Theis solution for partially penetrative wells (e.g., Sternberg 1973). All of these methods involve simplifications but can be useful for initial investigation and for the specific verification of numerical modelling results. Numerical models can retain the detail of the geothermal system but can be computationally demanding, particularly for 3D problems. Numerical models can also allow for a greater range of parameters to be incorporated into the simulation giving more realistic results.

For practical use, any model solution must be designed to be flexible (such that varying geological and engineering conditions can be modelled), simple to use and efficient on standard computers allowing the model to be used further after the PhD (e.g., by the industrial partner). The key components of a low-enthalpy geothermal model include fluid and heat flux, and to a lesser extent mechanical stresses and contaminant or solute transport. As the primary aim of this research is to simulate the extraction of hot, deep fluids from a single well without any enhancement

(fracturing) or injection of a fluid with varying salinity, the focus of the modelling is on simulating fluid and heat flux within the geothermal reservoir. The key governing equations and numerical methods for this approach are discussed in the chapter with justification and rationale provided for their use.

3.2 Key governing equations for heat and fluid fluxes in a geothermal system

Fluid flux is modelled in an aquifer or reservoir that is assumed to be fully saturated below the water table with pores filled with groundwater. Groundwater models are derived from two principles: conservation of mass, such that water is not destroyed or created, and Darcy's Law, where fluid flows from areas of high to low head (Anderson et al., 2015). Darcy's Law and the Darcy velocity (v) can be expressed as (e.g., Bear et al., 2010):

$$Q = K.A \, \frac{(h1-h2)}{L} \qquad\qquad 3.1$$

and

$$v = \frac{Q}{A} = -K\nabla h \qquad\qquad 3.2$$

where Q is the rate of fluid flux, K is hydraulic conductivity, L is the distance between two different piezometric heads (h) and A is the area. Assuming the fluid is a constant density and the rock is non-deformable (i.e., porosity is constant) the groundwater flow equation can be derived by substituting the Darcy velocity into the continuity equation (e.g., Rushton, 2003; Sachse et al., 2015):

$$\rho\frac{\partial\emptyset}{\partial t} + \rho\nabla(\emptyset V) = W \qquad\qquad 3.3$$

Dividing the continuity equation by the density (ρ) gives:

$$\frac{\partial\emptyset}{\partial t} + \nabla(\emptyset V) = \frac{W}{\rho} \qquad\qquad 3.4$$

where $\emptyset$ is the porosity, V is the average fluid velocity, W is a source or sink and t is time. To establish the governing equation for groundwater flux, a further assumption must be made; there is a linear relationship between porosity and pressure change. The time derivative can therefore be approximated using the storage coefficient (Ss) as $\frac{\partial \emptyset}{\partial t} = Ss\frac{\partial h}{\partial t}$ (Sachse et al., 2015). Substituting in the Darcy velocity where $\emptyset V = v = -K\nabla h$, the governing equation for groundwater flux in an isotropic, homogeneous aquifer is (Anderson et al., 2015):

$$K\nabla^2 h = Ss\frac{\partial h}{\partial t} - W \qquad\qquad 3.5$$

Hydrodynamic dispersion is not modelled as it is assumed that for the single well schemes modelled in this thesis that only the original fluid in the aquifer will be present and dispersion is most influential when two fluids with different solute concentrations come into contact (Todd and Mays, 2005).

Heat flux in low-enthalpy systems (temperatures <100 °C) will be transferred in two-phases; a saturated fluid component and the solid rock component. Both phases rely on different mechanisms to transfer heat; advective forces that transmit heat in the fluid and conduction in the solid and fluid phases. Heat flow (q) within a rock, where heat transfer is purely conductive, can be determined by the thermal conductivity (λ) and temperature gradient (∇T) (e.g. Rühaak et al., 2015):

$$q = -\lambda_s \nabla T_s \qquad\qquad 3.6$$

The energy balance of the solid phase (subscript s), using Fourier's Law can be described as (e.g. Nield and Bejan, 1992; Saeid et al., 2013):

$$(1 - \emptyset)\rho_s C_s \frac{\partial T_s}{\partial t} - [(1 - \emptyset)\nabla.(q)] = 0 \qquad\qquad 3.7$$

where $\emptyset$ is the porosity, ρ is the density, C is the specific heat capacity, T is the temperature and t is time. This can be simplified to:

$$\frac{\partial T}{\partial t} = \alpha_s \nabla^2 (T) \qquad\qquad 3.8$$

where the thermal diffusivity α is calculated by:

$$\alpha_s = \frac{\lambda_s}{\rho_s C_s} \qquad\qquad 3.9$$

Transient heat transfer in the fluid within the pore space (subscript f) can be modelled as both conductive and advective processes:

$$\emptyset \rho_f C_f \frac{\partial T_f}{\partial t} + \emptyset V \rho_f C_f \nabla . (T_f) - \emptyset \nabla . \lambda_f \nabla T_f = 0 \qquad\qquad 3.10$$

Assuming both solid and fluid components are in equilibrium ($T_f = T_s = T$), and that heat transfer in the conductive and advective phases occur instantaneously such that there is no heat transfer between phases, the combined continuity equation for heat transfer can be written as (Nield and Bejan, 1992):

$$\left((1-\emptyset)\rho_s C_s + \emptyset \rho_f C_f\right)\frac{\partial T}{\partial t} + v\rho_f C_f \nabla . T - \nabla . ((1-\emptyset)\lambda_s + \emptyset\lambda_f)\nabla T = 0 \qquad 3.11$$

3.3 Numerical methods for solving heat and fluid fluxes

Presently, the most commonly used numerical techniques for solving fluid and thermal fluxes in the literature include finite-difference, finite-element and finite-volume methods (Fig. 3.1). Finite-difference methods solve partial differential equations using an approximation of their derivatives on a discretised (usually rectangular) grid (Zhou, 1993). The finite-element method solves the same governing equations but is more flexible geometrically than the finite-difference method and allows the original structure of the physical domain (e.g., the reservoir) to be divided into individual

elements to produce a better fit to the true physical boundaries (Bofang, 2018). The finite-volume method is similar to the finite-difference method with the exception that it evaluates the thermal and fluid fluxes on the faces of discretised finite-volumes before solving the fluxes as a series of algebraic equations (Moukalled et al., 2016; Rapp, 2016). The finite-volume method also has the additional benefit that it can be solved on unstructured polygonal grids (e.g., Chow et al., 1996; Lipnikov et al., 2007). Typically, finite-element and finite-volume techniques use finite-difference approximations when discretising the time domain as other methods add unnecessary complexity (Griffiths, 1986). All three of the numerical methods listed above are currently used to evaluate geothermal systems in modern industrial computational programs. MODFLOW is based on the finite-difference method (and later the finite-volume) (Anderson et al., 2015), TOUGH 2 on the finite-volume method (O'Sullivan and O'Sullivan, 2016), whilst FEFLOW and COMSOL are based on the finite-element method (Zimmerman, 2006; Diersch, 2013; Dickinson et al., 2014).

Comparison of spatial discretisation of different numerical methods
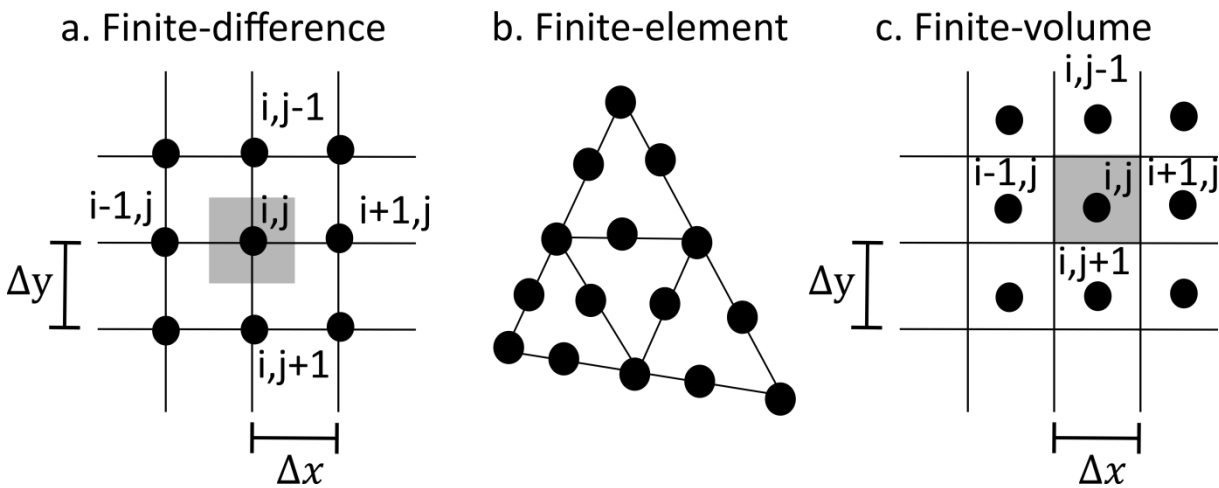
Figure 3.1: *Comparison between the spatial discretisation of different numerical methods (a) the finite-difference method, (b) the finite-element method and (c) the finite-volume method. Note that the mesh of the finite-element method does not have to be triangular.*

The model developed in this thesis uses the finite-difference method to approximate the temporal and spatial derivatives of fluid and thermal flux. The modelled scenarios have regular geological boundaries (e.g., planar aquifer) and do not need to incorporate more detailed reservoir architectures and/or irregular boundaries. This is because the models simulate borehole heat exchangers and standing column wells over time periods that typically only affect the subsurface in close proximity to the wellbore. Longer 'parameterisation' simulations are modelled which affect a larger spatial domain (e.g., chapter 5); however, these are designed to evaluate the impact of changing geological and engineering parameters, rather than variations in reservoir geometry. A novel approach is also undertaken to model the borehole as a series of 1D nodes (after Al-Khoury et al., 2005; Al-Khoury and Bonnier, 2006; Saeid et al., 2013), rather than complex finely shaped elements to meet the boundaries. As such, the finite-difference method was preferred as it has the added benefit of being able to produce complex models on high resolution grids without the need of a high performance computer (Anderson et al., 2015). In contrast, the finite-element method can be computationally expensive for large domains in comparison (Chapra and Canale, 2010, Pang et al., 2016). It has also been shown when using MATLAB the finite-difference method has similar errors and accuracy in comparison to the finite-element and finite-volume methods (Ng, 2011), with studies for heat flux suggesting the same (Mazumder, 2017).

3.4 The finite-difference method

The finite-difference method uses a series of nodes to represent the modelled space, where i,j,k are indices for the directions x,y,z respectively (Fig. 3.1a) (Anderson et al., 2015). The node represents the average modelled parameter (i.e., head or temperature) within the cell where the node is located (e.g., shaded area in figure 3.1a). The partial derivatives in the key governing equations can be replaced by approximates of the derivatives. The space or time domains can be divided into a series of discrete points which can then be solved numerically. The finite-difference

scheme is largely based on the Taylor series approximation of the spatial/temporal derivatives operating across neighbouring nodes (Causon and Mingham, 2010). The approximation contains a truncation error (i.e., a residual) and the magnitude of which reduces with decreasing time and space steps (Fletcher, 1988). When ignoring the truncation error, a first order derivative in space (x) can be approximated as a forward difference for temperature (T) (Wang and Anderson, 1982):

$$\frac{\partial T}{\partial x} \approx \frac{T_{i+1,j,k} - T_{i,j,k}}{\Delta x} \qquad 3.12$$

The backwards difference can be approximated as:

$$\frac{\partial T}{\partial x} \approx \frac{T_{i,j,k} - T_{i-1,j,k}}{\Delta x} \qquad 3.13$$

whilst the central difference approximation is:

$$\frac{\partial T}{\partial x} \approx \frac{T_{i+1,j,k} - T_{i-1,j,k}}{2\Delta x} \qquad 3.14$$

The second-order central difference can be approximated as:

$$\frac{\partial^2 T}{\partial x^2} \approx \frac{\frac{T_{i+1,j,k} - T_{i,j,k}}{\Delta x} - \frac{T_{i,j,k} - T_{i-1,j,k}}{\Delta x}}{\Delta x} \qquad 3.15$$

which can be simplified to:

$$\frac{\partial^2 T}{\partial x^2} \approx \frac{T_{i+1,j,k} - 2T_{i,j,k} + T_{i-1,j,k}}{\Delta x^2} \qquad 3.16$$

The first-order forward and backward differences can be used for time marching schemes; however, the central difference should not be used as it is unconditionally unstable (Remson et al., 1971). When using forward differences for temporal approximations, the variable at the next time step (T^{n+1}) is evaluated for known values of T and is referred to as the explicit finite-difference approximation (Wang and Anderson, 1982):

$$\frac{\partial T}{\partial t} \approx \frac{T^{n+1} - T}{\Delta t} \quad\quad 3.17$$

There is a strict stability criterion that has to be applied for transient solutions that are solved explicitly which is discussed in chapter 4.

In contrast to explicit approximations, implicit approximations evaluate all the variables of T at the next time step rather than known values of T (Wang and Anderson, 1982). A series of equations in the form of a matrix must be solved at each time step, which can increase the computational time, particularly for 3D problems (Chapra and Canale, 2010). When using the diffusion equation for a 1D example (assuming homogenous solid rock) the implicit solution can be written as:

$$\frac{T_i^{n+1} - T_i^n}{\Delta t} = \alpha_S \frac{T_{i+1jk}^{n+1} - 2T_i^{n+1} + T_{i-1jk}^{n+1}}{\Delta x^2} \quad\quad 3.18$$

when $S = \frac{\Delta t . \alpha_S}{\Delta x^2}$ the equation can be re-written as (e.g., Chapra and Canale, 2010):

$$T_i^n = -S.T_{i+1jk}^{n+1} + (1 + 2.S)\, T_i^{n+1} - S.T_{i-1jk}^{n+1} \quad\quad 3.19$$

which can then be written in matrix form. Assuming a 5 node system where T_1 and T_5 are constants equation 19 can be re-written in matrix form as (for nodes 2-4):

$$\begin{bmatrix} (1+2.S) & -1 & 0 \\ -1 & (1+2.S) & -1 \\ 0 & -1 & (1+2.S) \end{bmatrix} \begin{Bmatrix} T_2^{n+1} \\ T_3^{n+1} \\ T_4^{n+1} \end{Bmatrix} = \begin{Bmatrix} T_2^n \\ T_3^n \\ T_4^n \end{Bmatrix} \quad 3.20$$

The matrix is tridiagonal and the first square bracket represents the matrix of the coefficients. The second bracket represents the array of unknown temperatures whilst the final bracket represents the known variables. The matrix equation can then be solved using direct or iterative methods. A combination of explicit and implicit methods can be used to model the partial differential equations

with a higher temporal order of accuracy, with the Crank-Nicolson Method the most popular of these (Chapra and Canale, 2010).

3.5 Solution methods

Typically, the algebraic set of governing equations for a matrix in the form of $[A]\{x\} = \{b\}$ (e.g., eq. 3.20) can be solved using direct or iterative methods. Direct methods use matrix solvers to give an exact solution but are subject to round-off errors as computers can only store a finite number of digits. They also require large amounts of computer memory and are most suitable for small spatial domains or steady-state models (Anderson et al., 2015). Iterative methods use a general finite-difference approximation for all nodes (or cells) and solve them consecutively for the given problem (Wang and Anderson, 1982). They can be used effectively for large spatial domains due to their operational simplicity; however, they also result in round off errors due to iterations requiring a large number of calculations (Anderson et al., 2015). As a result iterative solvers, or iterative solvers combined with direct methods, are more suited to transient simulations for faster computational speed.

In this thesis, fluid flow and thermal fluxes in the aquifer and overburden will be modelled using explicit approximations, whilst the 1D wellbore is modelled using implicit methods solved for each time step using direct methods. This is due to the aquifer and confining beds being comprised of up to a few million nodes, whilst the wellbore is a series of 1D nodes generally reaching up to a few kilometres in length (e.g., for a 10 m nodal spacing for 2 km then 201 nodes would be required). To implicitly solve a computational domain containing a few million nodes using direct methods would take vast amounts of computational time and current industry software tends to only be able to model up to about 1 million nodes effectively (e.g., FEFLOW) (Anderson et al., 2015). In contrast, the small amounts of nodes in the wellbore lead to an implicit scheme being suitable (chapter 5). The implicit scheme also gives stability as a range of flow rates will be modelled. The implicit scheme can

be solved using the Thomas Algorithm or the Tridiagonal Matrix Algorithm (e.g., Chapra and Canale, 2010). This is effectively a Gaussian elimination for tridiagonal systems which can be solved by forward elimination and back substitution (Wen-mei, 2011). One of the benefits of using MATLAB is that a predefined function can be used to implicitly solve equations in the form of $[A]\{x\} = \{b\}$ (e.g., eq. 3.20) which allows for a relatively fast computational time for the 1D finite-difference equations (Ford, 2014).

The explicit solutions for the groundwater flow in the aquifer can be solved using a forward in time and central in space scheme (e.g., Causon and Mingham, 2010). When modelling the advective component of the governing equation for heat flux (eq. 3.11), an upwind scheme is used (e.g., Patankar, 1980). Explicit modelling allows for the temporal domain to be modified to have smaller time steps for time periods of interest or dramatic changes in the operational/performance functions (e.g., at the start of production when there is a rapid drawdown in the well). Implicit schemes using direct solvers are more limited in this respect in MATLAB as component 'A' (the matrix in eq. 3.20) can only be stored in the memory as fixed time steps and therefore, requires multiple matrices to be stored for different time steps, using more computer memory. When modelling the wellbore this is not an issue as the small amount of nodes modelled (in comparison to the reservoir) will only require a relatively small matrix.

Summary

The key governing equations for groundwater flow and heat transport in the aquifer have been outlined. Numerical methods have also been reviewed and the finite-difference method was chosen to develop the model with. Although the finite-volume and finite-element methods can aid in spatial discretisation, the models in this thesis use simple geometrical boundaries. In addition, the software used (MATLAB) has built-in functions to enhance computational speed and accuracy when using the finite-difference method.

When using numerical methods it is important to validate the models and test their accuracy. This can be done by comparing numerical results to analytical solutions and checking the code against real case studies (Anderson et al., 2015). In chapter 4 an extensive verification study is undertaken on the model, simulating against analytical and case studies.

CHAPTER 4 - MODELLING GEOTHERMAL SINGLE WELLS: INSIGHTS FROM THE GEOTHERMAL WELLS IN SOUTHAMPTON, UK

This chapter outlines the numerical model utilised in the thesis, verifying the model against analytical solutions and case studies. Standing column wells and coaxial borehole heat exchangers were then modelled for the Southampton Marchwood Well case study.

4.1 Introduction

The most recent focus of numerical modelling techniques for simulating deep geothermal systems has been on developing 'doublet' well models using the finite-element (e.g., Blöcher et al., 2010; Saeid et al., 2013, 2015; Major et al., 2018), finite-difference (e.g., Mottaghy et al. 2011) or finite-volume techniques (e.g., Le Brun et al., 2011), with little attention paid to modelling the potential of lower cost deep single well schemes. For low-enthalpy systems, a doublet scheme may be considered efficient for yielding high flow rates from the aquifer, however, such schemes have a high initial capital expenditure. For this reason, a single well scheme (where fluid is only extracted out of the reservoir without replenishment (Fig. 4.1a)) may be a viable option in the UK where the potential investment risk is high. Most single well schemes will have the problem of disposing of the extracted brines at surface level, which for the case study of the Southampton scheme was solved by disposal to the sea. This is a fortunate and unique situation as it allowed for a cost-efficient and simple disposal scenario to be adopted. Such measures are not suitable for the rest of the UK's 'inland' Mesozoic basins and the disposal of brine needs to be considered carefully if single well schemes are to become feasible across the UK.

An alternative method of dealing with the produced brine is considered in this study. Closed and open loop borehole heat exchangers (Fig. 4.1b) where fluid is circulated in the well are investigated, with modelled production data compared to the Marchwood Well, Southampton. In

this study, closed borehole heat exchangers (BHEs) with central coaxial pipes will be referred to as coaxial BHEs (Diersch et al. 2011a,b), whilst BHEs with an open base, interacting with groundwater will be referred to as standing column wells (SCWs). Coaxial BHEs allow the fluid to be re-circulated within the wellbore, therefore removing the issue of brine waste water disposal above ground. For SCWs, in peak periods where more energy and thus higher production temperatures are required, hot water in the aquifer can be drawn into the well and discharged elsewhere. This concept is called bleed flow (Rees et al., 2004; Pasquier et al., 2016). Although the production temperature is likely to be less than standard single well schemes, the associated waste water disposal costs of single well schemes are removed. Recent studies on deep BHEs and SCWs in the UK suggest they provide a cost benefit to doublet schemes as they allow minimal costly exploratory work and can operate in poor geological scenarios (e.g., low hydraulic conductivities (Law et al., 2015)). As such, deep SCWs and coaxial BHEs may be used in areas where energy demand dictates the placement of wells, rather than the geology. Currently, few deep geothermal wells utilise the SCW configuration, with only few modelling (Law et al., 2015) and exploratory studies (Cho et al., 2016) undertaken on their operation and feasibility. Although there has been more attention to closed loop deep BHEs in the past few years (Fang et al., 2018; Liu et al., 2019), few numerical studies have investigated the concept of a deep SCW with the potential to be open at depth. However, many shallow-to-medium depth closed loop BHE studies (<500 m) have been undertaken (e.g., Nguyen et al., 2015) and recent work by Westaway (2018) focusing on deep closed loop BHEs, highlighted the need for a validated model that is based on physical assumptions designed to match BHEs against the heat load. The work of Westaway (2018) presents a useful analytical solution; however, it fails to incorporate the more complex thermal changes present in the working fluid within the central pipe and annulus. In contrast, the model used here investigates the thermal response of all the components of the model and can use a predefined heat load or thermal power output.
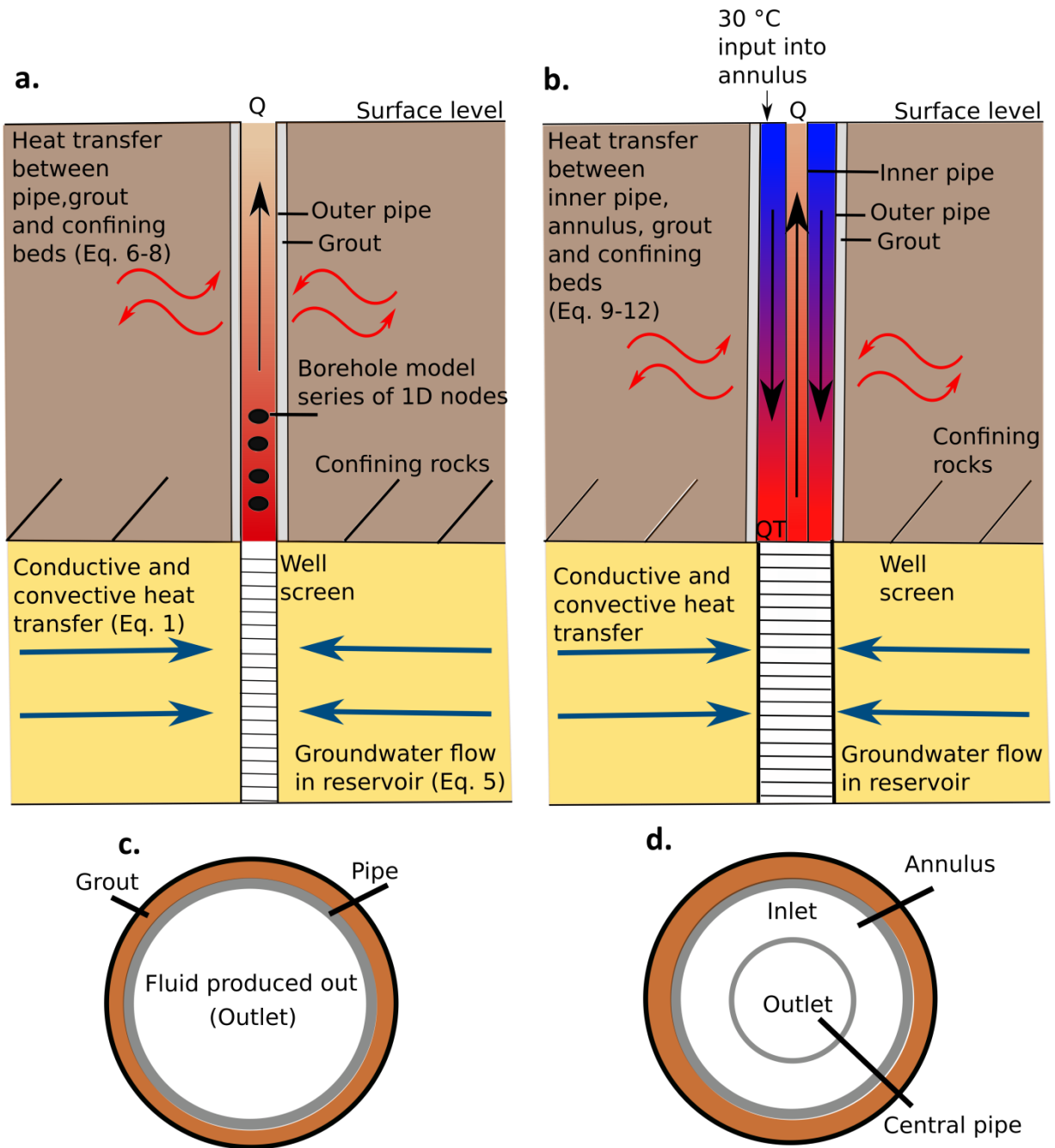
Figure 4.1: *(a) Schematic of a normal configuration deep single well, (b) schematic of an open standing column well, (c) cross section example of standard single well configuration in comparison to (d) standing column well.*

In this study, a single well geothermal model was designed and simulated using MATLAB software (produced by Mathworks), based on the finite-difference method to simulate advective and conductive heat transfer. The model was discretised using an orthogonal 3D mesh and explicit

approximations of derivatives (Fig. 4.2). Although the reservoir and surrounding confining beds were modelled in 3D, the wellbore was simulated in 1D. The thermal wellbore model was modified for the finite-difference method and coaxial BHE/SCW application from that of Al-Khoury et al. (2005), Al-Khoury and Bonnier (2006), Al-Khoury (2011) and Saied et al. (2013). Tests against analytical solutions and case studies of the Southampton wells were conducted to validate the model as these were the only examples of a single well deep geothermal scheme targeting a hot sedimentary aquifer (HSA) in the UK. The model was then used to assess the potential of geothermal extraction in the Wessex Basin. Previous models of the Marchwood Well have focused on a multi-layered analytical solution (Barker, 1981), without matching production data exactly (Price and Allen, 1982). Here, both Southampton wells were modelled numerically in 3D (Marchwood and Western Esplanade – page 92/93), and incorporated thermal and hydraulic interactions in the wellbore and reservoir. Further validation was undertaken by matching modelling results for the coaxial BHE example against real inlet and outlet data from China (Wang et al., 2017). This was chosen as a case study as no data for deep coaxial BHE is currently publicly available in the UK.

4.2 Method of numerical modelling

Heat within a geothermal system can be transferred through conduction in the solid phase of the system and by convection or diffusion through the fluid phase. Initially, the conductive transfer of heat can be useful for modelling a geothermal system as it helps identify potential regional thermal barriers (Cacace et al., 2010). The coupling of heat transfer through advection and conduction can help predict thermal changes in a reservoir, the lifetime of a well and the recharge of a system. The system was considered to only include single phase fluid flow within a fully saturated reservoir. All the symbols used in the governing equations are listed in Table 4.1.

Symbol	Parameter	Units
t	Time	seconds
λ	Thermal conductivity	W/m/°C
T	Temperature	°C
q	Heat flow	$W \cdot m^{-2}$
C	Specific heat capacity	J/kg °C
ρ	Density	kg /m^3
$\emptyset$	Porosity	%
α	Thermal diffusivity	m^2/s
R_d	Retardation factor	-
K	Hydraulic conductivity	m/s
v	Darcy velocity	m^3/s
Ss	Storage coefficient	-
h	Hydraulic head	m
Pr	Penetration ratio	-
PC	Pricketts penetration constant for additional drawdown	-
A	Area	m
u	Fluid velocity in the pipe	m/s
b_{pg}	Reciprocal of thermal resistance between pipe and grout	W/m^2 °C
Q	Production rate	m^3/s
W	Source or sink	m/s
rw	Radius of the well in the reservoir (screened interval)	m
re	Extrapolated radius	m
Subscripts		
b	Bulk	-
s	Solid phase	-
f	Fluid phase	-
p	Pipe	-
g	Grout	-
$prod$	Production temperature	-
rej	Rejection temperature	-
i	Inlet pipe	-
o	Outlet pipe	-

Table 4.1: *List of parameters used in the numerical model for deep geothermal wells.*

A 3-D orthogonal mesh, which can either be uniform or non-uniform, was used. The finite-difference method is defined with a Cartesian coordinate system, with (x,y) representing horizontal limits and (z) the vertical limits or depth (Fig. 4.2). The lateral extent (boundary) of the model was set to extend as wide as possible so that the boundary conditions of the model were inconsequential to

the modelling of the well itself (which was placed in the centre of the 3D computational grid). The governing equations used in the model incorporate both fluid and thermal changes within the reservoir and are commonly used in shallow (e.g., Nabi and Al-Khoury, 2012a, 2012b) and deep geothermal modelling (e.g., Saeid et al., 2013, 2015; Poulsen et al., 2015).
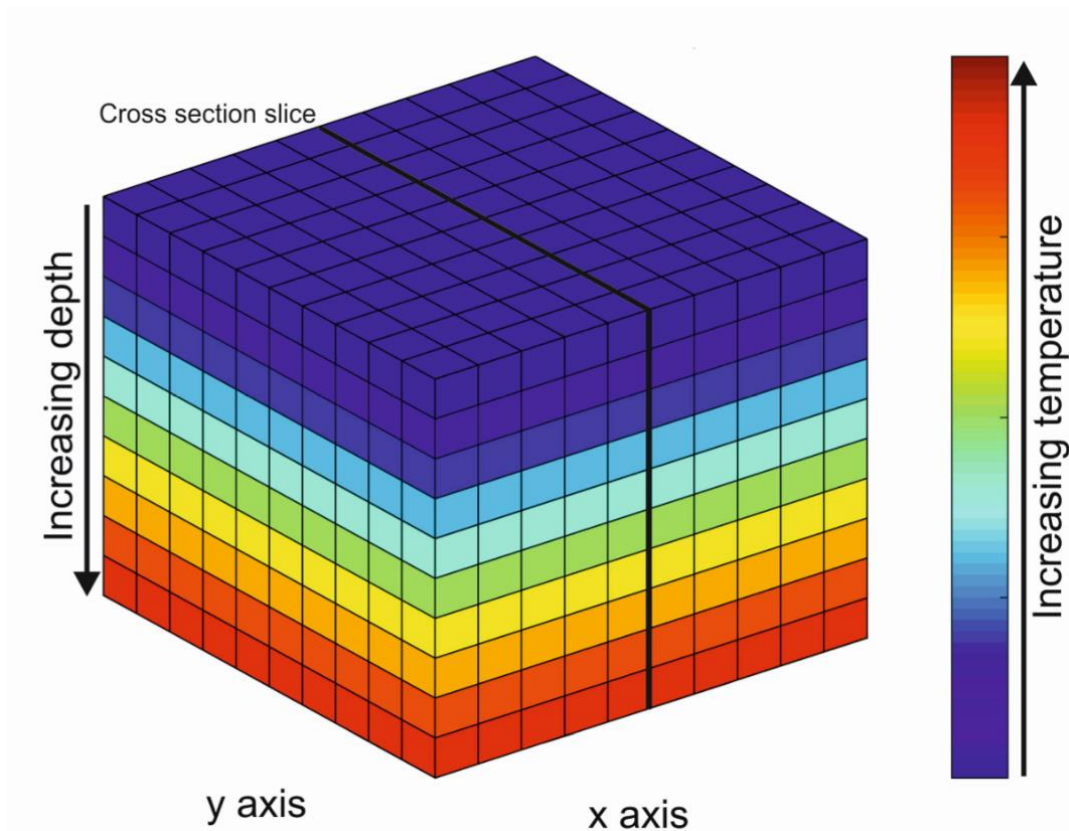
Figure 4.2: *Example 3D Cartesian grid with uniform nodal spacing.*

4.2.1 Governing equations for modelling reservoir interactions

The solid and fluid components in a reservoir can be modelled to give the advection-diffusion equation (e.g., Saeid et al., 2013):

$$\frac{\partial T}{\partial t} = -R_d . \, \mathrm{v}. \nabla \mathrm{T} + \alpha_b \nabla^2 \mathrm{T} + Q_T \qquad\qquad 4.1$$

where T is the temperature, t is time, Q_T is the source input term for SCWs, v is the Darcy velocity and R_d represents the thermal retardation factor, which signifies the change of temperature based

on the specific heat capacity (C) for both the fluid and solid phases of the system (subscript f and s respectively) (e.g., Molina-Giraldo et al., 2011).

$$R_d = \frac{\rho_f C_f}{(1-\emptyset)\rho_s C_s + \emptyset \rho_f C_f} \qquad\qquad 4.2$$

The bulk thermal diffusivity (α_b) is the sum of the solid and fluid phases (e.g., Saeid et al., 2013):

$$\alpha_b = \frac{\lambda_b}{\rho_b C_b} = \frac{(1-\emptyset)\lambda_s + \emptyset\lambda_f}{(1-\emptyset)\rho_s C_s + \emptyset \rho_f C_f} \qquad\qquad 4.3$$

where ρ is density, $\emptyset$ is porosity and λ is the thermal conductivity. The Darcy velocity is equal to:

$$v = -K(\nabla h) \qquad\qquad 4.4$$

where K is the hydraulic conductivity.

The fluid flow in the system is a function of hydraulic head and Darcy velocity, which can be modelled in the system by the continuity equation (Guo and Langevin, 2002; Anderson et al., 2015):

$$Ss\frac{\partial (h)}{\partial t} + \nabla \cdot (v) = W \qquad\qquad 4.5$$

where Ss is storativity, h is hydraulic head and W is a sink (i.e., the amount of fluid extracted).

4.2.2 Governing equations for modelling thermal borehole interactions

The boreholes were modelled to account for thermal interactions between the wellbore and the surrounding rock. The model proposed by Al-Khoury et al. (2005) and Al-Khoury and Bonnier (2006) was used, which consists of a series of 1D nodes designed to simulate heat flow in a borehole. It incorporates the outer solid rock, grout material, the pipe and the geothermal fluid in a closed loop system and has been widely used and verified for shallow systems (e.g., Al-Khoury et al., 2010; Diersch et al., 2011a, 2011b; Nabi and Al-Khoury, 2012b; Haslam, 2013). However, few studies utilised it in a deep geothermal setting, particularly for SCWs. The 1D borehole model has been

developed further to focus on heat flow in deep, low-enthalpy, open systems by Saeid et al. (2013, 2015). The model includes the heat exchange between the grout and the solid rock for the 1D wellbore and was adopted for use in this study (Figs. 4.1a, 4.1c & 4.3). However, it is worth noting the model can be simplified further when there is no interest in recording thermal changes within the grout (Saeid et al., 2015).
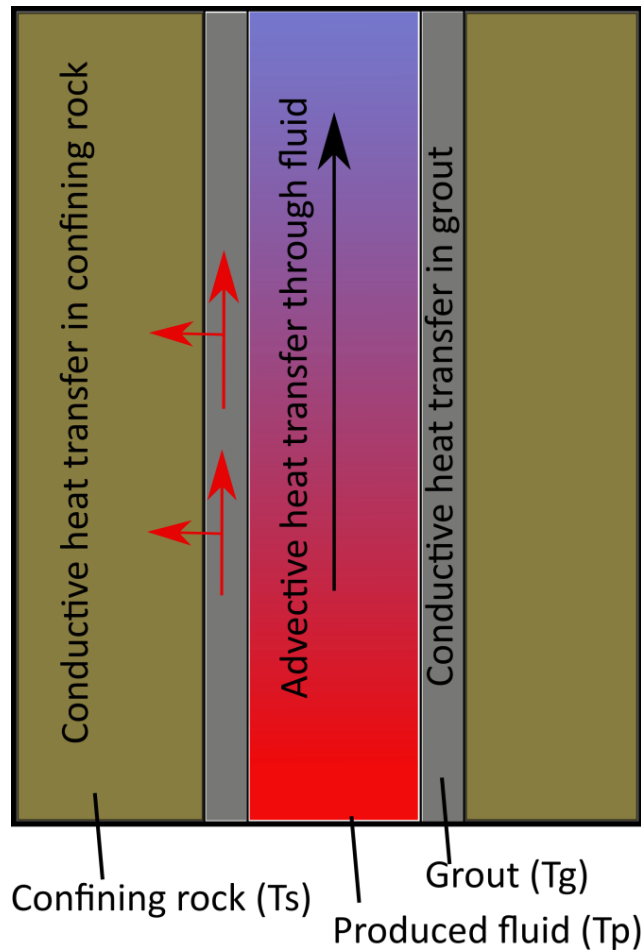
Figure 4.3: *Heat fluxes between the different components in governing equations 4.6-4.8.*

The governing equations for the heat flux in the wellbore (including the grout material) are (Fig. 4.3):

$$\rho_f C_f \frac{\partial T_p}{\partial t} A_p - \lambda_f \frac{\partial^2 T_p}{\partial z^2} A_p + \rho_f C_f u_p \frac{\partial T_p}{\partial z} A_p = b_{pg}(T_g - T_p)2\pi r_p \qquad 4.6$$

$$\rho_g C_g \frac{\partial T_g}{\partial t} A_g - \lambda_g \frac{\partial^2 T_g}{\partial z^2} A_g = b_{pg}(T_p - T_g)2\pi r_p + b_{sg}(T_s - T_g)2\pi r_g \qquad 4.7$$

$$\rho_s C_s \frac{\partial T_s}{\partial t} A_s - \lambda_s \frac{\partial^2 T_s}{\partial z^2} A_s = b_{sg}(T_g - T_s)2\pi r_g \qquad 4.8$$

The subscript p is representative of the respective property of the piping, subscript g is for the grout, subscript s for the solid rock mass, T_p is the temperature of the pipe, λ_f is the thermal conductivity of the fluid, b_{pg} is the reciprocal of thermal resistance between the wellbore pipe and grout, b_{sg} is the reciprocal of the contact thermal resistance between the grout and rock, A_g is the area of the grout etc, whilst other symbolic notations are as described in the reservoir formulation (e.g., used in equations 4.1-4.3). When investigating the thermal interactions in a coaxial BHE or SCW with a central co-axial pipe, equations 4.6-4.8 are modified to include the heat exchange between the central pipe and annulus (Figs. 4.1b & 4.1d) (Al-Khoury, 2011):

$$\rho_f C_f \frac{\partial T_{po}}{\partial t} A_{po} - \lambda_f \frac{\partial^2 T_{po}}{\partial z^2} A_{po} - \rho_f C_f u_{po} \frac{\partial T_{po}}{\partial z} A_{po} = b_{poi}(T_{pi} - T_{po})2\pi r_{po} \qquad 4.9$$

$$\rho_f C_f \frac{\partial T_{pi}}{\partial t} A_{pi} - \lambda_f \frac{\partial^2 T_{pi}}{\partial z^2} A_{pi} + \rho_f C_f u_{pi} \frac{\partial T_{pi}}{\partial z} A_{pi} = b_{poi}(T_{po} - T_{pi})2\pi r_{po} + b_{pig}(T_g - T_{pi})2\pi r_{pi}$$

$$4.10$$

$$\rho_g C_g \frac{\partial T_g}{\partial t} A_g - \lambda_g \frac{\partial^2 T_g}{\partial z^2} A_g = b_{pg}(T_{pi} - T_g)2\pi r_{pi} + b_{sg}(T_s - T_g)2\pi r_g \qquad 4.11$$

$$\rho_s C_s \frac{\partial T_s}{\partial t} A_s - \lambda_s \frac{\partial^2 T_s}{\partial z^2} A_s = b_{sg}(T_g - T_s)2\pi r_g \qquad 4.12$$

where the subscript o is for the outlet pipe (central pipe) and i is the surrounding annulus. For SCWs, the wellbore configuration is considered identical to that of the coaxial BHE, however, is assumed to have a liner penetrating the HSA (Fig. 4.1b).

The heat transfer coefficients for the thermal wellbore models can be described using an analogy to electrical circuits (as described by Al-Khoury et al. (2005), Al-Khoury and Bonnier (2006), Al-Khoury (2011) and Saied et al. (2013)).

For the standard configuration borehole (Eq. 4.6-4.8) the thermal resistance between the central producing pipe and surrounding grout is made up of the advective flux of the fluid and the conductive flux of the pipe material (Fig. 4.4a):

$$b_{pg} = \frac{1}{R_{pg}} \qquad\qquad 4.13$$

where R_{pg} is calculated as:

$$R_{pg} = R_{convection} + R_{pipe\ material} = \frac{1}{r_o/r_i \bar{h}} + \frac{r_o \ln(r_o/r_i)}{\lambda_p} \qquad\qquad 4.14$$

where $\bar{h} = Nu\ \lambda_f/D$ and D is the inner diameter of the producing wellbore pipe. Nu is the Nusselt number which can be calculated using the Dittus Boelter correlation (e.g., Saeid et al., 2013). The thermal resistance between the grout and surrounding solid is made up of only conductive heat transfer:

$$b_{gs} = \frac{1}{R_{gs}} \qquad\qquad 4.15$$

where R_{gs} is calculated as:

$$R_{gs} = R_{grout\ material} = \frac{r_g \ln(r_g/r_o)}{\lambda_g} \qquad\qquad 4.16$$

The formulation of thermal resistance in the SCW / coaxial BHE is similar to that of the single extraction only well, however, the transfer of heat between the central pipe and annulus involves advective heat transfer from both central pipe and annulus, and conductive heat transfer through the pipe (Diersch, 2011a) (Fig. 4.4b).

$$R_{pipo} = R_{poconvection} + R_{pipe\ material} + R_{piconvection} \qquad\qquad 4.17$$

a. Thermal resistance of standard configuration borehole

b. Thermal resistance of SCW configuration borehole
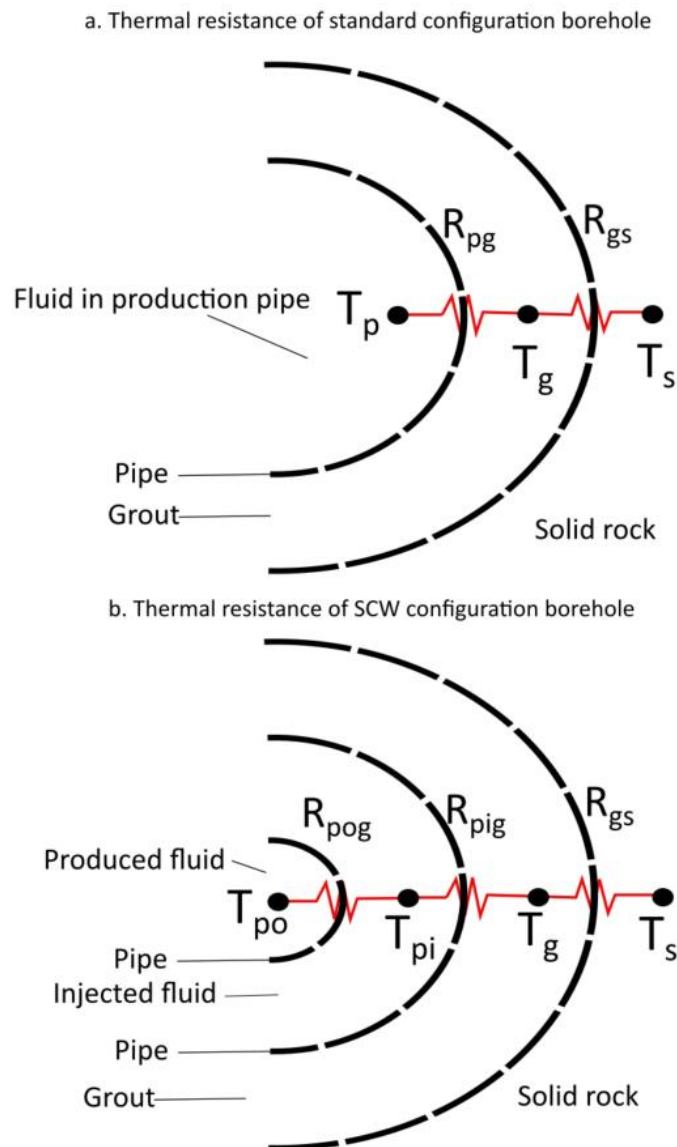
Figure 4.4: *Cross sectional areas of boreholes showing (a) thermal resistance of standard configuration deep single well and (b) thermal resistance of an SCW well (Al-Khoury, 2011).*

4.2.3 Governing equations for modelling head in the borehole

The method for calculating head in the wellbore in this model is commonly used in groundwater finite-difference models (e.g., Halford and Hansen, 2002; Konikow et al., 2009), and similarly to calculate pressure in the wellbore (e.g., Peaceman, 1978; Dogru, 2010). Neglecting

wellbore storage, the change in head due to fluid extraction (Eq. 4.5) can be modelled as $W = \frac{Q}{\Delta x.\Delta y}$, where Q is the volume of fluid produced and Δx or Δy are the nodal spacing around the source points (Trescott et al., 1976). The source function (W) allows an estimate of head to be solved within the reservoir. The head in a fully penetrative wellbore can then be modelled using the Thiem equation (Thiem, 1906; Prickett and Lonnquist, 1971; Akbar et al. 1974; Anderson and Woessner, 1992; Chen and Zhang 2009):

$$h_w = h - \frac{Q}{2\pi Kb} \ln\left(\frac{r_e}{r_w}\right)$$ 4.18

where h_w is the well head, r_w is the wellbore radius and r_e is the effective nodal radius equivalent to the head in the reservoir which is equal to that in the well (Konikow et al., 2009). The effective radius is calculated using the equation $r_e = \frac{r_1}{4.81}$ where r_1 is the mesh spacing ($\Delta x = \Delta y$) (Prickett, 1967). This method provides a higher level of accuracy for finer mesh sizes in the reservoir, with a closer fit to the analytical solution (Afshari et al., 2003).

Additional drawdown in partially penetrative wells, caused by the well extracting fluid from a smaller area, can be calculated (subtracted from Eq. 4.18) (Kozeny, 1933; Prickett, 1967):

$$\frac{\Delta h_{pp}}{\Delta h_{th}} = PC = \frac{1}{Pr\left[1 + 7\sqrt{\frac{r_w}{2bPr}}\cos\left(\frac{\pi Pr}{2}\right)\right]} - 1$$ 4.19

where Δh_{pp} is the change in head due to partial penetration (where the wellbore is only in contact with a predefined thickness of the aquifer), PC is an additional penetration constant, Δh_{th} is the change in head in the wellbore calculated from the Thiem equation and Pr is the penetration ratio, calculated as the length of the well screen divided by the thickness of the aquifer. When calculating wellbore head for partially penetrative systems, the average head at nodal source points in the reservoir along the well screen are used to calculate the wellbore head.

4.2.4 Energy output from a geothermal well

It is important to consider both the total energy in a system and the energy that can be produced in a system prior to the geothermal resource reaching its economic cut off point. Currently, most authors calculate the geothermal resource basin-wide prior to modelling (e.g., Muffler and Cataldi, 1978; Allen et al., 1985; Downing and Gray, 1986b; Campbell et al., 2016a, 2016b). Whereas numerical models allow the calculation of the total energy produced from a single well in a system (modified from Crooijmans et al., 2016):

$$E_{prod} = \sum_{t=1}^{n} Q.\Delta t.c_f\rho_f.(T_{prod} - T_{rej}) \qquad\qquad 4.20$$

where E_{prod} is the total amount of energy produced per time increment of production, Δt is the change in time, n is the number of time steps, Q is the production rate and T_{prod} and T_{rej} are the production and rejection temperatures, respectively. The rejection temperature is the point that the fluid is no longer viable in a district heating scheme, which can be as low as 30 °C (Downing and Gray, 1986b).

The total energy in the system can also be estimated (Crooijmans et al., 2016):

$$E_{total} = \sum_{t=1}^{m} L^3.\emptyset.c_f\rho_f.\left(T_i - T_{rej}\right) + L^3.(1-\emptyset).c_s.\rho_s.\left(T_i - T_{rej}\right) \quad 4.21$$

where E_{total} is the total energy in the system, L is the distance between each node, T_i is the initial temperature and m is the number of nodes. By calculating the total energy in a system it can allow us to identify the recovery factor for the resource and determine whether the prospect will be economic or not.

4.2.5 Boundary and initial conditions

The effects of lateral boundaries were designed to be insignificant by increasing the horizontal spatial domain of the model for any given problem (Poulsen et al., 2015), however, were assigned constant temperatures/heads. This was checked to ensure they had no influence on model outputs.

The confining beds were considered as 'no flow' boundary conditions (i.e., fluid cannot pass through the impermeable seal) (e.g., Anderson et al., 2015). The base of the model was assigned a constant temperature boundary condition, whilst the surface level was initially assigned a fixed surface temperature with the heat flux set to zero. The temperature input to the base of the production well was the averaged well screen temperature.

Initially, the temperature at time (t=0) at any node of the model was considered to be in a steady state condition (Saeid, 2015):

$$T(x, y, z, 0) = T(x, y, z) \qquad\qquad 4.22$$

The temperatures of the borehole components were assumed to be in equilibrium with the system at initialisation, where at time (t) = 0:

$$T_s = T_g = T_p \qquad\qquad 4.23$$

By substituting Darcy velocity into the continuity equation for head (Eq. 4.5), the initial head conditions can be expressed as:

$$\nabla^2 h = 0 \qquad\qquad 4.24$$

The initial aquifer temperature was established by taking a linear gradient and set using the equation (e.g., Saeid et al., 2013):

$$T_{(z)} = T_{(0)} + \Delta T . z \qquad\qquad 4.25$$

where $T_{(0)}$ is the initial surface temperature, typically set at $10 - 12$°C (BGS, 2011).

4.2.6 Discretisation, grid convergence and stability

The partial differential equations (Eq. 4.1, 4.5, 4.6-4.12) were solved using the finite-difference method using an orthogonal grid mesh to define each node point (e.g., Smith, 1985;

LeVeque, 2007). The orthogonal grid has fixed Cartesian coordinates (i,j,k relating to x,y,z in space) and the approximations can be solved for both uniform and non-uniform grids using forward differences in time and central differences in space (FTCS). Boundary conditions, however, employ forward and backward differences where appropriate to the nature of the boundary. The explicit method of solution relies on the standard stability criteria for the diffusive component (β) (e.g., Patankar, 1980):

$$\beta = \frac{\alpha_b \Delta t}{\Delta x^2} \leq \frac{1}{6}$$
4.26

and the advective component for the Courant Friedrich Lewy (CFL) condition (Courant et al., 1928):

$$CFL = \frac{|R_d.v|\Delta t}{\Delta x} \leq 1$$
4.27

where the parameters are: α_b is the bulk diffusivity, t is the temperature, ∇x is the nodal spacing, R_d is the thermal retardation factor and v is the Darcy velocity. The ratio between advection and diffusion can be calculated as the Peclet number (Pe) (e.g., El-Kadi et al., 1993; Bijeljic et al., 2004):

$$Pe = \frac{R_d.\text{v}.\Delta x}{\alpha_b} = \frac{CFL}{\beta}$$
4.28

The Peclet number is stable for 3-dimensional problems such that the stability criteria can be written as (Dehghan, 2004):

$$CFL^2 \leq \beta \leq \frac{1}{6}$$
4.29

or

$$6CFL \leq Pe \leq \frac{1}{CFL}$$
4.30

It can be seen (Table 4.2) that the diffusion stability component can remain stable for a large range of mesh sizes and for time steps greater than a day. The advective component is, however, more prone to causing oscillatory behaviour and if the stability criteria is not met the solution will not

converge. Stability in a solution is achieved when the criteria is met, thus reducing errors, otherwise these errors are amplified and may not grow, but oscillate instead (Chapra and Canale, 2010). As a result, the stability criterion controls the time step and nodal spacing in the model (Table 4.2). For both the Southampton (Marchwood and Western Esplanade) examples, Peclet numbers throughout the simulation were always within the stability criteria (Eq. 4.30). The nodal spacing around the well screen and wellbore was also set to 1 m. It is also worth noting that the equivalent diffusive stability criterion (Eq. 4.26) is applicable for fluid flow (Eq. 4.5).

Nodal Spacing variations (m)	Marchwood			Western Esplanade		
	Diffusive	CFL	Peclet	Diffusive	CFL	Peclet
1	1.28E-05	2.75E-06	2.14	1.21E-06	1.94E-06	1.6
2	3.22E-07	1.37E-06	4.27	3.03E-07	9.69E-07	3.2
4	8.04E-08	6.87E-07	8.54	7.57E-08	4.85E-07	6.4
8	2.01E-08	3.44E-07	17.09	1.89E-08	2.42E-07	12.8
16	5.03E-09	1.72E-07	34.18	4.73E-09	1.21E-07	25.6
Time step variations						
	Diffusive	CFL	Peclet	Diffusive	CFL	Peclet
1 second	1.29E-06	2.75E-06	2.14	1.21E-06	1.94E-06	1.6
1 minute	7.72E-05	1.65E-04	2.14	7.27E-05	1.16E-04	1.6
1 hour	0.0046	0.009	2.14	0.0044	0.007	1.6
1 day	0.1112	0.24	2.14	0.1047	0.17	1.6

Table 4.2: *Stability parameters compared under different time steps and nodal spacing. Diffusive stability parameter, Courant Friedrich Levy (CFL) number and Peclet number for a range of mesh sizes and time step variations for both Southampton scenarios, Marchwood and Western Esplanade. Stability parameters were calculated for heat flow in the* advective *-diffusive equation.*

4.2.7 Implementation of the finite-difference model in a computational environment

The finite-difference model was programmed using MATLAB software (R2016a) and the systematic sequential solution is simplified as a flow chart in figure 4.5. MATLAB was selected for this investigation as it provides high-level programming functions and high-quality 3D images of the system at various time steps, whilst also providing various other data visualisations. Although

MATLAB is slower than other programming languages (such as C++) it is easier for program development and adaptation.

The model is initialised with hydraulic- and thermal- parameters defined within the model and a static set-up is undertaken. The static set-up establishes initial conditions and is set up to meet equations 4.22-4.25. The iterative solution consists of four main processes:

1.) Solving fluid flow at the points of the wellbore extraction.

2.) Solving fluid flow in the reservoir.

3.) Solving the thermal interaction between the wellbore and confining beds.

4.) Solving thermal interaction in the reservoir.
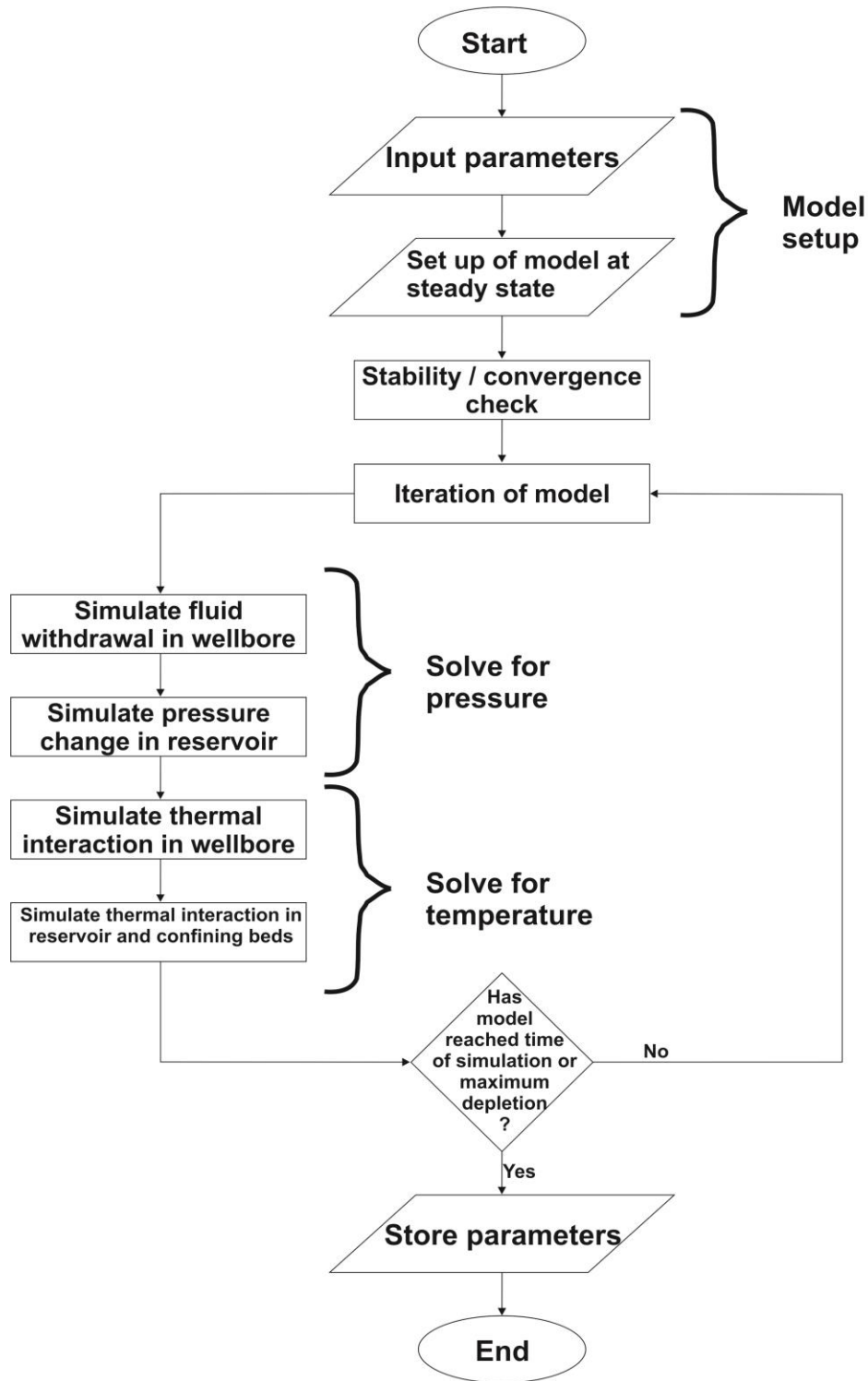
Figure 4.5: *Flow diagram of a model run for the finite-difference based single wellbore simulation.*

The data (e.g., drawdown in the well, production temperature, 3D plots of the mesh at specific pre-determined time intervals etc.) is then stored and can be displayed in a format as

determined by the user. The final saved model files can vary in size depending on the amount of variables stored (and the frequency of storage). In this study, the file size ranged from a few MBs to 40 MBs. The speed of the code is determined by the nodal quantity and the size of the time step. On an Intel Core i5-4590 3.3 GHz PC, the CPU time when modelling heat and fluid fluxes in the reservoir for an area of 224 m by 224 m by 64 m, took 21,278 seconds to run for a simulation period of 2 year (mesh analysis case study). This was for an hourly time step and a nodal spacing of 1 m (i.e., 3,290,625 nodes). If the nodal spacing is increased to 16 m (i.e., 1,125 nodes), the same simulation took 14 seconds (Table 4.3 and Fig. 4.6). The simulation time is therefore proportional to the amount of nodes used. For a typical simulation of the lifetime of a geothermal system (25 years), computational times can be kept below 2 hours.
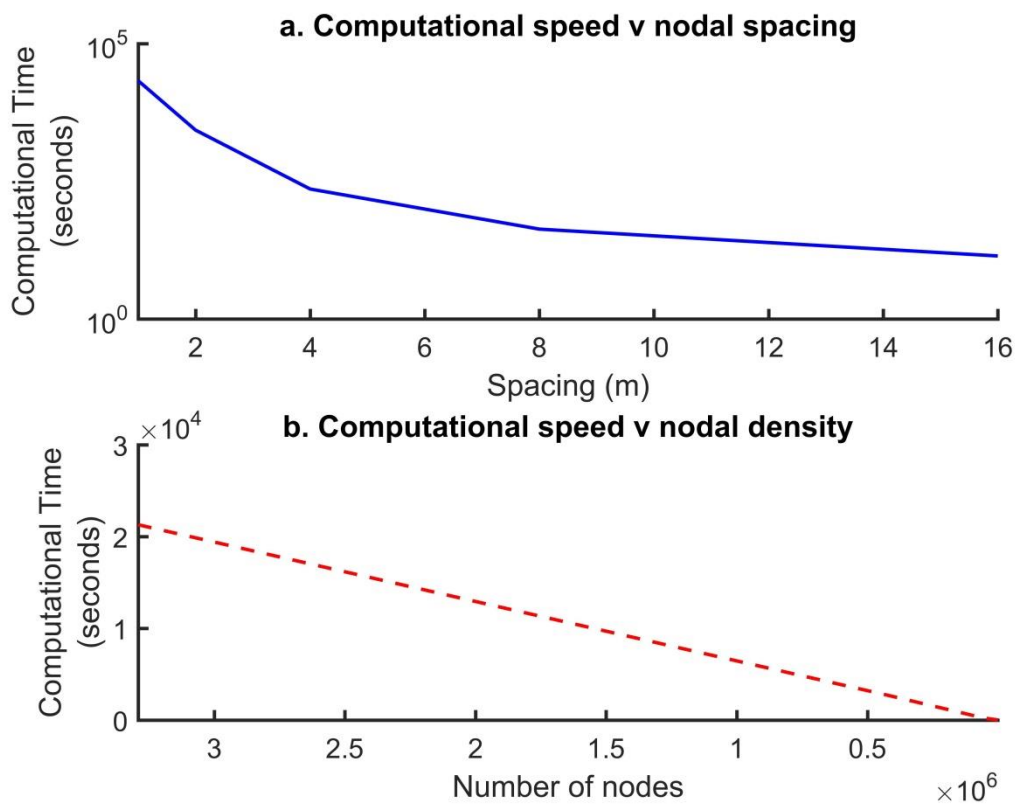
Figure 4.6: *Computational time plotted against (a) nodal spacing and (b) number of nodes.*

Nodal Spacing (m)	Simulation time (seconds)
1	21278
2	2701
4	230
8	43
16	14

Table 4.3: *Table of simulation time and nodal spacing. The simulation time increases when a greater quantity of nodes is used by refining the size of the finite-difference mesh. The simulation uses the same parameters and set up as for the reservoir in the mesh analysis study.*

4.2.8 Utilising non-uniform grid meshes

In areas of high pressure/ temperature contrast (e.g., around the borehole), the mesh must be fine enough to reduce error and retain stability. However, to produce an explicit model across a fine, uniform mesh with a spatial domain of a few kilometres will be computationally intensive. To solve this, the mesh can be discretised to coarsen away from the borehole using discretisation approximations after Turkel (1986), Sanmiguel-Rojas et al. (2005), and Kajishima and Taira (2017). It is likely that by increasing the mesh sizes with distance from thermal and hydraulic contrasts, any errors can remain low even with larger nodal spacing. Using the Marchwood case study as an example (Sect. 4.1), a non-uniform grid (Figs. 4.7 and 4.8) had little impact on the results in comparison to the uniform grid (1 m spacing (e.g., Fig 4.2)). In figure 4.7, there is near identical fit between the uniform and non-uniform meshes for both temporal change in head within the wellbore (Fig. 4.7a) and spatial changes of head within the reservoir (Fig. 4.7b). The mesh sizes outlined in figure 4.7b show for the same nodal quantities you can have a far greater spatial domain (150 m radially away from wellbore for uniform and 2370 m for non-uniform). Errors can be minimised further by having small expansion factors discretising away from the wellbore at a rate of 1.2-1.5 (Barrash and Dougherty, 1997). The graduation can be user definable, however, in this thesis the mesh was always set to expand by 1.2, unless otherwise stated. The verification of mesh discretisation gives confidence in using non-uniform meshes.

Comparison of fluid drawdown for uniform and non-uniform grids

a. Temporal head drawdown in the borehole

b. Spatial head drawdown in the reservoir
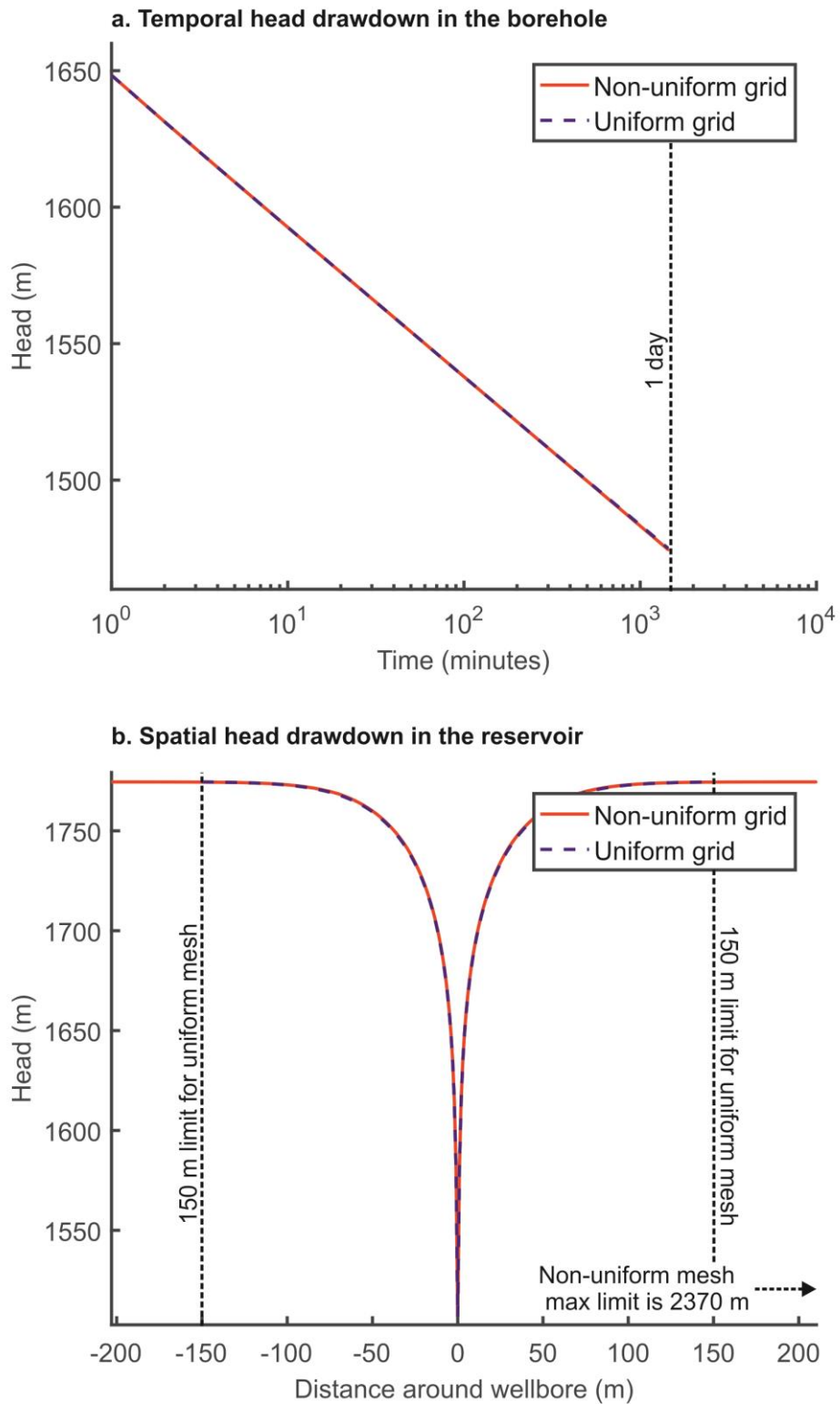
Figure 4.7: *Comparison of non-uniform and uniform mesh performance for hydraulic head both (a) temporally and (b) spatially. Note the initial head in the aquifer at time t=0 is 1775 m.*
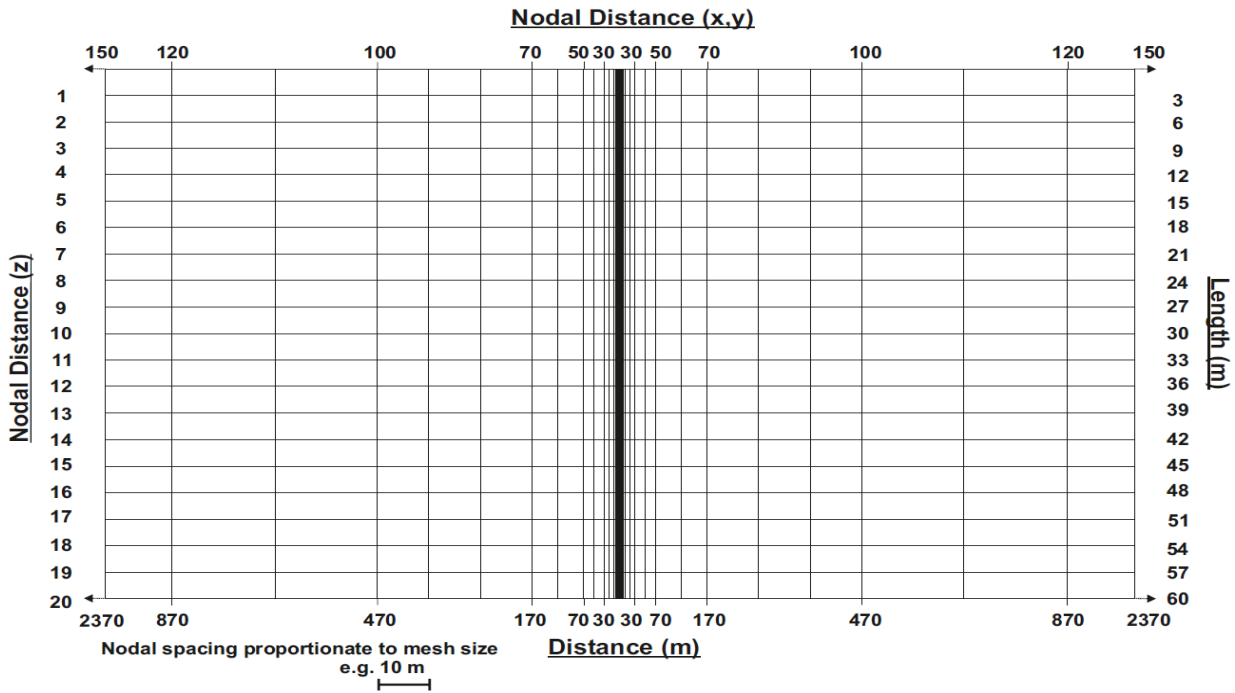
Figure 4.8: *Example non-uniform mesh used for the Marchwood case study.*

4.3 Analytical validation and mesh analysis of the finite-difference model

4.3.1 Validation of the reservoir model for temperature

The reservoir model was validated thermally against an analytical solution for advection and diffusion. The model was simplified to a 1D uniform mesh, neglecting viscosity and density changes and had an imposed head gradient in the reservoir that imitated head drop during production. Temperature was assumed to be initially constant in the reservoir and the time taken for a cold fluid moving from high to low head in the reservoir was measured. The boundary conditions were set as $(z, 0) = T_i$ and $T(0, t) = T_u$. The analytical solution was simulated as (Lapidus and Amundson, 1952; Ogata and Banks, 1961; Van Genuchten and Alves, 1982):

$$T(z, t) = T_i - \frac{T_i - T_u}{2} \left(erfc \left(\frac{z - V.t}{2\sqrt{\alpha.t}} \right) \right) + \exp \left(\frac{V.z}{\alpha} \right) \left(erfc \left(\frac{z + V.t}{2\sqrt{\alpha.t}} \right) \right) \qquad 4.31$$

T_i is the initial temperature of the reservoir, T_u is the temperature where the reservoir meets the upper confining beds, $erfc$ is the complimentary error function term and V is the true velocity of the fluid:

$$V = R_d.(K.\Delta h) \qquad\qquad 4.32$$

R_d is the retardation factor and K is the hydraulic conductivity.

Reservoir - temperature	Parameters	Units
Initial temperature (T_i)	70	°C
Depleted temperature (T_u)	30	°C
Retardation factor (R_d)	1.4019	-
Bulk thermal diffusivity (α)	9.55 E-7	m²/s
Hydraulic conductivity (K)	2 E-9	m/s
Wellbore - temperature		
Flow rate (u)	0.015	m/s
Initial temperature (T_i)	10	°C
Fluid injection temperature (T_{in})	50	°C
Thermal diffusivity (α)	1.6 E-7	m²/s
Reciprocal of thermal resistance and surrounding rock (b_{pg})	8.0856	-
Radius of pipe (A)	0.15	m
Reservoir - head		
Initial head (H_i (x,t))	1000	m
Depleted head (H_i (0,t))	900	m
Storativity (Ss)	1E-5	-
Hydraulic conductivity (K)	4.32E-7	m/s

Table 4.4: *Parameters used for the analytical comparisons to the numerical model.*

The reservoir was assumed to be 100 m thick (z), with a bulk diffusivity (Eq. 4.3) of 9.5527e-07 m²/s (Table 4.4). The hydraulic conductivity (K) was set at 2 e-9 m/s and the retardation factor (R_d) was set at 1.4019. The initial temperature of the reservoir was assumed to be constant at 70 °C and a temperature of 30 °C was imposed at the top of the reservoir to emphasise the spread of temperature in the simulation.
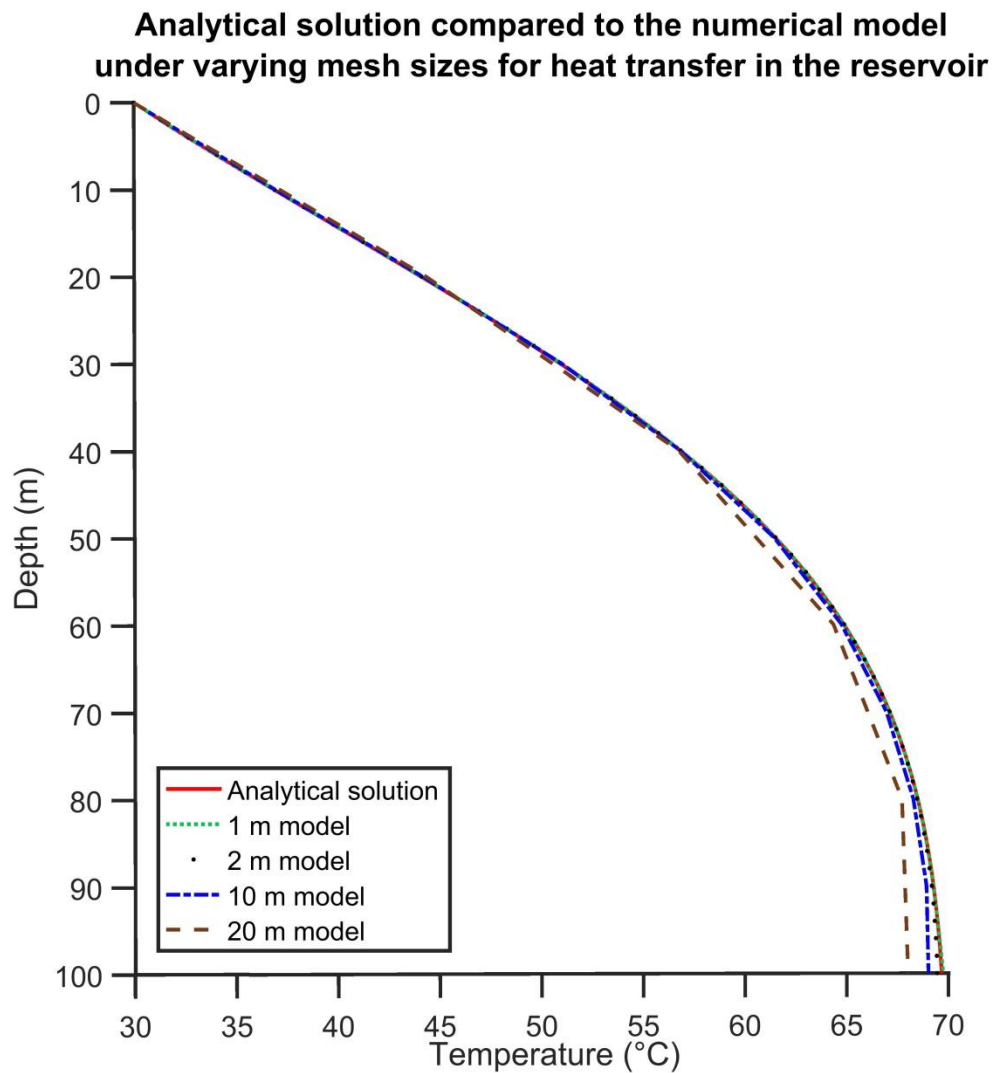
Figure 4.9: *Analytical versus the numerical solution for the reservoir temperature change. The temperature distribution over the reservoir after 20 years is shown with the cold water front moving away from the axis origin. Mesh sizes of 1, 2, 10 and 20 m were used for a reservoir thickness of 100 m.*

The analytical and numerical solutions both predicted similar thermal drawdown times for the modelled data. The numerical model showed a higher accuracy and closer match to the analytical solution with a higher quantity of nodes and finer mesh. The 1D model was simulated for a mesh size of 1, 2, 10 and 20 m using 101, 51, 11 and 6 nodes, respectively. After 20 years' simulation with hourly time steps, it can be seen that the spatial difference in temperature change was minor between a 1 m and 20 m mesh size (Fig. 4.9). The most noticeable difference is between depths of 40

and 100 m (Fig. 4.9) within the 20 m nodal spacing. In comparison to the 1 m spacing the maximum

error is 2.5 %.

4.3.2 Validation of the borehole model for temperature

The accuracy of the thermal borehole model was verified by comparing the numerical

solution to a 1D analytical solution. The analytical approach (of van Genuchten and Alves, 1982) gives

the solution to convective-dispersive, solute transport. The borehole model was verified for shallow,

geothermal systems by both Al-Khoury et al. (2010) and Nabi and Al-Khoury (2012b), for finite-

element and finite-volume methods, respectively. The finite-difference solution used here was

compared to the analytical solution (taken from van Genuchten and Alves, 1982; Nabi and Al-Khoury,

2012b):

$$T(z,t) = T_i - \frac{T_i - T_{in}}{2}\left(e^{\left(\frac{(u-w).z}{2\alpha}\right)}.erfc\left(\frac{z-wt}{2\sqrt{\alpha t}}\right) + e^{\left(\frac{(u+w).z}{2\alpha}\right)}.\left(erfc\left(\frac{z+wt}{2\sqrt{\alpha t}}\right)\right)\right) \qquad 4.33$$

T_i is the initial temperature of the surrounding rock, T_{in} is the temperature of the fluid entering the

pipe, z is the length of the pipe, u is the velocity of the fluid and α is the thermal diffusivity. w is

given by:

$$w = u\sqrt{1 + \frac{4\eta\alpha}{u^2}} \qquad 4.34$$

where

$$\eta = \frac{2b_{pg}}{\rho_f C_f \pi r_p} \qquad 4.35$$

b_{pg} is the reciprocal of thermal resistance between the pipe and surrounding rock, ρ_f is the density

of the fluid, C_f is the specific heat capacity of the fluid and r_p is the radius of the pipe.

A flow rate of 0.015 m/s was used, the initial temperature of the system was set at 10 °C, the

fluid injection temperature was 50 °C, the thermal diffusivity was 1.6e-7 m²/s, the reciprocal of

thermal resistance was 8.0856 W/m^2 °C and the radius of the pipe was 0.15 m (Table 4.4 and Fig.

4.10). Mesh sizes of 1, 2, 10 and 20 m were compared to the analytical solution for a 1,000 m long

pipe located within bedrock. The analytical solution aims to investigate heat transfer along the piping

and the accuracy in comparison to an analytical solution.
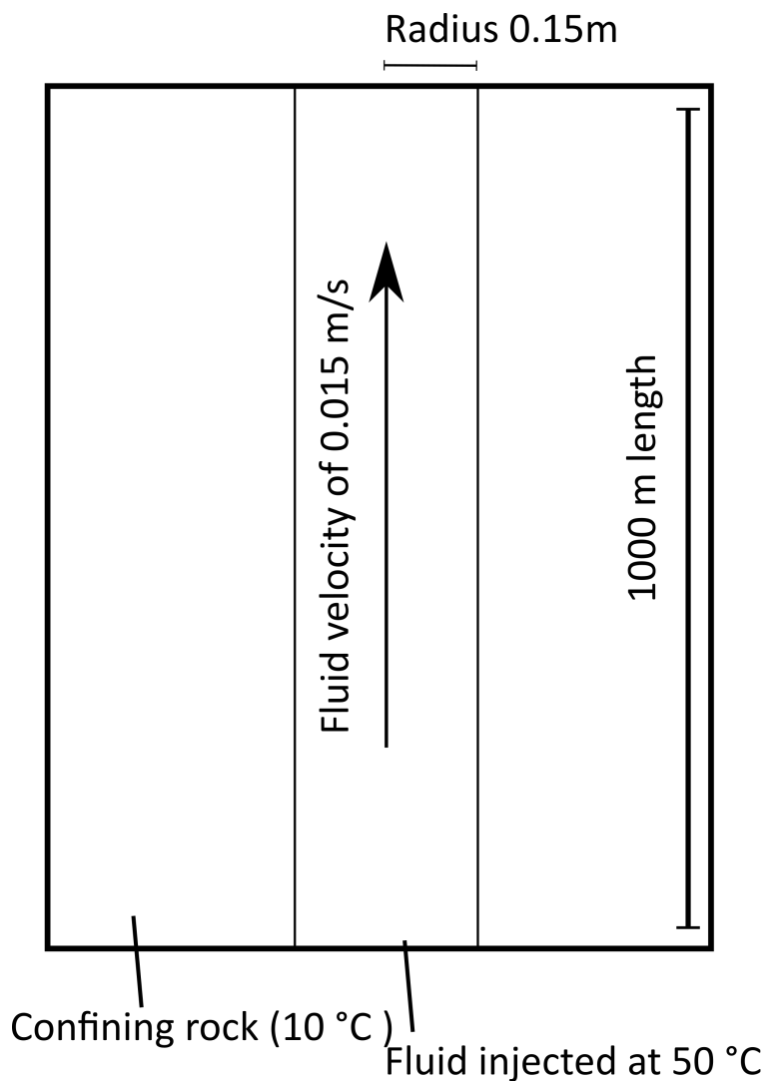
Figure 4.10: *Schematic of analytical solution showing input fluid and boundary conditions.*

Figure 4.11 shows the spread of temperature along the pipe after 30,000 seconds (i.e.,

approximately 8 hours), simulated using a one second time step. This value was utilised to allow time

for the thermal front to propagate down the pipe. Similarly to the analytical and numerical solution

of advection-diffusion in a reservoir, the finer the mesh size the more accurate the numerical model

in approximating the analytical solution. Once the hot fluid had propagated through the pipe, the temperature difference between the different mesh sizes was minimal. Reducing the nodal spacing further produces an even closer fit to the analytical solution (Nabi and Al-Khoury, 2012b).
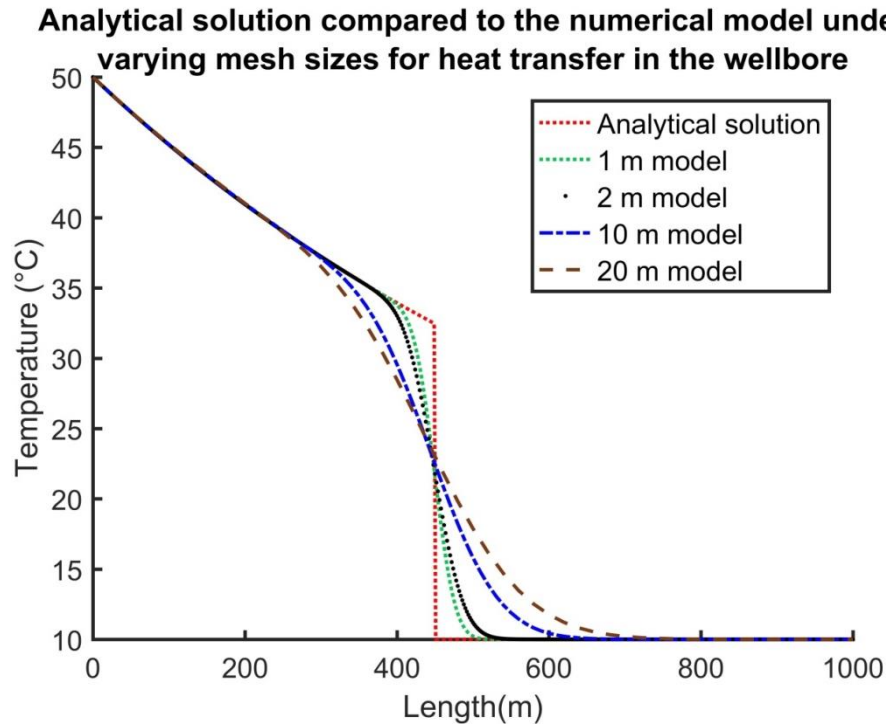
Figure 4.11: *Analytical versus the numerical solution for the wellbore temperature change. The temperature distribution over the wellbore after 30,000 seconds shows a closer fit between the numerical and analytical solution for finer mesh sizes. Mesh sizes of 1, 2, 10 and 20 m were used for a pipe with a length of 1000 m.*

4.3.3 Validation of the reservoir model for hydraulic head

The continuity equation for hydraulic head in the reservoir was validated as a 1D model compared to the analytical solution of the diffusion equation (Carslaw and Jaeger, 1959):

$$H(x,t) = Hi(x,t) - Hi(0,t)\left(1 - \mathrm{erf}\left(\frac{x}{\sqrt{4Dt}}\right)\right) \qquad 4.36$$

where $Hi(x,t)$ is the initial head in the reservoir and $Hi(0,t)$ is the depleted head around the well, x is the spatial distance, erf is the error function and t is time. The diffusion coefficient is given as:

85

$$D = \frac{K}{Ss}$$ 4.37

where K is the hydraulic conductivity and Ss is the storativity.

The initial head was set at 1,000 m in the reservoir and was then reduced to 900 m for point (0,t). The hydraulic conductivity was set at 4.32e-7 m/s and the storativity (Ss) at 1e-5 (which is similar to that of the Marchwood Well (e.g., Price and Allen, 1984)) (Table 4.4). Meshes of 1, 2, 10 and 20 m were used for a 100 m interval around the depleted pressure point. Figure 4.12 shows the hydraulic head change after 5,000 seconds (1 hour 23 minutes), using a one second time step. This was to allow the head to deplete spatially away from the sink, giving a representation of the reservoir for different mesh sizes. Differences between the numerical and analytical solution were small even when mesh sizes coarsen and minimal nodes were used. At a 20 m mesh size the numerical solutions appeared asymptotic to the analytical solution, such that at any given node it was still a close fit (Fig. 4.12). It is important that a high level of accuracy is obtained when modelling the fluid movement in a low-enthalpy, geothermal system as the performance of any district heating scheme will be determined by the level of head depletion. The validation in these analytical studies showed the numerical model provides a high level of accuracy.
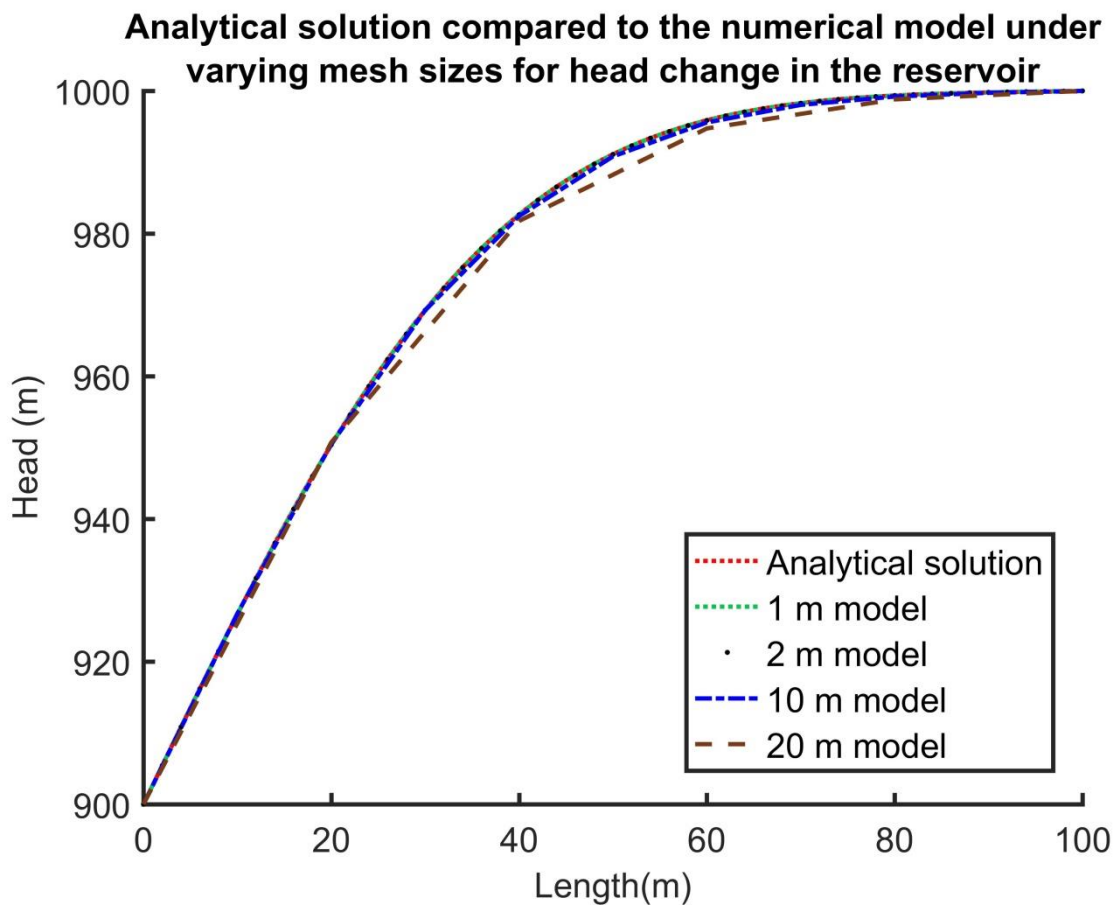
Figure 4.12: *Analytical versus the numerical solution for hydraulic head in the reservoir at 5,000 seconds. Mesh sizes of 1, 2, 10 and 20 m were used.*

4.3.4 Mesh analysis

Numerical errors can occur in computational simulations from round-off errors, iterative convergence errors and discretisation error, with the latter being the most dominant (Roy, 2005; Nick et al., 2009). Therefore, discretisation errors were focused on and the Roaches Grid Convergence Index method, a version of the Richardson Extrapolation approach, was used to identify the discretisation error and observed order of accuracy using a series of mesh sizes to solve the same solution (Richardson, 1911; Richardson and Gaunt, 1927; Roache, 1994; Roy, 2010).

When analysing mesh discretisation error, constant grid spacing is required. In this example, a fluid extraction point was assigned in the reservoir at one boundary of the model with a constant

temperature value assigned to the opposite boundary (i.e., the base of the aquifer). The model then recorded the changes in temperature and head across the spatial domain. The accuracy of the model was tested after 2 years of run time for the reservoir and 30 days for the wellbore. The model was discretised for a mesh of 224 x 224 x 64 m for the reservoir section with the reservoir situated 640 m below the ground. A grid refinement factor of 2 was used, with the spacing of the mesh set at 1, 2, 4, 8 and 16 m (Fig. 4.13), which in the reservoir amounts to 3,290,625, 421,377, 55,233, 7,569 and 1,125 nodes, respectively. When modelling the wellbore and confining beds, the horizontal spatial domain was limited to 21 x 21 nodes, giving the equivalent amount of nodes as 141,561, 71,001, 35,721 and 18,081. The reservoir and wellbore were assumed to contain the same parameters as the Sherwood Sandstone Group for the Marchwood Well case study (Table 4.5 and 4.6, Sect. 4). The only changes were a thermal diffusivity of 1.38e-6 m²/s in the confining beds around the wellbore, a lower hydraulic conductivity of 2e-9 m/s and higher thermal conductivity of 3.41 W/m/°C in the reservoir.

The Roaches Grid Convergence Index indicated a discretisation error ranging from 0.13 to 3.48 % (Fig. 4.14). The global order of accuracy ranged from 0.67 to 1.4. As the example used here was monotonically convergent, the range for accuracy was close to first order (where p=1), giving a reliable error estimate for a mixed order scheme (Roy, 2003). Coarser meshes tended to allow temperature or head difference to propagate quickly through the mesh (Figs. 4.15 and 4.16). This affected the reservoir more greatly than the wellbore, with the discretisation error in the reservoir far higher than that in the wellbore (Fig. 4.14). This can be mitigated by reducing the mesh size around areas of high temperature/ pressure contrast, such as the well screen. To account for systems with larger spatial domains, a non-uniform grid that increases incrementally away from the borehole can be considered. This does however require a slightly different finite difference approximation technique (e.g., Turkel, 1986; Sanmiguel-Rojas et al., 2005; Kajishima and Taira, 2017). In the examples in this chapter the mesh proximal to the wellbore was set at 1 m.
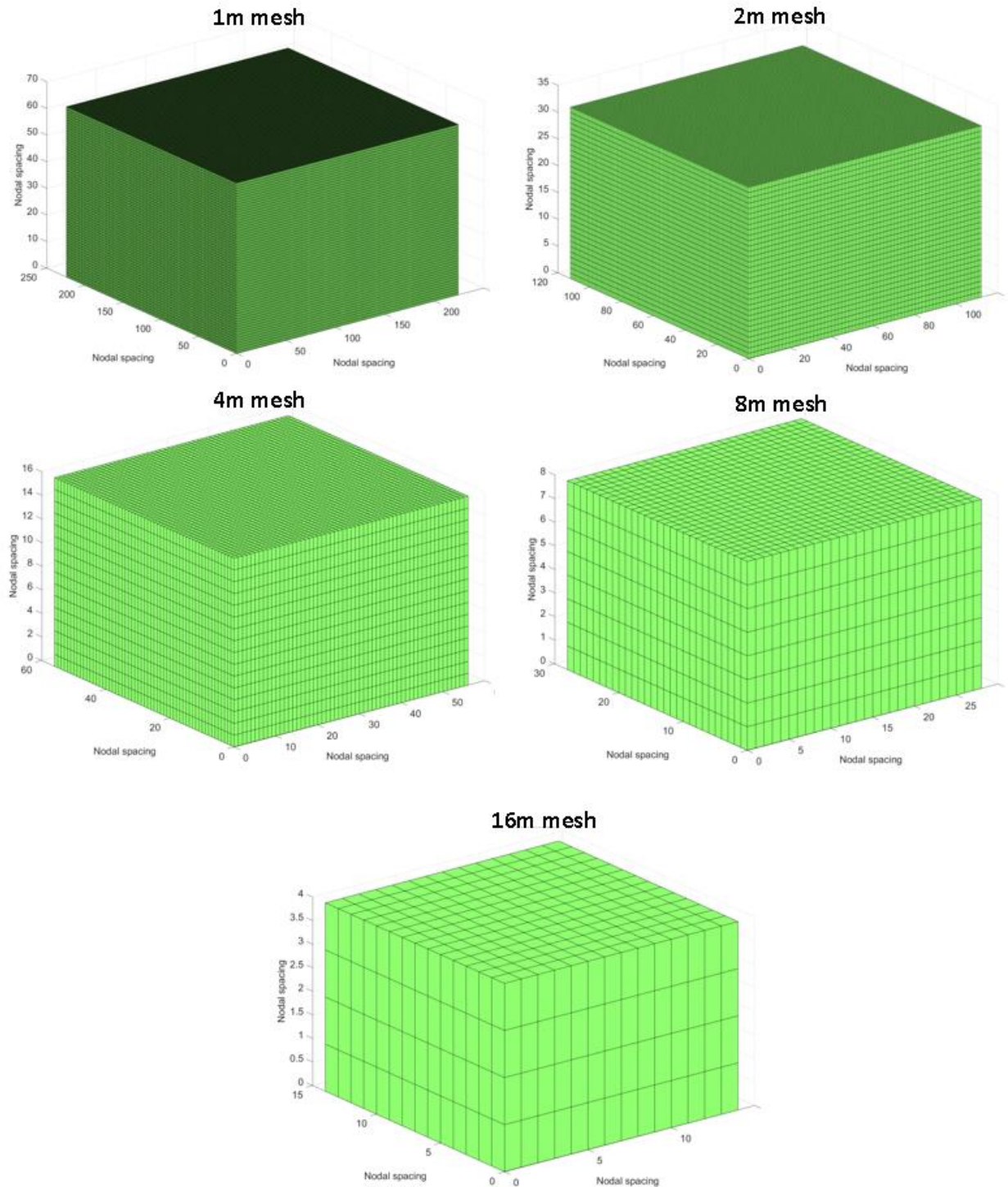
Figure 4.13: *Example discretised meshes for the reservoir volumes used in the discretisation tests. Mesh spacing was increased by a factor of 2.*
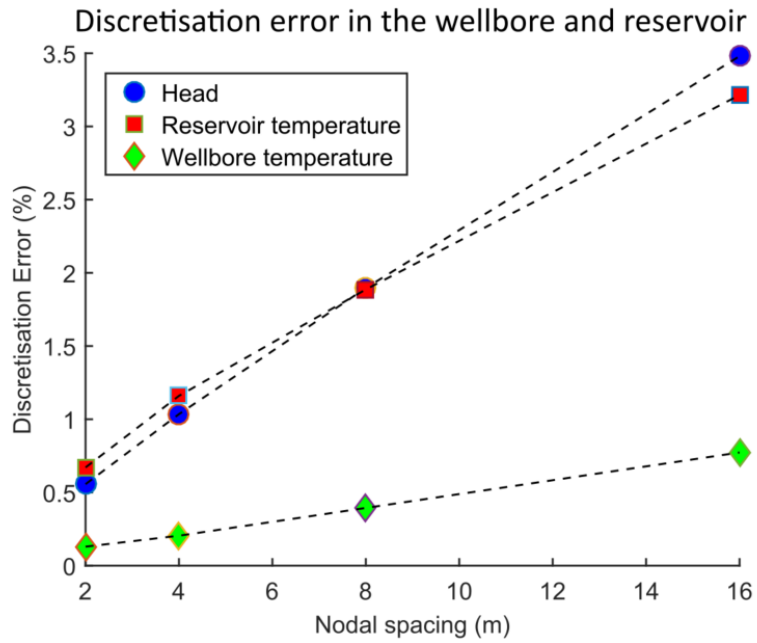
Figure 4.14: *Discretisation error for the wellbore and reservoir. The reservoir temperature points are shown as red squares and the hydraulic head as blue circles. The wellbore error is shown as green diamonds.*
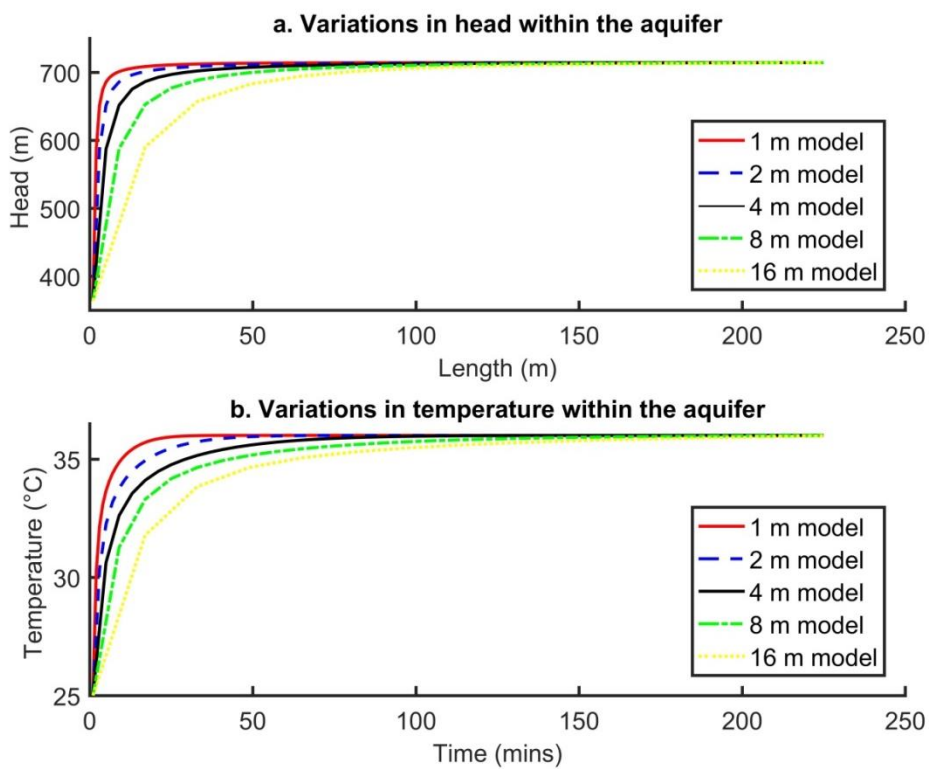
Figure 4.15: *Spatial variations in the aquifer for variation in (a) head and (b) temperature.*
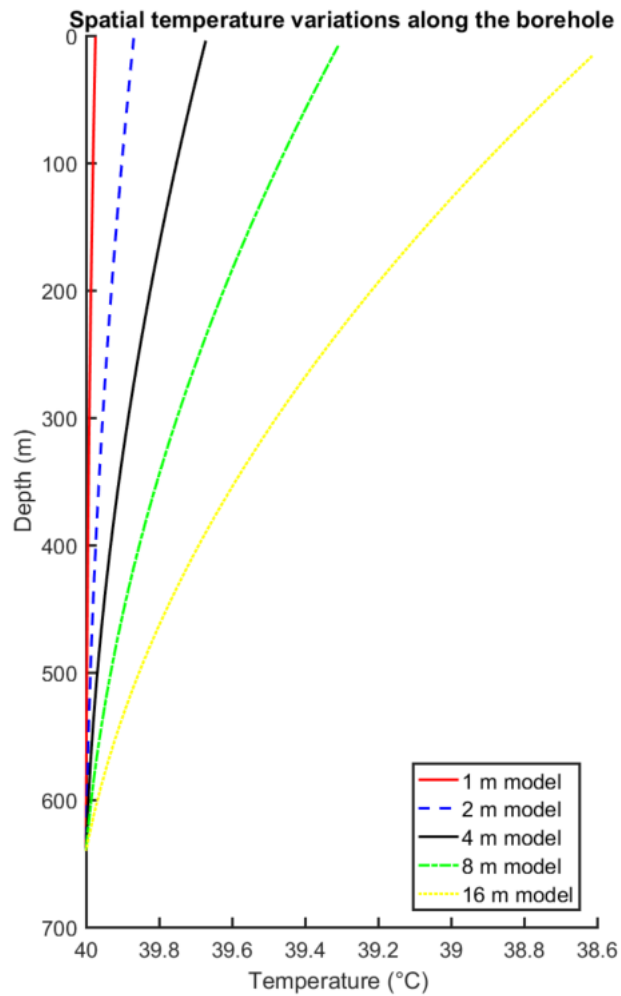
Figure 4.16: *Spatial variations in temperature along the wellbore.*

4.4 Application of the model to Marchwood and Western Esplanade Wells, Southampton, UK.

Two case studies from the UK were used to verify the model; both based on well tests from the geothermal exploration wells drilled in the Mesozoic aged Wessex Basin near Southampton in the 1980s: 1) the Marchwood Well, and 2) the Western Esplanade Well. In both cases, flow in the aquifer was horizontal as the well screen is fully penetrative; meaning that temperature in the aquifer remains the same as under static (initial) conditions (Figs. 4.17 and 4.18). Such assumptions are typical when modelling geothermal systems (particularly in doublet systems; e.g., Saeid et al., 2013), but in the models provided here energy losses in the wellbore were simulated to give a more

likely production temperature. Reservoir temperature change was also modelled for a hypothetical partially penetrative scheme using the Marchwood Well data. Partially penetrative wells in thicker aquifers in the UK, such as within the Cheshire and Worcester Basins (Downing and Gray, 1986b), may be more viable and the change in the reservoir temperature may impact energy production. A coaxial BHE model was also validated against the field test data from Wang et al. (2017). This example was chosen as limited data from deep BHEs is available publicly.
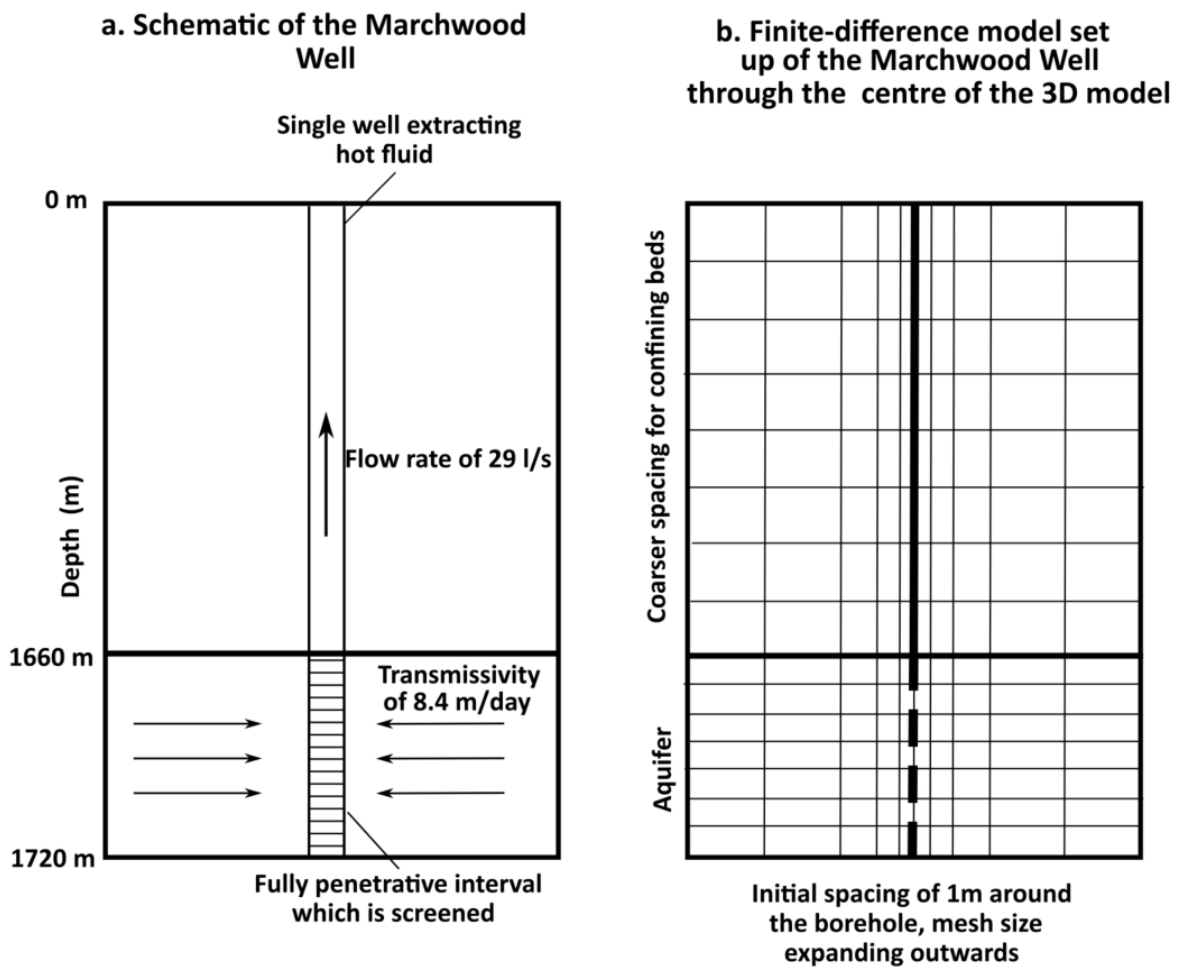
Figure 4.17: *(a) Schematic of the Marchwood Well and (b) an example of the finite-difference model.*

a. Schematic of the Western Esplanade Well

Single well extracting hot fluid

0 m

Depth (m)

Flow rate of 20 l/s

1729 m

Transmissivity of 6.8 m/day

1796 m

Fully penetrative interval which is lined

b. Finite-difference model set up of the Western Esplanade Well through the centre of the 3D model

Coarser spacing for confining beds

Aquifer

Initial spacing of 1m around the borehole, mesh size expanding outwards

Figure 4.18: *(a) Schematic of the Western Esplanade Well and (b) schematic of the finite-difference model.*

4.4.1 Verification against the Marchwood Well, Southampton

Reservoir	Parameters	Units
Storage coefficient	1E-4	-
Surface temperature	10	°C
Thermal conductivity	1.88 UCB / 3.1 R	W/m/°C
Specific heat capacity	860 UCB / 920 R	J/kg °C
Density	2170 UCB / 2450 R	kg/m^3
Wellbore		
Screened interval	212	mm
Wellbore diameter	306	mm
Thermal conductivity	43 Pi / 2.7 G / 0.67 F	W/m/°C
Specific heat capacity	1250 G / 4200 F	J/kg °C
Density	1600 G / 1000 F	kg/m^3

Table 4.5: *Reservoir and wellbore data used for both the Marchwood and Western Esplanade wells. The upper confining bed is denoted by UCB, the reservoir by R, the piping by Pi, the fluid by F and the grout by G. Information is collated from: Kappelmeyer and Hänel (1974), Price and Allen (1984), Downing et al. (1984), Knox et al. (1984), Downing and Gray (1986b), Allan (1997), BGS (2011), Eppelbaum et al. (2014), ETB (2017), Rosen and Koohi-Fayegh (2017).*

The Marchwood Well was completed in March 1980 (Fig. 4.19) and yielded a true transmissivity of 7 m^2 / day and an apparent transmissivity of 11.21 m^2 / day due to 'leakage through a less permeable' formation (Price and Allen, 1984). Transmissivity is the rate of groundwater flow horizontally through an aquifer. The Sherwood Sandstone Group was targeted as a geothermal resource from depths of 1,660 m to 1,720 m. These units were underlain by a thick sequence of red Devonian sandstone, which is strongly heterogeneous and consists of a series of mudstone, siltstone and sandstone (Knox et al., 1984) (Fig. 4.19). The Devonian sediments were more indurated and fractured than the overlying unconformable Triassic sandstone (Thomas and Holliday, 1982) and had lower intergranular-porosity but, potentially high fracture-related porosity. The Sherwood Sandstone Group was considered as the reservoir unit and the underlying Devonian sandstone the low-permeability basal confining seal in the model. It is important to note, however, that although the Devonian unit was not considered the target aquifer during the well tests, it is more than likely that the high porosity spikes identified in the logging data (Knox et al., 1984) could be responsible for

the leakage into the aquifer causing the apparent higher transmissivities (Price and Allen, 1984) (Fig. 4.19c).

	Marchwood	Western Esplanade	Units
Production rate	29	20	l/s
Reservoir temperature	73.6	76	°C
Depth of reservoir	1660 - 1720	1729 - 1796	m
Porosity	11.4	15	%
Transmissivity	8.4	6.8	m^2/day
Time of test	33	28	days

Table 4.6: *Modelling parameters for the Marchwood and Western Esplanade wells. Information was collated from: Allen et al. (1983), Downing et al. (1984), Price and Allen (1984), Barker et al. (2000), Knox et al. (1984).*

The well was tested for 33 days from 6th April 1979 producing brine at an average flow rate of ~29 l/s with an average formation temperature of ~73.6 °C and a maximum production temperature of 71.6 °C (Price and Allen, 1984). Hydro- and thermo-physical parameters used in the model were collected from literature: Kappelmeyer and Hänel (1974), Knox et al. (1984), Price and Allen (1984), Downing and Gray (1986b), Eppelbaum et al. (2014) and ETB (2017) (Table 4.5 & 4.6). In the reservoir, a thermal conductivity of 3.1 W/m/°C was used, porosity was 11.4 % and the initial pressure was ~17.3 MN/m^2. The specific heat capacity in the reservoir was modelled as 920 J/kg °C, with a density of 2,450 kg/m^3. The upper confining Mercia Mudstone Group have a thermal conductivity of 1.88 W/m/°C, density of 2,170 kg/m^3 and heat capacity of 860 J/kg °C. Porosity and hydraulic conductivity of the confining beds were assumed to be low and in the simulated time, the fluid would not propagate through either boundary. The wellbore was modelled to have a diameter of 306 mm with a screened interval of 212 mm (Downing et al., 1984). Skin or formation damage around the wellbore was neglected in the model as the well was filled with calcium chloride solution to remove mud-cake (Burgess et al., 1981).
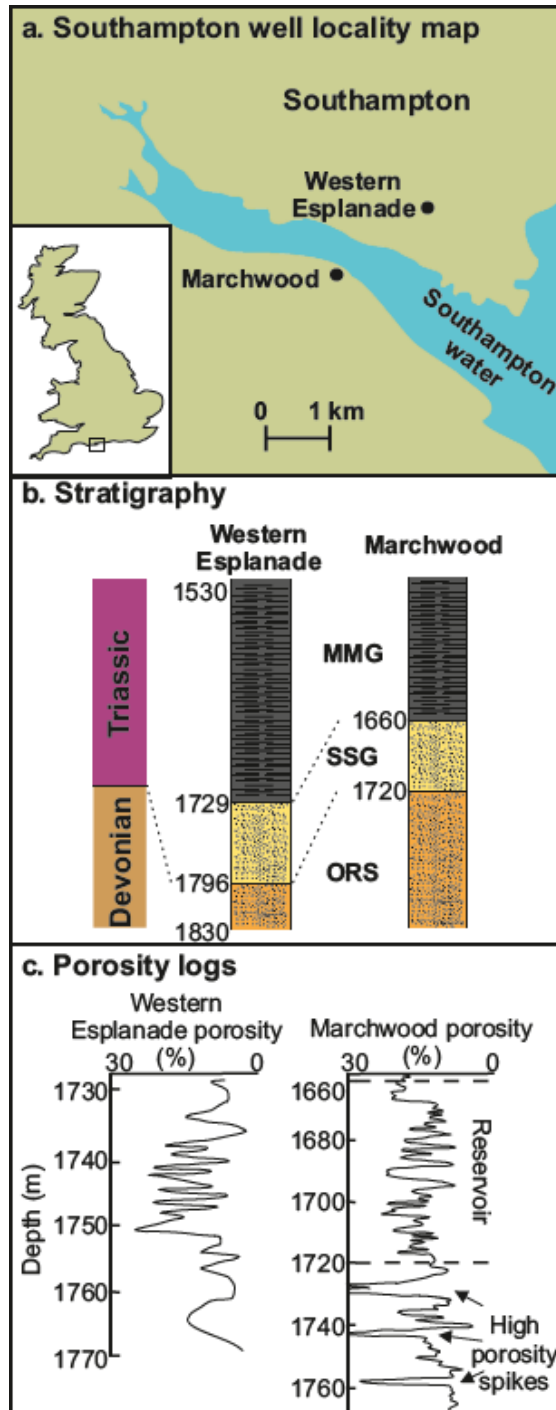
Figure 4.19: *(a) Southampton locality map highlighting borehole locations (modified from Downing et al., 1984 and Barker et al., 2000), (b) stratigraphic logs for the Marchwood and Western Esplanade wells (Thomas and Holliday, 1982; Knox et al., 1984) and (c) porosity logs (after Downing et al., 1984 and Knox et al., 1984). MMG = Mercia Mudstone group, SSG = Sherwood Sandstone group and ORS = Old Red Sandstone. Logs show depth from surface level in metres.*

Other models suggest that a transmissivity of 10 m^2/day was the likely rate of fluid flow proximal to the borehole, decreasing with distance from the wellbore (Barker, 1981). In this model, a bulk transmissivity of 8.4 m^2/day was used to account for enhanced permeability around the wellbore and leakage into the aquifer. This is equivalent to a hydraulic conductivity of 0.14 m/day. The model was constructed as a 3D orthogonal mesh with fixed boundary conditions. The temporal domain was discretised to a time step of 10 seconds. The mesh had a non-uniform spacing, increasing in nodal distance away from the well to a distance of 2,370 m on each side of the wellbore. The vertical spacing was uniform with a 3 m mesh size, whilst the reservoir/aquifer had a nodal domain set at 301 x 301 x 21 (x,y,z), which equates to 1,902,621 nodes. The borehole is located in the overburden above the reservoir and was modelled with a uniform vertical spacing of 10 m between nodes and a 1 m lateral spacing (Fig. 4.17).

During the 33 day well test, down-hole pressure reduced from 17.39 to 13.63 MN/m^2, which is equivalent to ~383 m fall in head. The model matched the real data closely and the analytical Theis equation (Theis, 1935), with head reducing by 377.5 m, which is equivalent to a fall in pressure of 3.67 MN/m^2 (Fig. 4.20a). Early head data (<10 minutes) did not match as well, which was interpreted as an effect of higher transmissivities closer to the borehole (Barker, 1981). The zone of influence around the well screen was 870 m (Fig. 4.21). This reflects the change in head in the aquifer radially away from the well screen (i.e., distances greater than 870m away from the well screen are still under static conditions). The production temperature reached a maximum of 71.43°C, which is slightly lower than the recorded production temperature (Fig. 4.22a). The grout around the wellbore also acted as an insulator, limiting the heat loss to the confining beds and resulting in temperature change to be minor in the near well strata (<6 m radially) (Fig. 4.22c and 22e). Recharge pressure curves also matched the real data and the 'Theis' recovery analytical solution (Theis, 1935), recharging to 17.28 MN/m^2 or 1,763.2 m (Fig. 4.20b). Assuming a reject temperature of 30 °C, 14.4 x 10^{12} J of energy were produced from a possible total of 0.12 x 10^{18} J within the spatial domain (Fig.

4.23a). This is the equivalent of 0.01 % of the energy within the reservoir, which is only a minor amount of energy as it was only for a production test, however, it is extremely important to model energy production during the lifetime of a well as it can be matched to public demand and input into a district heat network. Energy production increased with time as thermal fluxes cooling the wellbore initially reduce the amount of energy produced, particularly in the first two days (Fig. 4.23b).

Head drawdown and recharge semi-log plots for the Southampton case studies
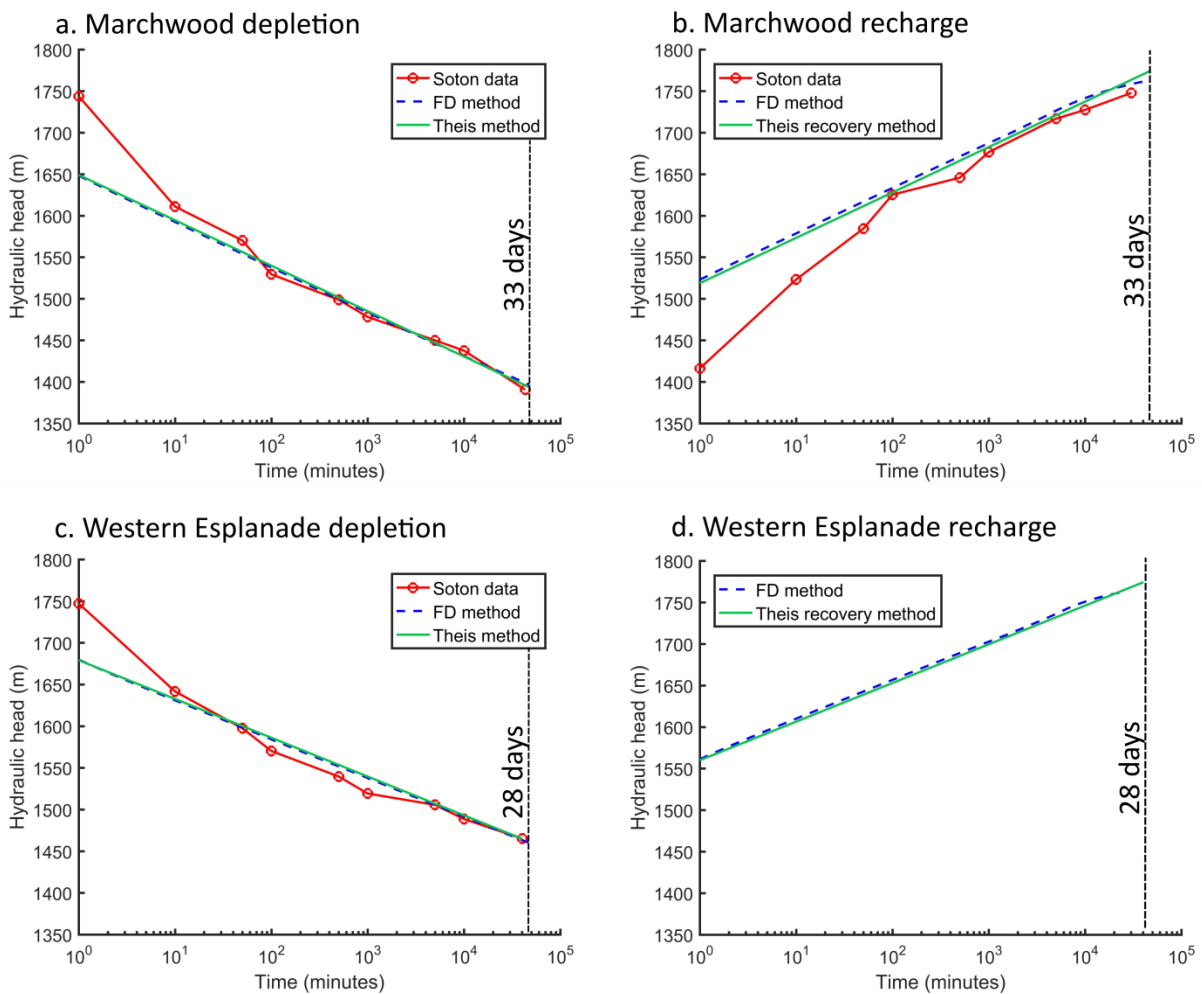
Figure 4.20: *Comparison of real data to modelled head drawdown data for (a) Marchwood depletion, (b) Marchwood recharge, (c) Western Esplanade depletion and (d) Western Esplanade recharge. The analytical solution (Theis method) was also compared to the finite-difference method (FD) with a near perfect fit. Drawdown data was obtained from Downing et al., (1984) and Price and Allen, (1984). Note initial conditions for both have starting head of 1775 m.*
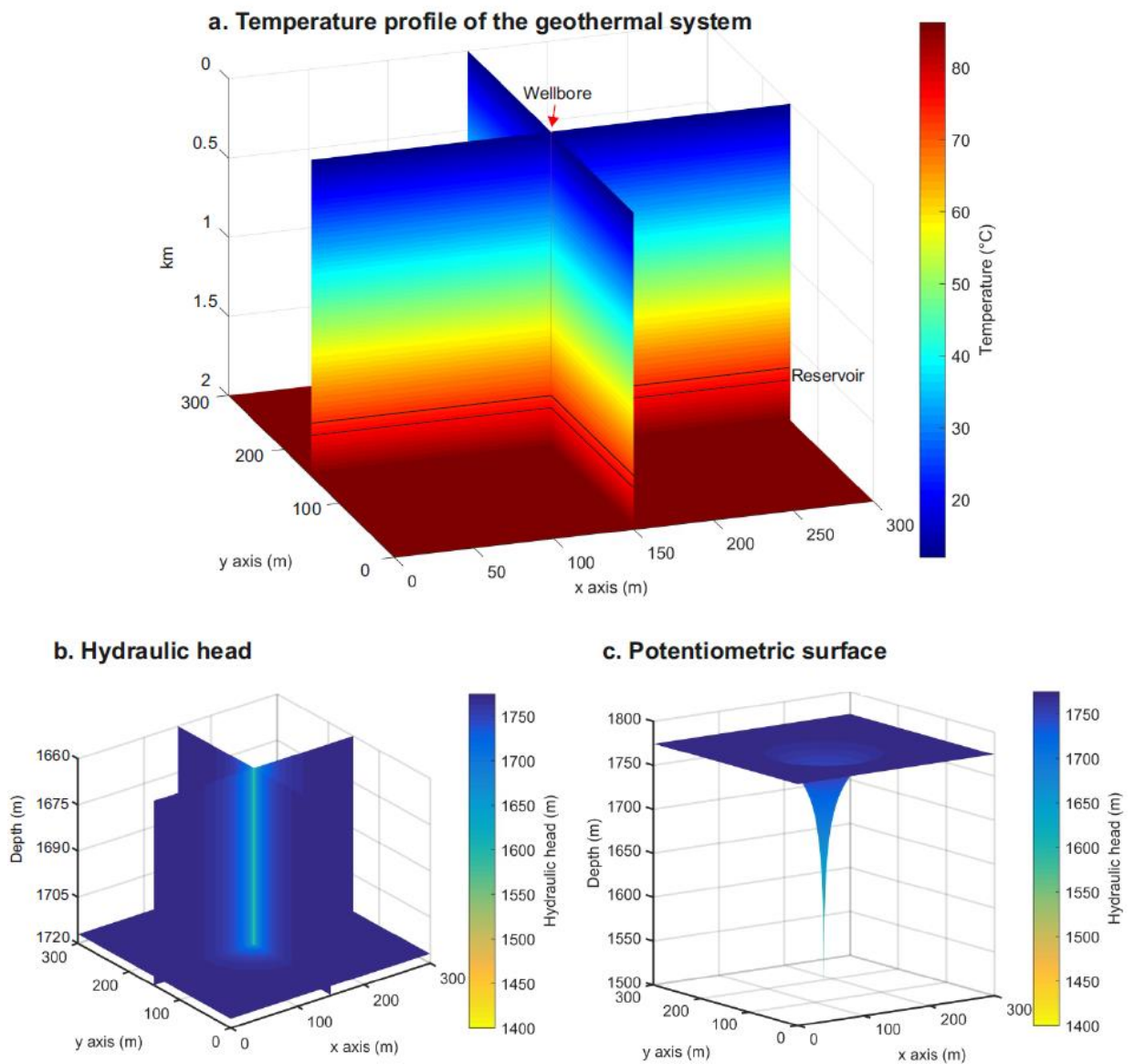
Figure 4.21: *3D representation of head and temperature change in the reservoir for the Marchwood Well, (a) is a 3D representation of the entire subsurface in proximity to the wellbore, (b) is the hydraulic head change around the wellbore in the reservoir (after 1 day of depletion) and (c) is a cross section showing the potentiometric surface near the wellbore in the reservoir (after 1 day of depletion).*
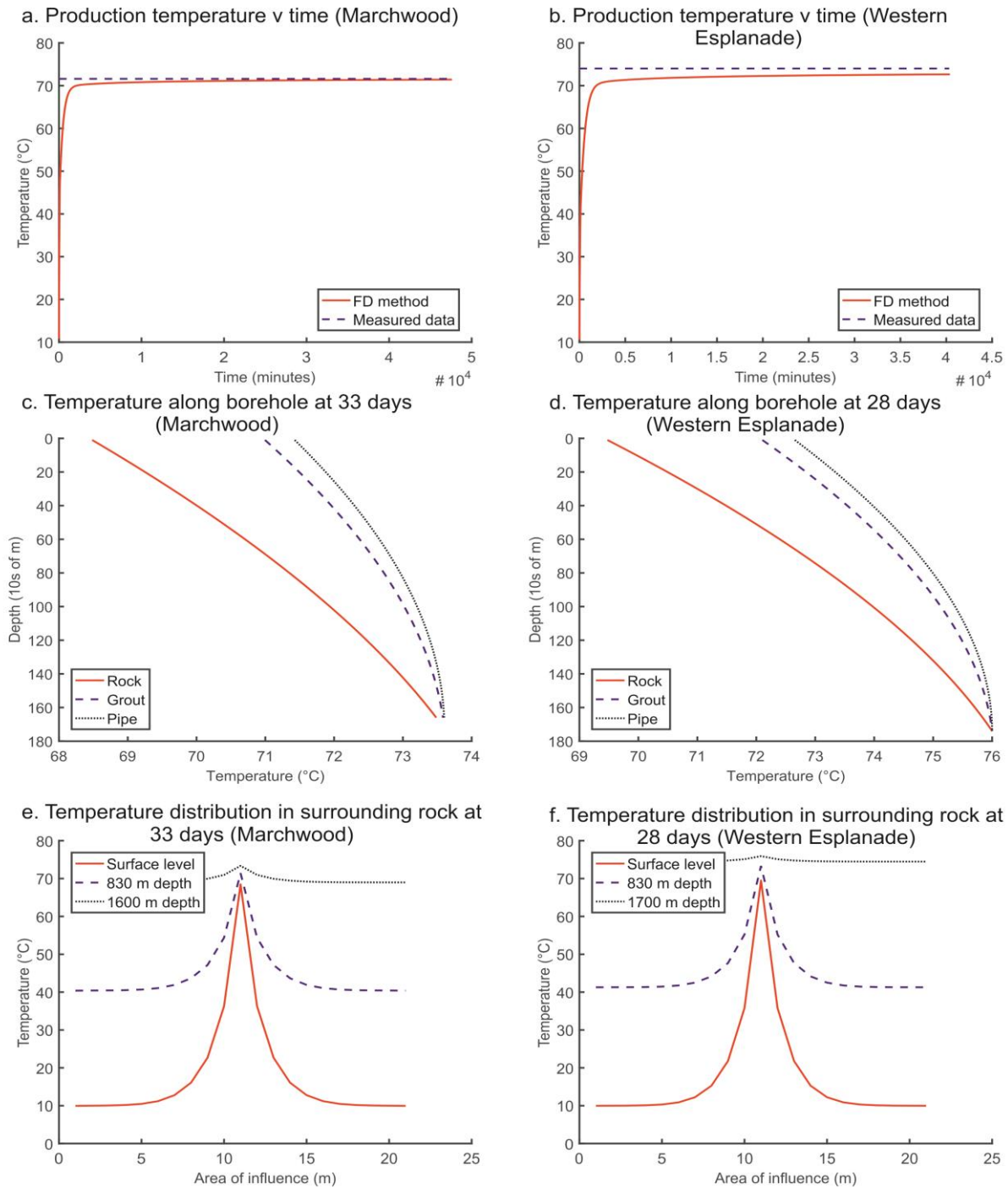
Figure 4.22: *Comparison of modelled Southampton wellbore data between Marchwood and Western Esplanade. Temperature in the pipe (a,b), vertical temperature distribution of the temperature in surrounding rock, grout and pipe (c,d) and the thermal zone of influence around the wellbore are shown at different depths respectively (e,f). The Marchwood wellbore is represented in figures (a), (c), (e) and the Western Esplanade in (b), (d), (f).*
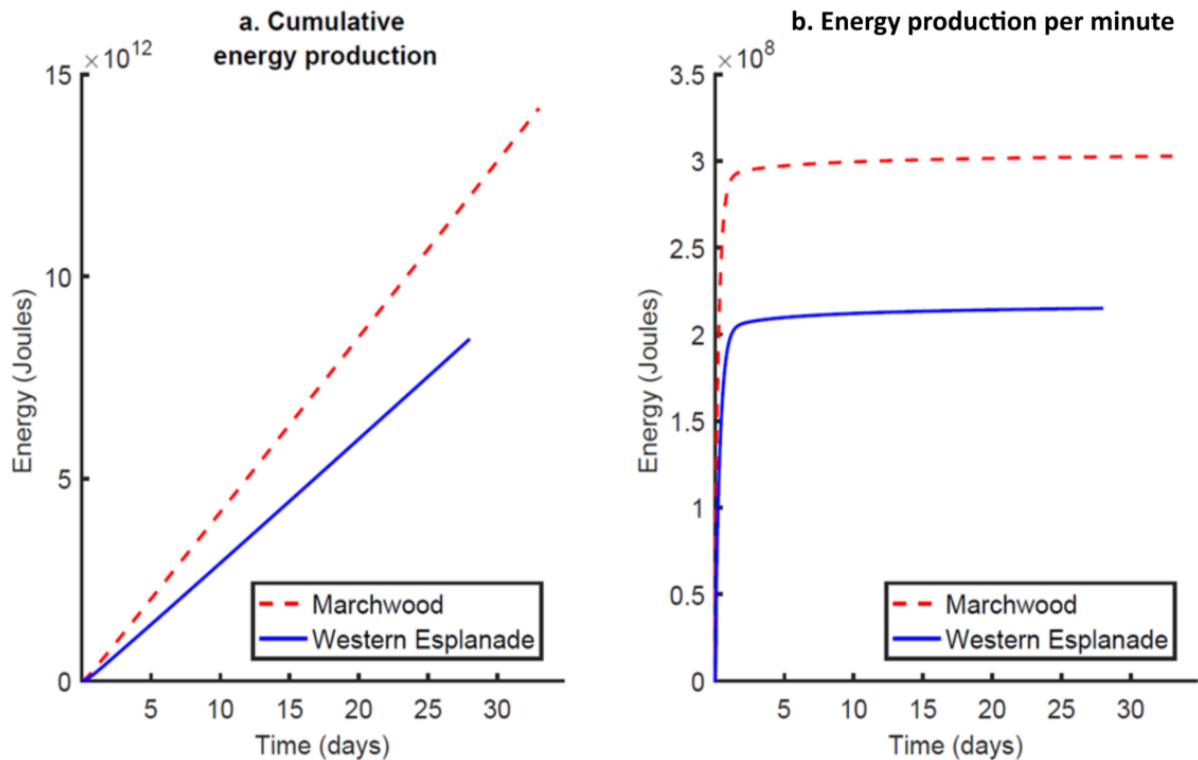
Figure 4.23: (*a) Cumulative energy and (b) energy per minute produced for the Southampton production test models.*

4.4.2 Verification against the Western Esplanade Well, Southampton

The Western Esplanade Well was drilled 1.85 km away from the exploratory Marchwood Well on 26th September 1981, confirming the Sherwood Sandstone Group was at a depth of 1,729 to 1,796 m and underlain by the indurated Devonian sandstones (Downing et al. 1984) (Fig. 4.19). The average reservoir temperature was recorded at 76 °C and the wellhead encountered temperatures of 74 °C (Barker et al., 2000). The hydro-thermal parameters and model set up were considered identical to the Marchwood Well, other than depth, initial temperature, flow rate of 20 l/s, which was sustained for 28 days, with a porosity of 15 % and transmissivity of 6.8 m^2/day (Allen et al., 1983; Downing et al., 1984) (Table 4.5 & 4.6). This is the equivalent to a hydraulic conductivity value of ~0.1 m/day. Head was assumed to increase with depth at the same rate as the Marchwood Well and was assigned the same initial head. The Western Esplanade Well was left as an 'open-hole' in the

reservoir below 1,717 m due to unstable conditions in the well. However, a liner of 240 mm was deployed (Downing et al., 1984). In the model, the liner radius was assumed to be equivalent to that of a well screen. The mesh was again non-uniform, laterally reaching a distance of 2,370 m, but had a uniform vertical spacing of 1 m. The spatial domain consisted of 301 x 301 x 68 nodes for the reservoir (Fig. 4.18).

During the 28 day test, the pressure in the wellbore dropped by 3.03 MN/m^2, which is equivalent to a ~ 309 m fall in head (Downing et al., 1984). A transmissivity of 6.8 m^2/day was used to account for an enhanced transmissivity from leakage into the reservoir (similar to that at Marchwood). The model matched the real data and analytical solution, with a drawdown of 307.5 m or a pressure drop of 3.01 MN/m^2 during the production test (Fig. 4.20c). The model was not an exact fit due to problems with the high pressure surface pump limiting pumping times to irregular periods during the test (Downing et al., 1984). Although post-test recharge data was unavailable, the reservoir recharged to 1,761.9 m head (Fig. 4.20d). The zone of influence around the well screen in the reservoir was recorded at 570 m (Fig. 4.24). As a result of the irregular pumping periods, the predicted temperature at ground level in the pipe (72.65 °C) was lower than that recorded (74 °C) (Fig. 4.22b). Similar to the Marchwood case study, the confining rocks take longer than the pipe to heat up, with a minor zone of influence (Figs. 4.22d and 4.22f). 8.9 x 10^{12} J of energy was produced from a possible total of 0.13 x 10^{15} J within the spatial domain (Fig. 4.23). The produced energy was, therefore, only 0.007 % of that within the system.
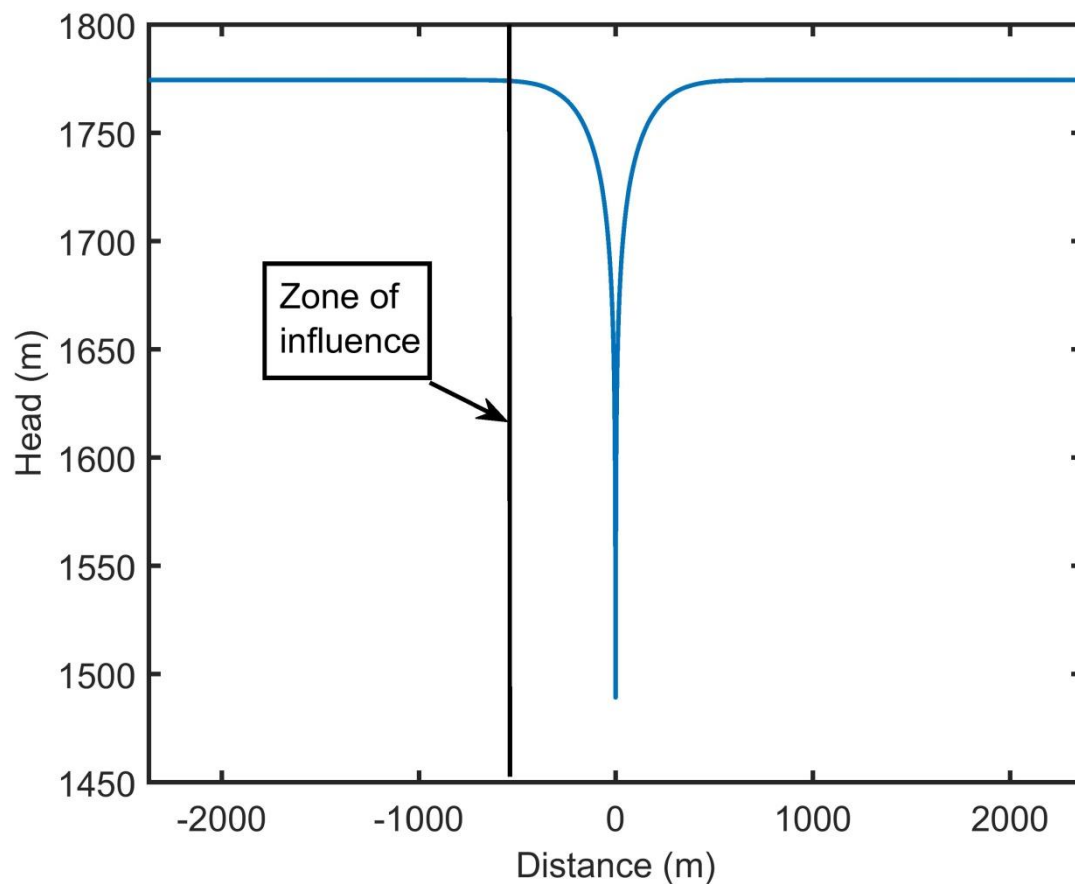
Figure 4.24: *Zone of influence around Western Esplanade well at the end of production test.*

4.4.3 Modelling of partial penetration scenarios for the Marchwood Well

A range of short simulations, designed to model a series of penetration ratios, were undertaken to investigate the effects of partial penetration on drawdown and temperature change in a geothermal system using the Marchwood case study. Partial penetration occurs when the well screen is only open in part of the reservoir and the penetration ratio can be calculated as the length of the well screen divided by the thickness of the reservoir. In aquifers of greater thickness a smaller percentage of wellbore penetration is required, typically at the top, middle or bottom of the reservoir (Fig. 4.25). The different penetration ratios modelled showed an initial rapid depletion in head, increasing with smaller penetration ratios. The model was set up with the same conditions as the Marchwood case study (Fig. 4.26). The aquifer was penetrated from the top, starting with a

penetration ratio (Pr) of 0.2 and increasing the Pr by 0.2 until the well screen was fully penetrative (Fig. 4.27).
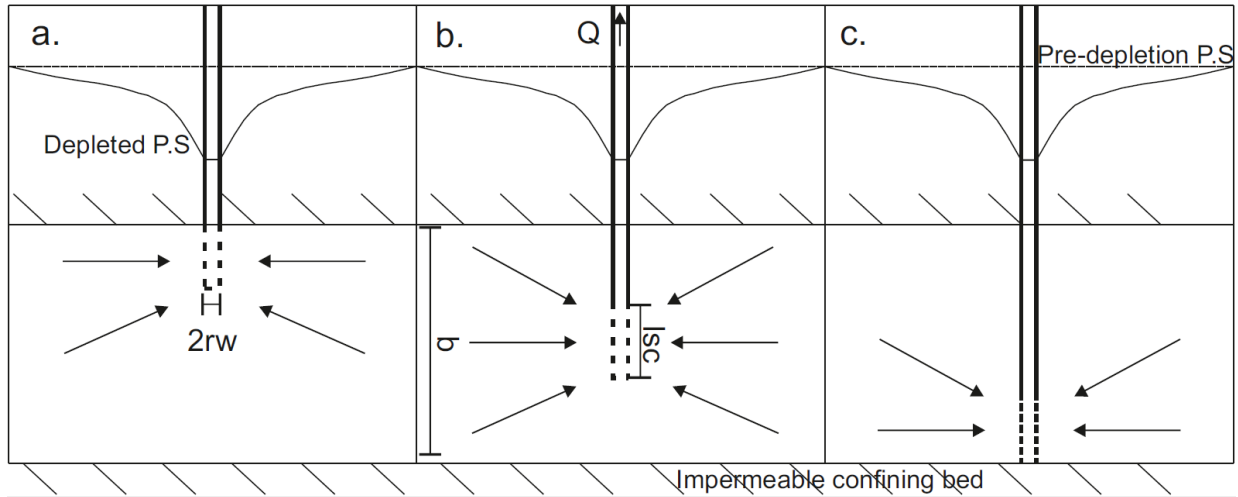
Figure 4.25: *Partial penetration scenarios as shown for varying locations in the aquifer; at the top (a), middle (b) and bottom (c). Abbreviations are as follows: length of well screen (lsc), radius of the well (rw), flow rate Q), potentiometric surface (P.S). Note scenario (a) is used for the comparison to analytical (i.e., well screen at top).*
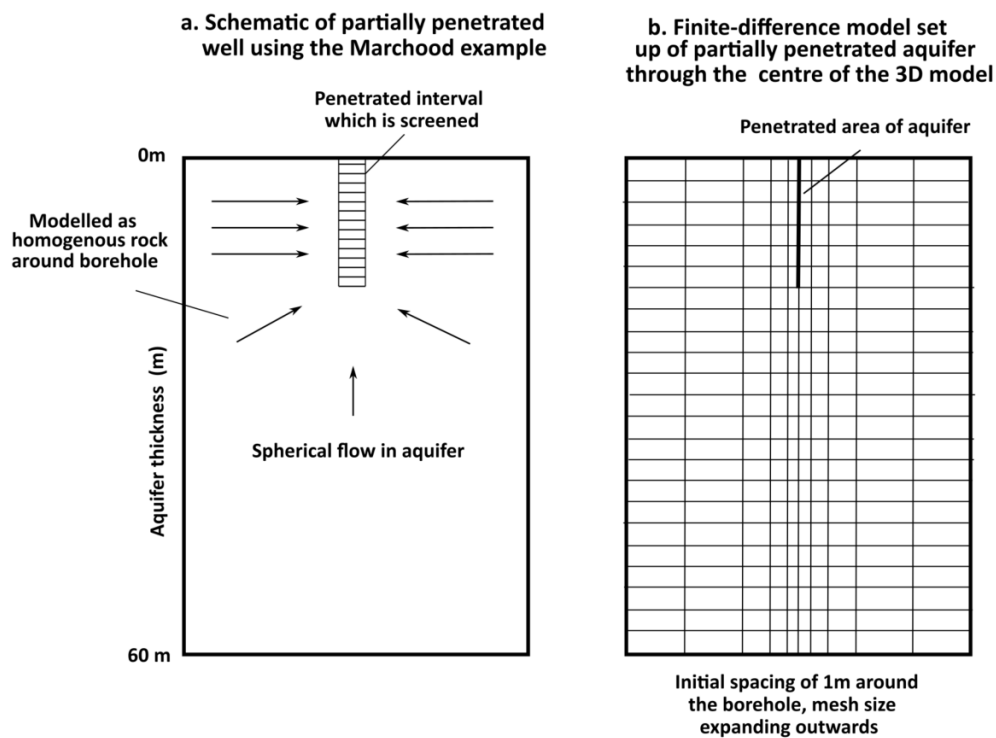
Figure 4.26: *(a) Schematic of the reservoir model used and (b) finite-difference mesh.*
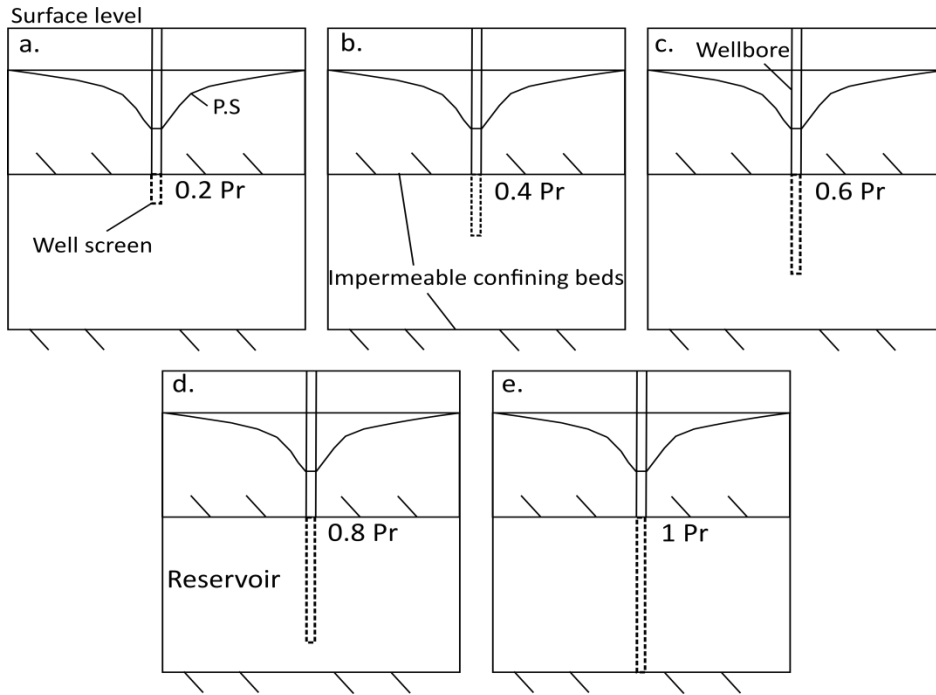
Figure 4.27: *Partial penetration scenarios modelled in comparison to the analytical (results in fig. 4.28 & 4.29).*
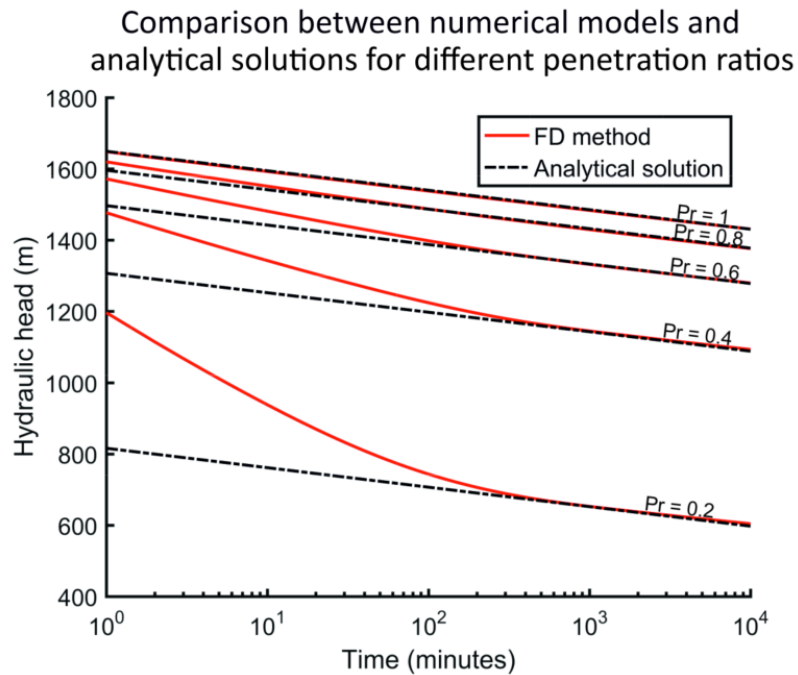
Figure 4.28: *Comparison of the finite-difference method (FD) with the analytical solutions for varying penetration ratios (Pr). The analytical solutions are based on the modified version of the Theis solution (Huisman, 1972).*

Drawdown in partially penetrative wells was validated by modelling an extended version of the Theis equation (Hantush, 1961). The analytical solution can be calculated by solving a series of equations, or by using tabulated approximations (Boonstra, 1992). For validation against the numerical solution in this study, the tabulated values from Huisman (1972) were used. It is important to note that Sternberg (1973) suggested that approximations from Brons and Marting (1961) were a closer match to the smaller radius-to-thickness ratios of Hantush (1962), whilst Huisman (1972) approximations were a closer fit for the higher values. In this example, the latter values were used due to the higher radius-to-thickness ratios.
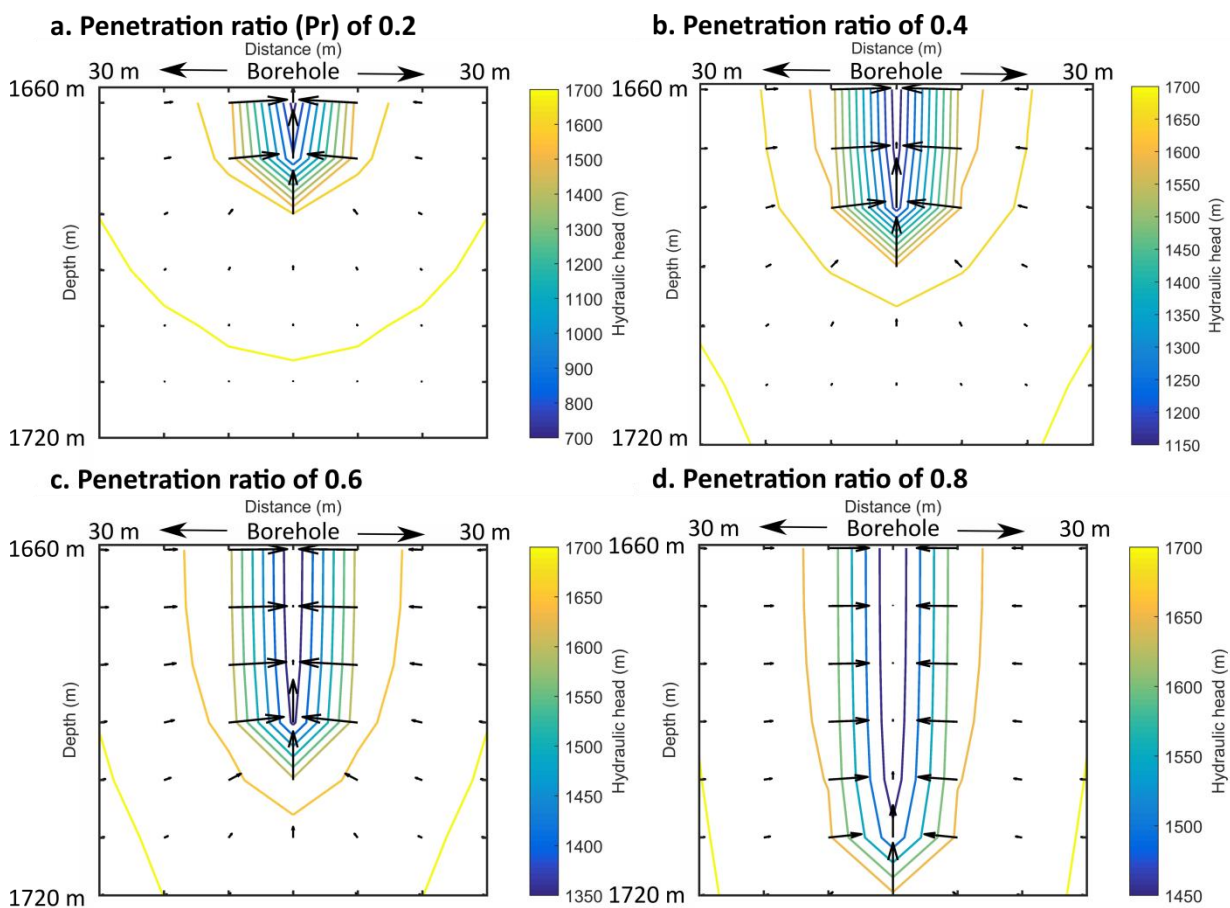
Figure 4.29: *Flow nets of different penetration ratios highlighted in Fig. 4.27 (a-d).*

The finite-difference model provided a near perfect fit to the analytical solution for values after ~500 minutes (Fig. 4.28). Most lifetime evaluations will focus on the drawdown at times greater

than a few hours so the method chosen here was deemed suitable. The initial difference in drawdown is likely to be due to the implementation of the steady-state Thiem approximation (equation 4.18), which estimates additional drawdown as a fixed constant. Similar errors are observed in industry software (MODFLOW (Konikow et al., 2009)). Flow in the models ranged from perpendicular to the well screen to semi-spherical (Fig. 4.29). Temperature change was minimal in the reservoir during the simulations, increasing with decreasing penetration ratios.

When the well screen (top location (Fig. 4.25a)) penetrated 40 % of the Marchwood reservoir, the change in temperature was 0.05 °C (Fig. 4.30). Over the course of a lifetime this could be far greater, particularly for thicker aquifers when the change in temperature between the upper and lower boundaries will be greater. The changes in temperature within the reservoir were also dependent on the position of penetration. Higher temperature contrasts were found proximal to the end of the well screen where the flow is no longer horizontal; this is an important aspect to consider and will affect the final production temperature. From the analysis of the Marchwood case study, it is shown larger penetration ratios can help to limit drawdown and by having the penetrative interval at the base of the aquifer hotter temperatures can be produced.
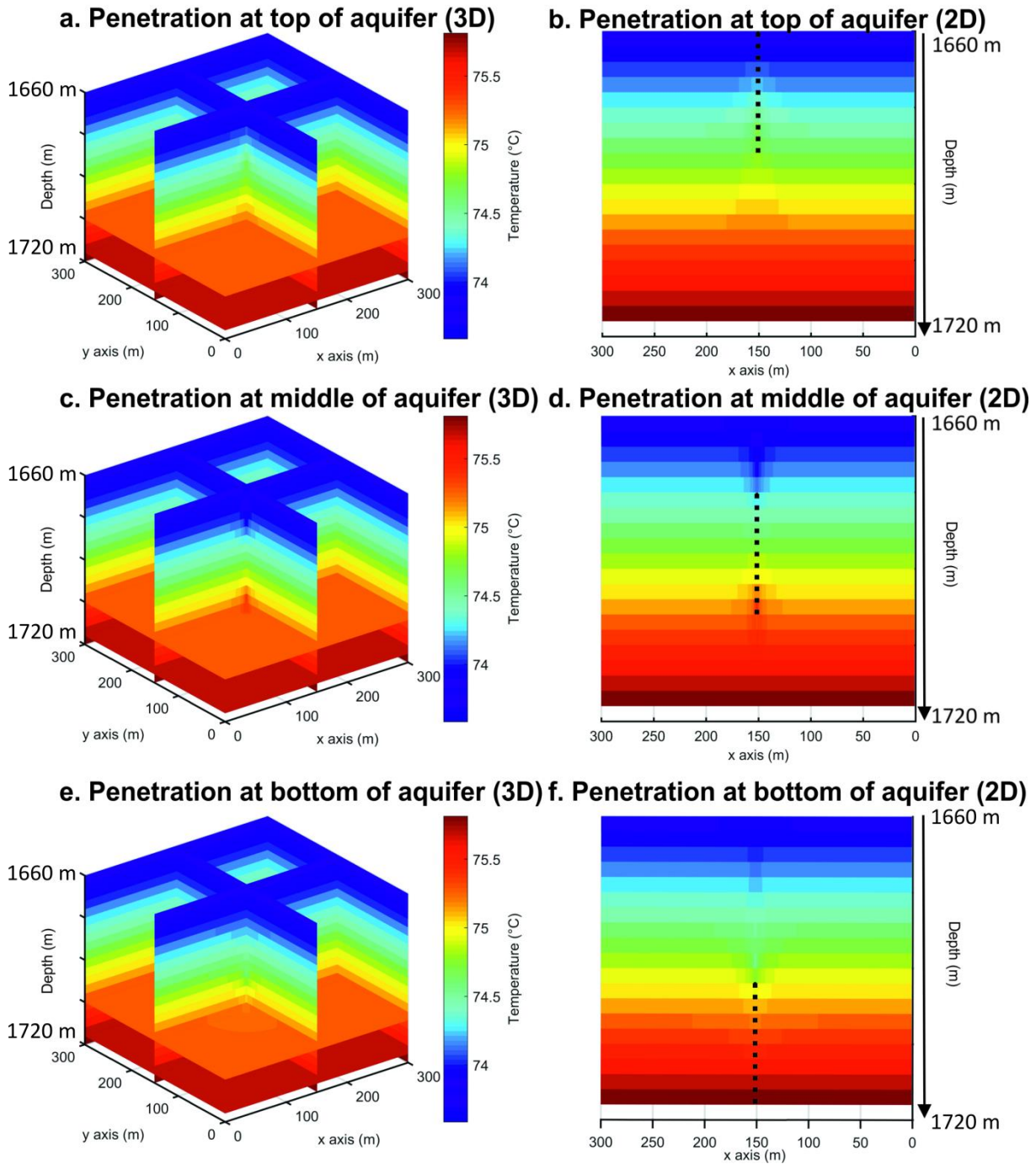
Figure 4.30: *Thermal plots for the partially penetrative well models (reservoir section only). (a and b) penetration at the top of the reservoir, (c and d) penetration at the middle of the reservoir, (e and f) penetration at the base of the reservoir. (b, d and f) are 2D vertical cross slices, with the dashed line highlighting the perforated interval. A penetration ratio of 0.4 was used for all the models illustrated. The PR is 0.4.*

4.4.4 Comparing model results to real data for the deep coaxial borehole heat exchanger

Field data from a test in Xi'an China was used as a comparison against the deep closed loop coaxial borehole heat exchanger (BHE) model (Fig. 4.31) (taken from Wang et al., 2017). This was due to the fact that no deep closed loop borehole heat exchangers currently exploiting geothermal resources exist in the UK. The study was undertaken for a duration of 4 days after 1 month of field tests (Liu et al., 2019), with physical parameters for the model highlighted in Table 4.7.

Parameter	Value
Thermal conductivity	0.6 (F) / 0.45 (IP) / 45 (OP) / 4 (G) / 4.5 (R)
Density	998.2 (F) / 4 (G) / 2551 (R)
Specific heat capacity	4182 (F) / 4 (G) / 1250 (R)
Mass flow rate	26.3 m³/h
Depth	2000 m
Diameter of pipe	110 mm (10 mm thickness) (IP) / 178 mm (9 mm thickness) (OP)
Thermal gradient	30 °C/km
Inlet flow temperature	17.6 °C
Field test outlet fluid temperature	26.6 °C
Field test transfer capacity	286.4 kW

Table 4.7: *Table of parameters taken from Wang et al. (2017). The average specific heat capacity, density and thermal conductivity are used in the model, with the confining rocks assumed isotropic and homogeneous. F = fluid, IP = inner pipe, OP = outer pipe, G = grout and R = confining rocks.*

To investigate the thermal performance of the coaxial BHE the heat load or thermal power (P) needs to be calculated (e.g., Dijkshoorn et al., 2013; Liu et al., 2019):

$$P = \rho_f c_f Q(T_{out} - T_{in}) \qquad\qquad 4.38$$
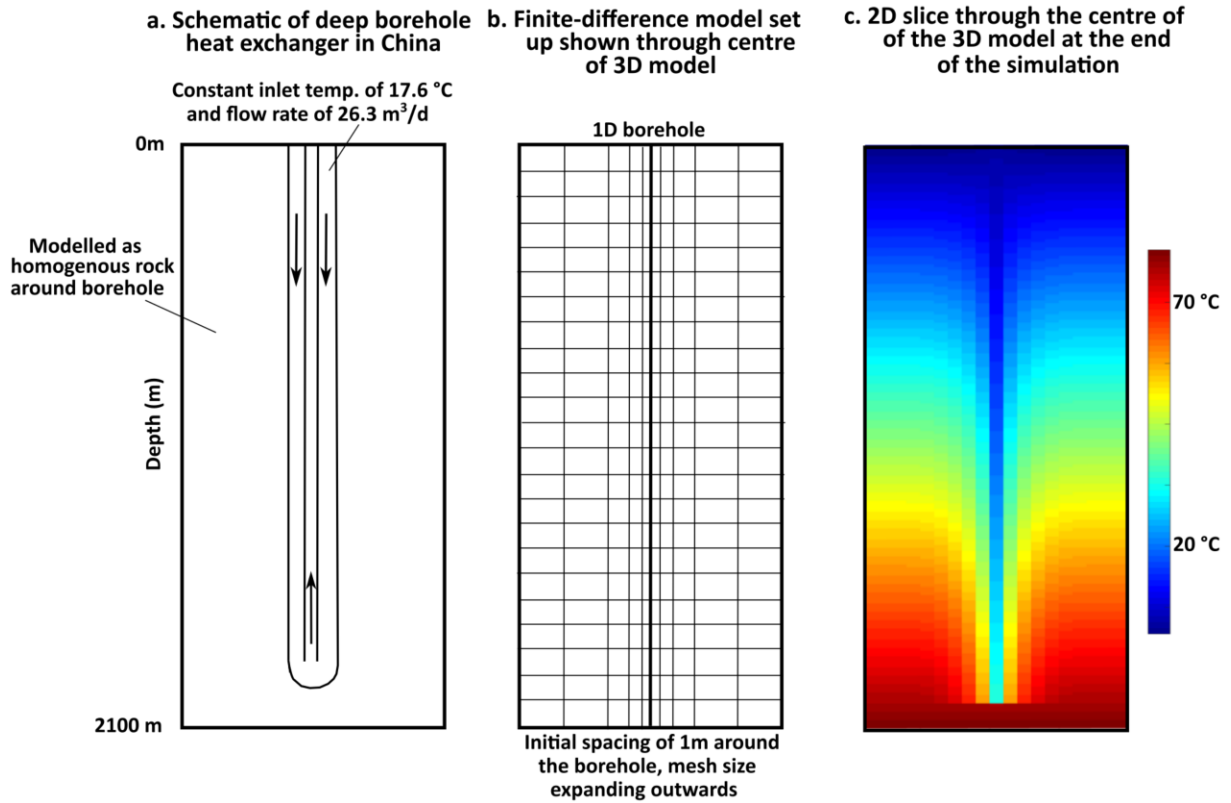
Figure 4.31: (a) Schematic of the deep borehole heat exchanger from China, (b) discretised finite-difference mesh and (c) temperatures in the surrounding rock after the simulation.

The heat loss ratio ($\propto$) can be established by (Liu et al., 2019):

$$\propto = \left(\frac{T_{base} - T_{out}}{T_{base} - T_{in}}\right) \qquad\qquad 4.39$$

where T_{base} is the temperature at the base of the borehole, T_{out} is the outlet temperature and T_{in} is the inlet temperature. Modelling undertaken by Wang et al. (2017) had a relative error of 12.6 % for the outlet temperature and 10.9 % for the heat transfer capacity. This corresponds to an average temperature and heat extraction of 27.9 °C and 317.8 kW (Fig. 4.32). In the model utilised in this study, the error was reduced for temperature, but slightly increased for thermal power.
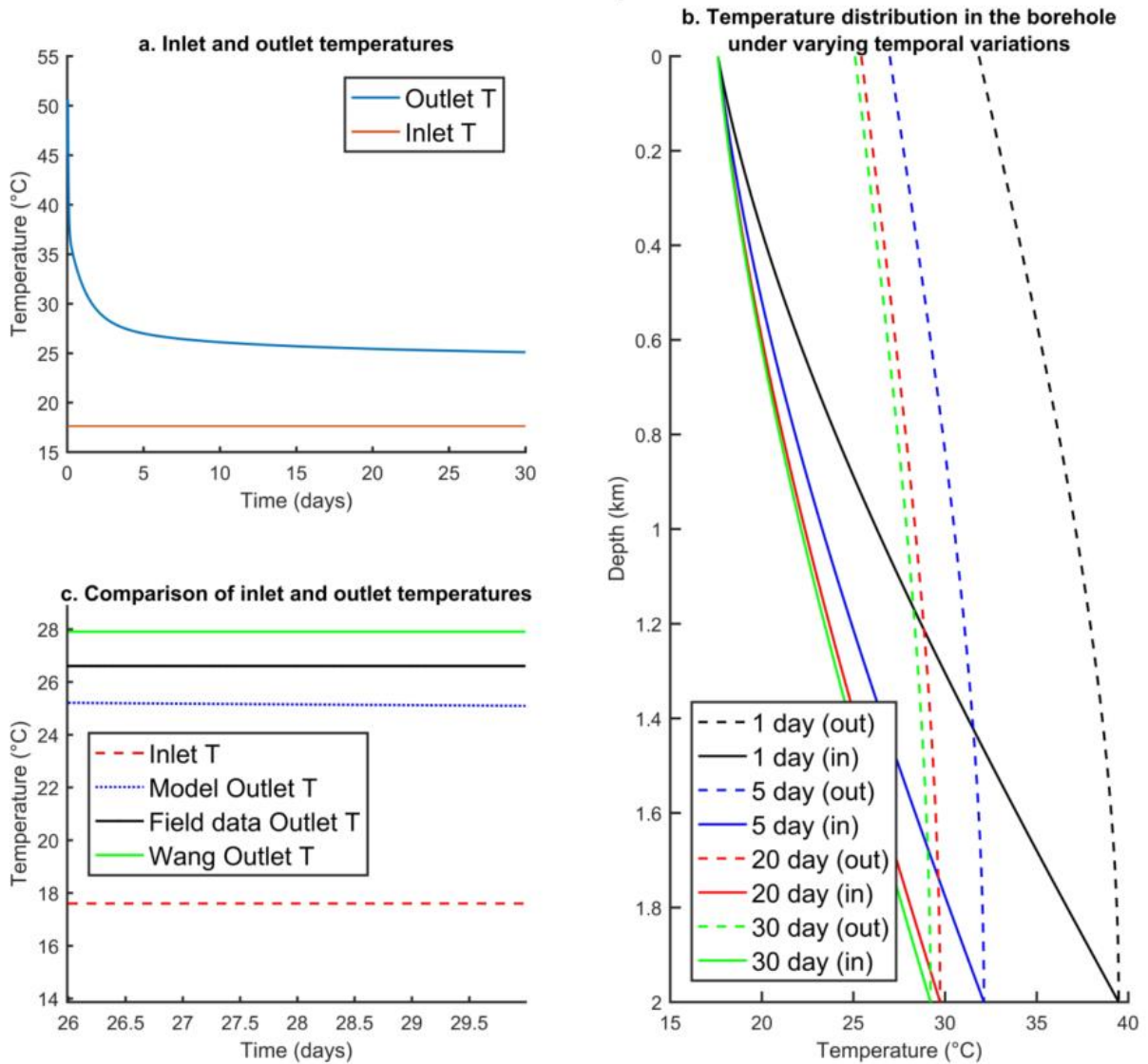
Figure 4.32: *(a) Modelled data for the China borehole heat exchanger study for a time period of 30 days, (b) comparison of inlet and outlet temperatures for varying time scales and (c) comparison of modelled results versus field data and other models.*

Most of the thermal interaction occurred in the first 10 days, with temperature rapidly increasing, and then decreasing (Fig. 4.32a and 4.32b). Over the final four days the average temperature calculated was 25.1458 °C, producing a heat load of 220.5 kW with a maximum heat load of 333 kW (Fig. 4.32c). This is similar to that from the field study, where the mean outlet

temperature was given at 26.6 °C and mean outlet power at 286.4 kW. The error for this was 5.5 % and 23 %, respectively. The error was less than that for the temperature predicted by Wang et al. (2017), and gives confidence for the accurate performance of the model. The lower prediction of temperature is attributed to low thermal conductivities encountered in the upper geological layers and higher thermal conductivities in deeper layers, leading to higher heat transfer at depth (Liu et al., 2019). Irregular flow rates and an unknown service regime for the month prior to recording may also influence the results. The heat loss ratio for the model utilised here was 0.338.

4.5 Future forecasting at Southampton for the Marchwood Well

In this section, the model's ability to forecast wellbore performance during production was tested under a range of wellbore configurations including borehole heat exchangers and standing column wells. The Marchwood Well was deemed unsuitable to be developed for a district heating scheme as a predicted drawdown of ~550 m was expected after 20 years of pumping, which was calculated by extrapolating a semi-log time-drawdown plot (Pr = 1). (Price and Allen, 1984). As a result, the Marchwood Well was used as an example of where different borehole configurations could allow heat to be extracted from the ground in an otherwise unsuitable development scenario. The alternate configurations allow high drawdowns to be mitigated as both borehole heat exchangers and standing column wells re-circulate fluid. Deep borehole heat exchangers circulate a fluid in a closed loop borehole (Fig. 4.33a). As the cold fluid moves downwards it warms under the Earth's natural thermal gradient and is then pumped back to the surface. The deep borehole heat exchanger modelled here involves fluid moving downwards in an annular space between an outer pipe and central pipe at slow velocities and then returning upwards in a narrow central pipe under high velocities. The standing column well involves the same configuration borehole; however, has the option to extract fluid from the aquifer through a screened/lined area which is open (Fig. 4.33b). Fluid is drawn in through the screened interval when not all the fluid is re-circulated in the wellbore,

causing an increase in the outlet temperature. This is commonly referred to as bleed. The borehole was modelled to be cased from the surface to the top of the aquifer.
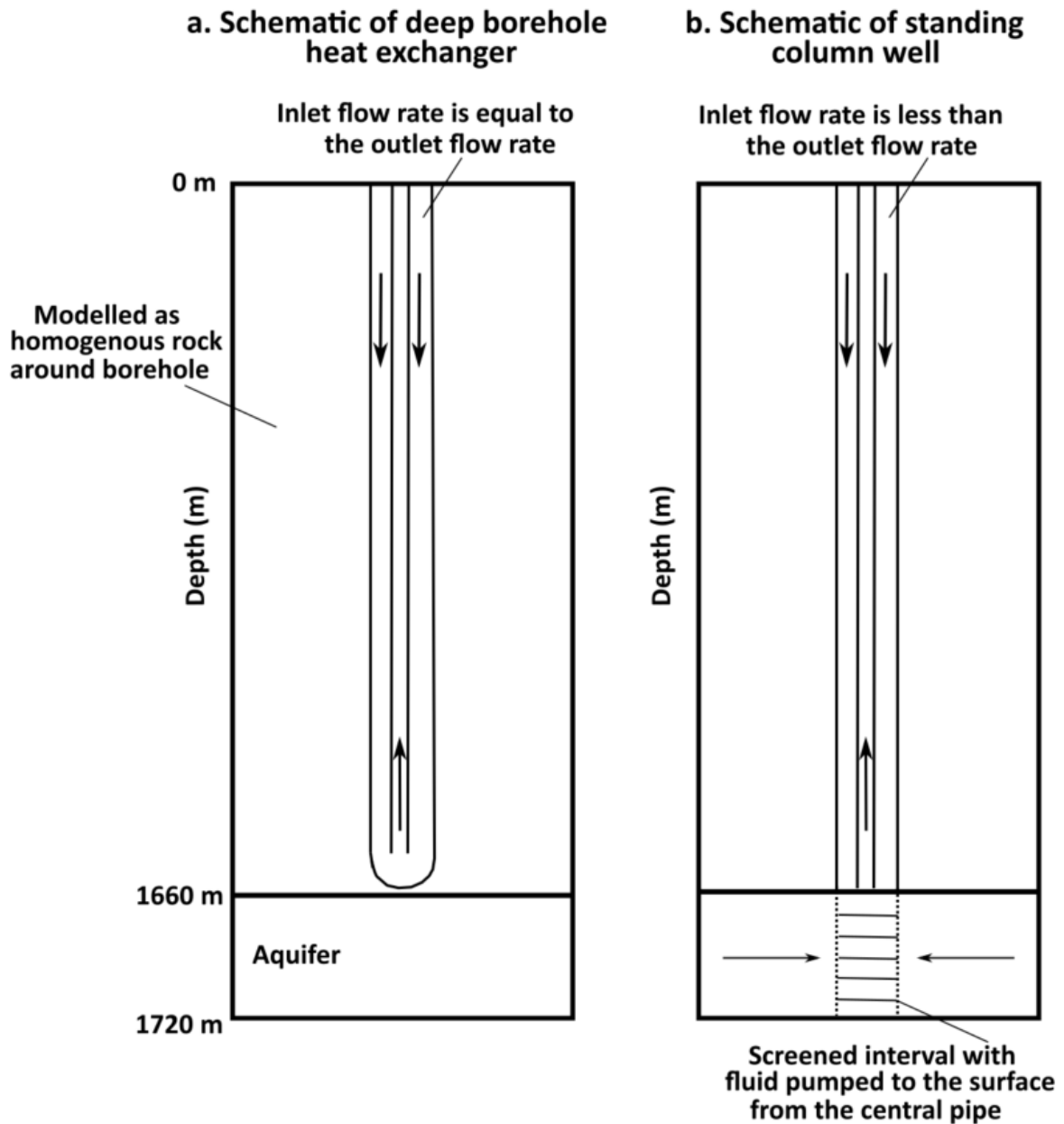
Figure 4.33: *(a) Schematic of the deep borehole heat exchanger modelled and (b) schematic of the standing column well.*

To optimise results and maximise the outlet temperatures for both the standing column well and borehole heat exchanger scenarios, the borehole was assumed to be insulated with a small

radius of the inner pipe to ensure higher velocities in the inner pipe than the outer pipe (Liu et al., 2019). The simulations used the same parameters as the Marchwood model (Sect. 4.4.1) and a series of short simulations were undertaken for a period of 4 months, which was considered the time period for peak demand in winter. The aims of this section were: to evaluate the effect of parameters (such as input temperature, ratio of inner pipe radius to outer pipe thickness, and flow rate) on outlet temperatures and heat load for borehole heat exchangers, to investigate the influence of different bleed ratios on outlet temperatures and heat load for standing column wells, to determine the highest heat load under optimal conditions for deep borehole heat exchangers and standing column wells, and to consider long term performance of different borehole configurations.

4.5.1 Application of deep coaxial borehole heat exchangers to the Marchwood Well

The influence of varying engineering parameters on the outlet temperatures and heat load were tested in this section. The parameters tested were input temperature, ratio of central pipe radius to outer annulus thickness and production rate. These parameters were all tested as they influence the amount of energy produced, allowing optimal conditions to be identified. Starting conditions used typical properties found in literature for similar systems. These included a constant input temperature of 30 °C (to reflect typical reject temperatures of district heat networks (Downing and Gray, 1986b)), an outer wellbore diameter of 0.15 m (e.g., Dijkshoorn et al., 2013) and an internal wellbore diameter of 0.08 m. The pipe thickness was set to 0.01 m (Wang et al., 2017), the grout surrounding the wellbore at 0.04 m and a flow rate of 3 l/s was implemented (Law et al., 2015). Under these initial conditions the outlet temperature at the end of 4 months was 31.4245 °C, giving a heat load of 17.949 kW. Most of the heat transfer in the borehole occurred in the first 20 days, with a rapid increase in the outlet temperature in the first hour, followed by a rapid decrease (Fig. 4.34).
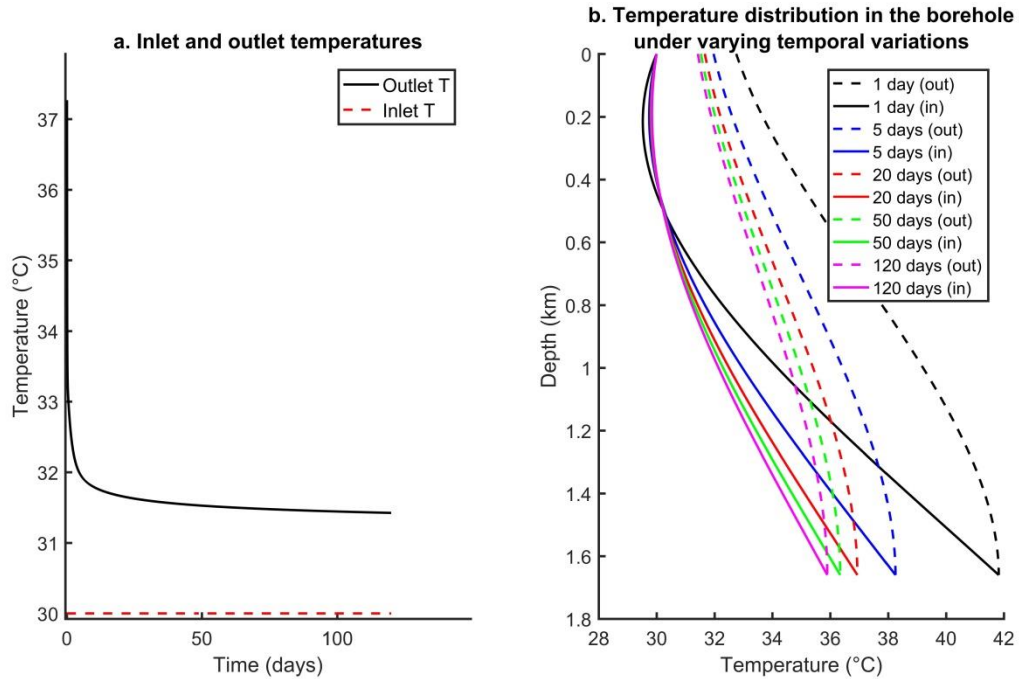
Figure 4.34: *(a) Inlet and outlet temperatures used in the study with a constant inlet temperature of 30 °C and (b) the spatial temperature change in the inlet and outlet pipes within the borehole heat exchanger for various times periods (ranging from 1 day to 4 months).*

4.5.1.1 The effects of different input temperatures on a deep coaxial borehole heat exchanger

The inlet temperature of the borehole heat exchanger (BHE) was gradually reduced (starting at 50 °C), with the aim of increasing the thermal power of the BHE. The inlet temperature into the BHE had a significant effect on the outlet temperatures and heat load. In general, lower inlet temperatures produce a greater heat load. This was due to there being a larger difference between the inlet and outlet temperatures, and thus a larger thermal power (Eq. 4.38). Temperatures were reduced incrementally by 10 °C until the inlet temperature was close to ambient conditions (20 °C).

At the end of the simulation the minimum and maximum outlet temperatures from the BHE were attained at 23.1 °C and 48.1 °C for inlet temperatures of 20 °C and 50 °C, respectively (Fig. 4.28a). Colder inlet fluids were heated giving larger outlet than inlet temperatures. As shown in figure 4.35a, the inlet temperatures of 20 °C, 30 °C and 40 °C show an initial rapid increase in outlet

temperature in the first few days, followed by a gradual reduction in temperature. This shows the borehole cooling with time under the influence of the cold inlet temperatures. For the 50 °C inlet scenario the outlet fluid rapidly warmed, followed by a gradual increase in temperature after the first few days of production. This is because the fluid was warming the shallow sub-surface and the fluid in the borehole subsequently cooled. The maximum amount of energy produced over the duration of the simulations was for the 20 °C inlet temperature, producing 4.46×10^{11} J of energy or a heat load of 39 kW (at the end of the simulation). At the start of the simulations when the temperature difference between the inlet and outlet temperatures was greatest (Fig. 4.35a) a higher heat load was achieved.

4.5.1.2 The effects of different volumetric flow rates on a deep coaxial borehole heat exchanger

Different volumetric flow rates were modelled to investigate the sustainability of higher flow rates in a borehole heat exchanger (i.e., if higher flow rates can produce high temperatures for a sustained period). The volumetric flow rate directly relates to the amount of thermal power that can be produced (Eq. 4.38) (Dijkshoorn et al., 2013), thus higher flow rates result in a higher power output. The flow rates tested were increased from 0.25 l/s until the final outlet temperature after 4 months simulation was less than the previously tested flow rate, this occurred when the flow rate reached 5 l/s. This approach was undertaken to find the optimal flow rate in the borehole and higher flow rates were likely to be unsustainable for long periods due to rapid cooling of the circulatory fluid.

Volumetric flow rates which were less than 1 l/s showed a rapid increase in outlet temperature within the first 5 days, followed by an extremely slow increase during the following 4 months (Fig. 4.35b). When the volumetric flow rate was modelled as less than 1 l/s the outlet temperature was always less than the inlet temperature and thus no energy was extracted. This was due to the low velocity in the central pipe allowing the fluid to cool as it approached the ground

level. When investigating flow rates >1l/s the outlet temperature for the duration of the simulation always exceeded the inlet temperature. In the first few days there was a rapid increase in outlet temperature, followed by a gradual cooling (Fig. 4.35b). At the end of the 4 month simulation the highest outlet temperature (31.4 °C) was produced under the 3 l/s flow rate. The reason for a lower final outlet temperature for the 5 l/s scenario was due to the higher velocity in the outer annulus resulting in less time for the surrounding rock to warm the fluid, thus cooling the borehole. Although this shows the 3 l/s flow rate may be more sustainable for longer periods the higher 5 l/s flow rate was able to produce a higher heat load. The heat load increased from 17.6 kW to 21 kW for 3 l/s and 5 l/s, respectively.
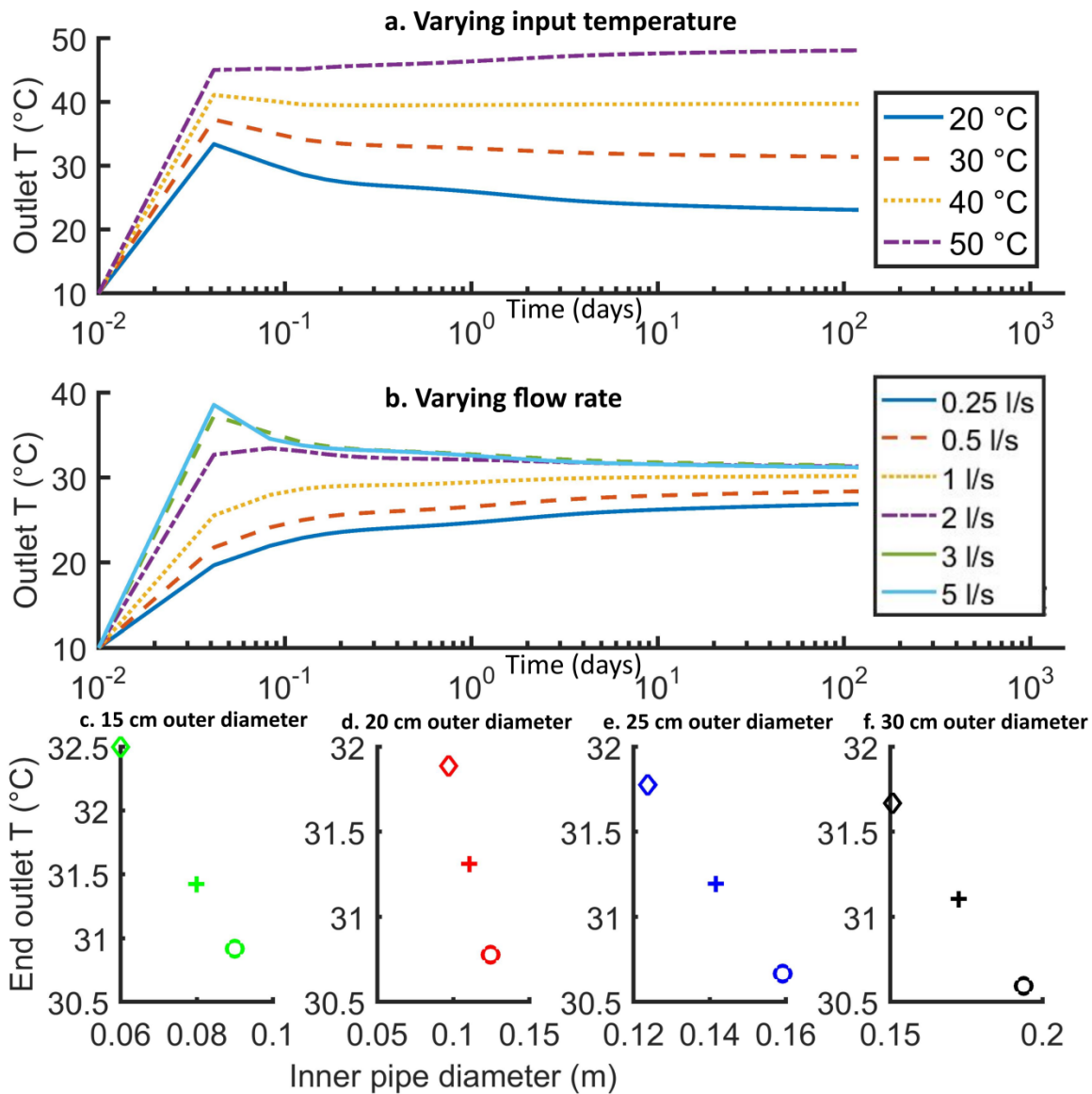
Figure 4.35: *Modelling of a closed loop coaxial BHE adapted for the Marchwood Well: (a) the effect of different input temperatures on outlet temperature, (b) the effect of different flow rates on outlet temperature, (c - f) the effect of different outer pipe and inner pipe diameters on end outlet temperature, recorded at the end of the simulation. The different shapes represent different outer to inner pipe diameter ratios. The diamond is 0.54, the cross is 0.62 and the circle is 0.69.*

4.5.1.3 The effects of different borehole diameters on a deep coaxial borehole heat exchanger

Different ratios of the inner pipe radius to outer annulus thickness were modelled for a range of outer pipe diameters (Fig.4.35c-f). A lower ratio (i.e., smaller production pipe radius to annulus

thickness) resulted in faster velocities in the central outlet pipe, which led to advective vertical heat transfer being dominant – with less interaction with the outer pipe. In contrast, the outer velocity was slower leading to increased thermal interaction with both the central pipe and outer confining rocks. As such, higher outlet temperatures were produced. Conversely, by having a larger inner pipe and smaller annulus area in the outer pipe, lower production temperatures were attained. The effects of different ratios were modelled for a range of fixed outer wellbore diameters to test the effects on both large diameter borehole and slim-borehole designs. The smallest inner pipe radius of 0.03 m had a velocity of 1.07 m/s, whilst the largest (0.09 m) had a velocity of 0.12 m/s.

The outlet temperatures were dependent on both the size of the inner pipe and outer pipe diameter. Smaller inner pipe diameters and smaller ratios (i.e., smaller inner pipe to outer annulus) produced higher outlet temperatures. When the outer annulus cross sectional area was larger than that in the central pipe the circulatory fluid was warmed with increasing depth from the outer rock, but also from the high temperature fluid in the central pipe. A borehole diameter of 0.15 m and inner pipe diameter of 0.05m were found to be optimal in this study (Fig. 4.35c). At the end of the simulation these optimal settings produced an outlet temperature of 32.5 °C and heat load of 31.5 kW. The results in this study are in agreement with that of Liu et al. (2019) who suggested large outer pipe diameters and small inner pipe diameters are able to achieve high outlet temperatures. They did however, suggest the feasibility of having larger borehole diameters would increase the initial costs when drilling a borehole and therefore, may not be practical.

4.5.2 Application of deep standing column wells to the Marchwood Well and varying bleed flow

An open standing column well (SCW) involves extraction and injection into the reservoir from a single well. Typically, under a scenario with no bleed, most of the water injected into the aquifer is re-circulated back into the well, leading to greater thermal drawdown and a reduction in production temperature (similar to that of a coaxial BHE). By adding periods of bleed, where re-circulation of

fluid into the aquifer is less than that being extracted, increases in the production temperature can be achieved with bleed levels of 10 and 50% simulated for production rates of 3, 5 and 7 l/s. Bleed flows are usually less than 25 % as this reduces the quantity of fluid that is needed to be disposed of, whilst maintaining production temperatures. The largely atypical 50 % bleed flow for standing column wells was modelled as it was assumed fluid disposal could be simple and direct into the sea, similar to the current wastewater disposal scheme at Southampton. The tested flow rates were lower than that of the production tests for the Marchwood Well to ensure that any thermal and hydraulic interactions with the currently producing Western Esplanade Well would be minimal. The configuration of the borehole was kept the same as for the closed loop coaxial BHE. Again all simulations were undertaken for four months with the bleed rate kept constant for the duration. Note that typically most periods of bleed will vary annually, to coincide with high and low demand periods.

The final minimum (10% bleed) and maximum (50 % bleed) outlet temperatures for flow rates of a) 3 l/s were 38.73 °C and 45.72 °C, b) 5 l/s were 39.86 °C and 48.26 °C and c) 7 l/s were 38.89 °C and 48.79 °C, respectively (Fig. 4.36). The results showed a rapid increase of outlet temperature, followed by a period of gradual cooling. Under a bleed flow of 50 % the final outlet temperature was highest for the production rate of 7 l/s, whilst for a bleed flow of 10 % the highest outlet temperature was for 5 l/s. This showed cooling was rapid when bleed was low and the larger flow rate of 7 l/s cannot be maintained for long periods. For flow rates of 7 l/s and 50 % bleed flow a heat load of 552 kW was produced. For the same scenario with 10 % bleed flow 261 kW was attained. This showed a significant increase of the energy produced in comparison to a deep closed loop borehole heat exchanger. This was due to an increased flow rate and higher temperatures sustained for longer periods.
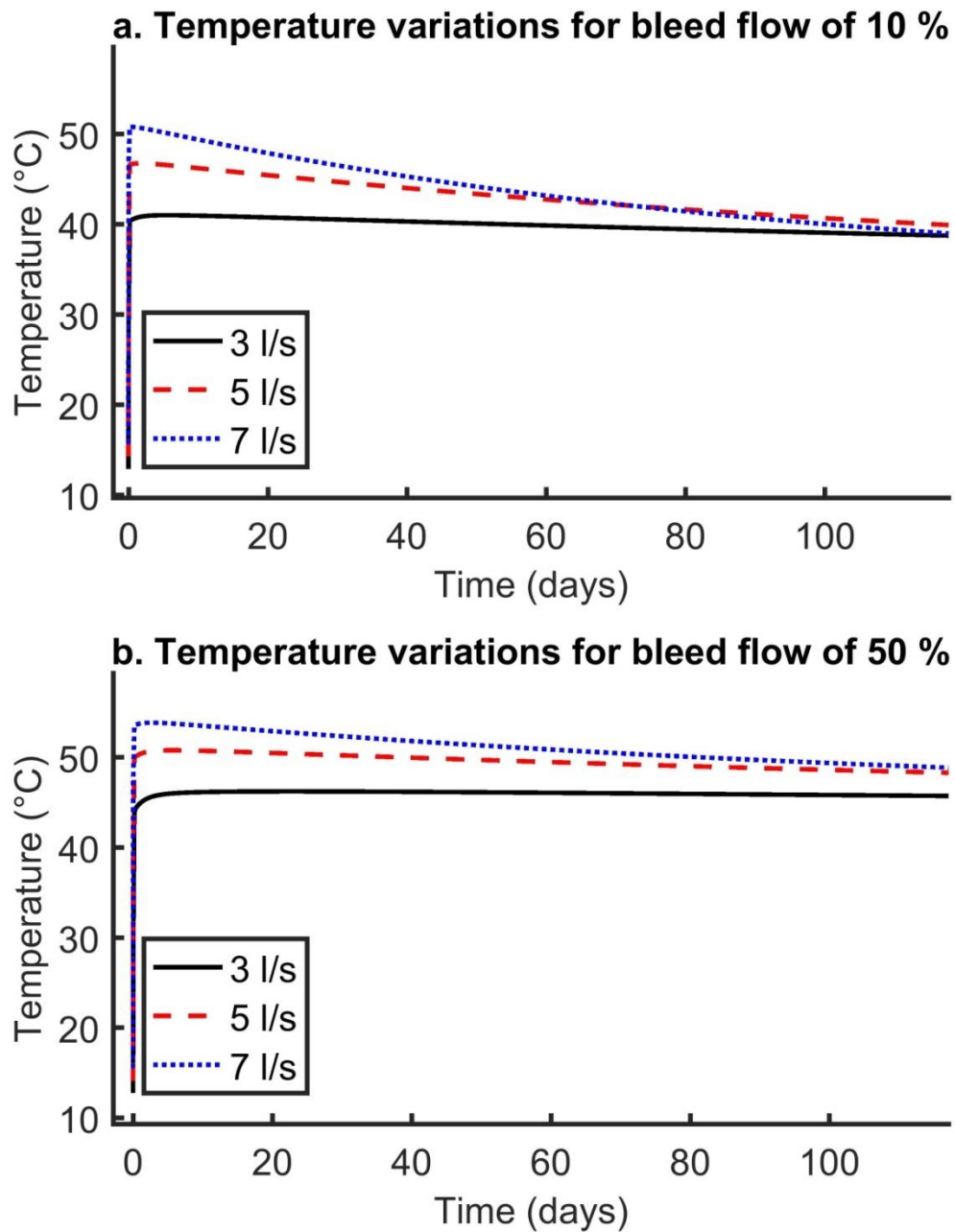
Figure 4.36: Temporal variations of the outlet temperatures for production rates of 3, 5 and 7 l/s for bleed flow of *(a) 10 % and (b) 50%.*

4.5.3 Long term simulations of the Marchwood Well

To evaluate whether the Marchwood Well could be converted/repurposed to an open SCW or closed BHE system for long-term production, models were run for a 20-year production cycle.

Although production would vary annually to meet demand, under the scenario here the production rate was set as a constant for the 20 year duration. The modelled conditions were: a ratio of 0.54 for the inner pipe radius to outer annulus thickness (for both configurations), an inlet temperature of 10 °C and a flow rate of 3 l/s for the borehole heat exchanger and an inlet temperature of 20 °C and a flow rate of 7 l/s for the standing column well. These were the optimal conditions found in section 5.1 and 5.2, although a slightly lower inlet temperature was used for the borehole heat exchanger to extract more energy and the bleed flow for the standing column well was set at 25 %, which was lower than the optimal amount of bleed identified in the short term simulations due to typical bleed rates being less than 25 % of the pumping rate (Spitler et al., 2002).

Lower outlet temperatures were produced for both BHEs and SCWs (in comparison to the standard configuration well – i.e., when fluid is extracted only) due to lower flow rates and circulation of fluid at cold temperatures in the wellbore. For the open SCW with a bleed flow of 25 %, the final production temperature was 30.17°C and 1.95×10^{14} J of energy was produced (Fig. 4.37 and 4.38). For a closed loop coaxial BHE, the final production temperature was 15.01 °C and 4.12×10^{13} J of energy were produced. If the exploratory well (Fig. 4.17 & 4.19) at Marchwood produced fluid under the same conditions as during exploration the final production temperature would be 72.28 °C, giving a total energy output of 3.2433×10^{15} J.

The significant reduction in energy in the BHE and SCW in comparison to the standard configuration model was largely due to the lower production temperatures and reduction in volumetric flow rate (i.e., 3 l/s for the coaxial BHE, 5 l/s for the SCW and 29 l/s for the normal configuration). For the open SCW, the zone of influence after 20 years (to 1 m of original head) reached a distance of 1.5 km radially around the well screen. This would be likely to have a minor influence on the Western Esplanade Well which is situated 1.85 km to the northeast. The zone of influence may also encounter hydraulic interactions with the boundaries of the interpreted wedge

shape geometry of the aquifer (Barker et al., 2000). The large zone of influence and interactions with the aquifer boundary contradicts research by Law et al. (2015), who suggested SCWs can be utilised in almost any geological scenario. In this case, the model showed significant hydraulic interactions may occur within the reservoir.
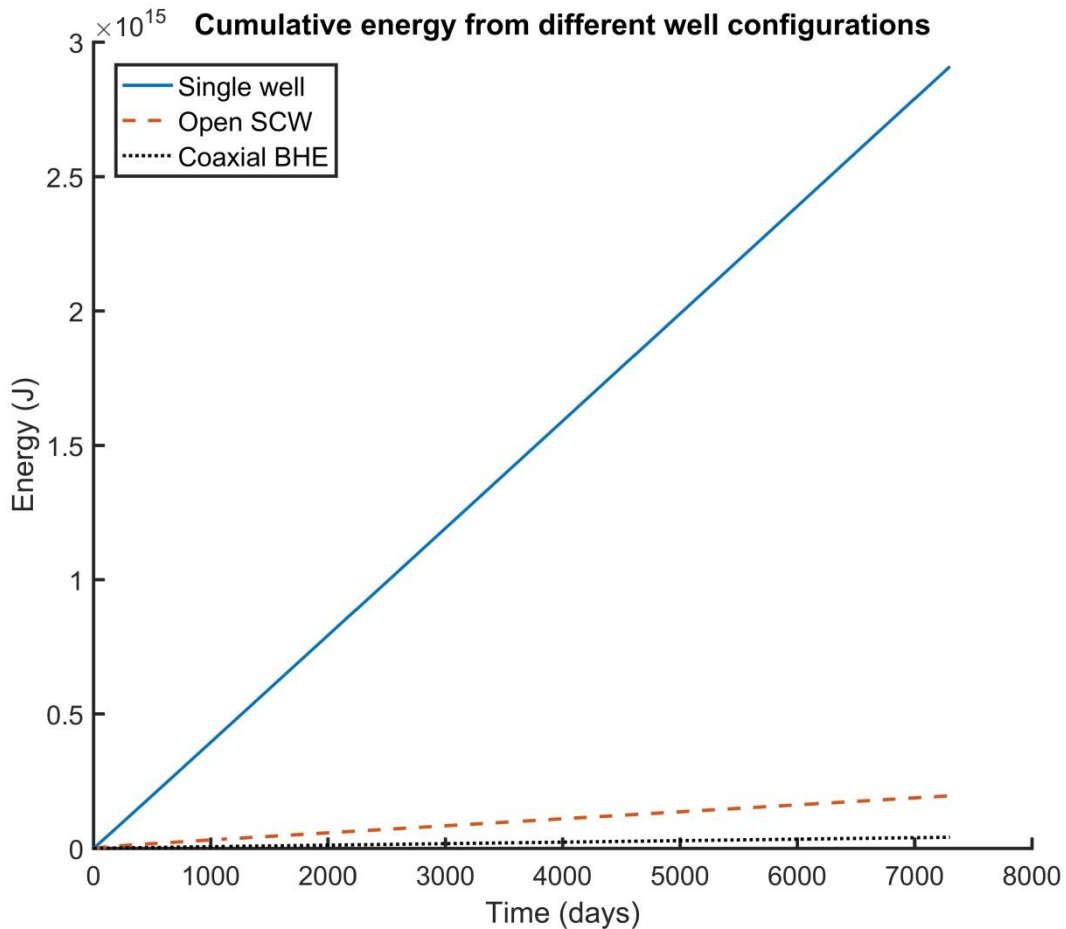
Figure 4.37: Ene*rgy produced for standing column wells (open and closed) and the normal configuration single well for the Marchwood case study. The open SCW has a consistent bleed flow of 25 %.*

The final thermal power output (Fig. 4.38) for each scenario was 63 kW (coaxial BHE), 299 kW (SCW) and 5.2 MW (the standard configuration (Fig. 4.17 & 4.19)). From the results, it seems apparent that an open well would be more beneficial due to the greater amount of thermal power and energy produced. The lack of fluid disposal costs, reduced risk of hydraulic interactions in the

reservoir, minimal operating costs and the option of having periods of bleed flow with minimal geological risk, may make either the SCW or coaxial BHE option more desirable and sustainable. It is also worth noting that periods of bleed are likely to be matched to periods of high demand, with no bleed for the majority of operation. This would lead to a reduced risk of interactions with the Western Esplanade Well and lateral aquifer boundaries.
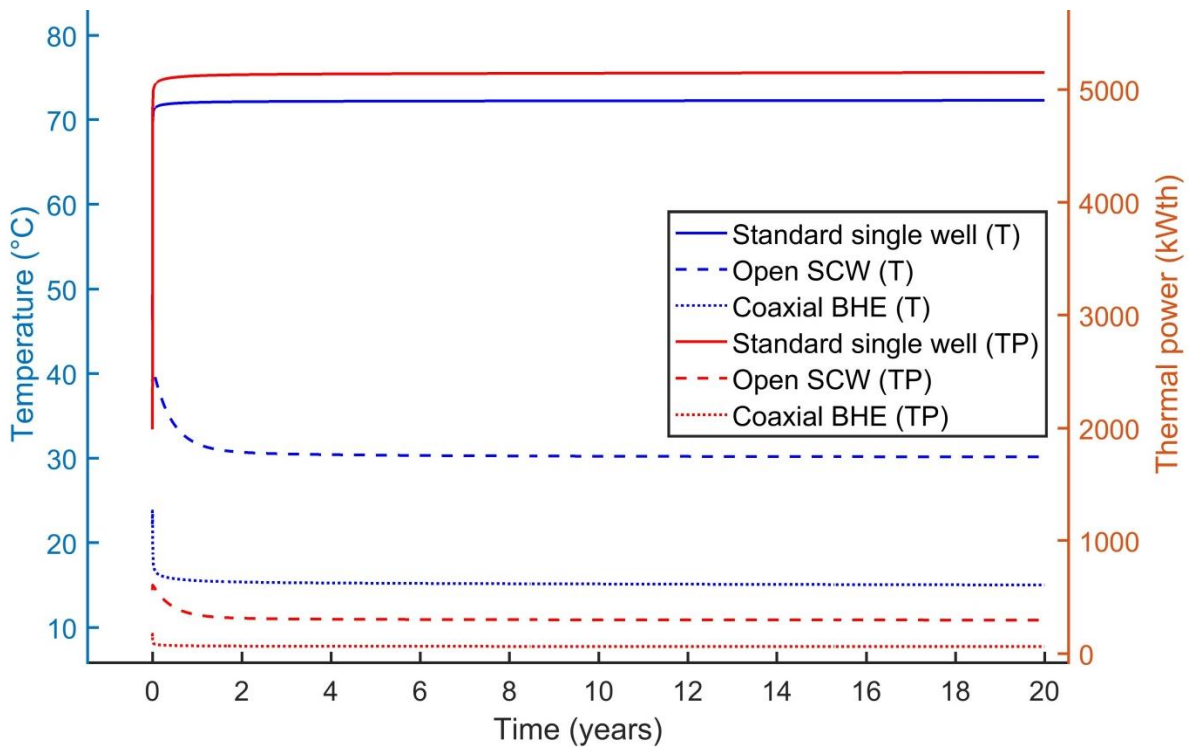
Figure 4.38: *Outlet temperature and thermal power produced for standing column wells (open and closed) and normal configuration single well for the Marchwood case study example. TP is thermal power and T is for the outlet temperature.*

Further analysis was undertaken using optimal conditions derived from other studies to assess the likely performance gains. A lower thermal conductivity was set for the inner pipe of 0.0001 W/m/°C (Dijkshoorn et al., 2013) and an even smaller central pipe to annulus ratio, where the inner pipe diameter was reduced to 0.05 m (Liu et al., 2019). The closed loop BHE model had an increased outlet temperature of 18.1 °C after 20 years. The total energy produced also increased to 6.69 x 10^{13}

J and the heat load produced was 102 kW. The heat loss ratio was also extremely small at 8 x 10^{-5}. Similarly, the performance of the SCW was improved with the final outlet temperature being 31.2 °C, producing a total of 2.2 x 10^{14} J of energy. The final heat load was 331 kW.

From the results it can be seen that inclusions of a lower thermal conductivity inner pipe and further reductions of the central pipe diameter can increase the performance of the Marchwood Well. For the coaxial BHE, the performance increased significantly (increased outlet temperature and heat load by 21 % and 62 % respectively), whilst the effect on the SCW was less prominent (increased outlet temperature by 1 % and increased heat load by 11 %). The smaller influence on SCWs was due to the interactions and input of hot geothermal fluids from the aquifer. It must also be noted that higher velocities in the central pipe can reduce the effect of low thermal conductivities (Holmberg et al., 2016).

4.5.4 Impact of energy demand on modelled well performance

Typically, when using a heat exchanger or pump in shallow geothermal BHE schemes a known priori of the heat load is given, resulting in a constantly changing inlet temperature being observed (Nabi & Al-Khoury, 2012b). The impact of this on the simulated Marchwood BHE was modelled by altering the inlet temperature based on the power demand (Eq. 4.38).

Power inputs of 20, 30 and 40 kW were modelled for 1 month and the results show that the inlet temperature changes had a significant effect on the outlet temperature (Fig. 4.39). The low power demands (20 and 30 kW) were all met, however, power demands of over 40 kW are likely to be unattainable for long periods of time due to the inlet temperature dropping towards a temperature approaching 0 °C (freezing). Faster flow rates approaching 5 l/s may allow for increased power production but are unlikely to be sustainable over time. The final outlet temperatures for each case (20, 30 & 40 kW) were 28.34 °C, 24.14 °C and 19.93 °C, respectively (Fig. 4.39), with an increased cooling of the outlet temperature observed with an increased thermal power output (Fig. 4.40). The

heat loss ratio also increased with higher heat loads (0.71, 0.76 and 0.86 for 20, 30 & 40 kW, respectively). The relatively poor results for the closed loop BHE may make a reduced flow rate standard single well or open SCW more viable for schemes with higher, fluctuating energy demands.
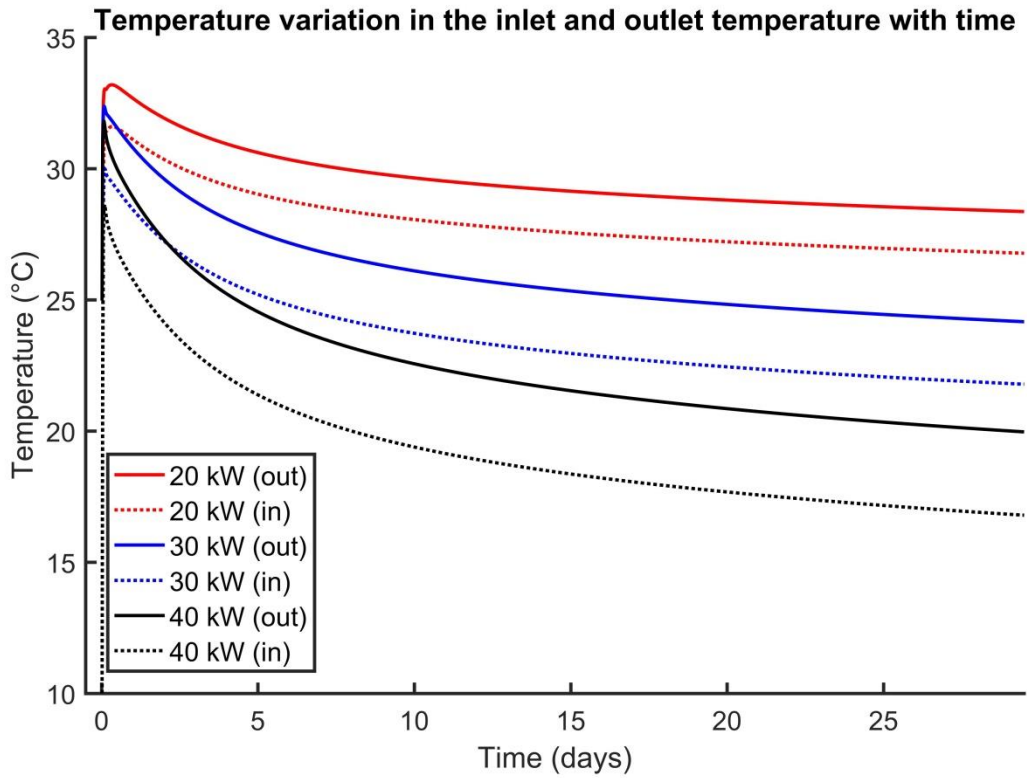
Figure 4.39: *Temporal changes in inlet and outlet temperatures for pre-defined power demands of 20, 30 and 40 kW.*
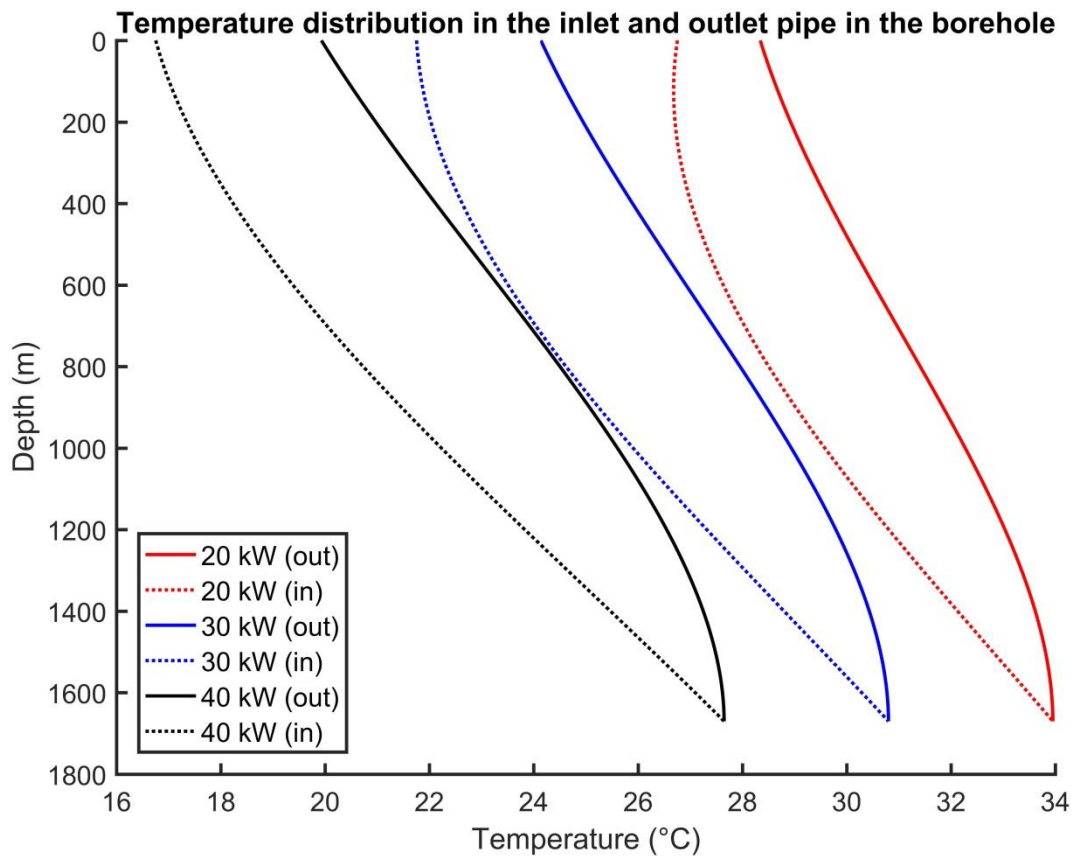
Figure 4.40: *Spatial changes at the end of the simulation (1 month) for the inlet and outlet pipe temperatures for a pre-defined power of 20, 30 and 40 kW.*

4.6 Model limitations

The model is only suitable for low-enthalpy systems (<100 °C) consisting of solid and liquid phases, and excluding any water content in the form of vapour. A key problem with the model (and others currently available), is that for fully penetrative wells the temperature in the reservoir is averaged and does not change with time. In most cases where the well is fully penetrative, the reservoir will be relatively thin and temperature change will be minimal; mostly as a result of heat loss through the wellbore, which was modelled in this study. With partially penetrative models, however, temperature can be predicted in the reservoir.

Another limitation is the physical description of the model which neglects deformation, and changes in both viscosity and density. Temporal evolution of density and viscosity is incorporated into the model in chapter 6, however, is anticipated to have a minor effect when no hot or cold fluid is injected into the aquifer.

The model also only accounts for homogenous reservoirs without a complex architecture (i.e., horizontally layered rocks). This model is suitable for initially assessing the lifetime of a geothermal system based on hydraulic head and production temperature but does not take into account heterogeneity. Although the model used here has not been discretised to account for heterogeneity, techniques similar to Cattaneo et al. (2015) for estimating head between nodes can be used in further work.

Summary

The aims of this chapter were to design and validate a numerical model for single well systems, and to investigate the potential of different single well configurations for deep geothermal systems. Standard configuration, coaxial borehole heat exchangers and standing column wells have been modelled for the Wessex Basin (Southampton Marchwood and Western Esplanade wells) as a comparative case study. This is the first time open and closed loop borehole heat exchangers have been modelled for the Basin, with a sensitivity analysis highlighting that the ratio of the internal pipe radius to the outer pipe thickness, flow rates and input temperatures should be carefully considered in order to maximise energy extraction. The results showed that the possible re-purposing of the Marchwood Well could allow further contributions to the district heating network from either an SCW or BHE with minimal hydraulic / thermal interaction expected with the currently operating Western Esplanade Well. They also showed that standing column wells could be beneficial for low-cost, geothermal schemes in Mesozoic Basins, whilst coaxial borehole heat exchangers may be used in almost any geological setting.

In later chapters, the model will be tested for other Mesozoic basins to investigate the potential of single well schemes for direct heat use. As such, the model is ideally suited for optimising the design of coupled geothermal district heating schemes where the economic risk factors (e.g., energy capacity, resource longevity, etc.) can be evaluated and realised ahead of costly physical investigations, allowing the method of extraction to be determined in advance. It also provides urban planners with tools to map low-carbon energy supply to future residential and commercial areas.

CHAPTER 5 - A SENSITIVITY ANALYSIS OF A SINGLE EXTRACTION WELL FROM DEEP, GEOTHERMAL AQUIFERS IN THE CHESHIRE BASIN, UK

This chapter investigates the effects of different geological and engineering parameters on the performance of a single producing geothermal well in the Crewe area of the Cheshire Basin by comparing the supply of geothermal energy to local heat demand. In addition, this chapter also explores ways to mitigate poor geological parameters at depth using engineering parameters. Seasonal fluctuations in production were also modelled.

5.1 Introduction

In this chapter, the explicit numerical model developed in chapter 4 is used to investigate the depletion, recharge and recovery of geothermal resources from the Collyhurst Sandstone Formation based on a single extraction well under varying geological and engineering scenarios. Permian aeolian to fluvial sandstones buried at depths of 2.8 - 3.5 km were investigated (Figs. 5.1a & 5.1b) due to their favourable temperatures (up to 100 °C) (Downing and Gray, 1986b; Barker et al., 2000; Busby, 2010, 2014). The low-enthalpy energy in the Mesozoic rocks in the Cheshire Basin and earlier Palaeozoic rocks can be used for direct heat use as a district heating scheme.

Currently, the geological risks associated with developing a geothermal scheme in the Cheshire Basin are too high for investors and this research aims to bridge this gap by presenting realistic results for a single well scheme under varying physical and engineering parameters, highlighting the key areas of risk in the basin and how they can be mitigated. This is vital for decision makers in the local authorities who wish to exploit the energy through a district heat network. The results are also of importance to other low-enthalpy, single well geothermal schemes targeting thick aquifers, stressing the importance of the key characteristics to well engineers.
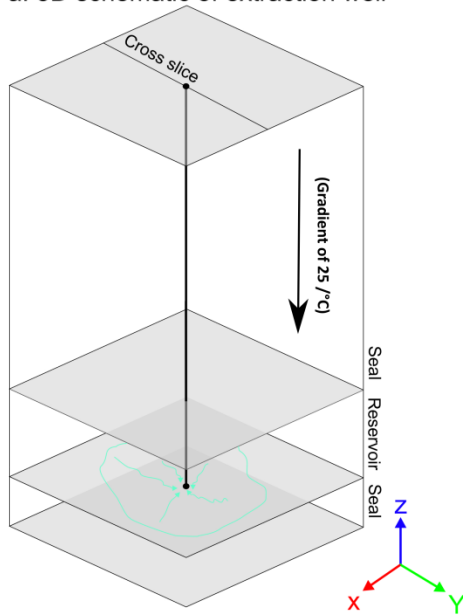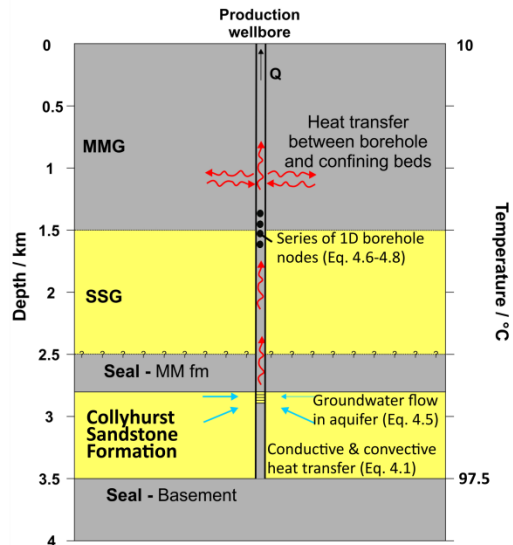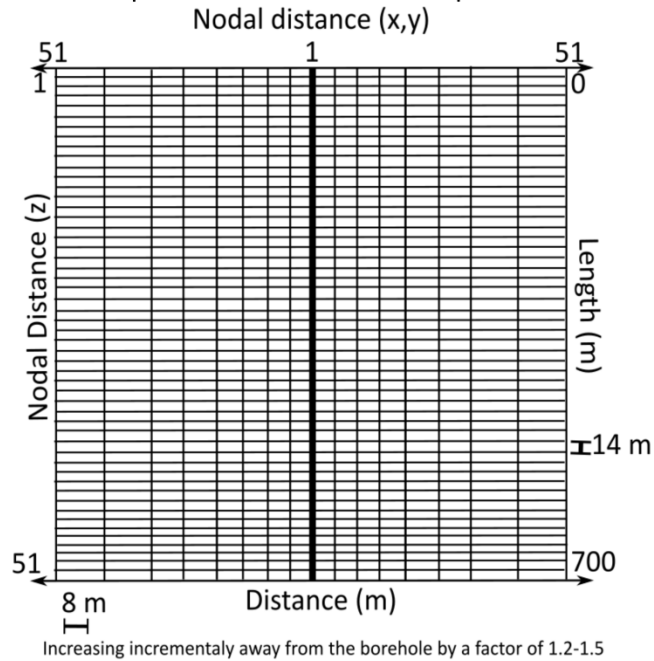
Figure 5.1: *(a) Schematic diagram illustrating the well design for extracting hot fluid around the wellbore in 3D, (b) the interpreted geological model in 2D (formation boundaries obtained from structural maps from Downing and Gray, 1986b) and (c) example discretised domain for the reservoir (Collyhurst Sandstone Formation). The vertical spacing is uniform and set at 14 m, whilst the horizontal spacing increases away from the well screen (thick black line) at an expansion factor of 1.2 to 1.5. Mercia Mudstone Group = MMG, Sherwood Sandstone Group = SSG and Manchester Marl Formation is MM fm.*

The Crewe area is located in the centre of the Cheshire Basin (Fig. 5.2a) with the highest geothermal resource expected to be concentrated around the thickest part of the aquifer. The modelled data can be used to aid the design and planning of future geothermal district heating schemes in the area providing planners with the information needed to match supply and demand. A single well approach is chosen to minimise the initial capital expenditure and explore the technical capacity to meet the heat demand in Crewe.

Currently, there are few wells penetrating depths of >2 km drilled in the Cheshire Basin, meaning that the quality, extent and temperatures of hot sedimentary aquifers (HSAs) in this region are unknown. The lifetime of a (doublet) well targeting low-enthalpy HSAs is controlled by both geological and engineering parameters, including porosity, pore fluid salinity, initial aquifer temperature and production rate, respectively (Saeid et al., 2015). Here, a parametric study is presented that investigates the exploitation of energy under varying engineering and physical conditions. The aim of this study is to help identify and mitigate the risks associated with the varying hydraulic and thermal conditions for single well schemes, particularly those with thick HSAs. The engineering parameters investigated were production rate, wellbore radial thickness, length of the well screen and position of the well screen. The geological factors investigated were aquifer thickness, hydraulic conductivity, thermal gradient, salinity of the pore fluid, thermal conductivity of the aquifer and porosity. The wellbore material was not investigated as it has a minimal effect on the lifetime of a geothermal system, only affecting the initial production temperature within the first month of operation (Saeid et al., 2015). Each parametric scenario was compared to a 'base case' scenario that was the best estimate of the real geological conditions (refer to the section 5.3.6 for details).

The geothermal system was modelled with MATLAB software using the finite-difference method coupling both advective and conductive heat transfer. The model was discretised by an

orthogonal 3D mesh and explicit approximations of derivatives (Fig. 5.1c). Although the aquifer and surrounding confining beds were modelled in 3D, the wellbore was simulated in 1D. The wellbore model used is based on that of Al-Khoury et al. (2005) and Al-Khoury and Bonnier (2006) with further development by Saied et al. (2013). The 1D wellbore reduces the nodal quantity used, saving computational time. An IMEX (implicit-explicit) scheme was used when modelling the wellbore for greater stability whilst maintaining accuracy, allowing larger time steps (e.g., Spiegelman, 2000; Geiser, 2008).

5.2 Geological setting

The Cheshire Basin is one of a series of Permo-Triassic extensional sedimentary basins located across the UK associated with the rifting of Pangaea and the breakup of Laurasia (Glennie, 1995; Rowley and White, 1998). Extensional collapse occurred after the Variscan Orogeny resulting in tilted fault blocks and graben structures (Figs. 5.2b & 5.2c) (Ruffell and Shelton, 1999). The Cheshire Basin has a thick succession of infill consisting of high-quality Permo-Triassic sandstone aquifers (Sherwood Sandstone and Appleby Groups) overlain by an insulating mudstone sequence (Mercia Mudstone Group) (Figs. 5.2a & 5.2c). The Permo-Triassic sandstones have been characterised thoroughly, retaining high micro-porosity at depth (e.g., Allen et al., 1985, 1997; Downing and Gray, 1986b; Griffiths et al., 2003; Ambrose et al., 2014). The most basal member, and target of deep geothermal extraction in this model, is the Collyhurst Sandstone Formation of the Appleby Group. The Collyhurst Sandstone Formation is an arenaceous, aeolian- to fluvial-sandstone with core data showing high porosities (13 – 32 %) and hydraulic conductivities (<10 m/day) (Allen et al., 1997). The formation is overlain by the Manchester Marl Formation, which is anticipated to be an insulating, low-porosity seal that was deposited during a marine incursion in the mid-Permian (Naylor et al., 1989). The Manchester Marl Formation is composed of mudstones intercalated with limestones that become siltier and thinner to the south of the basin (Evans et al., 1993). In Crewe, the formation is considered

an aquiclude as the cover of the formation is laterally continuous radially for 5 km around the wellsite (Fig. 2.16), preventing hydraulic continuity between the Collyhurst Sandstone Formation and Sherwood Sandstone Group.

Figure 5.2: *(a) Geological outcrop map of the Cheshire Basin (after Plant et al., 1999; Hirst et al., 2015; UKOGL, 2019). Permo-Triassic sandstones are the dominant infill (Appleby and Sherwood Sandstone Groups), capped by a sequence of thick insulating mudstones (Mercia Mudstone and Lias Groups). (b) Schematic of the tectonic history of the basin and (c) cross section of the basin (both modified after Plant et al., 1999), with the potential extent of Carboniferous strata in the subsurface.*

Carboniferous strata directly underlie the basal Permian sandstones and are predominantly fluvial, to semi- to open-marine in depositional environment. Marls, sandstones, limestones, coals and shales have all been identified in outcrop studies (e.g., Gibson, 1901; Smith, 1998; Powell et al., 2000). Early Carboniferous strata are deposited in a marine setting followed by a fluvial to lacustrine setting, representing a shallowing-upwards sequence, associated with uplift during the Variscan Orogeny. The lateral extent of the Upper Carboniferous strata underlying the Cheshire Basin has been widely debated, with some suggesting that in the deep, south-eastern part of the basin, basal Permian sandstones lie directly on low-grade metamorphic Palaeozoic rocks (Fig. 5.2c – with potential Carboniferous strata extent hypothesised) (Abdoh et al., 1990; Mikkelsen and Floodpage, 1997). This is due to fault reactivation during the Variscan Orogeny uplifting Carboniferous strata in the south of the basin (Fig. 5.2b). Although this could limit the thickness of the geothermal resource at higher temperatures, thick outcrop successions of Carboniferous strata in the east indicate the opposite (Hirst et al., 2015). In this study, both scenarios are considered; (1) the Collyhurst Sandstone Formation lies directly on low-grade metamorphic rocks, acting as an impermeable seal and (2) the Collyhurst Sandstone Formation overlies the Warwickshire Group – a thin succession of Carboniferous sandstone (Salop and Halesowen Formations) underlain by a bottom seal (Etruria Marl Formation/low-grade metamorphic basement). Although the Salop and Halesowen Formations are far more lithologically complex and heterogeneous (Gibson, 1901; Smith, 1998; Powell et al., 2000), they are considered to be an extension to the aquifer with the same properties (modelled as an extension to aquifer thickness in parametric study section 5.4.2.2). To understand the effects of the parameterisation of engineering and geological properties, the former scenario where the Collyhurst Sandstone Formation lies directly on impermeable low-grade metamorphic rocks is used when modelling the 'base case'.

5.3 Method of numerical modelling

5.3.1 Methodology for the modelling of the reservoir and wellbore

The finite-difference method was used to model the reservoir and wellbore, coupling thermal and fluid interactions. The orthogonal mesh was discretised on a non-uniform grid with fixed Cartesian co-ordinates (Fig. 5.1c) and an axis-symmetric model was used for faster computational time. The model assumed that the aquifer was initially fully saturated and the pressure head was equal to the depth. It is unlikely that the reservoir will be fully screened for an interval of ~700 m and it was, therefore, assumed that the wellbore would be screened for an interval of 70 m in the modelling base case. The varying effects of penetration ratio were also investigated. The model was set up using the key governing equations established in chapter 3 and 4 for heat and fluid flux in the aquifer and wellbore (Eq. 4.1 – 4.19).

5.3.2 Energy production

To assess the economic viability for any geothermal scheme, the total quantity of energy produced must be determined. For a single well scheme, the total energy production (E_{prod}) can be calculated using equation 4.2 (modified from Crooijmans et al. (2016) for a single well scheme). For this study, it was assumed that the rejection temperature (i.e., where the water temperature is deemed no longer suitable for a district heating scheme) was 30 °C, which is consistent with research for the Cheshire Basin (e.g., Downing and Gray, 1986b).

5.3.3 Discretisation, grid convergence and computational speed

5.3.3.1 Introduction of an implicit-explicit scheme for the wellbore model

The model was discretised using an orthogonal mesh with the spacing expanded horizontally using an expansion factor of 1.2 to 1.5. In the reservoir, thermal and fluid fluxes were modelled explicitly, whilst heat fluxes in the wellbore were modelled using an implicit-explicit (IMEX) operator

splitting procedure (e.g., Spiegelman, 2000; Geiser, 2008) where the diffusion component of equation 4.6 is modelled explicitly and the advective component implicitly. In explicit schemes, new parameters are calculated based on those at the previous time step whilst implicit schemes calculate the subsequent time steps by solving a series of equations dependent on other variables. This procedure allows a greater range of time steps to be used for the wellbore and provides increased stability in the model. This is because the implicit procedure makes the advective component unconditionally stable (Chapra and Canale, 2010). This method of wellbore modelling retains accuracy and produces results similar to the purely explicit method, both spatially and temporally (Fig. 5.3). There were minor discrepancies in the first few months of modelling; however, over the lifetime of the system this only has a minor impact. Computational time (when modelling heat flux in the wellbore) is dramatically reduced, nevertheless, the time step size must still be considered carefully to ensure accuracy is maintained.

a. **Variation in production temperature with time**

b. Temperature variations along the length of the pipe after 25 years
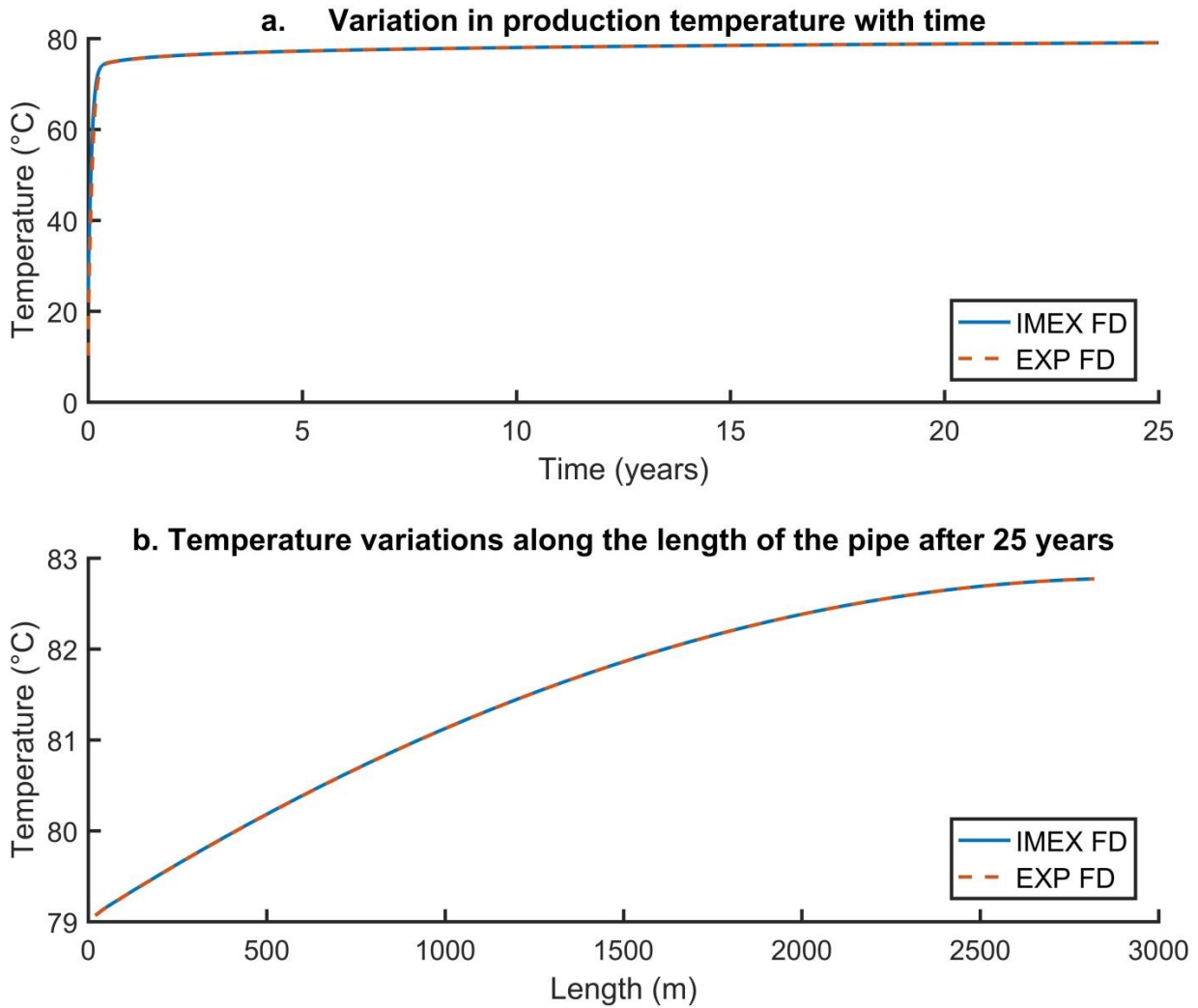
Figure 5.3: *Results for the wellbore heat flow model after 25 years, comparing the explicit finite difference (EXP FD) and operator splitting implicit-explicit method (IMEX FD). (a) Temperature variations at the top of the borehole with time, (b) temperature variations along the borehole piping after 25 years.*

5.3.3.2 Testing the mesh sizes for individual components used in the model

In contrast to the modelling undertaken in chapter 4, the computational speed of the program was extremely important so that multiple models can be simulated in a small amount of time. Analysis was undertaken to investigate the impact of different mesh sizes such that the accuracy of the results were not compromised, whilst increasing the computational speed by increasing the nodal spacing. Both the reservoir and wellbore model were initially tested separately

at different mesh sizes ranging from 1 m to 30 m (Figs. 5.4 and 5.5). The reservoir was simulated for 1 month due to the large computational times required for the smaller meshes, whilst the wellbore was simulated with a constant input for 10 years. This was an initial test to identify key areas of error and narrow down the mesh sizes simulated for the fully coupled system. It can be seen that the effect on reservoir temperature at the extraction nodes was minor, whilst there was a more significant effect on head in the wellbore. This was largely due to a small change in temperature over the simulation time. In other scenarios (such as doublets) where there is a more significant temperature difference, the spacing may have a greater effect on temperature.
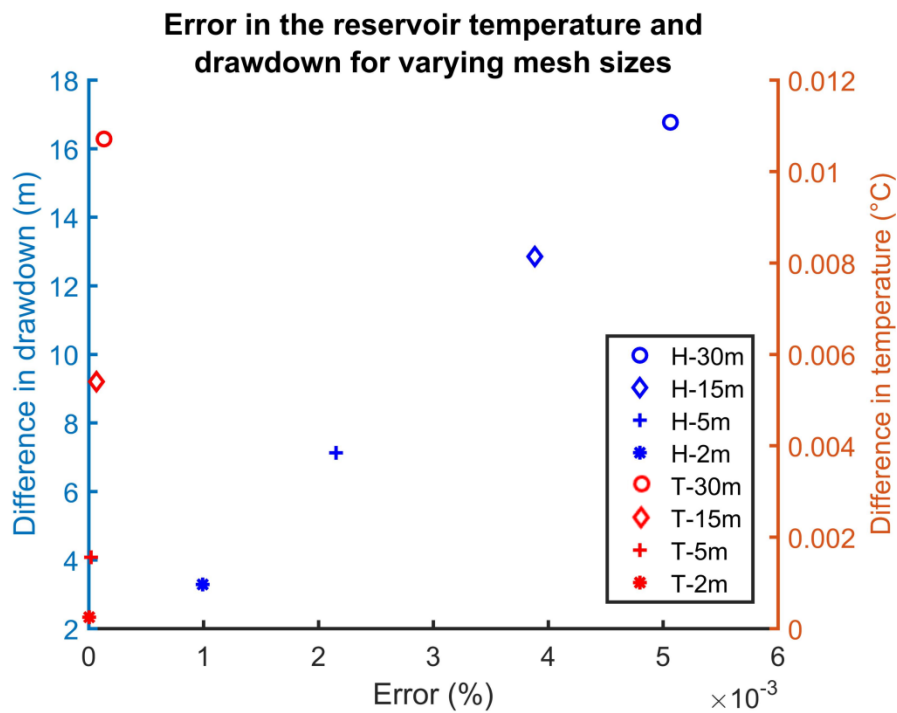
Figure 5.4: *Error in reservoir temperature and well head for different mesh sizes. The blue circle is for a 30 m mesh, the diamond 15 m, the cross 5 m and the asterisks are for 2 m mesh sizes. Error evaluated as difference in final head/temperature for each mesh compared to the 1 m scenario.*

When testing the varying lateral spacing around the wellbore and confining beds, it was noticeable the main issue was the delay in heat reaching the surface within the wellbore, with coarser lateral spacing emphasising this. This will result in an underestimation in production

temperature and energy. A mesh spacing of 15 m takes nearly a year to reach the same production temperature to that of 1 m, whilst 5 m takes less than a day (17 days). The final percentage error between different mesh sizes and the 1m mesh were 0.6 %, 1.5 %, 3.2 % and 4.7 % for 2, 5, 15 and 30 m lateral mesh spacing, respectively.
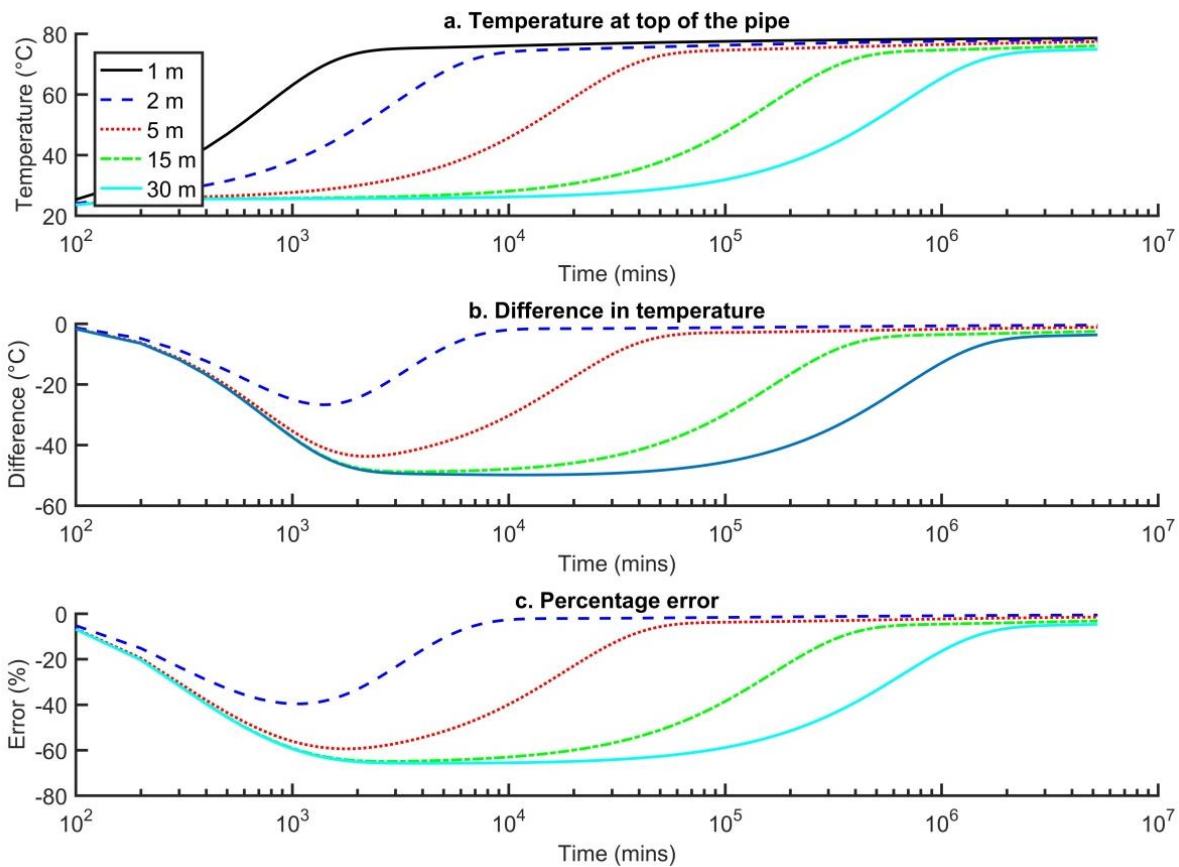
Figure 5.5: *Error in production temperatures for different modelling mesh sizes, (a) shows temporal changes in production temperature, (b) shows the difference in temperature between the 1 m scenario and alternate mesh sizes, and (c) shows their respective percentage error with temporal variations.*

5.3.3.3 Testing the mesh sizes for the fully coupled model

Testing the model components separately highlighted that the coarser mesh sizes (12 m and 15 m) were not going to be viable due to the significant error and difference in head, whilst also causing a significant delay in thermal fluxes in the wellbore. As such, further mesh analysis was

140

undertaken for the full model (reservoir and wellbore coupled), exploring a range of mesh sizes of 2 m, 4 m, 8 m and 12 m. A 1 m mesh was not considered as the initial analysis showed minimal variations between the 1 m and 2 m scenarios and to test the model over a longer simulation period (6 years) would have taken a number of days.
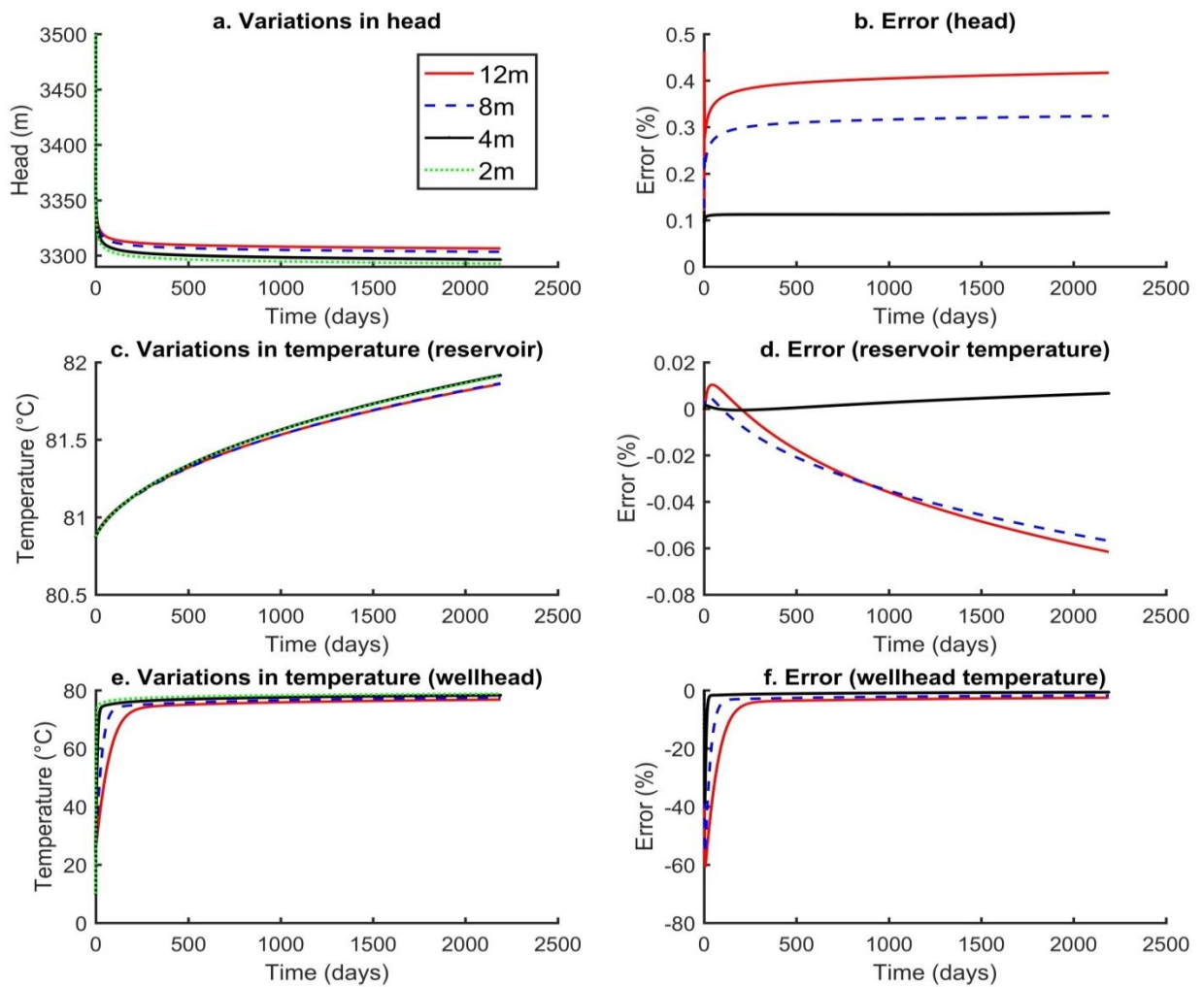
Figure 5.6: T*emporal variations in head (a), reservoir temperature (c) and production temperature (e), with corresponding error (b), (d) and (f) respectively for a range of mesh sizes. Error calculated at the well screen for b and d, whilst for f error is calculated at the top of the wellbore.*

Mesh sizes of 12 m were not suitable for this study as they increase the error in the first 250 days for the production temperature (Fig. 5.6), leading to significant underestimations in production temperature. They fall short of the 2 m mesh production temperature by over 2 °C. An 8 m mesh has a slight delay in the wellbore temperature reaching that of the 2m study; however this was only around a month and over the lifetime of 25 years would have a minor impact.

The computational times for the different mesh sizes were also significant. The 2 m mesh took in excess of a day to simulate, whilst the 12 m mesh took less than an hour. To achieve a balance in computational speed and accuracy, the mesh size of 8 m was chosen. This allowed the simulations to be undertaken for the base case of 25 years in just over 3 hours whilst allowing the maximum error to be ~1 %.

5.3.4 Model validation and accuracy

In this study, the model was compared to an analytical solution, which is a modified version of the Theis solution (Brons and Marting, 1961; Hantush, 1961, 1962; Huisman, 1972; Sternberg, 1973). Although thermal changes are important to any geothermal scheme, it is likely that any viability of a district heating scheme will be determined by the ability of a well to produce fluid sustainably. The partial penetration effects are additional to the Theis solution (Eq. 5.1), where the drawdown (s) in a well is calculated as:

$$s = \frac{Q}{4\pi K b} \left[W(u) + 2\,S_p \right] \qquad\qquad 5.1$$

where Q is the production rate, K is the hydraulic conductivity, b is the aquifer thickness, $W(u)$ is the well function and S_p is the additional drawdown caused by partial penetration. For the previous example of partial penetration in this thesis (Southampton Marchwood Well, chapter 4.4.3), the values for S_p were tabulated from a range of authors by Sternberg (1973). The S_p values correspond to various aquifer thickness (h) divided by (r_w) ratios. By extending the tabulated values listed in

Sternberg (1973), the S_p values for greater h/r_w values can be obtained (Fig. 5.7). The S_p value for a penetration ratio of 0.1 can be calculated using the equation:

$$S_p = 8.6714\ln(h/r_w) - 19.338 \hspace{4cm} 5.2$$
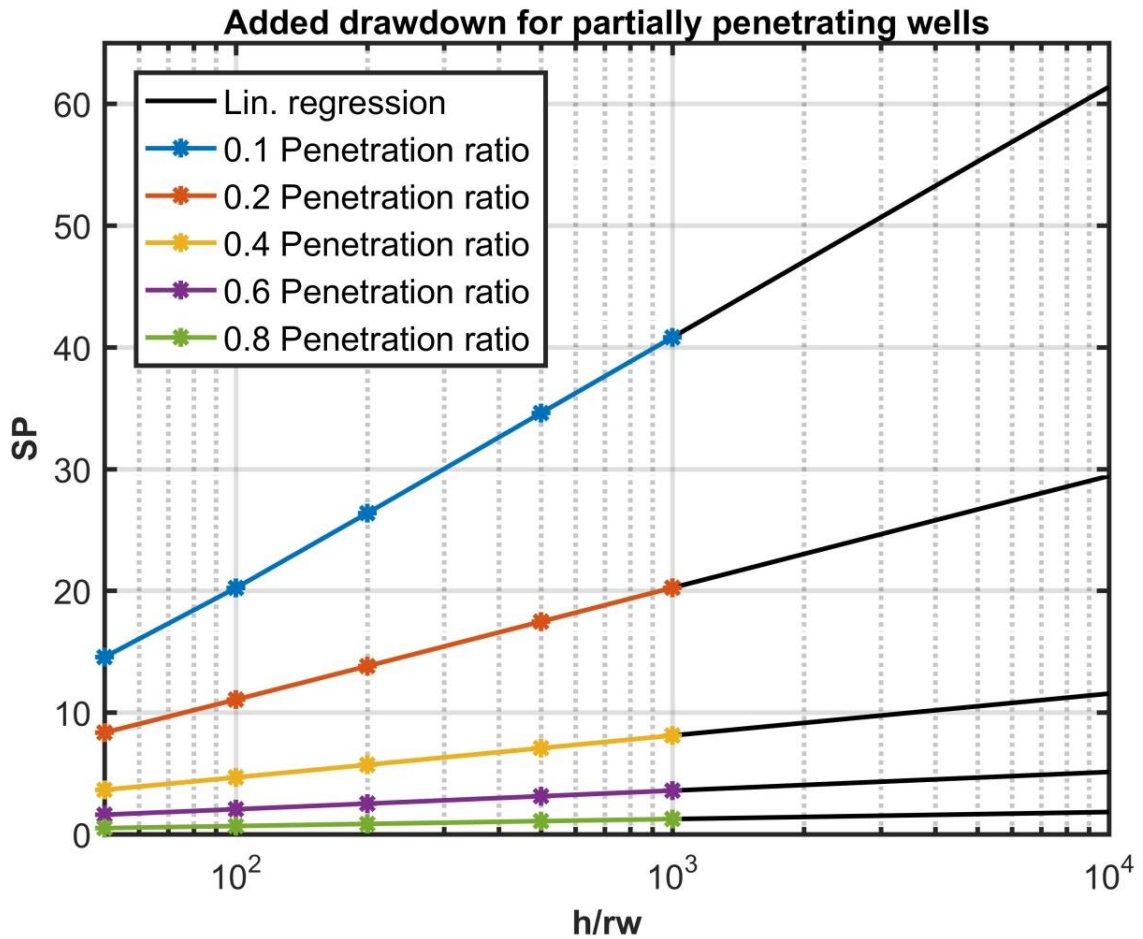
Figure 5.7: *Calculation of the additional drawdown ratio for partially penetrative wells.*

To compare the models against the analytical formulation, the aforementioned 'base case' scenario was modelled with the well screen located in the centre of the aquifer and a lateral and vertical mesh size of 8 m (expanded outwards) and 14 m, respectively. This model matched closely to the analytical solution (Fig. 5.8a) with the percentage error and difference in head higher in the first year, then reducing to <4.1 % and <10 m (Figs. 5.8b). As we are interested in changes in head

and temperature over the lifetime of a geothermal system under exploitation for 25 years, the initial

loss in accuracy is deemed acceptable. The end difference in two solutions is <8 m head (Fig. 5.8b).
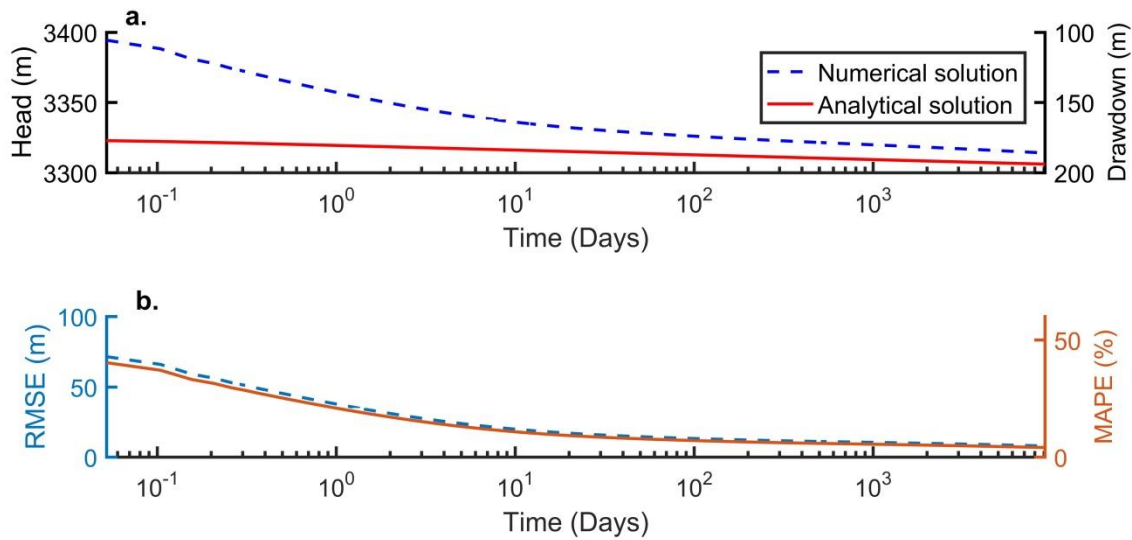
Figure 5.8: *(a) Comparison between the analytical modified Theis solution for partially penetrative schemes*

(modified Theis) and finite-difference method (FD) for drawdown in the wellbore, (b) RMSE difference in head

between the analytical and numerical solution and the percentage error in wellbore head.

5.3.5 Thermal dispersion

In recent years, the use of the thermal dispersion term when upscaling from micro-scale

(pore) to macro-scale (formation) has been widely debated. Thermal dispersion is heat flux caused by

local variations in fluid velocity between pore spaces (Molina-Giraldo et al., 2011; Saeid, 2015). It has

been suggested that thermal dispersion is extremely important to thermal fluxes in a geothermal

system with similar orders of magnitude to solute dispersion (De Marsily, 1986). Others suggest the

opposite, or that thermal dispersion is only important under certain conditions, and that the

enhanced thermal spreading is negligible (Bear, 1972). Some suggest that heat transport behaves in a

homogenous manner as it occurs in both the matrix and pore water; therefore, diffusivity is more

influential and dispersion only has a minor impact (Zeghici et al., 2015). When there is no

groundwater movement, thermal dispersion is set equal to zero (Anderson, 2005), and the bulk rock

thermal diffusivity is large, thus thermal dispersion only has a small effect except for when large

Darcy velocities are present (Hopmans et al., 2002; Saeid, 2015). It has also been suggested thermal

dispersion is only important when complex rock structures are present (Law, 2009). In this study, it

was anticipated that temperature change in the reservoir would be minor as shown in the mesh

analysis studies. Nevertheless, a brief comparative study of results with and without thermal

dispersion was undertaken.

To test the effects of thermal dispersion the model by Rau et al. (2012) was used. They used

a linear approximation based on laboratory tests:

$$\alpha_b = \frac{\lambda_b}{\rho_b c_b} + \beta_{l,t} \left(\frac{\rho_f c_f}{(1-\emptyset)\rho_s c_s + \emptyset \rho_f c_f} . v \right)^2 \qquad\qquad 5.3$$

where the longitudinal coefficient (along flow direction) is $\beta_l = 1.478$ and the transversal

(perpendicular to flow direction) is $\beta_t = 0.4$. A 1 m uniform mesh was used and the well simulated

for 1 month.

The results indicated that thermal dispersion was extremely minor for single well geothermal

systems with a temporal error of less than -1.0626 x 10^{-6} % and a spatial error of less than -7.1882 x

10^{-7} %. Both the thermal fluxes for the temporal and spatial changes showed a slight increase in the

temperature when modelling with thermal dispersion (Fig. 5.9). The difference in the end reservoir

temperature at the well screen was -8.6 x 10^{-5} °C and the highest spatial difference was -5.9 x 10^{-5} °C

(at the wellbore distance (point 0 in Figs. 5.9b and 5.9d)).

These results show that thermal dispersion only has a minor effect on a single well scheme

when the changes in temperature are minor within the system. It has, however, been shown that

thermal dispersion can be far more significant in doublet systems with errors ranging from 3 and 17

% when thermal dispersion is neglected (Saeid, 2015). As such, thermal dispersion is assumed to be

negligible in this study and is not modelled. It is also worth noting that the model by Rau et al. (2012) was used for higher Darcy velocities than those modelled here; as such, experimental thermal dispersion models based on data and laboratory experiments replicating conditions in the Cheshire Basin may be beneficial in future work to determine the true effects of thermal dispersion.
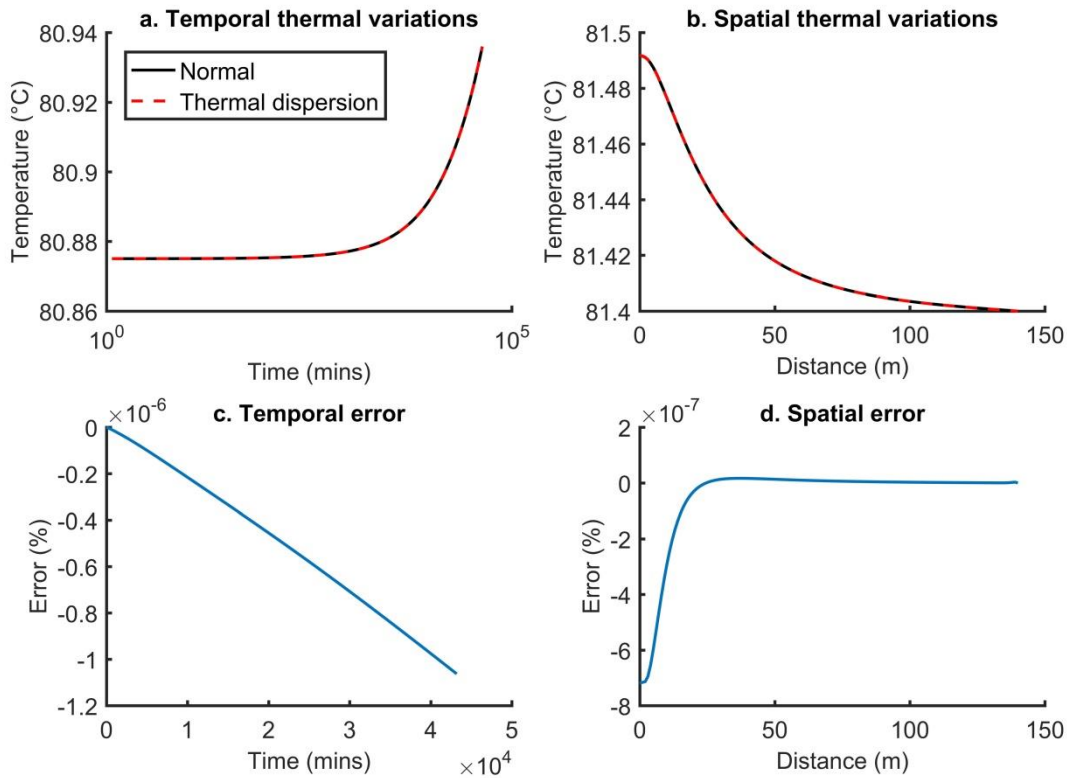
Figure 5.9: *Comparison of models with and without thermal dispersion for (a) temporal variations, (b) spatial variations and respective percentage error (c) and (d).*

5.3.6 Initial conditions

The setup of the model was similar to that in section 4.2.5 (Eqs. 4.22-4.25) and the surface temperature was set to 10 °C (BGS, 2011). The initial hydraulic head in the wellbore was set to 3,500 m, porosity to 15%, production rate 15 l/s, storativity to 4e-4 and the hydraulic conductivity to 0.1 m/d (Table 5.1) (Allen et al., 1997). The hydraulic conductivity was chosen as being slightly lower than the geometric mean (0.4 m/d) to reflect further reduction in permeability as few wells in the Cheshire Basin reach the depths targeted here. The hydraulic conductivity and porosity of the

confining upper seal (Manchester Marl Formation) and lower confining beds (considered to be low-grade metamorphic rock - Abdoh et al., 1990; Mikkelsen and Floodpage, 1997; Hirst et al., 2015) was set equal to zero. The thermal conductivity was set to 3.41 W/m/°C in the reservoir and 2.12 W/m/°C for the upper confining beds (Downing and Gray, 1986b). The heat capacity was set to 775 J/kg °C for the reservoir and 950 J/kg °C for the upper confining beds, whilst the density was set to 2,450 kg/m^3 for the reservoir and 2,720 kg/m^3 for the upper confining beds (Waples and Waples, 2004). The fluid salinity was set at 0.08 ppm/10^6 (similar to that of the Southampton geothermal fluid - Downing and Gray, 1986b), with a specific heat capacity of 4,200 J/kg °C (ETB, 2017) and a conductivity of 0.67 W/m/°C (Ozbek and Phillips, 1979). The density of the fluid was constant and calculated to be 1,024.7 kg/m^3 (Batzle and Wang, 1992; Adams and Bachu, 2002; Saied et al., 2015; Crooijmans et al., 2016).

Parameters	
Production rate (l/s)	15
Initial thermal gradient (°C/km)	25
Surface temperature (°C)	10
Thermal conductivity (W/m/°C)	2.12 UCB / 3.41 R / 0.67 F
Specific heat capacity (J/kg °C)	950 UCB / 775 R / 4200 F
Density (kg/m^3)	2720 UCB / 2450 R / 1024.7 F
Porosity (%)	15
Hydraulic conductivity (m/d)	0.1
Salinity (ppm/10^6)	0.08

Table 5.1: *Base case parameters used in this study (from Downing and Gray, 1986b; Burley et al., 1980; Allen et al., 1997; Waples and Waples, 2004; ETB, 2017). Upper confining bed = UCB, reservoir = R and fluid = F.*

For the base case scenario, the geological parameters were set in accordance with Table 5.1 and for the wellbore, Table 5.2. These were: a well screen radius of 0.106 m, piping thermal conductivity of 43 W/m/°C, grout thermal conductivity of 2.7 W/m/°C, grout specific heat capacity of 1,250 J/kg °C, grout density of 1,600 kg/m^3, pipe thickness of 0.02 m and grout thickness of 0.04 m (Allan, 1997; ETB, 2017; Rosen and Koohi-Fayegh, 2017). The radius of the piping in the wellbore was modelled at 0.153 m to match that of Southampton Marchwood Well (Downing et al., 1984).

Parameters	
Radius of well screen (m)	0.106
Thermal conductivity (W/m/°C)	43 P/ 2.7 G
Specific heat capacity (J/kg °C)	1250 G
Density (kg/m^3)	1600 G
Pipe thickness (m)	0.02
Grout thickness (m)	0.04

Table 5.2: *Borehole parameterisation of both materials and radius to test the thermal and pressure effects*

(from Allan, 1997; ETB, 2017; Rosen and Koohi-Fayegh, 2017). Pipe = P and grout = G.

5.3.7 Parameterisation of the models

The simulations will test a variety of geological and engineering parameters, covering the base case (BC) and three scenarios for each parameter (S1, S2 and S3). The parameters are outlined below (Table 5.3 and Fig. 5.10).

5.3.7.1 Geological variations

When considering the porosity of the Collyhurst Sandstone Formation, a range between 10 and 30 % was used for the parametric study, which corresponds to estimates by Allen et al. (1997), who gave a range for core plug studies of between 13 and 32 %. The average onshore porosity of the Collyhurst Sandstone Formation is estimated as 14 % (Rollin et al., 1995) but it has been suggested that the true porosity could be less, with the average porosity of 369 samples set at 11 % with porosity decreasing further with depth (Hirst, 2017). A porosity of less than 10 % was not modelled as aquifers are likely to be too tight to produce fluid at this level. The variance in Collyhurst Sandstone Formation porosity is highlighted further with Plant et al. (1999), highlighting porosities of 20 – 24 % in outcrop studies, whilst suggesting the porosity in the Prees-1 borehole to be 41 %. The high porosity value recorded at Prees-1 could indicate a high-quality aquifer, but for the purpose of this study was considered an anomaly. The base case porosity was chosen at 15 % to reflect the average onshore porosity value.

Case	S1	S2	S3	BC
(G1) Porosity (%)	10	20	30	15
(G2) Salinity (ppm/10^6)	0.04	0.16	0.2	0.08
(G3) Thermal conductivity (W/m/°C)	2	4	5	3.41
(G4) Reservoir thickness (m)	630	840	770	700
(G5) Hydraulic conductivity (m/day)	0.01	0.03	0.05	0.1
(G6) Thermal gradient (°C/km)	28	23	17	25
(E1) Well screen position (km)	2.94-3.01	3.29-3.36	3.43-3.5	2.8-2.87
(E2) Production rate (l/s)	20	30	40	15
(E3) Well screen length (m)	700	280	140	70
(E4) Radius of wellbore (cm)	5	15	20	15.3

Table 5.3: *Parameter ranges used in sensitivity analysis models. (G) highlights a geological parameter, whilst (E) highlights an engineering parameter. Parameters are highlighted in figure 5.10.*

Limited hydraulic conductivity values have been given at depth for the Cheshire Basin in the literature due to few wells exceeding (or reaching) the interval targeted in this study (i.e., >2 km). Hydraulic conductivities of up to 10 m/day have been encountered (Allen et al., 1997), which are unlikely (from primary micro-scale permeability) at a depth of 2.8 – 3.5 km. Therefore, they were not considered as they were potentially being recorded as a result of fluid flow in fractures or faults. Further suggestions of a high-quality aquifer were given by Plant et al. (1999) with hydraulic conductivity values ranging between 1.8 and 12 m/day for the Shropshire area. The lowest value recorded by Allen et al. (1997) was 3.7×10^{-5} m/day with only four values recorded less than ~0.05 m/day. The majority of samples tested in the study exceeded 0.1 m/day (base case scenario), with the high-quality properties interpreted due to the aquifer having medium- to coarse- grains, with limited cementation (Allen et al., 1997). As the focus of the study was on wellbore performance under potentially poorer, tighter conditions at depth, lower hydraulic conductivity values were used

for the models. The hydraulic conductivities modelled in the parametric analysis were 0.01 m/day, 0.03 m/day and 0.05 m/day.
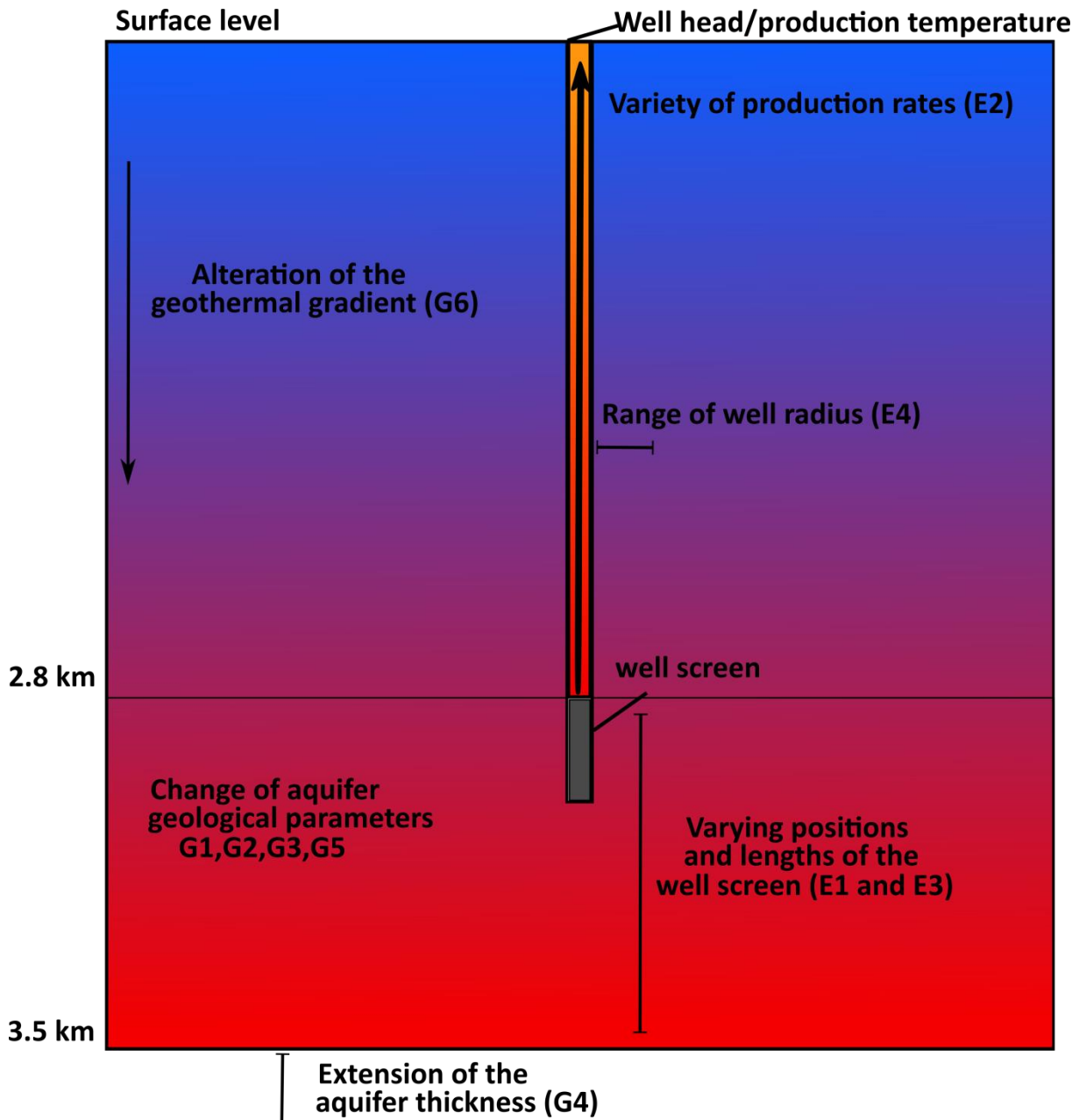
Figure 5.10: *Schematic showing different parameters tested in the model. Parameters listed in table 5.3.*

The base case thickness of the aquifer was chosen to be 700 m, based on structural maps (Downing and Gray, 1986b) (Fig. 5.11) and cross-section diagrams (Plant et al., 1999). Indications from well logs (Prees-1 and Knutsford) give an average thickness of the Collyhurst Sandstone

Formation of 514 m (Hirst 2017). It is anticipated that the sandstones will be thicker than that recorded for Prees-1 and Knutsford due to the position of the well in a deeper part of the basin. As such, a variation of -10 % was assigned to the first parameterisation model (S1) to reflect potential overestimations of the aquifer thickness. It was assumed that the Collyhurst Sandstone Formation overlies a metamorphic seal (Abdoh et al., 1990; Mikkelsen and Floodpage, 1997). The extent of Carboniferous sandstones is unknown and was considered as an extension of the thickness of Permian sandstones. To account for this, further thicknesses of +10 % and +20 % are modelled in the other parametric cases.

The geothermal gradient in the Cheshire Basin is disputed, with older estimations from uncorrected bottom-hole temperatures giving an average geothermal gradient of 20 °C/km (Downing and Gray, 1986b; Burley et al., 1980; Plant et al., 1999). Recent evaluations estimating the corrected geothermal gradient indicate the value could be closer to 27 °C/km (Busby, 2014). In this study, a range of values for the geothermal gradient were modelled, with the highest being 28 °C/km to cover the average of shallow gradients for the UK (less than 1 km) (Busby et al., 2011). The lowest gradient of 17 °C/km was used to represent the average Permo-Triassic gradients (Downing and Gray, 1986b). A gradient of 25 °C/km was used for the base case to reflect the recent higher estimates by Busby (2014); however, it is slightly lower than the suggested value as the data for the study is not published and the value of 27 °C/km seemed optimistic.
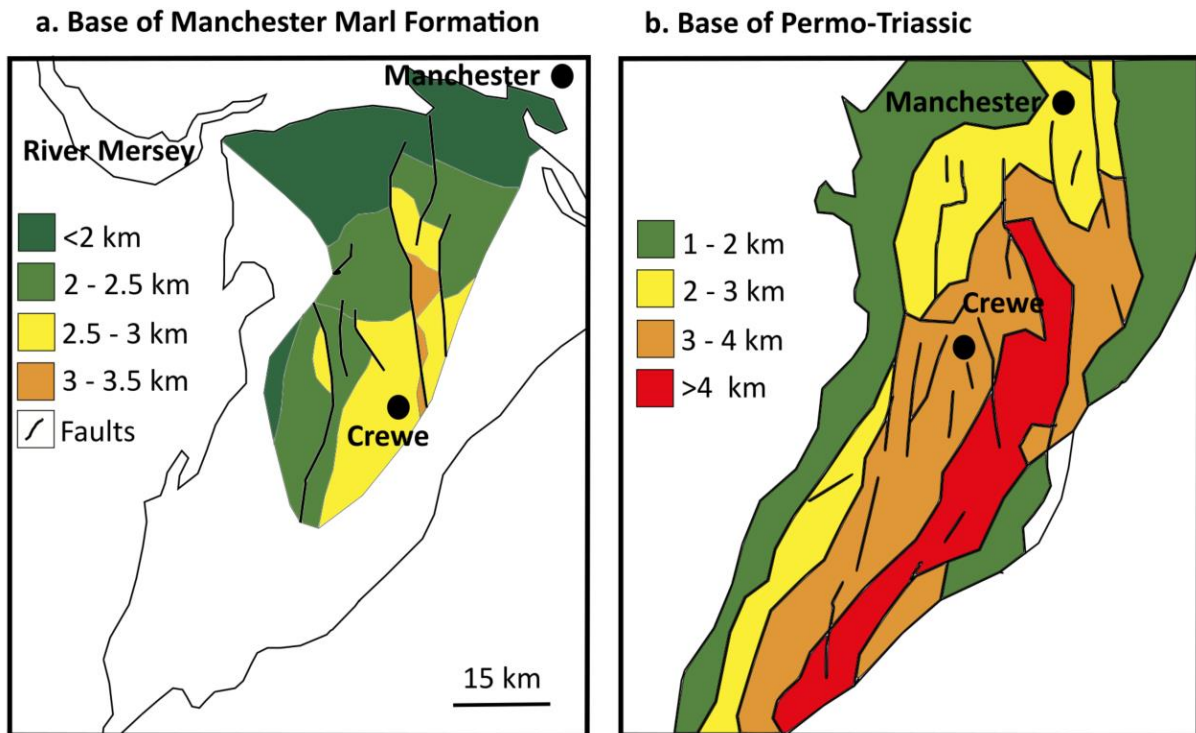
Figure 5.11: *(a) Base of Manchester Marl formation (modified from Downing and Gray, 1986b) and (b) base of Permo-Triassic, (modified from Plant et al. 1999 and Hirst 2017).*

Salinity data at depth is limited for the basin, however, the Prees-1 and Knutsford boreholes indicate that it is between 0.02 and 0.05 ppm/10^6 for the Collyhurst Sandstone Formation whilst the overlying formations (Wilmslow and Chester) have salinities approaching 0.08 ppm/10^6 (Plant et al., 1999). Due to the positions of both the Prees-1 and Knutsford boreholes being closer to the edges of the basin, with freshwater recharge encountered, it was anticipated that the central area of the basin may have higher salinity contents. Modelling from Plant et al. (1999) indicates that the groundwater flow in the centre of the basin (Crewe area) is likely to be influenced by the presence of salt in the overlying Mercia Mudstone Group. The base case salt content was therefore estimated at 0.08 ppm/10^6, whilst the lowest salt content for the parameterisation was set at 0.04 ppm/10^6. The highest estimate of salt content was based on data from the Southampton geothermal wells, which indicated a higher salt content approaching 0.3 ppm/10^6 (Downing and Gray, 1986b). As saline water influence is unlikely in the centre of the Cheshire Basin, a maximum value of 0.2 ppm/10^6 was used.

It is also worth noting that a change in salinity only affects the thermal flux component of the model where a new density for the geothermal fluid was calculated for each scenario. The density was considered constant for heat fluxes and was calculated using the initial average pressure and temperature of the reservoir (Batzle and Wang, 1992; Adams and Bachu, 2002; Saied et al., 2015; Crooijmans et al., 2016).

Base case thermal conductivity was estimated at 3.41 W/m °C for the aquifer whilst an estimate for similar rocks across the UK was utilised for other parametric scenarios (2, 4 and 5 W/m °C - Downing and Gray, 1986b).

5.3.7.2 Engineering variations

Unlike the geological parameters, which can vary considerably at depth, the engineering parameters can be pre-determined. Production rates were chosen using estimates from the Collyhurst Sandstone Formation from a range of authors. Hirst (2017) calculated production rates of 16 l/s may be attained at depth, whilst Griffiths et al. (2003) and Plant et al. (1999) stated rates of 20 - 30 l/s can be produced sustainably from wide diameter boreholes. The highest value utilised was 40 l/s, which is likely to be optimistic and based on a doublet scheme maintaining pressure along a fault line (Atkins, 2013). The base case was set at 15 l/s, whilst the alternate scenarios investigate how much more fluid and thus energy can be produced.

The well screen position and length were investigated to see if they can increase the performance of the single well. The well screen position was placed at the top of the aquifer (2.8 km – 2.87 km) for the base case. For the other parametric scenarios, the screen was positioned in the upper centre (2.94 km – 3.01 km), lower centre (3.29 km – 3.36 km) and base of the aquifer (3.43 – 3.5 km). The screen length was selected at 10 % of the aquifer thickness for the base case. The three scenarios tested in the parametric models were 100 %, 40 % and 20 %.

The final parameter tested was the radius of the wellbore and well screen. Typically, smaller diameter (slim-borehole) wells can be cheaper to drill. The profit in potential geothermal wells could therefore be increased, encouraging investors to exploit this energy from the basin. The scenarios tested assume the well screen radius was the same as the borehole diameter. The base case assumed the same parameters as the Southampton wells (Sect. 3.6), whilst the radii tested in parametric models are 0.05, 0.15 and 0.2 m.

5.4 Results for the parametric models

The depletion and recharge of a reservoir was modelled for 25 years, which was considered to be the maximum lifetime of a well for investment and operational purposes. Seasonal fluctuations in extraction were not modelled for the parametric analysis, whilst the base case geological scenario assumed that the Collyhurst Sandstone Formation was the only hot sedimentary aquifer (HSA) present, confined by underlying low-grade metamorphic rocks at the base and the overlying Manchester Marl Formation at the top. To test the varying parameters, the HSA was considered homogenous and isotropic. Although this is unlikely to be an accurate representation of any aquifer geologically, it will highlight the variance of depletion and recharge within the reservoir under the varying parametric conditions. It is also important to note that the reservoir model utilised a predefined production rate, which implies that the pressure in the aquifer was always maintained such that fluid can be produced.

The performance-related lifetime of the well was considered 'finished' when the head in the wellbore was equal to 3,000 m or the temperature was less than 60 °C. The wellbore head was considered to have a cut-off of 500 m below static conditions to match that of the submersible pump used in the Marchwood Well, Southampton. This was submersed to 617 m below the datum and capable of dealing with high temperatures (Price and Allen, 1984).
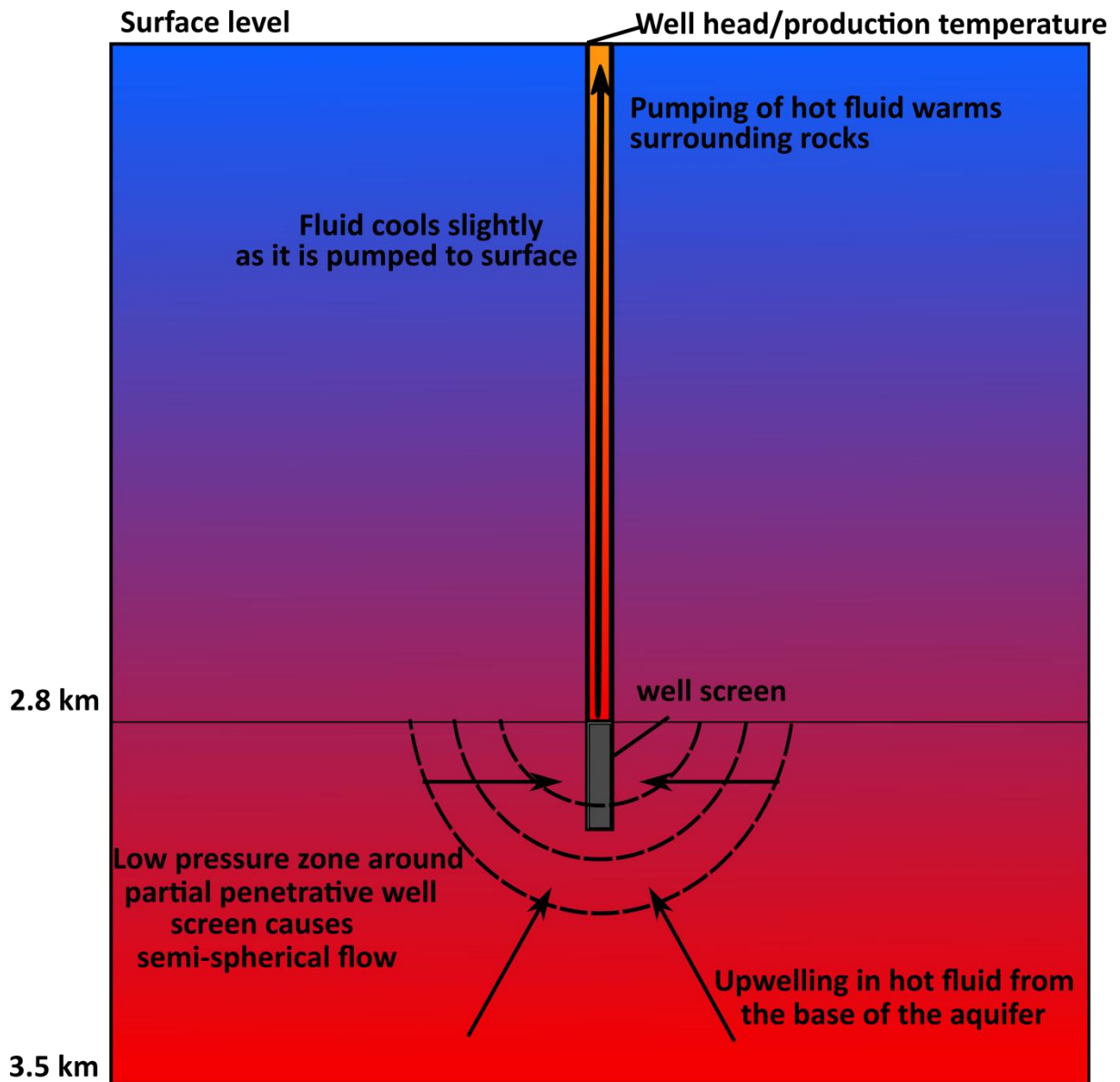
Figure 5.12: *Schematic of base case scenario highlighting upwelling of hot water caused by partial penetration. Note red is hot and blue is cold.*

5.4.1 Base case scenario model

As the base case thickness of the aquifer was set to 700 m it was expected that temperatures would be higher towards the base, assuming an increase in temperature with depth under static conditions. The well screen was located at the top of the reservoir and had a penetration ratio of 10 %. With time, the hot water front at the base of the aquifer was pulled upwards towards the well

screen, increasing the production temperature and decreasing the head in the HSA (Figs. 5.12 & 5.13). Vertical fluxes within the wellbore were the most significant with minimal temperature change in the reservoir and confining beds (Figs. 5.12, 5.13a, 5.13b & 5.13c). Over the lifetime of the single well (25 years of production), the head decreased by 200.2 m and the temperature at the well screen increased by 1.8952 °C (Fig. 5.13d). When the well ceased production, head rapidly increased by 198.3 m whilst temperature in the reservoir began to decrease when the change in temperature, via conduction, from the surrounding rocks was greater than that from advective heat fluxes. During recharge (when there is no fluid extraction), temperature in the reservoir decreased by 0.61 °C (Fig. 5.13d). Colder fluid fills the vacated pore-space, predominantly from regions directly adjacent to the borehole (horizontal movement), increasing head and decreasing temperature. Although recharge was only simulated for 25 years, it is likely that temperature recharge could take thousands of years to re-equilibrate (Axelsson et al., 2005; Pearson, 2012).

During the lifetime of the well 11,826,000,000 litres of water were produced, which is equal to 2.37×10^{15} Joules of energy. This was based on the assumption that production temperature was recorded at the top of the production well. If reservoir temperature was used to determine the energy return, the figure would be over-estimated at 2.59×10^{15} Joules. The total amount of energy produced would be enough to meet 35 % of the demand in Crewe town centre over 25 years, calculated using the annual demand of 76 GWh/year (Routledge et al., 2014). The zone of influence around the well within the HSA reached a maximum radius of 2.285 km, covering an area of 16.4 km^2 (taken at the middle of the length of the well screen to a depth of 1m of the static HSAs head). The greatest difference in temperature was near the well screen (within ~200 m - Figs. 5.13a & 5.13c); therefore, the zone of influence was based on the hydraulic interactions.

Figure 5.13: *(a) 2D cross slices through the entire subsurface after 25 years of production, (b) 'zoomed-in' section of the wellbore showing only small thermal propagation (within 30 m), (c) 'zoomed-in' section of the reservoir and (d) head and reservoir temperature at the well screen v time.*

Temperature distribution along the wellbore piping rapidly changed in the first 5 days, immediately increasing in the first 6 hours such that the temperature along the wellbore exceeded 25 °C (Fig. 5.14a). Thermal propagation in the confining strata around the borehole was minimal and radially only reached a distance of 50 m after 25 years of depletion (measured to greater than 1 °C change from initial conditions) (Figs. 5.13a, 5.13b & 5.13b). Within the first year, temperature in the pipe and grout were similar at 75.46 °C and 75.01°C respectively, whilst the temperature in the confining rock was slightly lower by 2.16 °C (Fig. 5.14c). Assuming the temperature at the top of the piping was similar to production temperature at the wellhead, there was a 3.7 °C loss in temperature

within the wellbore (between well screen temperature and production temperature) at the end of production.
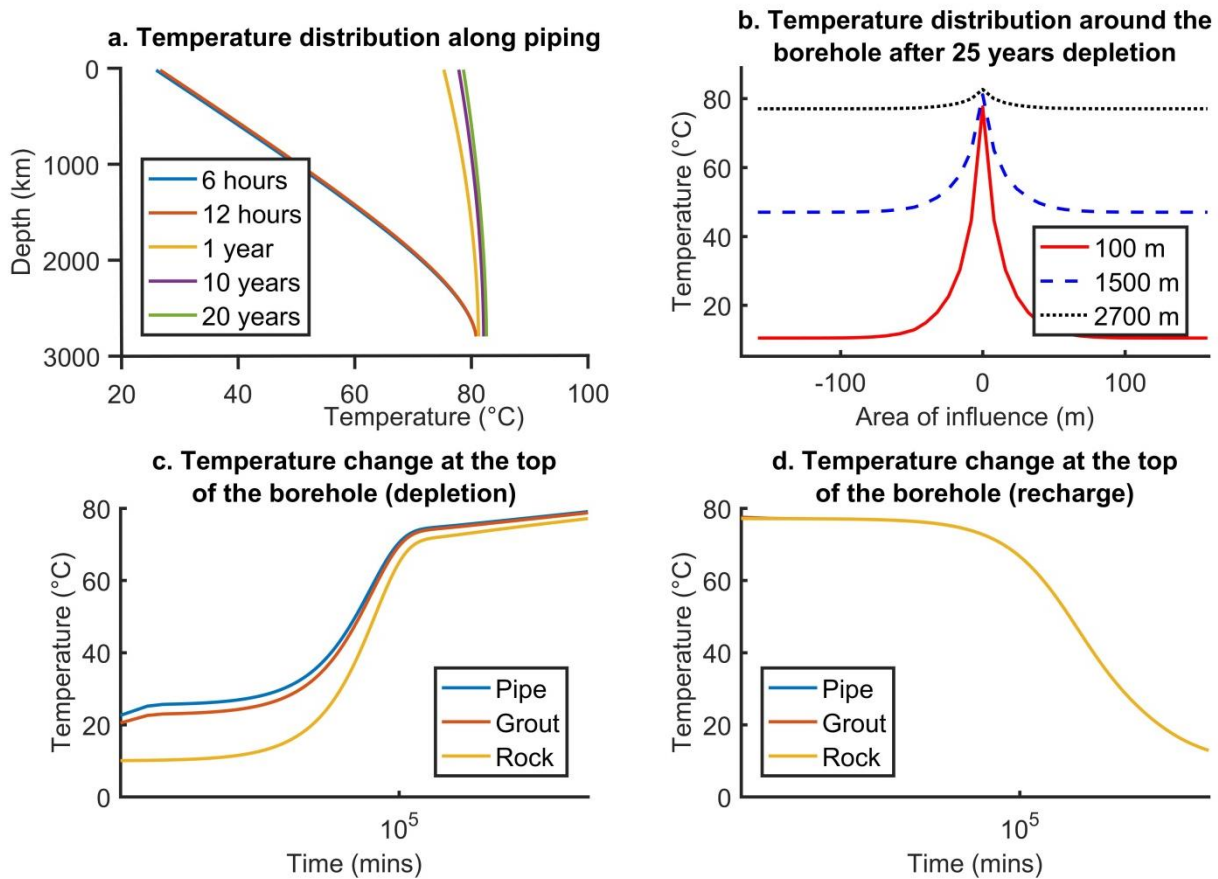
Figure 5.14: *(a) Temperature distributions in the wellbore after 6 hours, 12 hours, 1 year, 10 years and 20 years, (b) changes in temperature in the confining beds around the wellbore at the surface level (S.L), 1500 m and 2700 m, (c) temperature distribution of the pipe, grout and surrounding rocks with time during the depletion scenario and (d) recharge scenario. Note in figure d the pipe and grout have a similar temperature decline to the rock, such that the minor difference cannot be distinguished on the graph.*

At the end of the 25 year lifetime, the temperature in the aquifer (in the well screen interval) was 82.77 °C, the confining rocks around the wellbore at surface level was 77.13 °C, the grout at surface level was 78.74 °C and for the piping at surface level was 79.07 °C (Fig. 5.14c). Temperatures in the pipe, grout and surrounding rock took longer to equilibrate during recharge periods. This was

due to purely conductive heat transfer from the surrounding rock cooling the wellbore. After 25 years recharge, the temperature at the top of the borehole (surface level) for the pipe, grout and confining rock were all 12.88 °C (Fig. 5.14d). This highlights the slower thermal rate of recharge when only conductive heat transfer is present.

5.4.2 Parameterisation model results - geological conditions

5.4.2.1 Porosity, fluid salinity and thermal conductivity variations (G1, G2 & G3)

Porosity (Fig. 5.15) was modelled at 10 %, 20 % and 30 %, fluid salinity at 0.04 ppm/10^6, 0.16 ppm/10^6 and 0.2 ppm/10^6 (Fig. 5.16), and thermal conductivity at 2 W/m/°C, 4 W/m/°C and 5 W/m/°C (Fig. 5.17). All the above parameters only had a minor effect on the system, changing the production temperature in all cases by a minimal amount (i.e., less than 0.15°C). When testing porosity changes, temperature at the well screen only changed between the minimum and maximum scenarios by 0.14 °C. For alternate salinities the difference was 0.07 °C and for different thermal conductivities the change in temperature was 0.09 °C. None of the above parameters had an effect on the depletion or recharge of head in the system and only had a minor effect on energy production (Fig. 5.18).
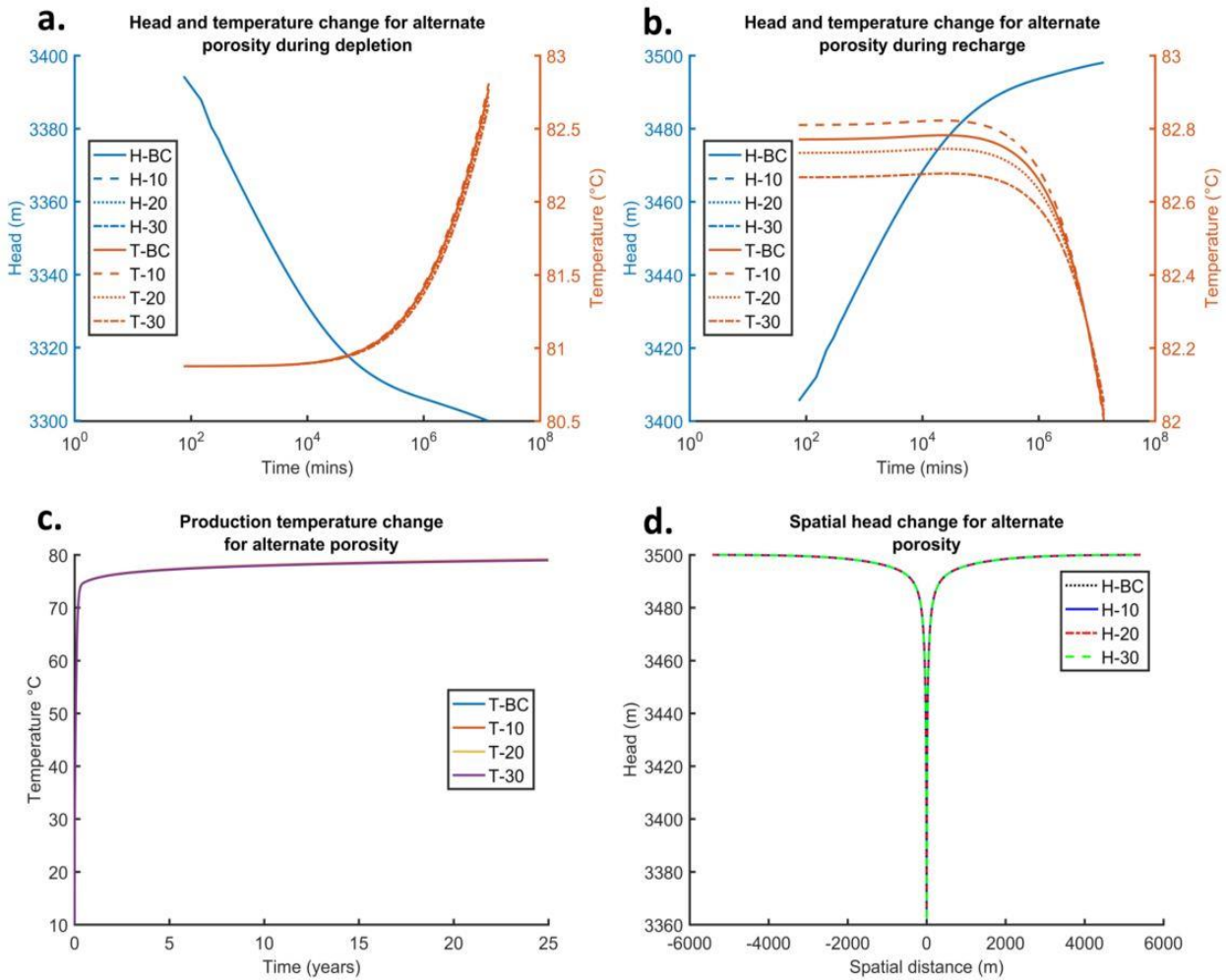
Figure 5.15: *Well screen temperature (T) and head variations (H) with time during depletion and recharge phases for varying porosity (a – b), (c) shows the change in production temperature and (d) is the zone of influence. Porosities shown for the base case BC (15%), S1 (10%), S2 (20%) and S3 (30%).*
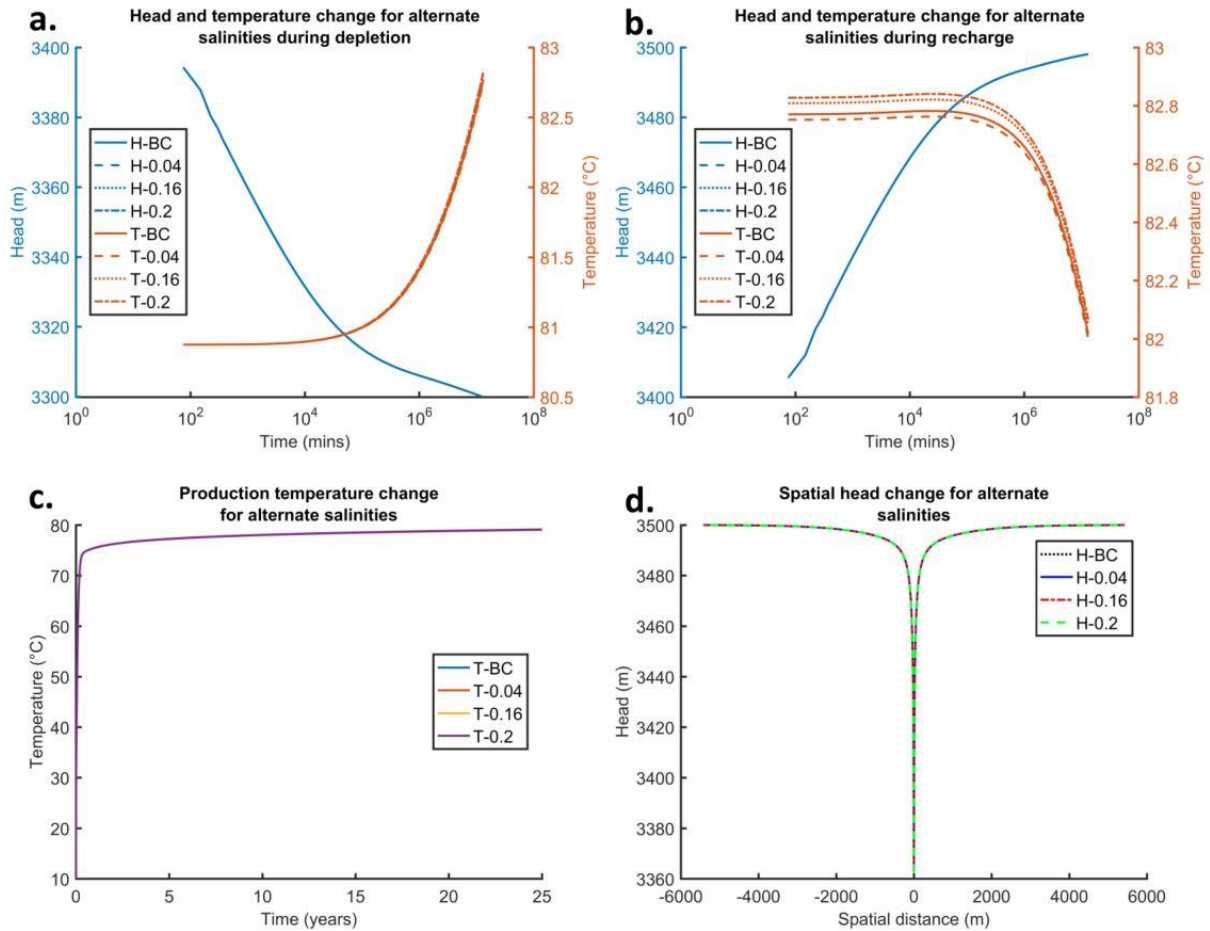
Figure 5.16: *Well screen temperature (T) and head variations (H) with time during depletion and recharge phases for varying salinities (a – b), (c) shows the change in production temperature and (d) is the zone of influence. Salinity shown for the base case BC (0.08 ppm/10^6), S1 (0.04 ppm/10^6), S2 (0.16 ppm/10^6) and S3 (0.2 ppm/10^6).*

Porosity and fluid salinity have been shown to have a more significant effect on temperature in doublet systems (Saeid et al., 2013, 2015) whilst thermal conductivity in the reservoir has been shown to have a significant effect on productivity in fractured systems (Aliyu and Chen, 2017). The reason for this difference is likely to be due to the higher contrast in temperature within a system. In the model presented by Saeid et al. (2013, 2015), the reservoir is of similar temperature, however, the injection fluid is 20 °C and 30 °C, respectively. This vast difference in temperature is far more influential in a doublet system, emphasising the effects of porosity and salinity. In a single well

system, however, temperature change in the aquifer is limited and these parameters have a less

significant influence. Similarly, the model presented by Aliyu and Chen (2017) uses multiple wells,

including an injection well, inputting cold fluid into a high-enthalpy system (200 °C reservoir). Both

the above studies are based on simulations that run for lifetimes in excess of double that modelled

here, again emphasising the effects. It is also worth noting that porosity and salinity may have more

of an effect if the model physical description were to include deformation, and temporal evolution of

density and viscosity.
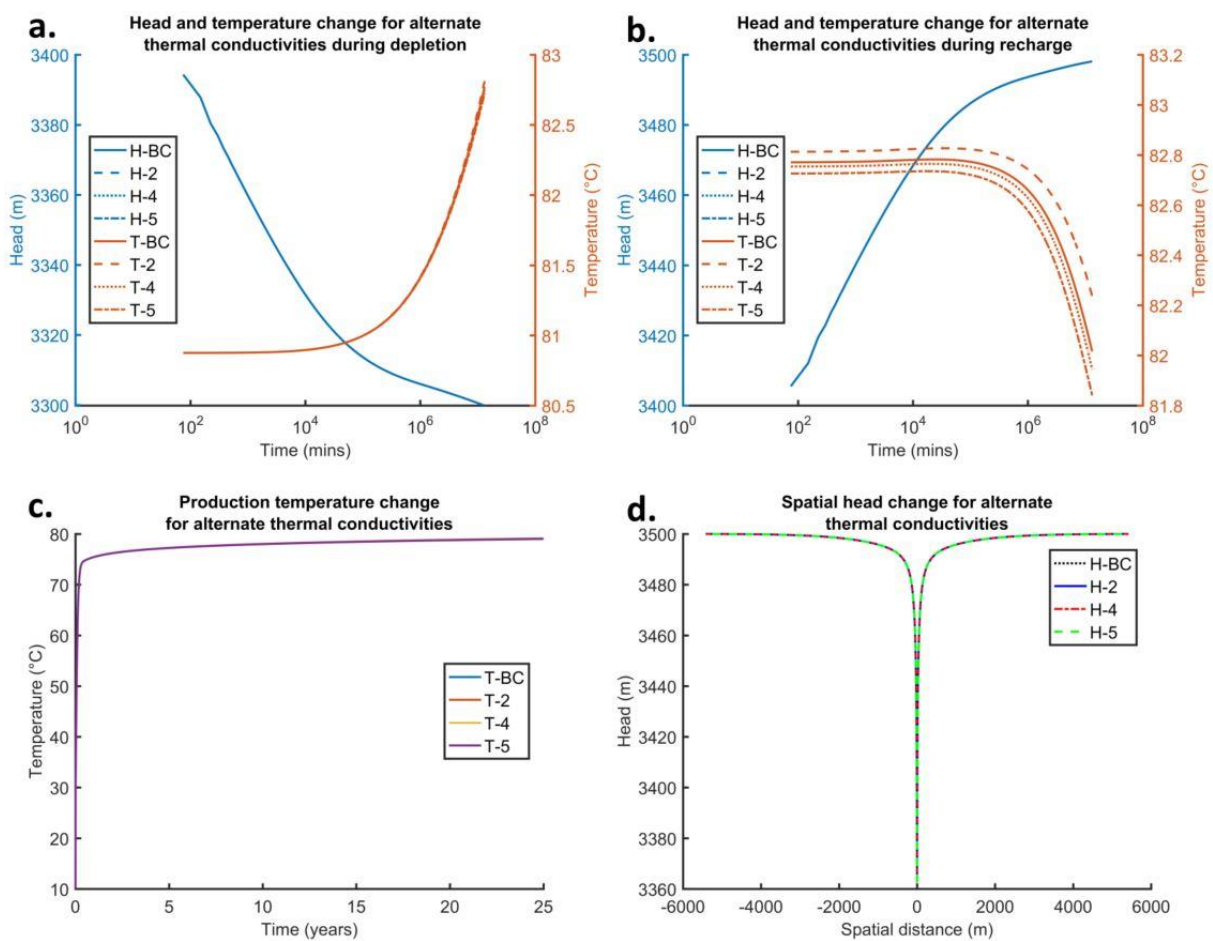
Figure 5.17: *Well screen temperature (T) and head (H) variations with time during depletion and recharge*

phases for varying thermal conductivities (a – b), (c) shows the change in production temperature and (d) is the

zone of influence. Thermal conductivity shown for the base case BC (3.41 W/m/°C), S1 (2 W/m/°C), S2 (4

W/m/°C) and S3 (5 W/m/°C).

162
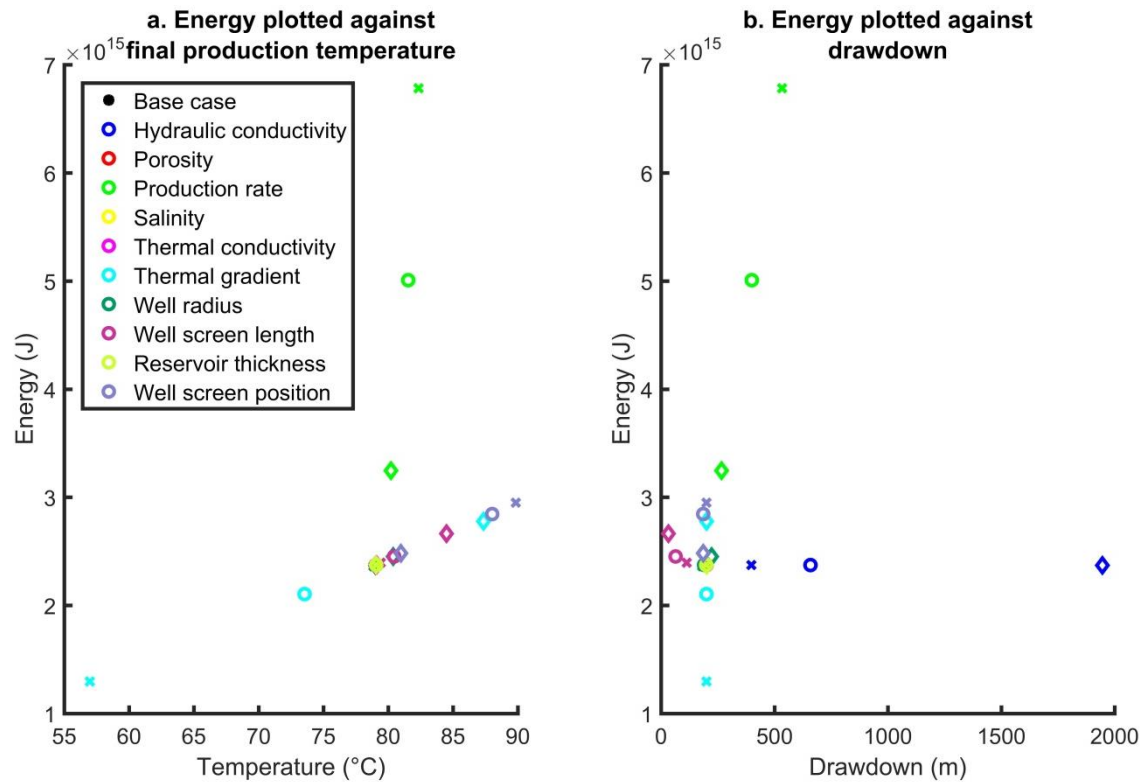
Figure 5.18: *The final production temperature at the wellhead and drawdown versus the total energy produced. The four outliers which reach the cut-offs for shorter lifetimes are for reservoir temperature (17 °C/km thermal gradient), production rate (40 l/s) and hydraulic conductivity (1e-2 and 3e-2 m/day). The cross represents scenario 1, the circle scenario 2 and the diamond scenario 3 for each parameter, respectively.*

5.4.2.2 Reservoir thickness variations (G4)

Thickness variations of (S1) -70 m, (S2) +140 m and (S3) +70 m were considered (Fig. 5.19). The thicknesses were added or removed from the base of the reservoir. The change in head in the aquifer was minor in comparison to the base case whilst lifetime and the amount of fluid produced were also identical to the base case scenario. Temperature difference at the well screen between the smallest reservoir thickness (S1) and largest thickness (S2) was 0.02 °C (Fig. 5.19a). The zone of influence increased when the thickness of the aquifer reduced with radii of 2.735 km, 2.06 km and 2.285 respectively for scenarios S1-S3 (Fig. 5.19d). For the time frame modelled, the thickness of the reservoir (within 140 m of the base case) lacked influence on productivity. Greater lifetimes, or

greater differences in aquifer thicknesses, may have a more significant effect on a system. During recharge, head recovered by 198.8 m, 197.5 m and 197.9 m, respectively for S1-S3, whilst temperature recovered by 0.75 °C at the well screen in all scenarios (Fig. 5.19b). The thickness of an aquifer should not be ignored completely in well planning when the hydraulic conductivity is unknown. The thickness affects the transmissivity of an aquifer and may have a more significant effect when the hydraulic conductivity is of poor quality.
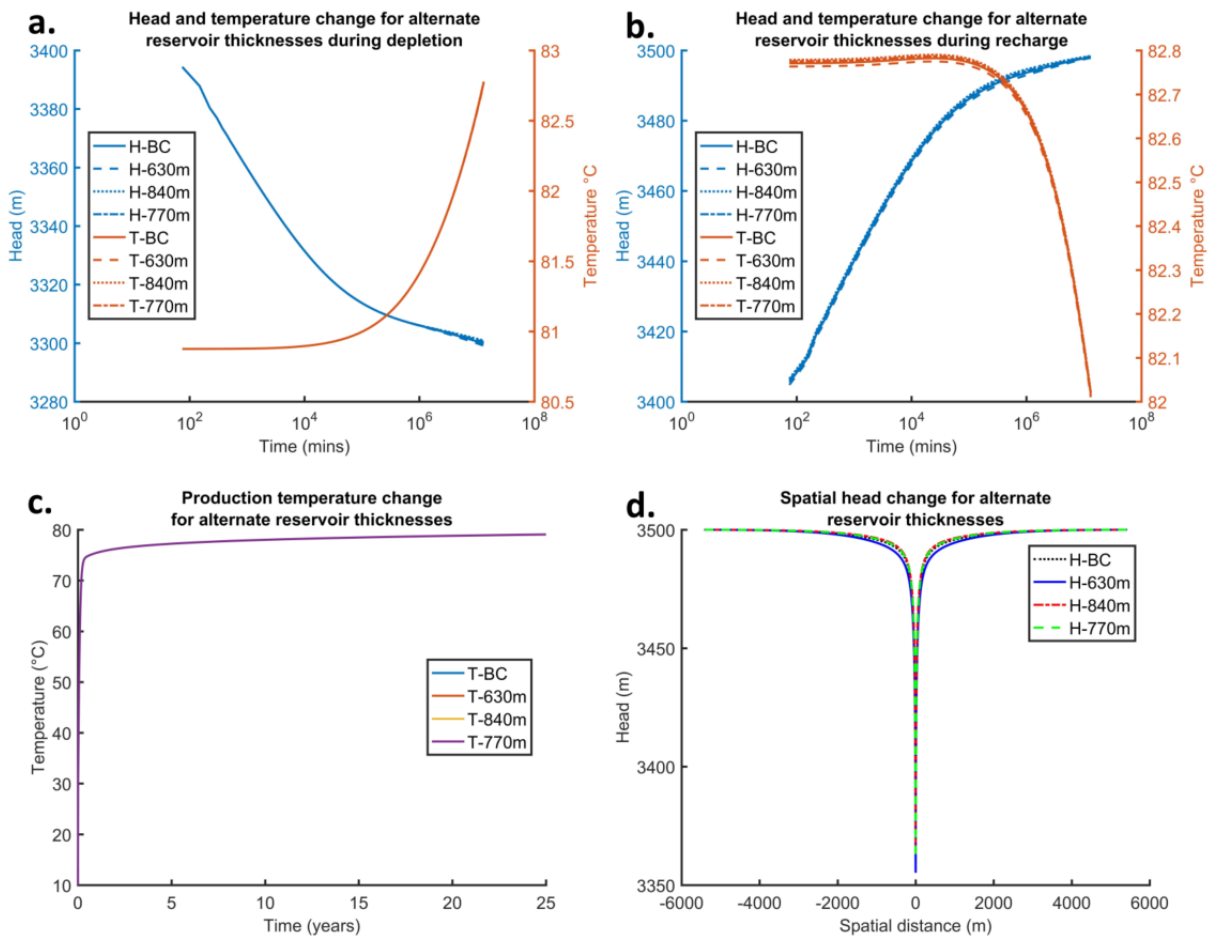
Figure 5.19: *Well screen temperature (T) and head variations (H) with time during depletion and recharge phases for varying reservoir thickness (a – b), (c) shows the change in production temperature and (d) is the zone of influence. Reservoir thicknesses shown for the base case BC (700 m), S1 (630 m), S2 (840 m) and S3 (770 m).*

5.4.2.3 Hydraulic conductivity variations (G5)

Three hydraulic conductivities were modelled: (S1) 0.01 m/d, (S2) 0.03 m/d and (S3) 0.05 m/d) (Fig. 5.20). Low hydraulic conductivities resulted in rapid pressure drops in the reservoir around the wellbore with the worst case scenario (S1) resulting in the well head immediately dropping below the cut-off. Similarly, scenario 2 also dropped below the cut-off within the first few days. Hydraulic head in the wellbore changed by 1946.1 m, 658.9 m and 398.1 m for scenarios S1-3 (Fig. 5.20a). Temperature, however, depleted at slower rates as fluid circulation was limited and, therefore, surrounding waters could not enter the pore space, with the reservoir temperature change modelled at 1.84 °C, 1.88 °C and 1.89 °C. The wellbore also only affected proximal areas within a radius of 1.235 km, 1.835 km and 2.06 km (S1-S3). The cone of depression was larger around the well screen for poorer hydraulic conductivities (Fig. 5.20d). The reason for the zone of influence increasing with better hydraulic conductivity is related to the connectivity between pore-spaces limiting the transmittance of fluid toward the wellbore for poorer conductivities. The cone of depression increasing with lower hydraulic conductivities highlighted the fact that head drop around the wellbore was rapid and that fluid flux radially towards the well screen was not enough to replenish the extracted fluid. During recovery, the temperature change at the well screen remained small at 0.68 °C, 0.73 °C and 0.75 °C, respectively for each scenario, whilst recovery from drawdown was 1,930.5 m, 653.2 m and 394.5 m (Fig. 5.20b). Hydraulic conductivity change did not have a significant effect on the production temperature or energy output. The key issue with hydraulic conductivity is that it may reduce inflow into the well such that drawdown in the well is too significant for it to produce water (e.g., S1, S2), resulting in a reduced lifetime. Further modelling analysis was performed with a hydraulic conductivity value of 0.5 m/day and drawdown in the well gave a final head of 3,458.9 m at the end of production.
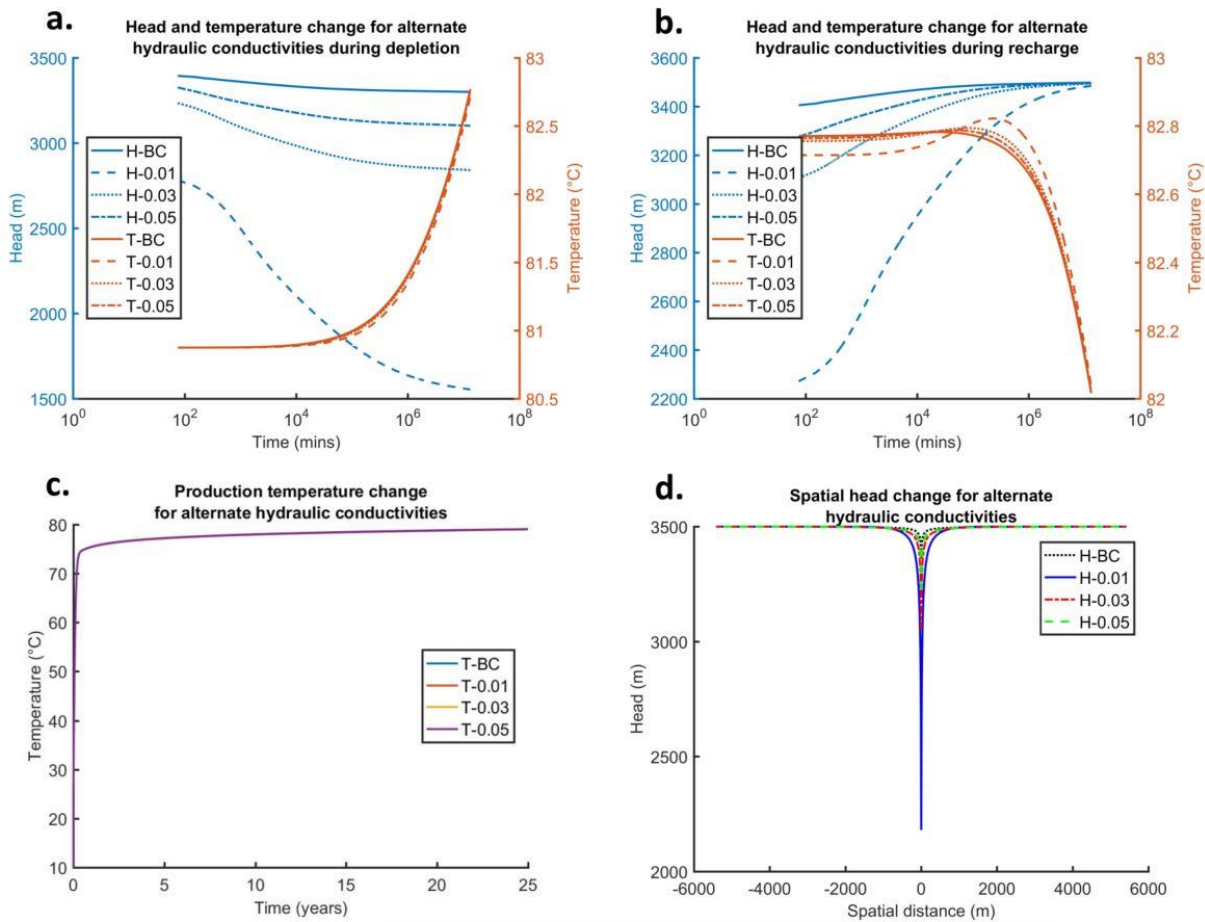
Figure 5.20: *Well screen temperature (T) and head variations (H) with time during depletion and recharge phases for varying hydraulic conductivities (a – b), (c) shows the change in production temperature and (d) is the zone of influence. Hydraulic conductivities shown for the base case BC (1e-1 m/day), S1 (1e-2 m/day), S2 (3e-2 m/day) and S3 (5e-2 m/day).*

5.4.2.4 Thermal gradient variations (G6)

Three thermal gradients were modelled: 28 °C/km (S1) (Busby et al., 2011), 23 °C/km (S2) (Atkins, 2013) and 17 °C/km (S3) (Downing and Gray, 1986b). Scenario 3 was immediately below the cut-off temperature as the initial temperature at the well screen was 58.2 °C (Figs. 5.21a & 5.21c), however, both scenarios 1 and 2 were within the cut-off for the entire production period (Figs. 5.21a & 5.21c). Temperature change during both depletion and recharge was significant due to the different initial temperatures. Change in temperature at the well screen during depletion was 2.11 °C

(S1), 1.75 °C (S2) and 1.3 °C (S3). A similar trend was reflected during recharge with temperature recovering by 0.84 °C (S1), 0.69 °C (S2) and 0.51 °C (S3) (Fig. 5.21b). The thermal gradient did not influence head in the model (Figs. 5.21a, 5.21b & 5.21d). The difference in production temperature caused by the initial aquifer temperature is a major factor to consider as it greatly influenced the energy production: 2.78×10^{15}J (S1), 2.1×10^{15} J (S2), 1.3×10^{15} J (S3) (Fig. 5.18). The final production temperatures for scenarios 1-3 were 87.35 °C, 73.55 °C and 56.97 °C (Fig. 5.21).
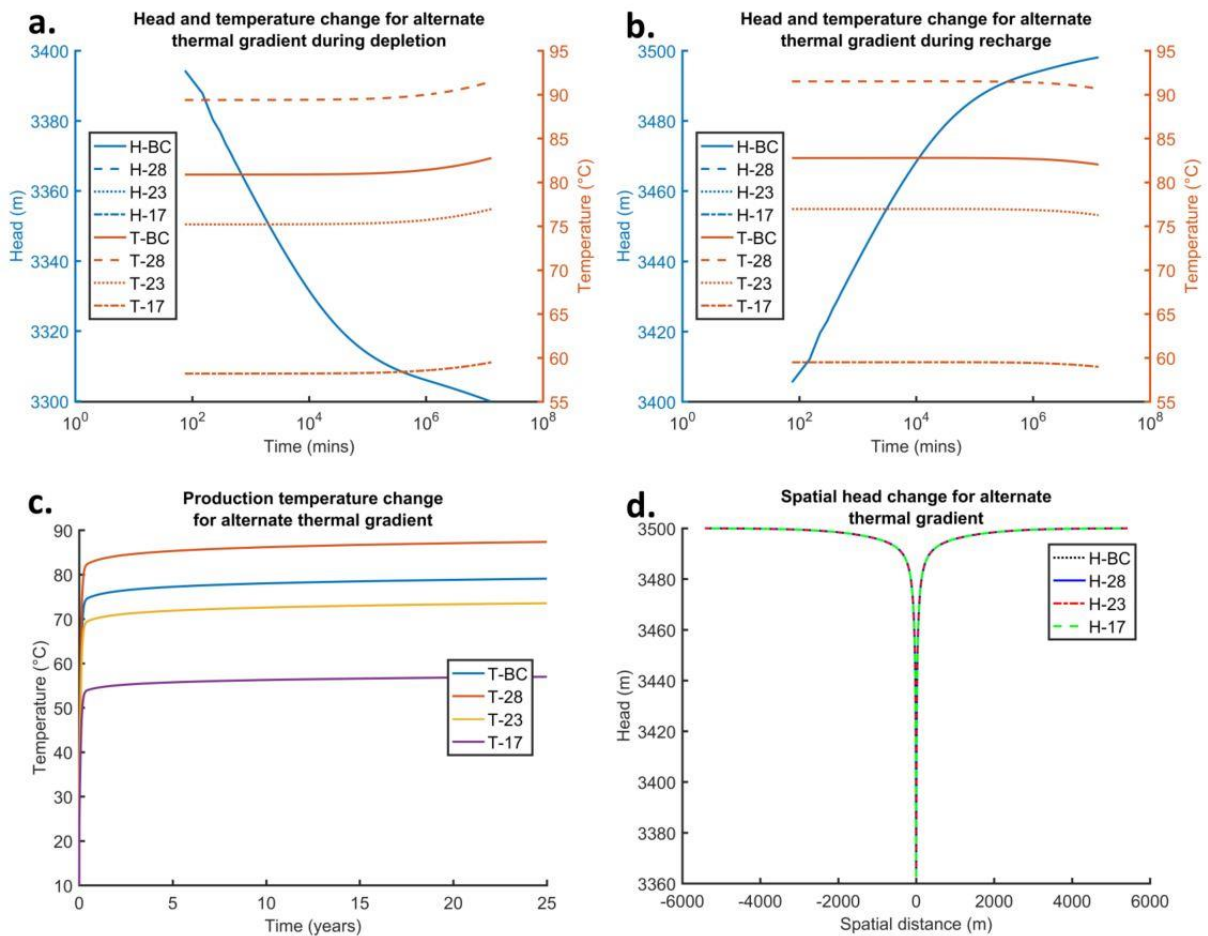
Figure 5.21: *Well screen temperature (T) and head variations (H) with time during depletion and recharge phases for varying thermal gradients (a – b), (c) shows the change in production temperature and (d) is the zone of influence. Thermal gradients shown for the base case BC (25 °C/km), S1 (28 °C/km), S2 (23 °C/km) and S3 (17 °C/km).*

5.4.3 Parameterisation model results - engineering conditions

5.4.3.1 Well screen position variations (E1)

The position of the well screen can be important for the depletion of fluid in the reservoir as the confining upper or lower boundary can reduce the proximal quantity of fluid that can be drawn into the wellbore. The position of the screen is also important for thermal fluxes in the wellbore as deeper localities result in higher temperatures and, therefore, increased energy production. The three parametric scenarios located the wellbore in the upper-middle (S1), lower-middle (S2) and base of the reservoir (S3) (Fig. 5.22, Table 5.3). The position of the well screen did have a minor influence on drawdown. The two cases (base case and S3) where the well screen was located at the upper and lower boundaries of the reservoir had a higher drawdown than the central location of the well screen by 14.2 m (Fig. 5.22a). Temperature varied between different scenarios due to the different initial temperatures at the screened interval. The middle screen position scenarios showed minimal variations in temperature over the lifetime of the well during depletion and recharge (S1 slightly increasing and S2 decreasing), whilst the basal well screen position (S3) showed a reduction in temperature at the well screen from 96.62 °C to 94.64 °C. The zone of influence was identical to the base case (Fig. 5.22d). The total energy produced was also slightly altered due to the change in production temperature: 2.48×10^{15} J (S1), 2.84×10^{15} J (S2), 2.95×10^{15} J (S3) (Fig. 5.18). During the recharge phase all scenarios recovered to 3,498 m head in the wellbore. Temperature changed by 0.016 °C in both scenarios 1 and 2 during recharge, but recovered by 0.77 °C in scenario 3 (Fig. 5.22b). The alternate positions of the well screen can be used when planning the well to mitigate lower initial aquifer temperatures. The final production temperatures at the wellhead for S1-S3 were 80.97 °C, 88.02 °C and 89.85 °C (Fig. 5.22c).
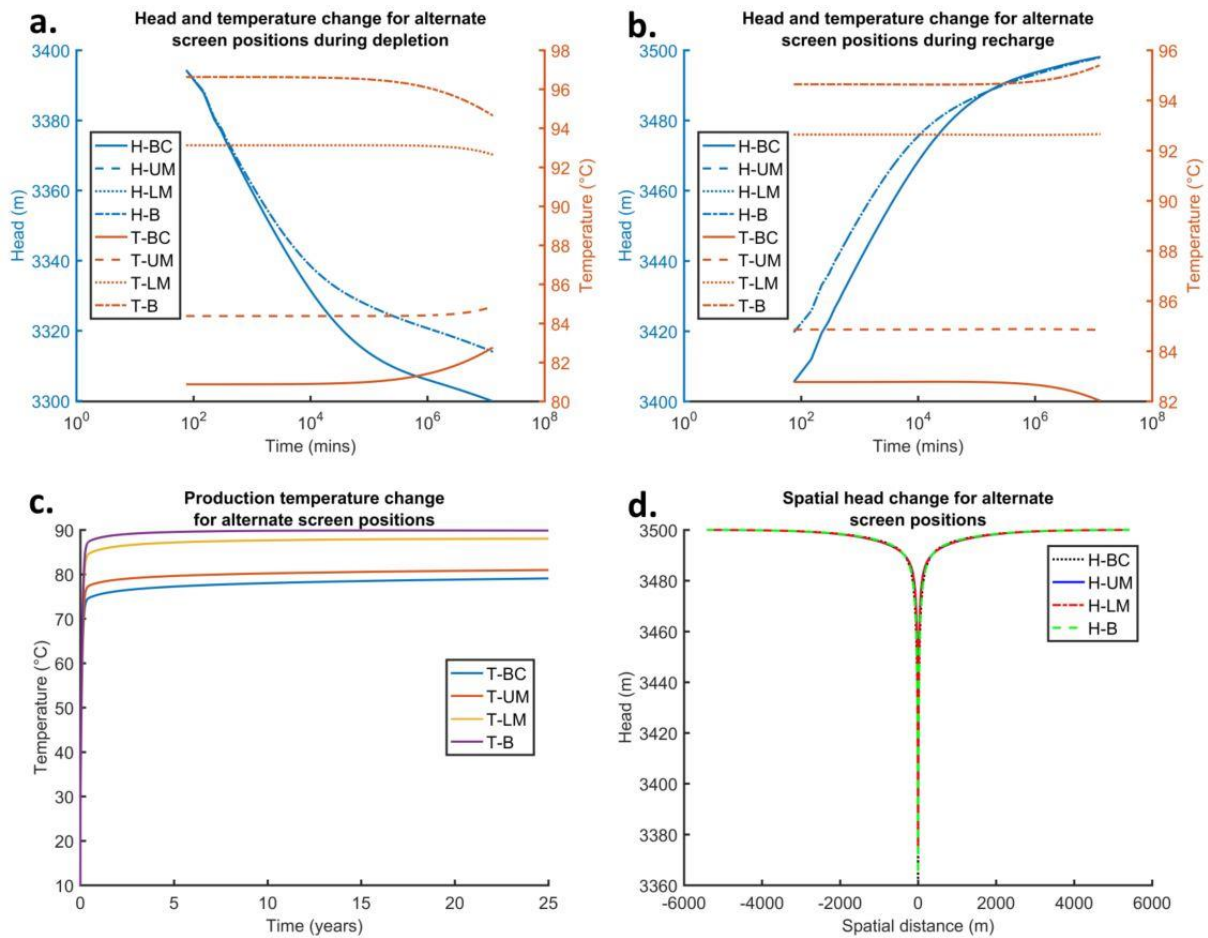
Figure 5.22: *Well screen temperature (T) and head variations (H) with time during depletion and recharge phases for varying well screen position (a – b), (c) shows the change in production temperature and (d) is the zone of influence. Well screen position shown for the base case BC (top HSA (2.8-2.87 km)), S1 (upper middle of the HSA (2.94-3.01 km)), S2 (lower middle of the HSA (3.29-3.36 km)) and S3 (base of HSA (3.430-3.500 km)).*

5.4.3.2 Flow rate variations (E2)

The Collyhurst Sandstone Formation can yield 20-30 l/s (S1 and S2) from large diameter boreholes in shallower areas of the Cheshire Basin (Griffiths et al., 2003); whilst some have estimated that at 4 km deep, 40 l/s (S3) extraction rates can be obtained (Atkins, 2013). Although the latter seems unlikely, all scenarios were modelled. For flow rates of 20 – 40 l/s, the head in the reservoir depleted more rapidly than the base case scenario (15 l/s), such that the head in the well fell by 266.9 m, 400.3 m and 533.7 m, respectively for S1-S3 (Fig. 5.23a). Scenario 3 reached the 3,000 m

head cut-off within the first year of production. Higher flow rates were unsustainable and the zone of influence of the well significantly increased with greater production rates. This was recorded for each scenario at 2.51 km, 2.735 km, and 3.063 km, respectively (Fig. 5.23d). Final reservoir temperatures in the well screen area reached 83.04 °C, 83.46 °C and 83.8 °C (Fig. 5.23c). Although flow rates limit the lifetime of the single well, a substantial amount of energy and fluid could still be produced for each scenario, i.e., 3.256×10^{15} J and 15,800,000,000 litres (S1), 5.01×10^{15} J and 23,700,000,000 litres (S2) and 6.78×10^{15} J and 31,500,000,000 litres (S3 – assuming production for 25 years) (Fig. 5.18). Under recharge conditions, head recovered by 264.4 m, 396.5 m and 528.6 m (Fig. 5.23b). For all scenarios, well screen temperature changed during recovery by 0.84 °C, 0.96 °C and 1.1 °C respectively. Higher production rates also resulted in increased production temperatures as the fluid is able to move up the pipe without cooling. The final wellhead temperatures for each scenario (1-3) were 80.22 °C, 81.54 °C and 82.34 °C (Figs. 5.18 & 5.23).
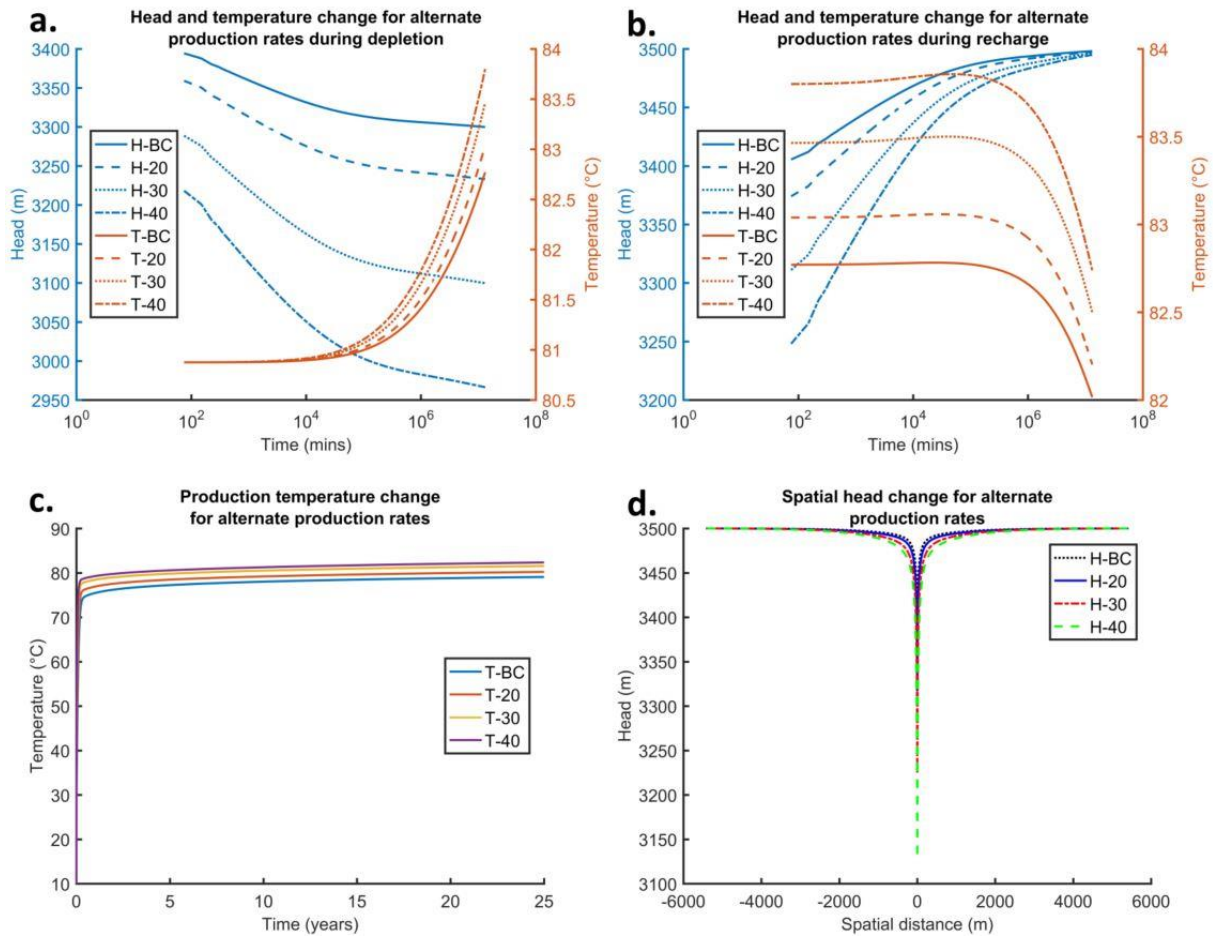
Figure 5.23: *Well screen temperature (T) and head variations (H) with time during depletion and recharge phases for varying production rates (a – b), (c) shows the change in production temperature and (d) is the zone of influence. Production rates shown for the base case BC (15 l/s), S1 (20 l/s), S2 (30 l/s) and S3 (40 l/s).*

5.4.3.3 Well screen length (E3)

A range of well screen lengths were modelled including fully penetrative in the reservoir (S1), and partially penetrative at 280 m (S2) and 140 m (S3) (Fig. 5.24). Lower penetration rates caused an increase in drawdown over the lifetime of the system: (S1-S3) 32.1 m, 64.2 m and 113.1 m (Fig. 5.24a). Similarly, temperature change at the well screen increased with reduced penetration with no change recorded for fully penetrative wells, and 0.8 °C and 1.28 °C for partially penetrated well screens of S2 and S3. The fully penetrative well did not show temperature change as only horizontal fluxes occurred in the system. The amount of energy produced also increased with greater

penetration due to a higher production temperature (Fig. 5.24c): 2.66×10^{15}J (S1), 2.45×10^{15}J (S2) and 2.39×10^{15}J (S3) (Fig. 5.18). Head recharged by 30.4 m (S1), 62.4 m (S2) and 111.3 m (S3), whilst temperature recovered by 0.14 °C and 0.36 °C for S2 and S3 respectively (Fig. 5.24b).
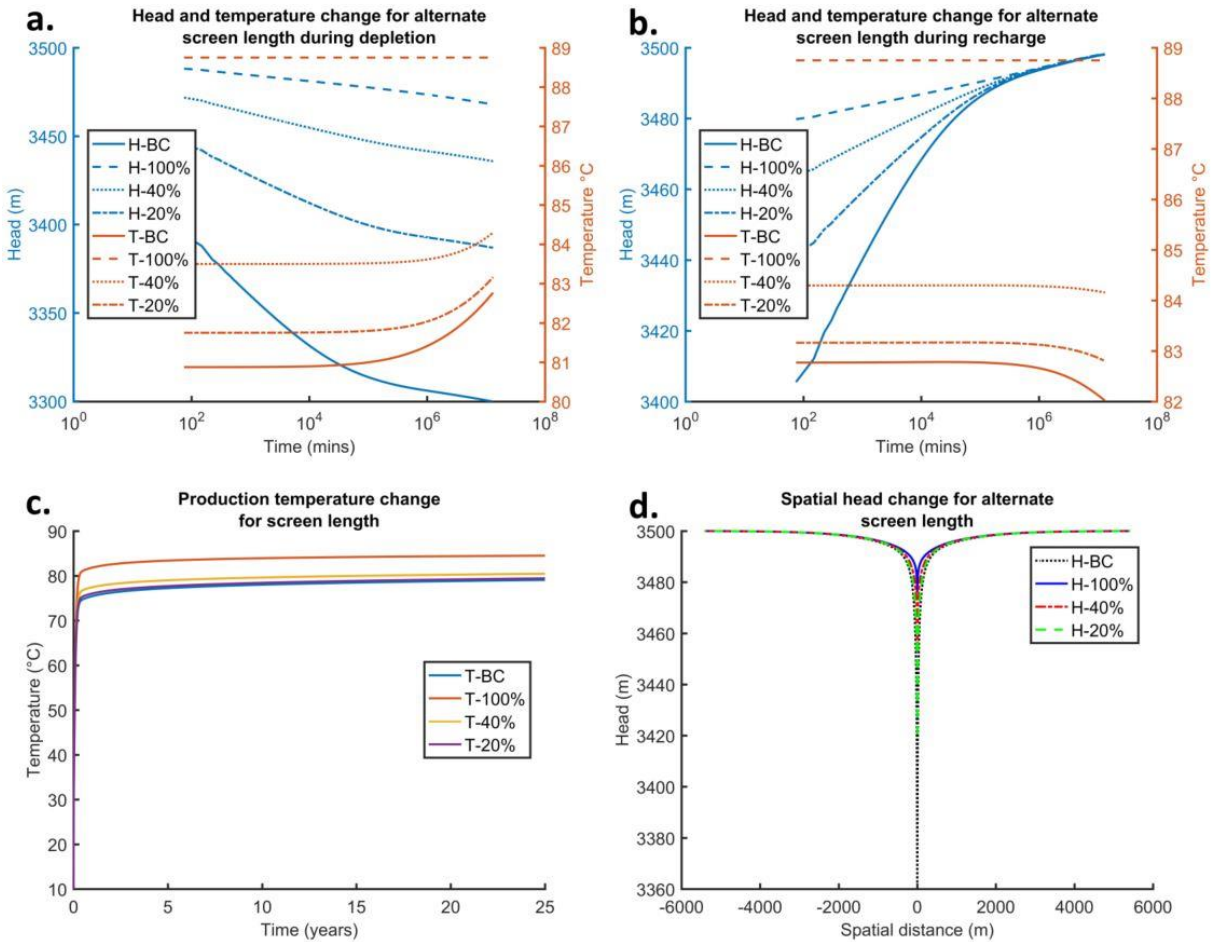
Figure 5.24: *Well screen temperature (T) and head variations (H) with time during depletion and recharge phases for varying well screen lengths (a – b), (c) shows the change in production temperature and (d) is the zone of influence. Well screen length is shown for the base case BC (penetrating 10 % of the HSA), S1 (100 %), S2 (40 %) and S3 (20 %).*

5.4.3.4 Wellbore radius variations (E4)

To investigate the effects of a slim borehole versus regular borehole, wellbores and well screen were modelled to be of equal diameter. The radii were set at 0.05 m (S1), 0.15 m (S2) and 0.2 m (S3), whilst the base case scenario had a borehole radius of 0.153 m and well screen radius of 0.106 m. A smaller radius resulted in greater drawdown in the well, with scenarios 1-3 recording a final well head of 3,276.7 m, 3,310.2 m and 3,318.5 m (Fig. 5.25a). As temperature in the reservoir was not influenced in the model by wellbore radius, the reservoir temperature was the same as the base case. During recharge, head re-equilibrated to 3,498 m in the 25 year simulated time period (Fig. 5.25b). Temperature in the piping was affected by the radius of the wellbore due to the higher velocities created in the pipe for the smaller radii, meaning less heat was lost. The energy recorded for scenarios 1-3 were: 2.45×10^{15}J (S1), 2.37×10^{15}J (S2) & 2.36×10^{15}J (S3) (Fig. 5.18). The final production temperature varied by 1.5 °C (S1 – S3) (Fig. 5.25 c); this was due to the faster velocities in the narrower wellbore.
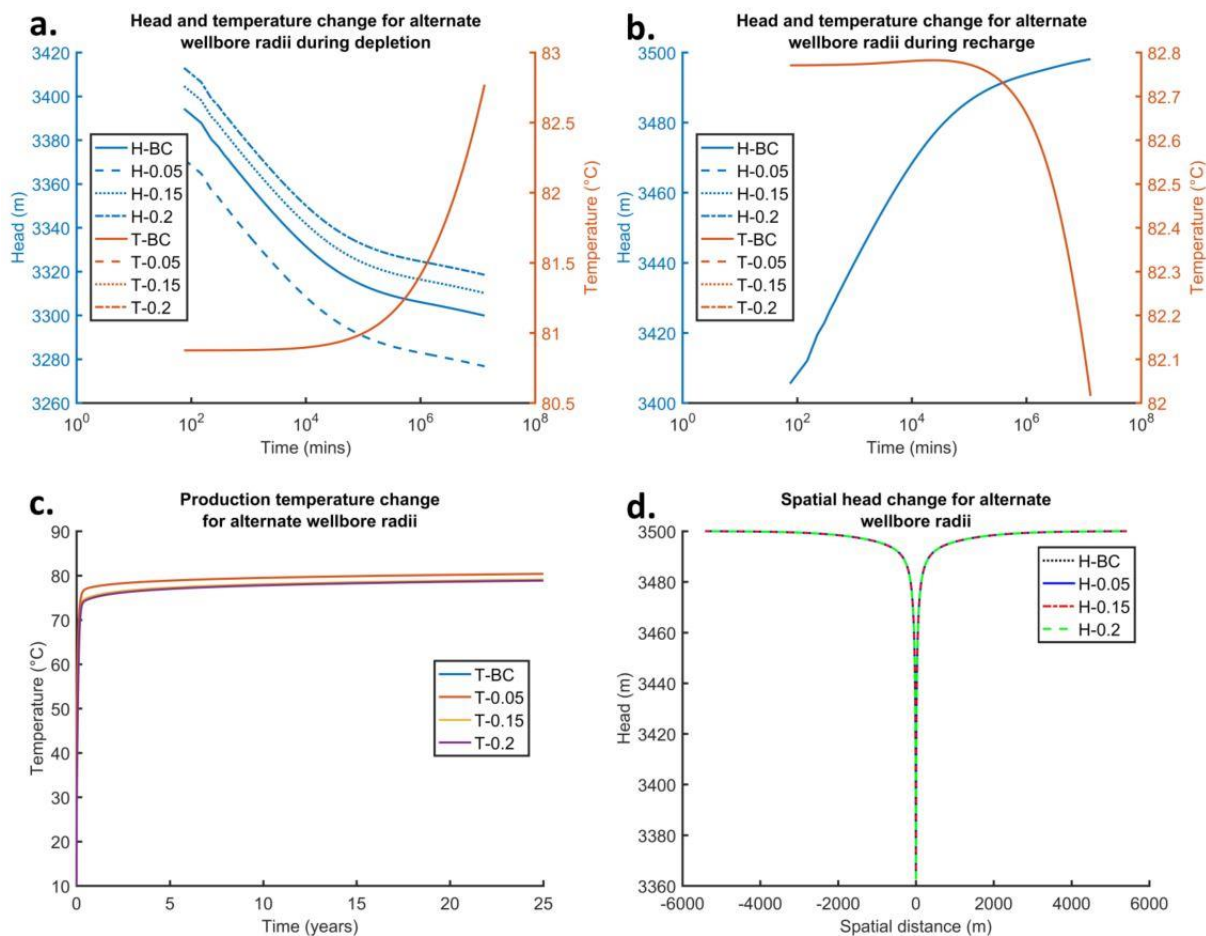
Figure 5.25: *Well screen temperature (T) and head variations (H) with time during depletion and recharge phases for varying wellbore radii (a – b), (c) shows the change in production temperature and (d) is the zone of influence. Wellbore radii shown for the base case BC (0.106 m), S1 (0.05 m), S2 (0.15 m) and S3 (0.2 m).*

5.4.4 Planning for low hydraulic conductivities

The initial results of the parametric modelling study indicated that thermal gradient, hydraulic conductivity, production rate, length and position of the well screen had the most significant effects on the energy output, the sustainability of aquifer head and the production temperature. Hydraulic conductivity, production rate and thermal gradient all resulted in reduced operational lifetime in the worst case scenarios. Although different thermal gradients can dictate the energy production in a reservoir, it is difficult to alter these in single well schemes as the temperature may already be below the threshold for economic viability. The only way to alleviate

this is by drawing in water at the base of the reservoir where the temperature will be greater, leading to the position of the well screen being influential. Low hydraulic conductivities, however, can be mitigated by increasing the length of the well screen or reducing the production rate.

To investigate this, hydraulic conductivities of 0.01 m/day and 0.05 m/day (S1 and S3) were modelled with both increased well screen length and decreased production rates. Well screen lengths were increased to a penetration ratio of 50 % and 100 %, whilst production rates were reduced to 5 and 10 l/s. Reducing the production rate did help to reduce the amount of drawdown, but did not reduce it enough to make the lower hydraulic conductivity scenario viable (0.01 m/day). Increasing the screen length, however, did ensure that the lower hydraulic conductivity could be viable and the well head/temperature did not reach the cut-off.

When increasing the well screen length, drawdown was dramatically reduced. A 50 % well screen length reduced the amount of drawdown to a final head in the wellbore of 3,015 m for hydraulic conductivities of 0.01 m/day and 3,395.7 m for 0.05 m/day (Fig. 5.26a), far higher than that for the 10% penetration ratio (1,553.9 m and 3,103.9 m). For the same scenarios, final head levels for a fully penetrating well were 3,229.8 m and 3,438.9 m, respectively (Fig. 5.26a). The variation in end temperature observed at the well screen for the different hydraulic conductivities was minor; for the 50 % well screen length the difference was 0.04 °C. When the well was fully penetrative there was no temperature change between different cases. Although having a longer well screen was beneficial for increasing lifetime and counteracting poor hydraulic conductivities, it would be far more costly. However, it may be more beneficial for energy output as the ability to draw hotter water from deeper in the reservoir would increase the produced energy to 2.66 x 10^{15} J and 2.48 x 10^{15} J for full and 50 % penetration ratios.

When decreasing the production rate, drawdown was slightly reduced. At a rate of 10 l/s the final head in the wellbore was higher than that for a flow rate of 15 l/s at 2,202.6 m for (0.01 m/day)

(Fig. 5.26b). Similarly, for slightly higher conductivities the wellbore head level increased to 3234.6 m (0.05 m/day) (Fig. 5.26b). The final head levels for a production rate of 5 l/s were 2,851.3 m (0.01 m/day) and 3,367.2 m (0.05 m/day). It is important to note that the energy produced was also significantly reduced to 1.51 x 10^{15} J and 6.57 x 10^{14} J, for 10 and 5 l/s respectively. Lowering the production rate limited the amount of drawdown; however, it also substantially limited the amount of energy that could be produced. In addition, the well did not meet the cut-off for the lowest hydraulic conductivity.

The best solution to mitigate poor hydraulic conductivities may be to optimise a range of engineering characteristics including production rate, position and length of well screen. Individually, increasing the well screen will help to maintain head, however, it may be more costly. Reduced production rates can also help to minimise drawdown, yet have the most influence on total energy extraction. In an ideal scenario this particular parameter will need to be kept as high as possible.
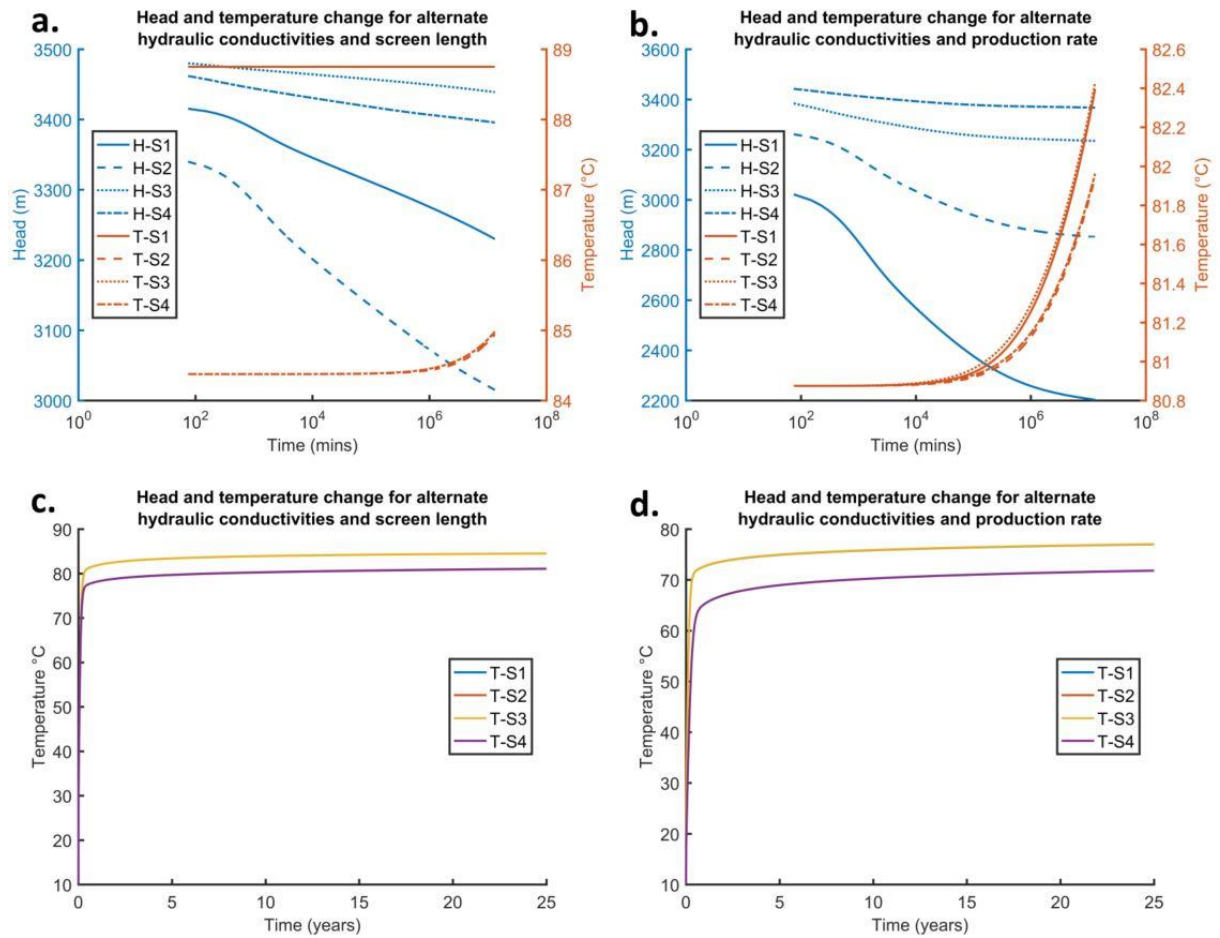
Figure 5.26: *Well screen temperature (T) and head variations (H) with time during the depletion phase for different hydraulic conductivities compared to varying length of the well screen (a) and production rates (b). In the plot (a) S1 is 0.01 m/day v fully penetrative well screen (FWS), S2 is 0.01 m/day v 50 % penetrative well screen (HWS), S3 is 0.05 m/day v FWS, S4 is 0.05 m/day v HWS. In plot (b) S1 is 0.01 m/day v 10 l/s, S2 is 0.01 m/day v 5 l/s, S3 is 0.05 m/day v 10 l/s, S4 is 0.05 m/day v 5 l/s. (c) and (d) are the respective production temperatures.*

5.4.5 Seasonal fluctuations in energy consumption

Over the lifetime of a geothermal energy scheme used for district heating there will be fluctuations in energy demand. Lower demand and consumption will coincide with warmer summer months when domestic spatial heating is unnecessary, leading to annual variations. There will also be smaller cycles of variation coinciding with daytime and evening use. The larger annual cyclicity in

heat usage was considered and in the summer months (when demand is lower), a period of recharge in the HSA was envisaged (Fig. 5.27). This will help to prolong the lifetime of the geothermal resource. Three cyclical scenarios were tested: 1) 6 months depletion and 6 months recharge, 2) 8 months depletion and 4 months recharge and 3) 10 months depletion and 2 months recharge. The base case parameters were used and the system was modelled for 25 years of operation.

a. Modelled flow rates for seasonal fluctuations
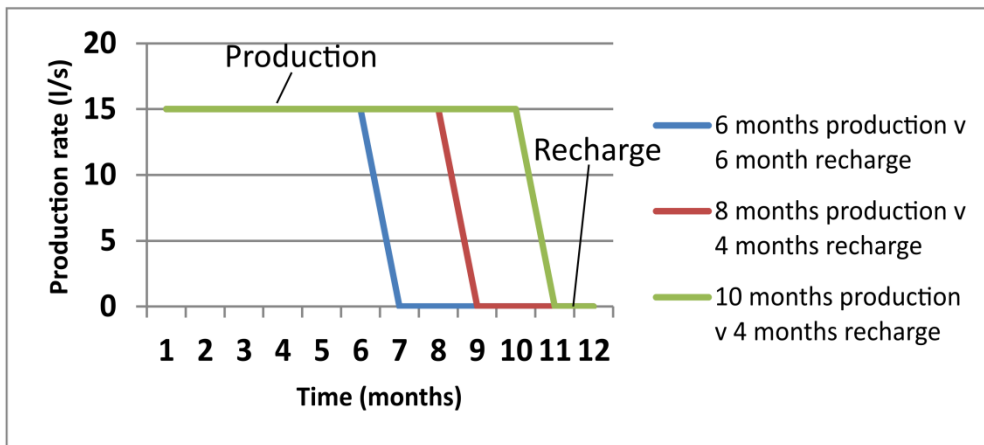
b. Schematic of production   c. Schematic of recharge
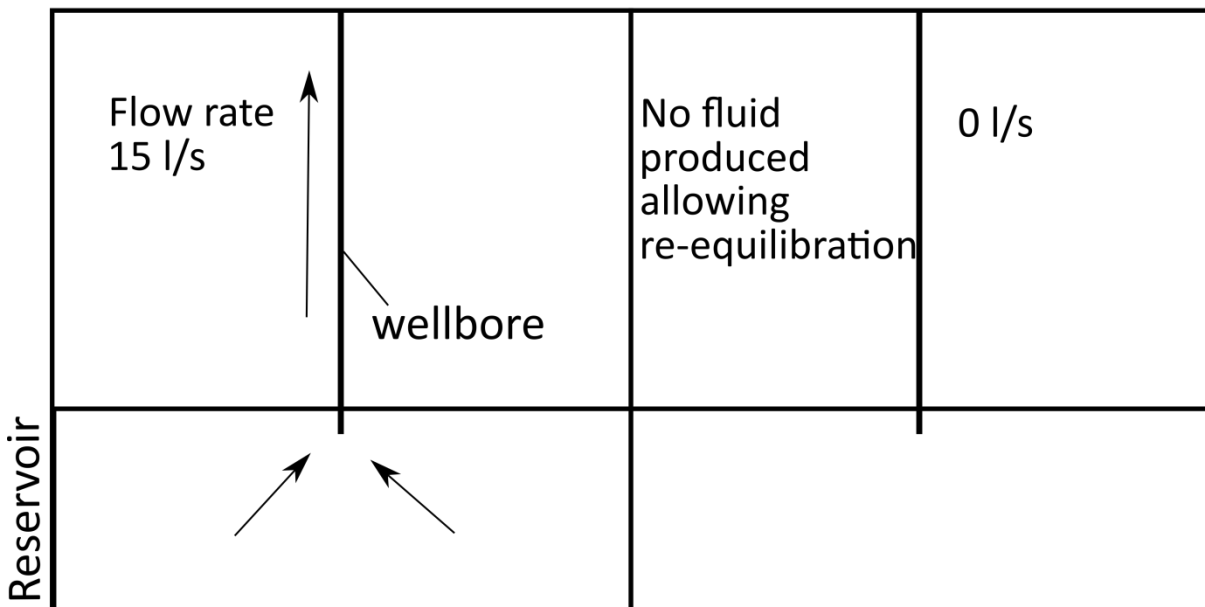
Figure 5.27: *(a) Modelled flow rates for each scenario, schematic of (b) production and (c) recharge.*

Head variations with lifetime were minor; however, periods of longer recharge allowed a greater recovery of head over the lifetime (Fig. 5.28). For the shortest to longest periods of recharge, the final recorded heads were 3,487 m, 3,491.6 m and 3,494.4 m respectively for the three scenarios. Similarly, after the final depletion cycle (year 24) recorded heads were 3,301.5 m, 3,303.3 m and 3,305.5 m, respectively.

The varying scenarios highlighted that shorter levels of annual recharge produced a larger change in temperature in the aquifer; however, this effect was still minimal over a 25-year period of extraction. The scenario with 2 months recharge had a final temperature in the reservoir at the extraction nodes of 82.6 °C, with 82.4 °C for the 4 months recharge and 82.2 °C for 6 months recharge (Fig. 5.28).

Similar variations were reflected in the production temperature. The final temperatures at the top of the wellbore were 52.76. °C, 59.6 °C and 67.5 °C for the varying annual variations from 6 months recharge to 2 months recharge respectively (Fig. 5.29). For the longer periods of recharge (i.e., no production) the change in production temperature was far more significant. This led to reduced production temperatures for longer periods of recharge. At the end of the final production temperature cycle (year 24), the final production temperatures were 78. 2 °C, 78.6 °C and 78.9 °C in order of descending amounts of recharge. The results of the seasonal fluctuation models highlighted that recharge periods should be minimised (if the parameters of the reservoir are similar to the base case model of this study). Higher production temperatures were attained for shorter recharge periods, whilst more energy could be extracted due to longer production periods. The change in head was minimal, with the most significant change in head occurring in the first few hours of production. Although the results show that head and production temperature can be optimised by limiting recharge it does highlight the small variations between different scenarios have minimal effects. It

should be noted for poorer hydraulic conductivities, variations in head could be far more significant and longer periods of recharge may be required.
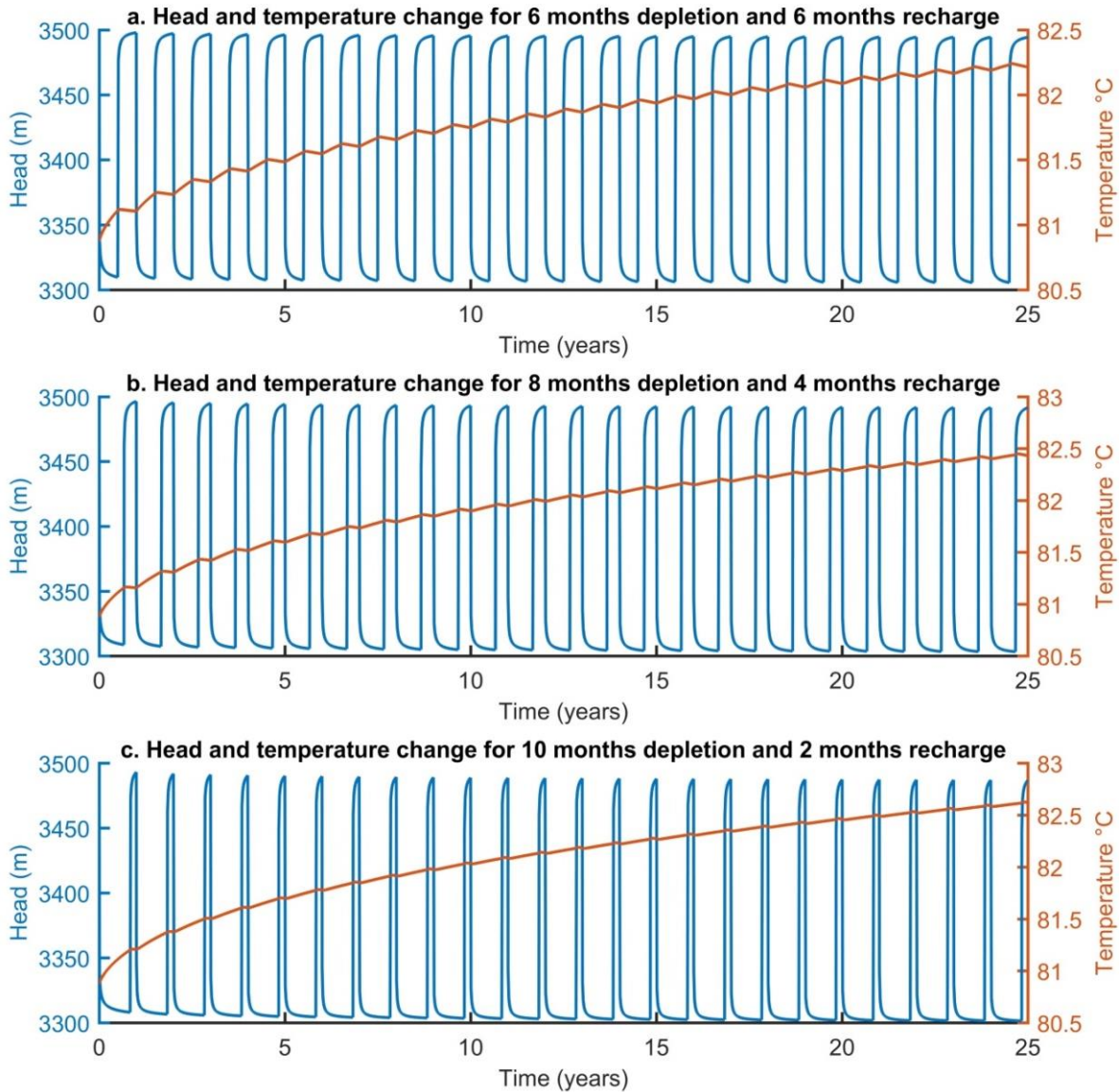
Figure 5.28: *Variations in well head and temperature in the reservoir extraction nodes for varying scenarios: (a) depletion for 6 months and recharge for 6 months, (b) depletion for 8 months and recharge for 4 months, (c) depletion for 10 months and recharge for 2 months.*
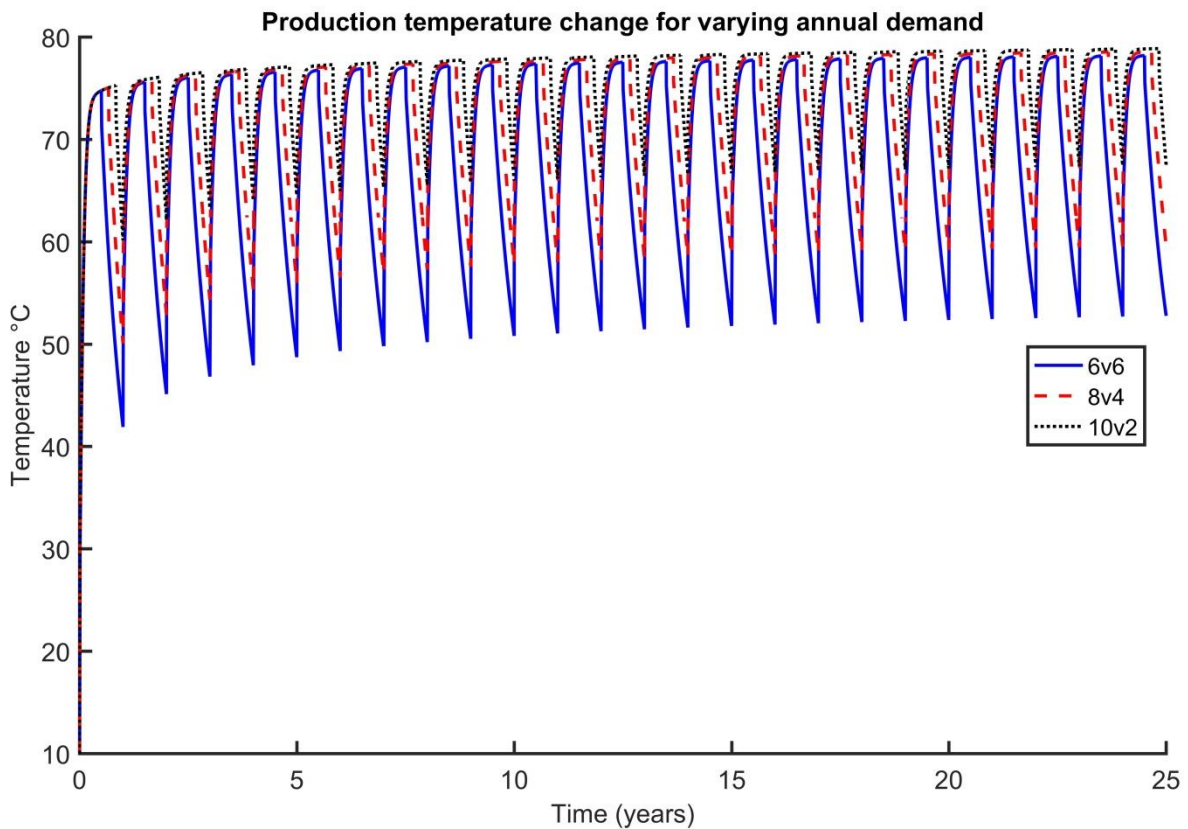
Figure 5.29: *Variations in production temperature (temperature at the top of the wellbore) for seasonal variations of 6 months depletion and 6 months recharge, 8 months depletion and 4 months recharge, 10 months depletion and 2 months recharge.*

5.5 Matching energy to demand in Crewe - the impact of the modelled zones of influence

Recent studies have considered the development of a multi-phase district heat network plan in Crewe (Cheshire, UK) that aims to gradually increase the energy supply to businesses in the town centre with a peak demand of 35 MW, or 76 GWh/year (Routledge et al., 2014). In this study, the total producible energy from the base case single well scheme in the Cheshire Basin was modelled at 2.37 x 10^{15} J or 658 GWh, matching only 35 % of the potential energy demand over 25 years. The development of an initial single well would, however, meet the demands of the core scheme (phase

1 of the current heat network development), which has an energy demand of 0.04 to 1.6 MW (Arup, 2018b).

The original district heat network development was planned as three phases by BRE and Greenfield Consulting Ltd, with the scheme to run on geothermal energy or a combined heat and power scheme. Phase 1 would connect the industrial areas in Leighton West, phase 2 would developing a separate heat network in the town centre and phase 3 would link the two heat networks using a transmission line (Routledge et al., 2014). However, a recent re-evaluation of the heat network scheme in 2019 considered the central area of the town as phase 1 and then spreading the heat network laterally to phase 2 (the train station) and phase 3 (Leighton West industrial park) (Fig. 5.30). This is problematic as the large zone of influence (base case 2.285 km radius) around the well screen in the aquifer would result in the wells being spread laterally away from the demand. The well heads could be located closer to the centre of town but this would likely involve directional drilling schemes, significantly increasing the cost. Alternatively, the well spacing could be moved closer, but a rejection well would be needed to help maintain pressure due to hydraulic interactions between wells. Future work in the basin would benefit from modelling of the development wells combined with a heat network development strategy. An energy and exergy analysis, considering losses in the heat network, would also substantially increase knowledge about the suitability of locating wellheads (from vertically drilled wells) away from high heat demand areas.

Another strategy to meet the heat demand could be to use a combination of shallow- to deep- open well systems extracting from the HSA and shallow closed loop borehole heat exchangers, or the utilisation of cascade schemes to maximise the use of energy (e.g., Rubio-Maya et al., 2015). Studies have also suggested that the demand in the Cheshire East borough (central location over the basin) could reach 198 GWh/yr from new developments (4,074 GWh/yr total demand) by 2030, giving a large energy void which must be filled (LDA design, 2011). To fill this void for new

developments in the Cheshire East borough, 8 wells operating at the base case capacity would be required. This is unlikely to be possible without reinjection wells to maintain pressure; however, further consideration would be required for thermal breakthrough.
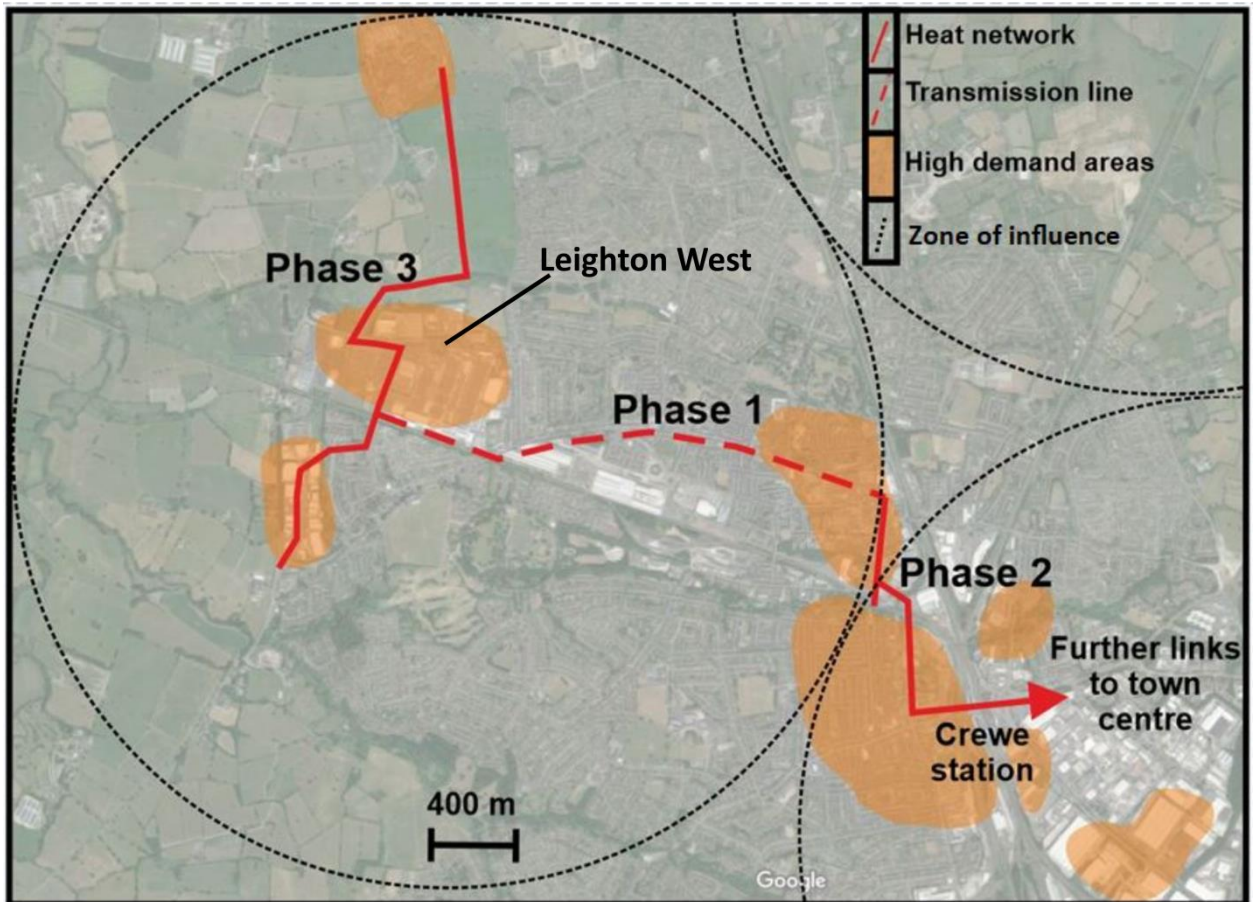
Figure 5.30: *Localities of the zone of influence around potential wellbore areas in the Crewe area. Phase 1 targets the high demand central town centre, whilst phase 2 and 3 link Leighton West and further areas of the town centre. Background image obtained from Google Maps (2018).*

Summary

A modelling sensitivity analysis of both the engineering and geological parameters associated with a single well geothermal scheme has been undertaken for the Cheshire Basin to highlight risk and uncertainty. The findings highlight that the key factors to consider are thermal gradient,

hydraulic conductivity, production rate and length of the well screen. Thermal gradients can be estimated with some confidence using existing nearby wells but it is difficult to estimate hydraulic conductivity at depth accurately. Core plugs and outcrop studies can give good estimations, however the uncertainty at depth is unpredictable. The analysis highlights that the negative effects of poor hydraulic conductivities can be mitigated by reducing the production rate and by increasing the length of well screen. Other engineering factors such as position of the well screen and radius of the wellbore (e.g., slim versus regular) can also aid in the alleviation of high drawdown during production caused by low hydraulic conductivities. Any development scheme must, therefore, be designed to incorporate the engineering factors outlined above to reduce the effects of poor aquifer hydro-physical parameters found during exploration. This will ensure that productivity is sustainable for the desired lifetime of a well. Interestingly, the findings also highlight that slim-boreholes (with smaller radii) have a slight positive impact on the total energy produced as the fluid travels up the borehole faster, cooling at a slower rate. The negative effect of larger drawdown is only minor, meaning a lower cost exploratory slim-borehole could be converted to an effective production well without the costly drilling of another development well.

The findings also show that for the base case scenario, 35 % of the identified district heat system demand in the Crewe area can be met, highlighting the need for more development wells in the area to meet the full demand. As such, the Cheshire Basin can produce energy for a district heating scheme in the Crewe area, assuming that favourable hydraulic conductivities are discovered at depth and the geothermal gradient is high enough to allow production temperatures in excess of 60 °C. Typically, over a period of 25 years, 2.37×10^{15} J of energy can be produced (for the base case). However, further investigation should be undertaken to understand heat losses for the 6.7 km core (phase 1) heat network with current estimates of losses to be 5-10 % (Routledge et al., 2014).

It is also important to note that the key parameters influencing single well schemes are different to those in doublet and multi-well schemes. Whilst the main concern with injection-extraction doublet schemes is the time of thermal breakthrough, the primary focus of single well schemes is the initial temperature and drawdown due to minimal temporal thermal changes. Thick aquifers, such as those in the Cheshire Basin, are more than capable of producing energy through single well partial penetration schemes for low energy demand schemes. For populous areas, such as Crewe, a multi-well or multi-method (both shallow and deep) geothermal scheme should be considered to meet the high demand and to account for the disposal of waste water. Further work on the basin should focus on establishing the true geology at depth in the Crewe area, particularly on whether Carboniferous rocks are present.

CHAPTER 6 – MODELLING ALTERNATIVE WELL CONFIGURATIONS TO REDUCE WASTE WATER FROM SINGLE WELLS IN THE CHESHIRE BASIN, UK

Presently, low-enthalpy geothermal schemes are usually developed by two-well schemes (doublets). Doublets have the benefit of maintaining pressure in the reservoir whilst also disposing of the extracted geothermal fluid. In some cases the benefits do not outweigh the increased initial capital expenditure, leading to an alternative method of extraction through a single well being explored. The methods proposed in this chapter involve returning brine to the reservoir / borehole to minimise fluid disposal cost via 1) seasonal injection-extraction, 2) coaxial borehole heat exchangers and 3) standing column wells.

6.1 Introduction

In the UK, the exploitation of low-enthalpy deep geothermal systems is in its infancy, with the only commercial scheme (supplying ~3,000 homes) located at Southampton targeting the Sherwood Sandstone Group at a depth of ~1.8 km (Barker et al., 2000; Lund et al., 2011). A single extracting well is used to produce the geothermal fluid with a submersible pump (Price and Allen, 1984), discharging the production fluid into the sea (Energie-Cités, 2001). Unfortunately, this disposal method is not always possible due to the majority of the Mesozoic basins in England being located inland. A number of single well strategies were considered for the Cheshire Basin, with the aim of mitigating the problem of waste water disposal, whilst reducing the initial cost involved with developing doublet schemes (i.e., by only drilling one well). The first strategy modelled a single well which extracted fluid from the reservoir in high energy demand months (winter) and re-injected the fluid back into the reservoir in summer months when demand was considered low (Fig. 6.1a). This does, however, require a vast quantity of water to be stored (discussed in section 6.3.2). The second strategy modelled deep closed loop coaxial borehole heat exchangers (BHE) (Fig. 6.1b), and the third

strategy modelled standing column wells (SCW) with bleed flow (Fig. 6.1c). BHEs operate by

continually circulating the fluid in a closed loop system, whilst SCWs circulate fluid in an open loop

system with periods where the fluid is not all returned into the borehole (referred to as bleed). This

induces groundwater flow towards the well and results in hotter temperature fluid being drawn from

the aquifer.
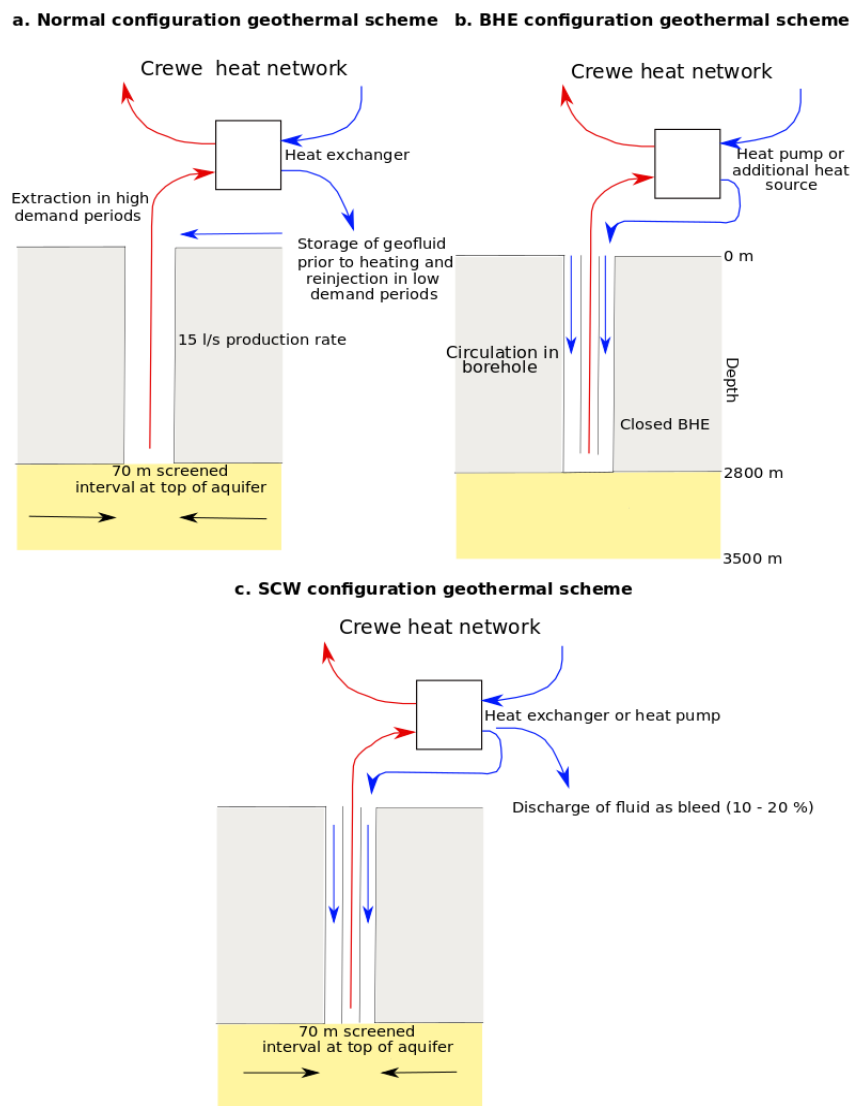
Figure 6.1: *Schematics of (a) deep single well scheme where fluid is extracted and injected seasonally, (b) a deep*

closed loop borehole heat exchanger (BHE) where fluid is constantly circulated and (c) a standing column well

(SCW) where the majority of fluid is circulated and some is discharged as bleed to induce a groundwater flow

towards the borehole.

The first strategy was investigated as an aquifer thermal energy storage scheme (ATESS). An ATESS operates by injecting high temperature fluid, rather than ambient fluid injection (such as in doublet systems), into the reservoir when demand is low and then extracting it in higher demand periods. An ATESS is useful as they can be used to store excess energy underground when demand is low. For example, thermal solar panels are most efficient in summer months; as a result, this energy can be stored underground and extracted in the winter for direct heat use with recovery factors of up to 95 % (Paksoy et al., 2000).

BHEs and SCWs are usually used in shallow to medium depth schemes (<400 m) (e.g., Rees et al., 2004), however, a substantially deeper configuration was considered in this case (>2.8 km). Increased drill depth results in a greater bottom-hole temperatures and surface areas for heat exchange. Preliminary trials in the UK (Law, 2014; Collins and Law, 2017) indicate these methods of geothermal extraction are sustainable from a geological perspective and can produce higher thermal yields than shallow geothermal wells (Cho et al., 2016), with further development of the SCW method ongoing at the 'Jubilee Pools' project, Penzance, UK (Collins and Law, 2017). Although SCWs will require periods of bleed, the amount of fluid requiring disposal will be 10 − 20 % of the volumetric flow rate, which will be constrained to short timescales coinciding with periods of high demand. The Crewe area of the Cheshire Basin is located away from the sea where the disposal strategy used at Southampton will not be possible. The Crewe area also has unique sources of excess energy to heat the fluid prior to injection for the potential use in an ATESS, including the Bentley factory in Leighton West and a planned combined heat and power fed district heat network.

6.2 Method of numerical modelling

The thermal and hydraulic interactions were coupled in the reservoir and wellbore using the finite-difference method described in chapters 4 and 5. A partially penetrative well intersecting a fully saturated reservoir was modelled using an orthogonal mesh, discretised as a non-uniform

grid. The penetrative interval extended over a well screen length of 70 m in the reservoir with a thickness of 700 m at a depth of 2.8 km (Downing and Gray, 1986b). The model was developed using MATLAB and tested stringently both analytically and against case studies as shown in chapters 4 and 5.

To more accurately model the influence of injected hot or cold fluid to the aquifer, the key governing equations were slightly modified from chapters 4 and 5 to include temperature-dependent viscosity and the buoyancy effect. Buoyancy, caused by a difference in fluid density between the hot injected fluid and aquifer temperature, can create a tilted thermal front, whilst viscosity can affect the rate of tilting (Schout et al., 2016). It has been shown in ATESS that the efficiency can be underestimated when buoyancy and viscosity effects are ignored (Zeghici et al., 2015), and, as such, both were incorporated to further develop the model in this chapter. The Oberbeck-Boussinesq approximation was used for both fluid and heat transfer equations, where fluid density variations were ignored, other than in the buoyancy effect (Eq. 6.2) (Oberbeck, 1879; Boussinesq, 1903; Nield and Bejan, 1992; Ackerer et al., 2000). This method is commonly used in numerical modelling of fluid and thermal fluxes (e.g., Kolditz et al., 1998), and is valid for low-density contrasts (Carlos et al., 2015). The buoyancy effect and varying viscosity were modelled here due to the substantial increase in temperature within the aquifer due to hot fluid injection.

The revised Darcy velocity is (e.g., Oude Essink, 1998; McKeown et al., 1999):

$$v = -K\mu_r(\nabla h - \rho_r) \qquad\qquad 6.1$$

where K, μ_r, h and ρ_r are hydraulic conductivity, relative viscosity, hydraulic head and relative fluid density. The relative fluid density was calculated as ($\rho_r = \rho - \rho_o/\rho_o$), where ρ_o is the reference density and ρ is the fluid density. It was assumed that the fluid entering or exiting the system had an equal concentration of salinity. Changes in fluid density were calculated as a function of pressure, temperature and salinity (Batzle and Wang, 1992; Adams and Bachu, 2002; Saeid et al., 2015;

Crooijmans et al., 2016). Changes in fluid density from pressure were, however, expected to have only a small effect in comparison to temperature and were consequently neglected (McDermott et al., 2006; Saeid et al., 2013). The revised Darcy velocity is then substituted into the key governing equations to couple fluid and thermal flux in the aquifer (eq. 4.1 and 4.5)

6.2.1 Evaluation of the thermal performance

To determine the thermal performance of the three different geothermal well schemes, the following operational terms were used;

The energy recovery is important for an ATESS and the energy recovery factor (E) was calculated as (Schout et al., 2013; Zeghici et al., 2015):

$$E = \frac{E_{prod}}{E_{inject}} = \frac{Q.c_f\rho_f(T_p - T_a)}{Q.c_f\rho_f(T_i - T_a)} \qquad 6.2$$

where T_p is the production temperature, T_i is the injection temperature and T_a is the ambient temperature.

The thermal performance of the coaxial BHE and SCW was determined by considering the heat load or thermal power (P) (e.g., Dijkshoorn et al., 2013; Liu et al., 2019):

$$P = \rho_f c_f Q(T_{out} - T_{in}) \qquad 6.3$$

Typically, BHEs will have a predetermined heat load. The maximum heat load in a BHE was calculated by utilising the temperature at the base of the borehole (T_{base}), rather than the outlet temperature (T_{out}). The heat loss ratio ($\propto$) is (Liu et al., 2019):

$$\propto = \left(\frac{T_{base} - T_{out}}{T_{base} - T_{in}}\right) \qquad 6.4$$

It was also important to consider the specific heat load, which was calculated as the difference between the temperature of the fluid in the annulus space and the outer piping wall. The

outer pipe temperature was considered equal to that of the grout such that the specific heat load (q_z) was expressed as (Liu et al., 2019):

$$q_z = b_{pg}(T_{pi} - T_g)$$ 6.5

6.2.2 Initial conditions and discretisation

In this study, the seasonal injection-extraction strategy (ATESS) used a lateral (x,y) spacing of 2 m for the mesh, expanding laterally away from the wellbore to a distance of just over 2 km, whilst a 1 m lateral mesh was used for the BHE and SCW models. The vertical spacing was set at 20 m for the borehole component in the confining beds and 14 m for the aquifer (Fig. 6.2). The initial conditions were set up identically to those in chapter 5 (Table 5.1 and 5.2), with a few minor changes highlighted in the following section.
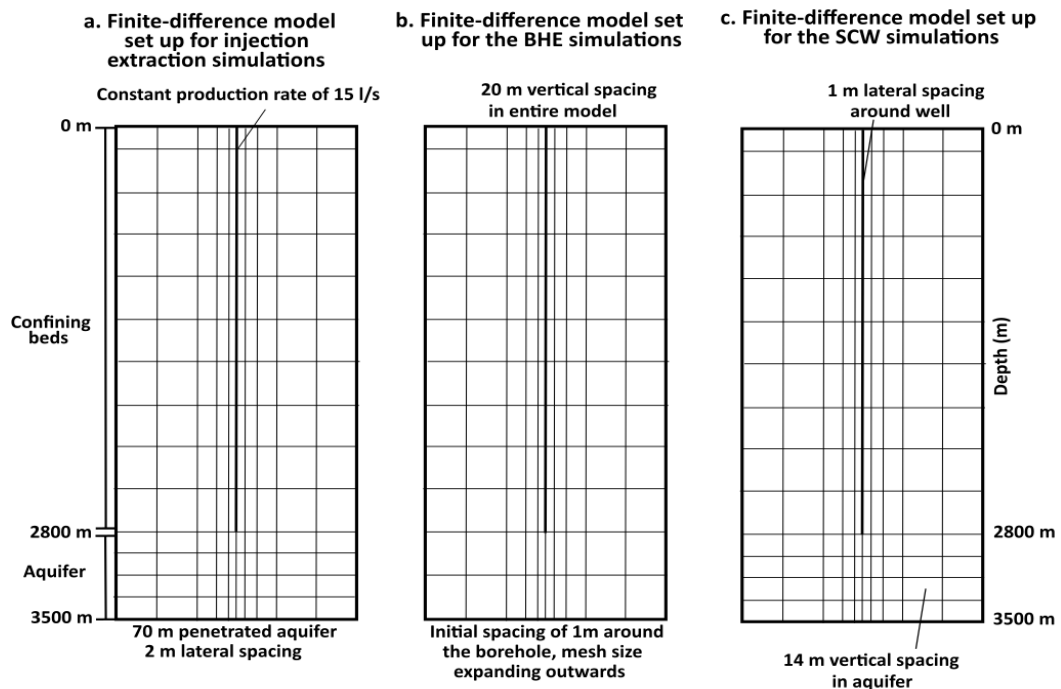
Figure 6.2: *Schematics of the finite-difference meshes for the respective model set ups of (a) deep single well scheme where fluid is extracted and injected seasonally, (b) a deep closed loop borehole heat exchanger (BHE) where fluid is constantly circulated and (c) a standing column well (SCW) where the majority of the fluid is circulated and some is discharged as bleed to induce groundwater flow towards the borehole.*

6.2.2.1 Injection-extraction modelling parameters

The injection volumetric flow rates were calculated such that the total volume of fluid injected was equal to the amount of fluid extracted during the production time period in an annual cycle (i.e., 75 l/s for 2 months injection, 30 l/s for 4 months injection and 15 l/s for 6 months injection – Table 6.1), where:

$$Q_{in}.t_{in} = Q_{out}.t_{out} \qquad\qquad 6.6$$

with Q_{in} being the injection rate, t_{in} the total time of injection in an annual cycle, Q_{out} the extraction rate (set at 15 l/s) and t_{out} the total time of extraction in an annual cycle. The injection temperature was set at 95 °C. Although this is high, it is hypothesised heat can be stored from the nearby Bentley factory or solar panels.

Injection period v Extraction period	Injection rate
2 months v 10 months	75 l/s
4 months v 8 months	30 l/s
6 months v 6 months	15 l/s

Table 6.1: *Comparison of flow rates under the different scenarios for the injection-extraction scheme.*

6.2.2.2 Borehole heat exchanger and standing column well modelling parameters

The BHE was modelled to a depth of 2.8 km with no fluid interactions with the aquifer. The volumetric flow rates in the borehole were modelled using a constant inlet temperature and the borehole parameters were set as the optimal conditions identified in chapter 4. To help increase the outlet temperatures and efficiency of the system, the outer thermal conductivity of the pipe was set at 45 W/m/°C, whilst the inner pipe was more insulating at 1 W/m/°C (Table 6.2). The initial inlet temperature was set at 10 °C based on the analysis in chapter 4 which showed reduced inlet temperatures were able to produce higher quantities of energy. Volumetric flow rates were modelled at variable rates to establish which were capable of producing the highest heat load for the

modelled time period with minor thermal drawdown in the borehole. Pre-defined heat loads were then analysed and subsequently increased to test the sustainability of high heat loads. The SCW had the same pipe components as the BHE; however, it was made open to the aquifer at the same screened interval as the injection-extraction scenario (70 m). Different bleed flows of 10 % and 20 % were then investigated under high volumetric flow rates.

Parameter	Value
Thermal conductivity	1 (IP) / 45 (OP)
Fluid inlet temperature	10 °C
Diameter of the inner pipe	0.05 m

Table 6.2: *Alternate parameters used in the borehole heat exchanger and standing column well models. IP = inner pipe, OP = outer pipe. The inner pipe is considered to have properties of a glass fibre reinforced plastic pipe and the outer pipe of steel (e.g., Dijkshoorn et al., 2013).*

6.3 Results of the modelling study

6.3.1 Single well injection-extraction annual simulations

A series of annual simulations were undertaken to investigate the response of the aquifer under varying time periods of injection, i.e., 2, 4 and 6 months, whilst the production period was the remaining period of the year (i.e., 10, 8 and 6 months).

When hot fluid was injected into the aquifer it quickly propagated away from the wellbore due to the decreased viscosity and high injection rates. As a result of the buoyancy effect, the temperature was hotter around the well screen interval at the top of the aquifer. In figure 6.3a & 6.4a, it can be seen the hot fluid injected at the top of the borehole (i.e., at 0 m) cools as it descended towards the aquifer, whilst in figure 6.3b & 6.4b the fluid cools as it moves from the

aquifer to the surface. Greater cooling in the wellbore is observed for slower extraction / production

rates.

a. 2D model showing the temperature profile after 2 months injection
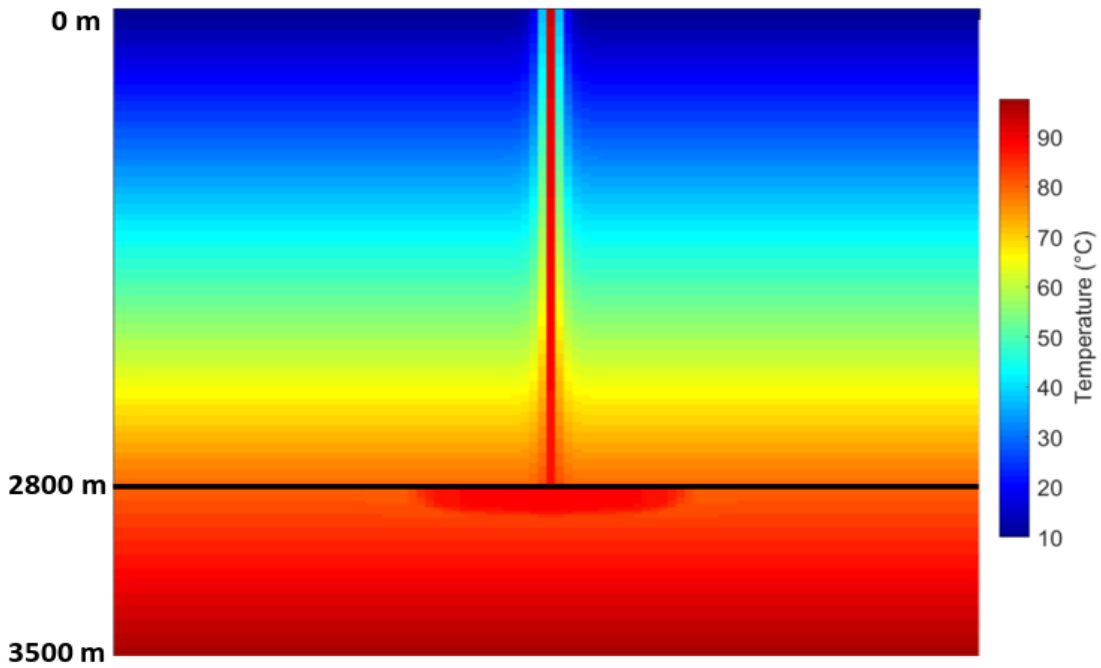
b. 2D model showing the temperature profile after 10 months production
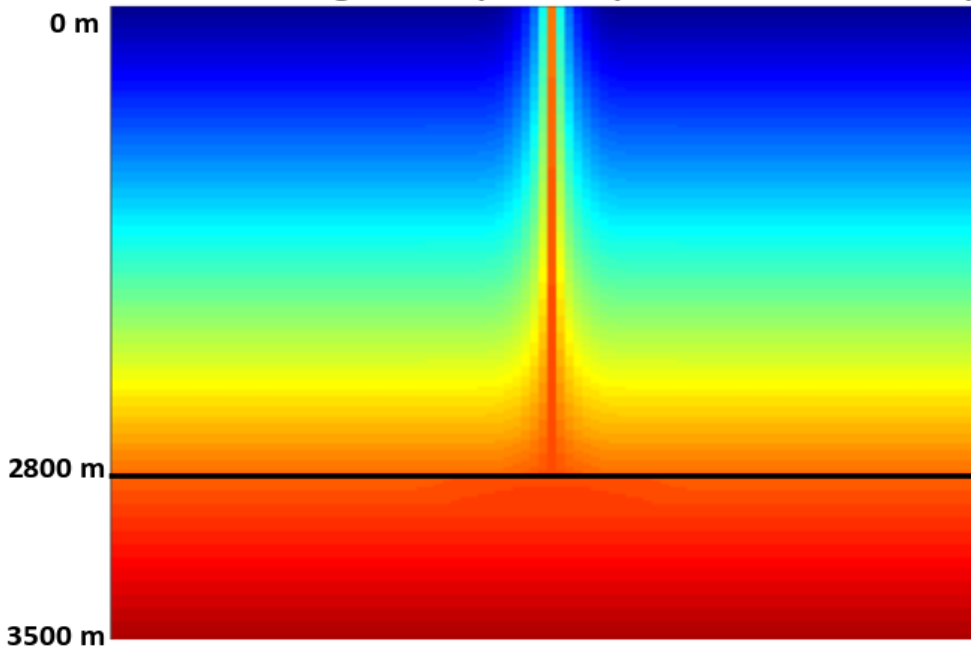
Figure 6.3: (a) *Temperature profile of the injection-extraction model after 2 months of injection and (b) 10 months of extraction.*

194

a. 2D model showing the temperature change after 2 months injection
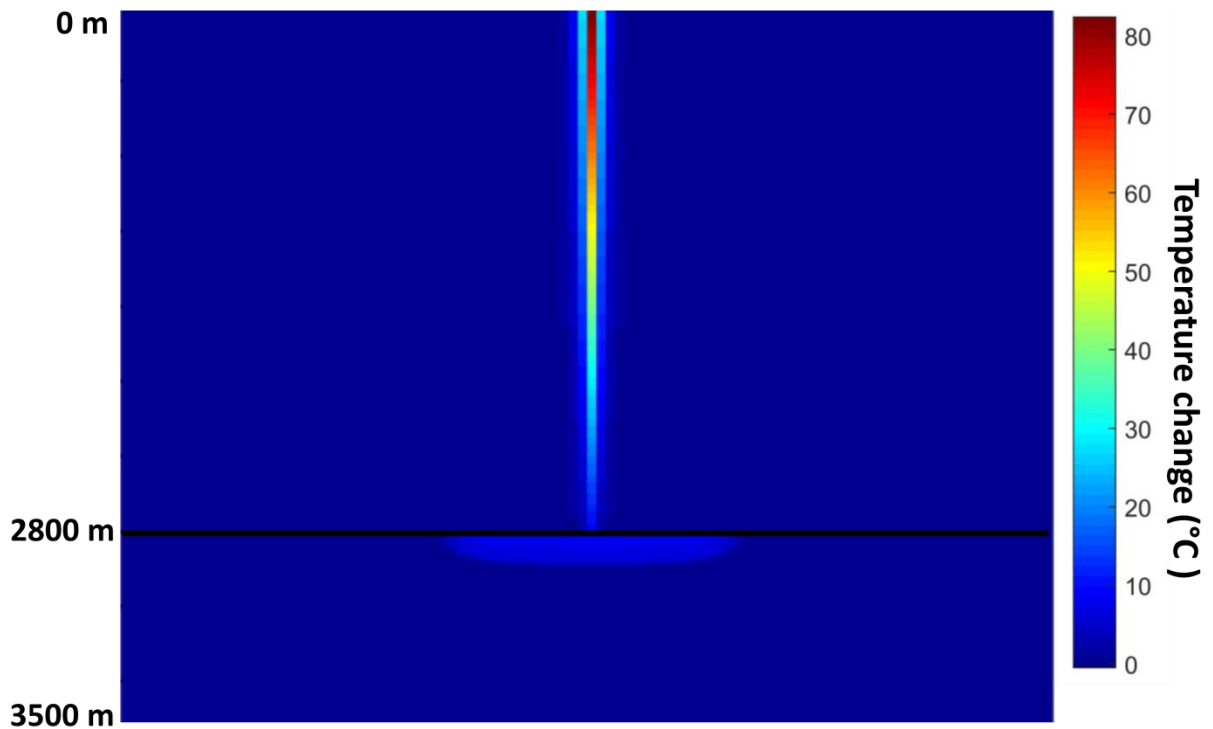
b. 2D model showing the temperature change after 10 months production
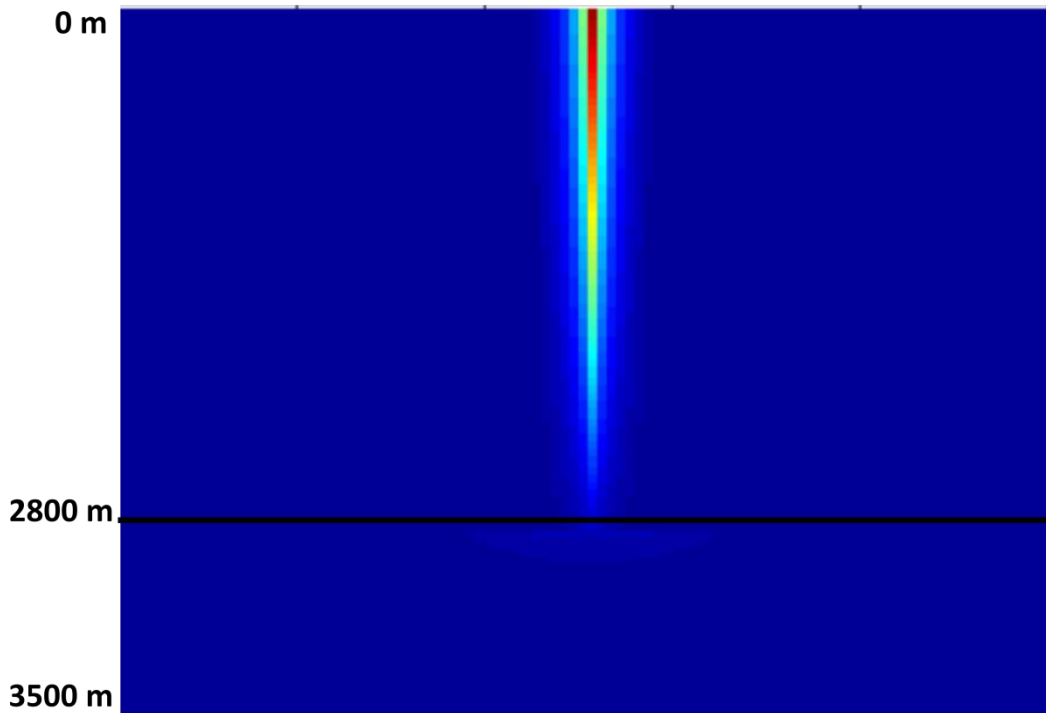
Figure 6.4: (a) *Cross-section profile of the injection-extraction model showing the change in temperature from static conditions after 2 months of injection and (b) 10 months of extraction.*

The results highlighted that shorter injection periods at higher injection rates, and therefore longer extraction periods, were less efficient at extracting energy over an annual cycle. An injection time of 2 months led to 22.9 % of the energy injected being recovered whilst increasing the injection time led to higher recovery factors (27.4 % for 4 months and 29.8 % for 6 months) (Fig. 6.5c). This was due to the slower injection rate causing less forced advection in the aquifer, such that the high temperature spread slowly within the aquifer. This is in contrast to the high injection rates which caused rapid thermal propagation away from the well screen resulting in lower energy recovery rates (Fig. 6.3a & 6.4a). In figure 6.5a, fluid is injected at 95 °C followed by a period of extraction. During extraction, the production temperature rapidly returns to near-aquifer temperature in an exponential like decline. At the end of the simulation period, the difference in temperature was 1 °C between the 2 month and 6 month injection periods. In figure 6.5b the energy recovery is far higher for the longer production period cases. As the cumulative energy produced increases in a linear fashion this is likely to be due to the additional production time.

The recovery factors identified were far lower than those cited in recent studies by Major et al. (2018) who found recovery factors of 67 % using similar injection and aquifer temperatures. This could be due to a number of factors, including higher volumetric flow rates for production or increased hydraulic conductivity; however, it could also be because losses in heat flux in the wellbore were not modelled and that the injection temperature into the reservoir was considered equal to that at the wellhead. In this study, heat losses of up to 7 °C were observed in the wellbore during injection and production, meaning much of the energy from the fluid was transferred to the confining beds (Fig. 6.3 & 6.4). Major et al. (2018) suggest that their recovery factors were valid at the surface; however, the results of this study suggest the opposite.

The total quantity of energy produced in this short series of simulations was 8.53×10^{13} J, 1.13×10^{14} J and 1.4×10^{14} J for 6, 8 and 10 month extraction periods (Fig. 6.5b).
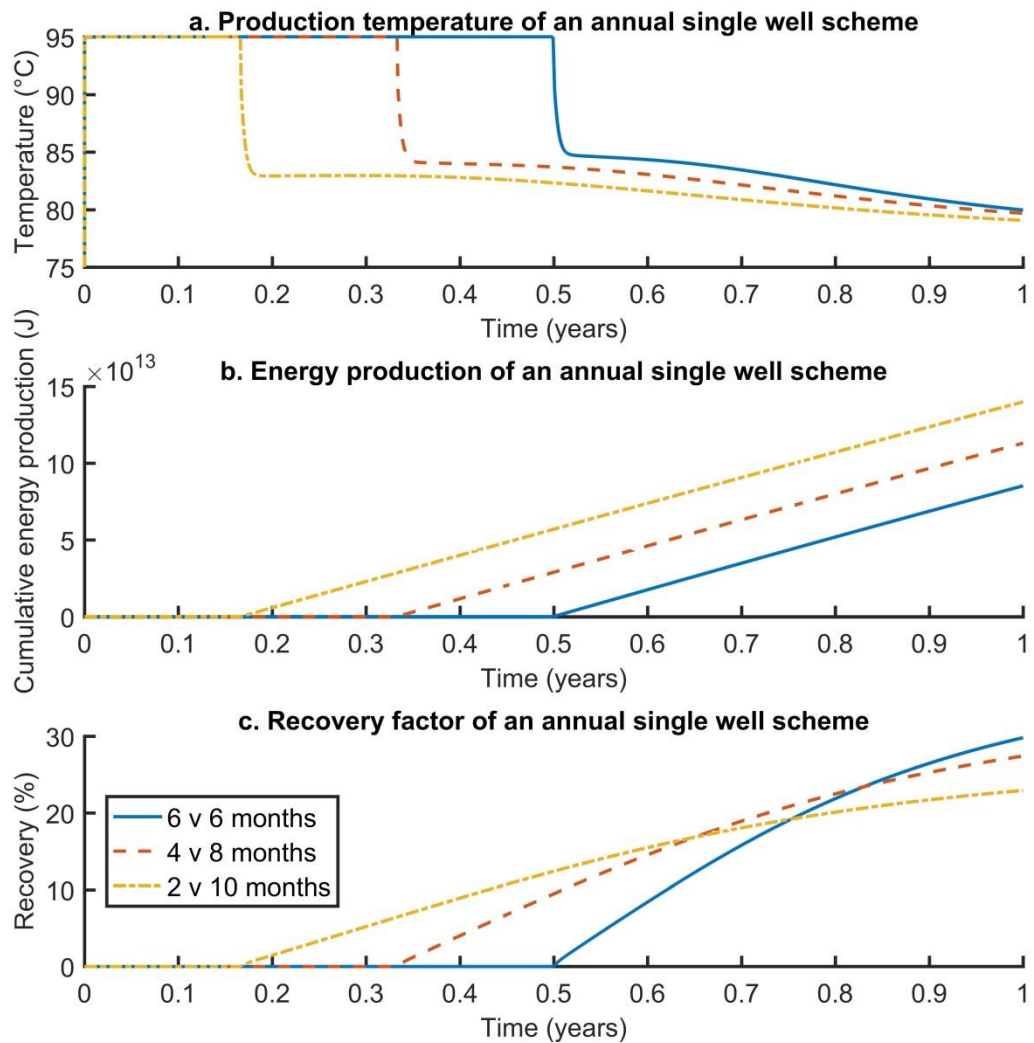
Figure 6.5: *Single well models:* (a) *annual variations in wellhead (production) temperature, (b) cumulative energy production and (c) recovery factors of energy. Note the different intercepts in (b) and (c) on the x-axis indicate the period from when production starts following injection.*

6.3.2 Single well injection-extraction 10 year simulations

To extend the analysis to longer-term performances the injection-extraction strategies were modelled for a period of 10 years to investigate the aquifer response and the impact on heating

schemes. It was hypothesised that the injection of hot fluid at the top of the aquifer would promote high production temperatures as the hot fluid is buoyant and stays at the top of the reservoir (as seen in Fig. 6.3), which could then be extracted in high demand months. With time, the aquifer temperature was expected to increase leading to higher recovery factors.

Although there are feasibility problems with this method, such as the storage of such a large quantity of water throughout the year, the potential of this single well scheme was evaluated from a technical viewpoint. The three simulations from the annual models were repeated for an operational period of ten years to evaluate the response of the aquifer over time. The net volume of water needed to be stored at any given time was also recorded so that potential storage needs can be considered. The long-term simulations were set up identically to those in section 6.3.1; however, in contrast to the short time-scale simulations, the longer time-scale simulations started with extraction followed by injection. This was to ensure no additional, externally sourced water (and subsequent cost) was required to be injected into the aquifer.

During the 10 year simulation, the aquifer temperature gradually increased, highlighted in figure 6.6a. This can be observed by the production temperature at the end of each subsequent extraction period being greater than the last. After the first cycle (i.e., after years 1.5, 1.6 and 1.8 for the extraction period of 6, 8 and 10 months, respectively) the extraction fluids temperature was far greater than that observed after the first 6, 8, or 10 months of extraction. For the 6 v 6 month cyclical scenario, fluid temperature increased between the first extraction cycles after injection (taken between years 0.5 and 1.5) by 3.9 °C. For the 8 v 4 month scenario, production temperature increased by 3.8 °C and 3.7 °C for the 10 v 2 month scenario. This increase in temperature corresponded to an overall increase in the recovery of heat over the total simulation time.
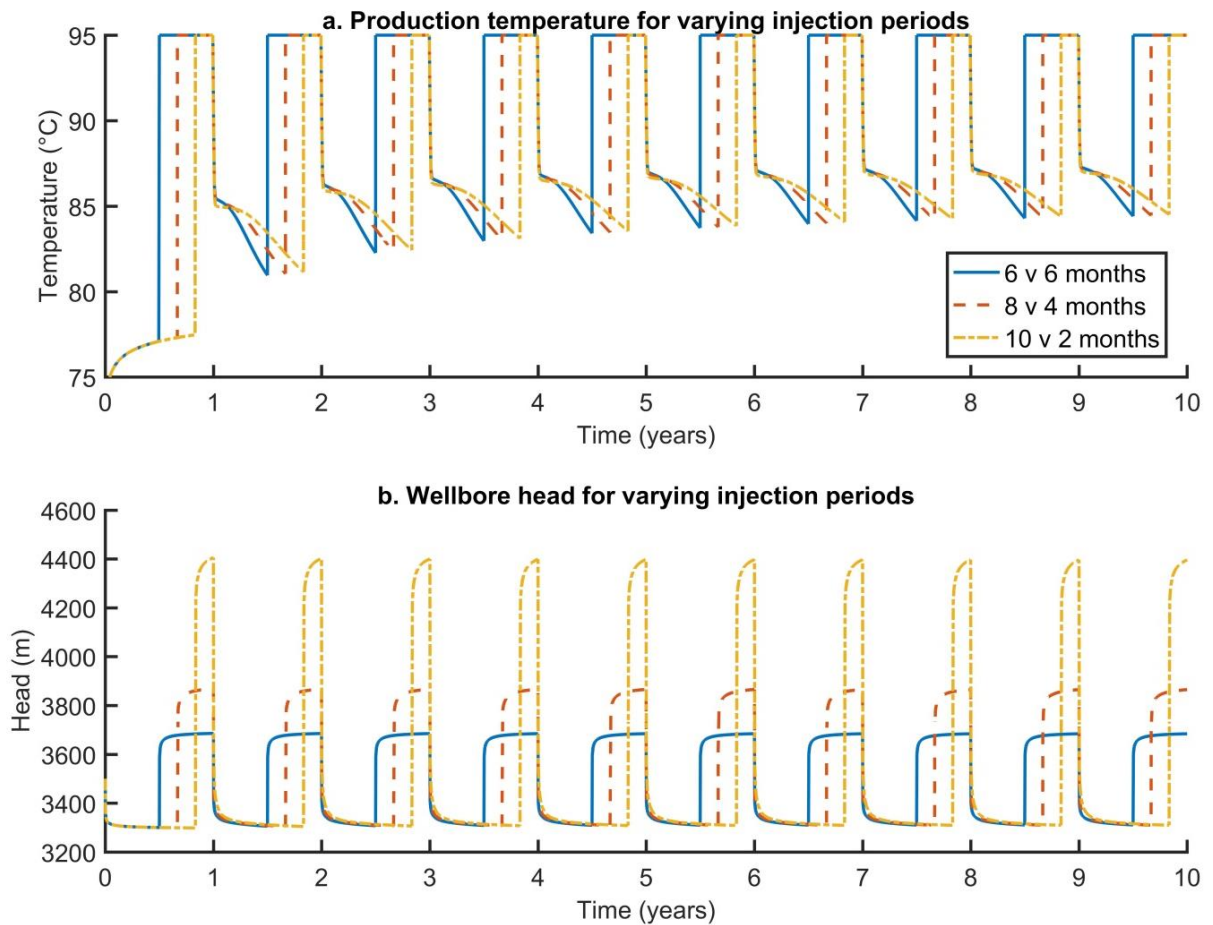
Figure 6.6: *Long term (10 year) simulations showing (a) annual variations in wellhead (production) temperature and (b) wellbore head.*

After each cycle, the relative increase in production temperature reduced. The second cycle (at years 2.5, 2.66 and 2.83 respectively) increased in temperature by ~1 °C in all scenarios, whilst the final cycle showed an increase of only ~0.3 °C. At the end of the first injection-extraction cycle all the recovery factors were similar at ~35.7 %. However, recovery factors after 10 cycles of injection increased for each time period. For the 6 v 6 month scenario the recovery factor increased to 50.5 %, 50.4 % for the 8 v 4 month scenario and 50.1 % for the 10 v 2 month scenario. The increase in recovery factors were similar, but slightly smaller, to the study of Poppei et al. (1998), who found recovery factors to increase by 21 %. They injected fluid of 70 °C into a reservoir with a temperature

of 19.3 °C. The recovery factors after one annual cycle were 61 % and 82.5 % after 5 annual cycles. The higher recovery factors in their study could be due to a greater difference between the injection and aquifer temperatures. The study also used a shallow aquifer that was within 300 m of the ground level leaving minimal interactions in the wellbore. This again emphasises the important role of thermal interactions in the wellbore during any ATESS.

When analysing the corresponding well heads (Fig. 6.6b) it can be seen that higher injection values (Fig. 6.7b) in the wellbore correspond to far higher head values (and therefore pressure). If any plan to develop geothermal in the area wanted to reinject fluid at high flow rates (as part of a seasonal scheme) this could lead to the aquifer becoming over-pressurised with the possibility of inducing seismicity in faults.

Another key issue is the volume of fluid that would be stored during the extraction months. When the duration of injection is low (i.e., 2 months) there is a significant quantity of fluid that would need to be stored during the production months (i.e., 8 months of extraction would produce 3.89 x 10^8 litres of geothermal fluid that would need storing) (Fig. 6.7b). Assuming that 2.5 million litres of water can be stored in an Olympic sized swimming pool then this equates to 156 pools of water that would be needed for storage, which is unlikely to be feasible. Even during lower extraction periods (6 months) water storage would require the equivalent of 93 Olympic swimming pools.
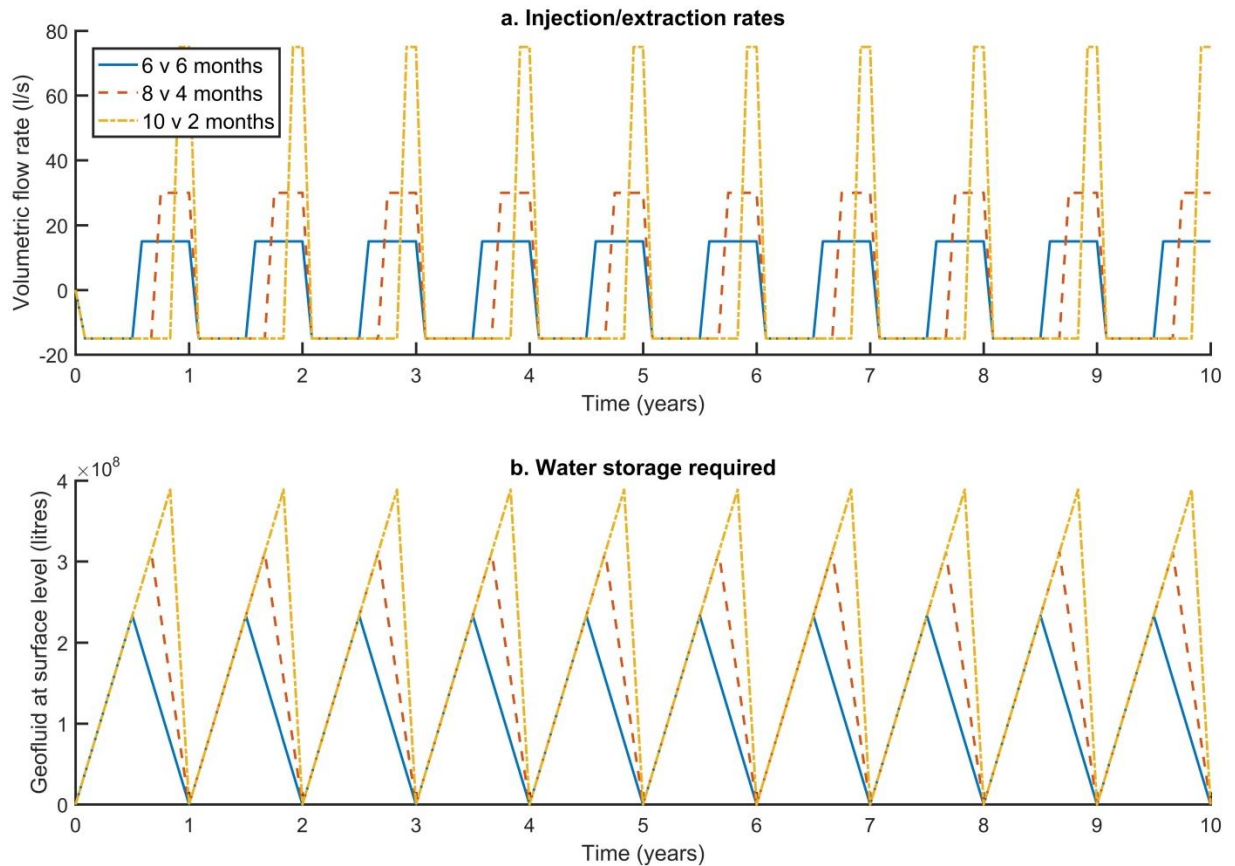
Figure 6.7. (a) *Annual variations in injection / extraction rates and (b) the cumulative water production during the 10 years of simulation. In figure (a) a negative value indicates the fluid is removed from the aquifer, whilst a positive value means it was injected into the aquifer.*

6.3.3 Coaxial borehole heat exchanger

The initial analysis of energy extraction using a BHE model focused on operation with a constant inlet temperature of 10 °C. A short simulation of 30 days was undertaken as the greatest change in temperature within a BHE occurs immediately after initialisation (as identified in chapter 4). Flow rates were increased incrementally by 2 l/s, from 2 to 12 l/s. A 15 l/s flow rate simulation was also undertaken to compare with the base case scenario for energy extraction in the parametric study (chapter 5). The analysis showed a rapid increase in thermal drawdown in the borehole under higher flow rates (Fig. 6.8), whilst the lower flow rates had a smaller reduction in temperature within the borehole. At the end of the simulation for the lowest flow rate of 2 l/s the bottom-hole

temperature (of the fluid) was 50.5 °C whilst for 15 l/s, the bottom-hole temperature was 14.6 °C. Even though higher flow rates rapidly reduced the temperature of the fluid in the borehole, the net energy produced was still greater in the higher flow rate scenarios (i.e., up to 12 l/s). When the flow rate exceeded 12 l/s, the total energy produced in the 30 day simulation began to reduce. This is due to rapid thermal drawdown caused by the high velocities.

a. 3D temperature plot of the subsurface surrounding the BHE   b. 2D Temperature plot through the BHE
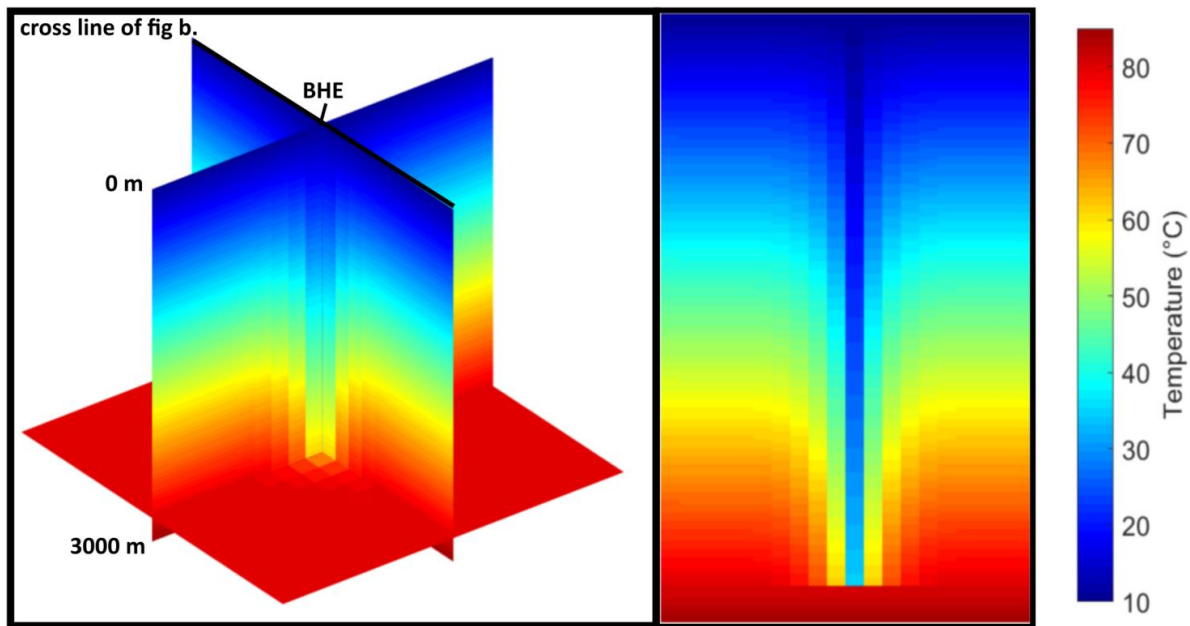
Figure 6.8: (a) *3D temperature plot of the subsurface for the 15 l/s borehole heat exchanger (BHE) model and (b) the 2D cross line through figure a.*

Modelling also showed that heat loads approached 3.5 MW (for 15 l/s flow rate), however, this decreased to 320 kW after 4 days (Fig. 6.9c and 6.9d). This is significant as the heat load produced in the parametric study for the base case example was 3 MW at the end of the 25 year simulation period. The reason that the thermal power in the parametric study was lower was due to the higher rejection temperature of 30 °C used in the energy equation (eq. 6.3). The high heat load observed for borehole heat exchangers does show that the demand for the core scheme (phase 1) of

the district heat network for Crewe town centre can be met for short periods (<1.6 MW as defined by Arup, 2018b).

In practice, when using the deep BHE, a range of flow rates may be used in combination to meet the variance in demand. At the end of the simulation, the lowest flow rate of 2 l/s produced 161 kW, whilst the greatest heat load was obtained when using the 8 l/s flow rate at 236.5 kW (Fig. 6.9d). It is worth noting that the flow rates between 4 l/s and 15 l/s were all grouped within 4.2 kW of each other. The vertical depth profiles for the inlet and outlet temperature also changed dramatically with higher flow rates. Steep, near vertical profiles were seen in the higher flow rates for both the inlet and outlet temperatures. This was due to the high velocities in the central pipe (in comparison to the outer annulus), reducing the amount of time for thermal interactions. In the outer annulus, where cold fluid was injected, a more significant difference in temperature for lower velocities was seen as the fluid had time to warm with depth.

The heat loss ratio reduced in the higher flow rate scenarios when compared to the lower flow rates; the heat loss at the end of 30 days for 2 l/s was 0.53, whilst it was 0.2 for 12 l/s. This was due to much of the heat in the 12 l/s model being extracted, leaving the bottom-hole temperature similar to the inlet and outlet temperatures. After 30 days, the highest bottom-hole heat load was found in the 4 l/s scenario at 378.2 kW, whilst the lowest bottom-hole heat load was in the 15 l/s scenario (289 kW), signifying the greatest thermal drawdown. The 4 l/s scenario was therefore taken forward in order to investigate predefined heat loads, due to it having the maximum heat load at the base of the BHE and only a small difference in actual heat load (by 2.2 kW) at the end of the simulations. The bottom-hole temperature was also the second largest after the 2 l/s flow rate (Fig. 6.9a). It should be noted that the higher volumetric flow rates have the potential to meet the maximum demand for the first phase of development in Crewe town centre and, as such, higher flow rates could be implemented for short operational periods. Across all the models, the specific heat

203

load was always negative and decreased with volumetric flow rate (Fig. 6.9b). The specific heat load shows the rate of heat loss between the surrounding rock and fluid in the annulus. The higher flow rates gave a near linear decrease in specific heat load at the end of the simulations. At the bottom of the wellbore, the maximum specific heat load was -79 W/m and the minimum specific heat load was -167.7 W/m for the 2 l/s and 12 l/s scenarios, respectively. The negative values for the specific heat load highlighted the heating of the fluid as it descended with depth in comparison to the hotter confining rock.
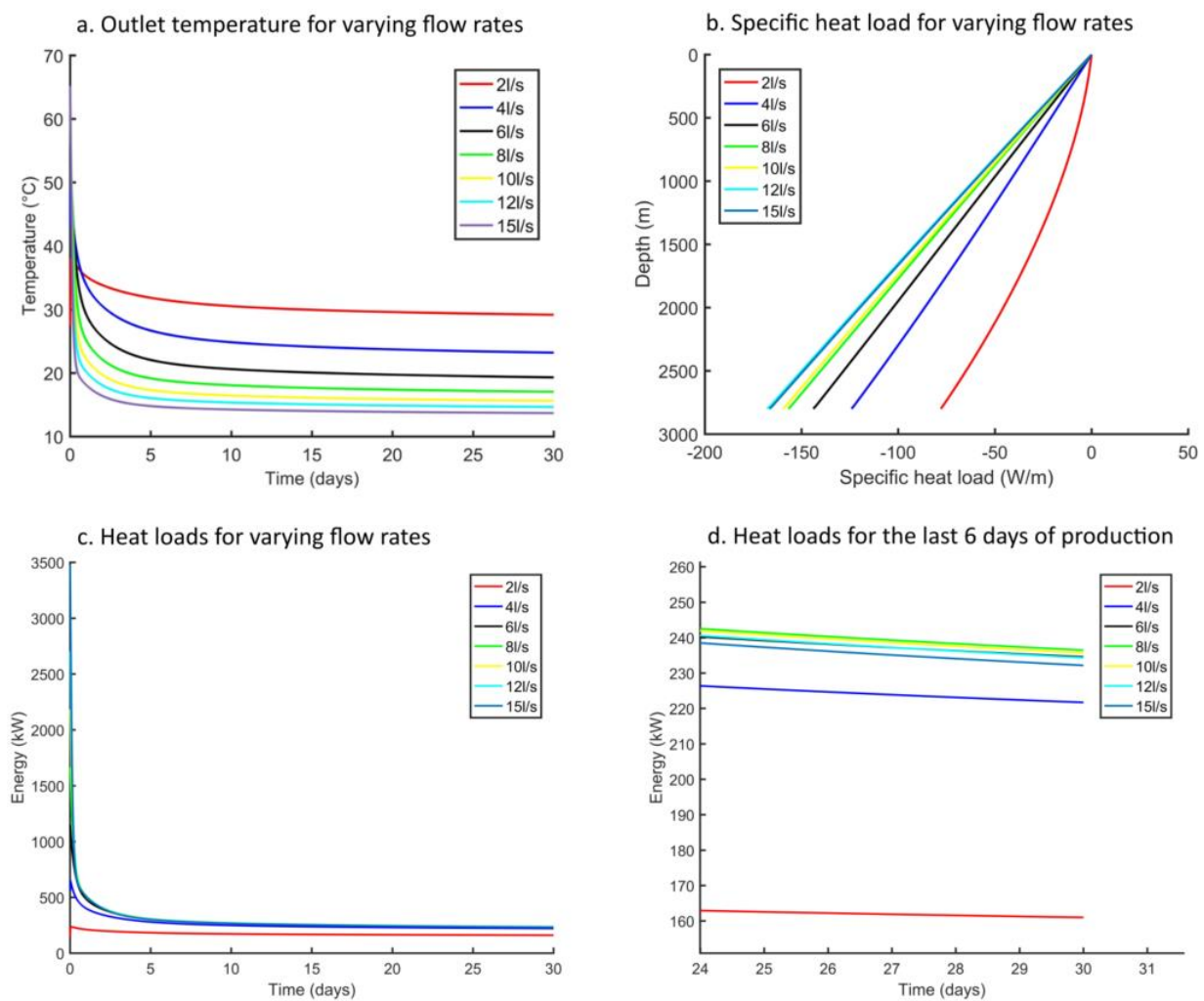
Figure 6.9: *Wellbore performance of borehole heat exchangers under different flow rates: (a) temporal variations in outlet temperature, (b) specific heat load variations with depth, (c) temporal variations in heat load over 30 days and (d) temporal variations in heat load over the last 6 days of the model.*

An analysis of predefined heat loads of 50 kW, 100 kW, 200 kW, 300 kW, 400 kW and 500 kW was undertaken to investigate the potential to supply the Crewe area's district heating scheme. Although these heat loads were less than that of the total initial demand in the first phase of district heat network development, it has been envisaged that a combined heat and power system and deep geothermal scheme (similar to the Southampton example) could supply the network. Increasing the heat load in the system showed a significant increase in the initial rapid thermal drawdown, both in terms of temperature reduction and by increasing the length of time of initial thermal drawdown. The initial thermal drawdown in the 500 kW heat load model resulted in the inlet fluid reducing to a sub-zero inlet temperature, making it unviable within the first few hours. Similarly, the 400 kW heat load reduced to sub-zero inlet temperatures after 3 days, and the 300 kW heat load after 19 days. To prevent freezing and rapid cooling of the borehole, temperatures greater than 0 °C must be maintained for longer borehole operating periods. Heat loads of 50 kW, 100 kW and 200 kW all showed positive results, with final outlet temperatures of 43.76 °C, 38 °C and 26.7 °C (Fig. 6.10a). For a period of constant operation that could be sustained for a period of a month, a heat load of 200 kW to 300 kW was deemed optimal. Typically, operation and heat load will vary depending on different timescales. Annually, less demand will be needed in summer months, whilst on a daily timescale demand will increase in the evening when temperatures are cooler. As such, the higher heat load demand of 400 kW to 500 kW may in fact be optimal for evening usage and a lower demand in the day, allowing time for thermal recharge.

The heat loss ratio decreased with increased heat loads due to cooler inlet temperatures. For the 3 scenarios (50 kW, 100 kW and 200 kW), where the heat load was delivered across the whole time period, the maximum heat loss ratio was 0.57 and 0.42 (50 kW and 200 kW respectively). The specific heat loads at the end of the simulation were different to the constant temperature scenarios. This was due to an increase in inlet temperatures in the annulus (in comparison to the surface ground temperature) giving a positive specific heat load near the surface (Fig. 6.11). The maximum

specific heat load was recorded as 76.8 W/m and the minimum was -118.3 W/m (for heat loads of 50

kW and 200 kW respectively).
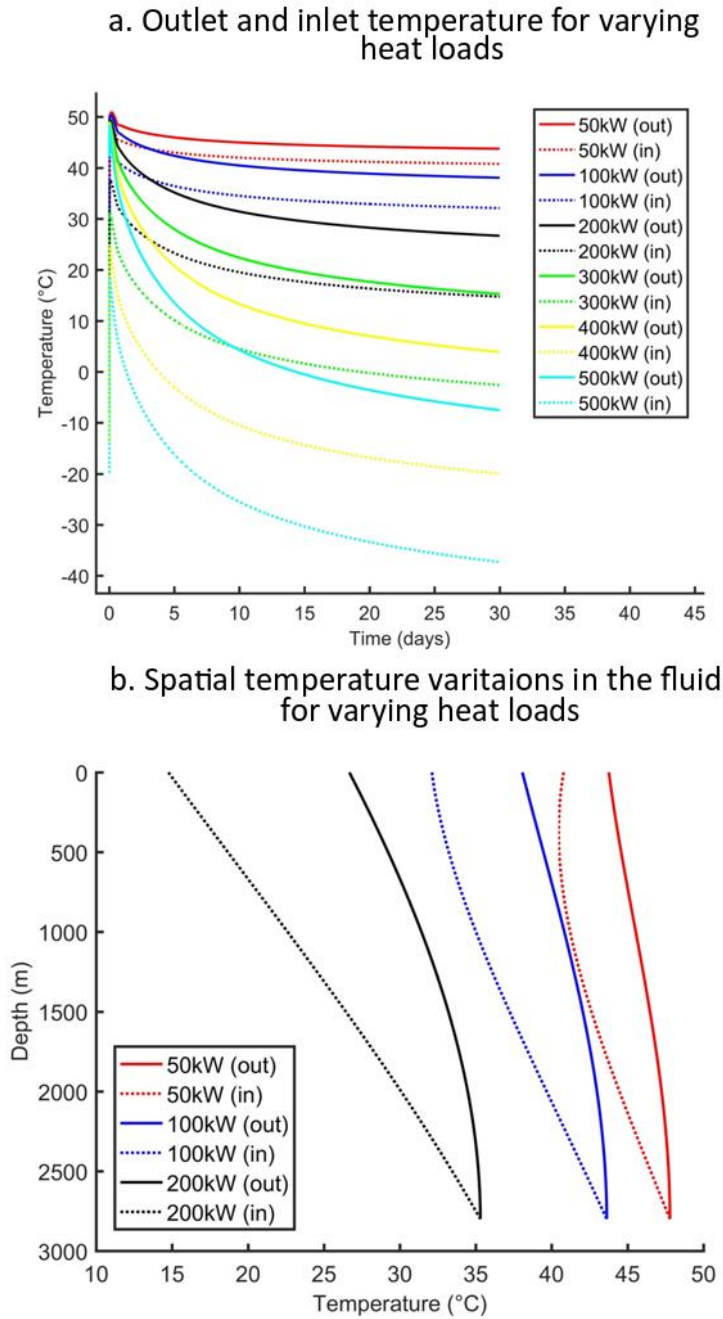
Figure 6.10: *Borehole heat exchanger performance for varying heat loads:* (a) *temporal variations in inlet and outlet temperature and (b) spatial variations in the borehole for the inlet and outlet fluids.*

The results indicated that a coaxial BHE could meet some, if not all, of the demand in the heat network's core scheme (i.e., Crewe phase 1), with heat loads peaking at 3.5 MW. Heat loads of 200 - 300 kW could be sustained with a constant inlet temperature of 10 °C for a month of operation, with it likely that they could be sustained for even greater periods. Similarly, operation of the BHE with a volumetric flow rate of 4 l/s could achieve predefined heat loads of 200 - 300 kW. Assuming houses in the UK have a demand of ~1 kW (Ovo, 2020) this is enough to power 200-300 homes. In the UK, tests on standing column wells with similar flow rates (3 l/s) indicate that a pump would require 7 kW of power to operate (Collins and Law, 2017). Assuming the same power would be required in this study, the coefficient of performance would be between 28.6 and 42.9 at the end of operation. This is far greater than those observed when using shallow ground source heat pumps in the UK which are typically around 4 (Ng, 2011).
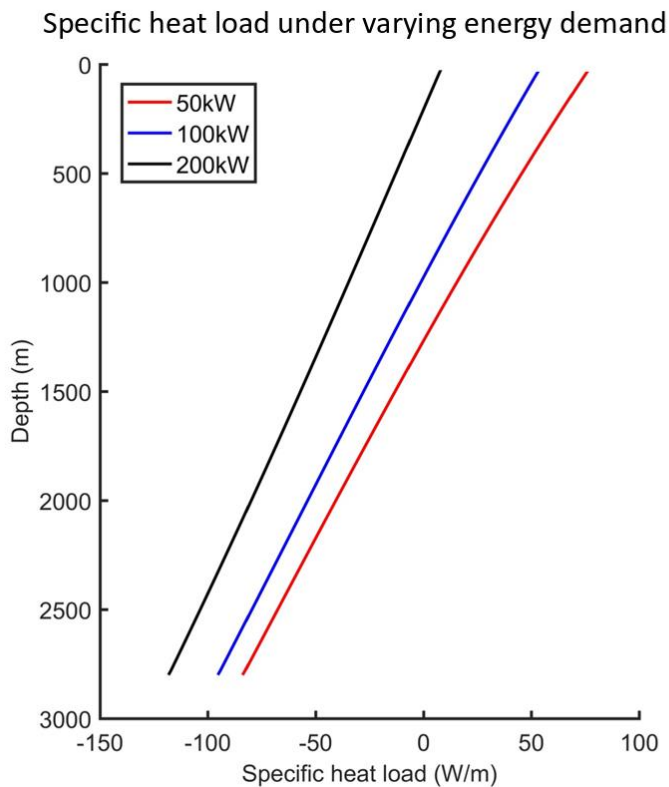
Figure 6.11: *Modelled specific heat loads under predetermined demand heat loads.*

6.3.4 Standing column well evaluation

The standing column well (SCW) configuration was chosen to investigate improved well performance using the same parameters as the coaxial BHE but with the wellbore open at the top of the aquifer in a perforated interval of 70 m. The inlet fluid was injected at the top of the well at a temperature of 10 °C and circulated at volumetric flow rates of 5 l/s, 10 l/s and 15 l/s. Bleed flows of 10 % and 20 % were used to evaluate the impact of the flows on operational performance.

The impact of injecting cool fluid had less of an impact on the surrounding rocks with temperature change in the aquifer being minimal, other than that seen at the well screen nodes (Fig. 6.12). The higher flow rates in the well also caused higher temperatures within the first day of production (Fig. 6.13a and 6.13b). Subsequently, the temperature rapidly dropped and higher flow rates produced cooler temperatures than the slower flow rates. Bleed flows of 10 % had a maximum outlet temperature of 53.6 °C, 63.7 °C and 68.3 °C, whilst bleed flows of 20 % had a maximum outlet temperature of 54 °C, 63.9 °C and 68.5 °C (for 5 l/s, 10 l/s and 15 l/s respectively) (Fig. 6.13a and 6.13b). At the end of production, for both bleed rates the outlet temperatures were greatest for the lower flow rates.

In comparison to the deep coaxial BHE, the achievable heat load was far greater for the SCWs. The greatest heat load achievable at the maximum outlet temperature occurred in the first day. The maximum heat load for 10 % and 20 % bleed flows were a) for 5 l/s - 915 kW and 924 kW, b) for 10 l/s - 2,256 kW and 2,264 kW, and c) for 15 l/s - 3,676 kW and 3,684 kW, respectively (Fig. 6.13c and 6.13d).

a. 3D temperature plot of the subsurface surrounding the SCW   b. 2D Temperature plot through the SCW
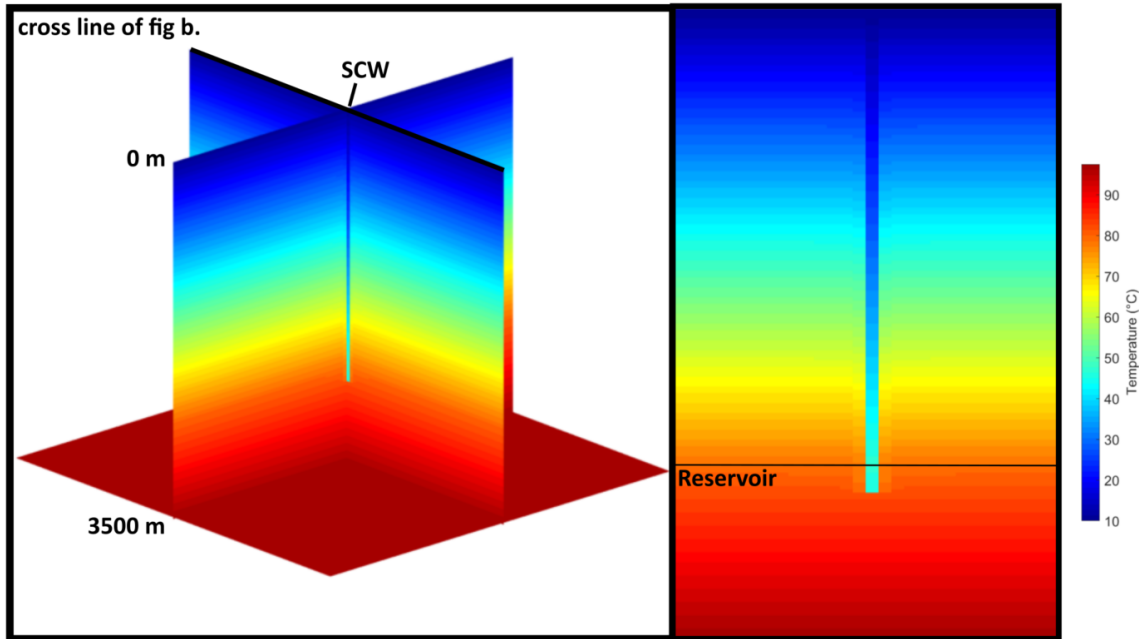
Figure 6.12: (a) *3D temperature plot of the subsurface for the 15 l/s standing column well (SCW) model scenario with 20 % bleed model and (b) the 2D cross line through figure a.*

At the end of the simulations, the heat loads were a) for 5 l/s - 654 kW and 684 kW, b) for 10 l/s - 1,207kW and 1,242 kW, and c) for 15 l/s - 1,692 kW and 1,725 kW, respectively (Fig. 6.13c and 6.13d). In this study, higher flow rates could achieve an initial high heat load (similar to the coaxial BHE); however, the reduction in temperature with time was less than the BHE. The different bleed ratios also had a minor impact on the outlet temperatures. At the end of the simulations, the coefficient of performance was calculated to be between 93.4 and 246.4 (assuming the power required to pump the fluid would be 7 kW after Collins and Law (2017)). Realistically, the pumping power required would be higher; meaning the coefficient of performance would be less.
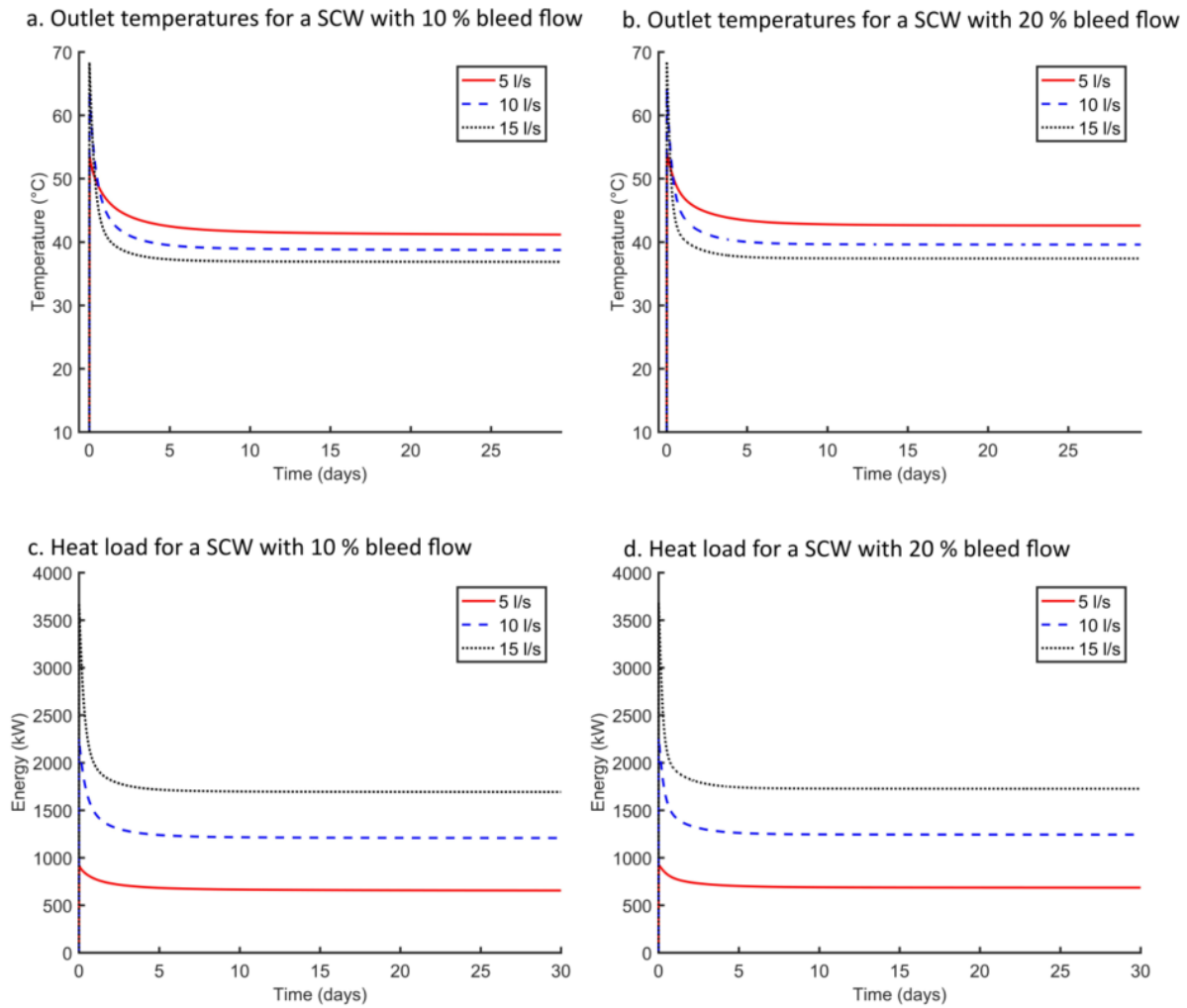
Figure 6.13: (a) *Outlet temperatures for a bleed of 10 %, (b) outlet temperatures for a bleed of 20 %, (c) heat load for a bleed of 10 % and (d) heat load for a bleed of 20 %.*

Summary

In this chapter, alternative geothermal production methods to the more common doublet scheme were modelled for use in the Cheshire Basin where fluid was recirculated in single wells, either annually or continually. The study highlighted that deep standing column wells and borehole heat exchangers hold the potential to supply enough energy for the initial core demand (<1.6 MW) in the Crewe town centre district heat network. Greater cooling (and a reduction in outlet temperature) was observed in borehole heat exchangers in comparison to standing column wells. This led to

210

standing column wells with bleed being capable of producing a significant sustainable heat load at the end of the simulated time period (<1.725 MW). Coaxial borehole heat exchangers could still operate at a reduced capacity and meet the maximum energy demand for short periods (<1 day). They also have the added benefit of not injecting or extracting fluid into the aquifer, leading to limited investigatory work or government consent.

Although the single well injection-extraction aquifer thermal energy storage scheme proved to be technically possible, giving reasonable recovery factors of up to 50 %; it seems unlikely to be developed due to practical feasibility issues. These include the requirement of vast amounts of space to hold the extracted geothermal fluid and the potential to induce seismic events due to injection over-pressurisation in the rocks. Further analysis of the injection-extraction scheme did highlight losses in temperature through the wellbore piping and grout which led to a significant reduction in temperature and, therefore, to reduced recovery factors. As such, any deep aquifer thermal energy storage schemes should include these losses, otherwise recovery factors may be over-estimated (e.g., Major et al., 2018). The observation of increased recovery factors with time (~36 – 50 %) are also similar to other authors (Poppei et al., 1998); however, it has been stated that in deep aquifer thermal energy storage schemes, these are not observed to such an extent due to the reduced temperature difference between the aquifer and injected fluids (Major et al., 2018).

CHAPTER 7 - A THERMAL AND ECONOMIC ANALYSIS FOR THE UTILISATION OF HEAT EXCHANGERS AS PART OF A GEOTHERMAL DISTRICT HEATING SCHEME IN THE CHESHIRE BASIN, UK

This chapter investigates the use and impact of different heat exchangers for the proposed geothermal scheme in Cheshire with a particular emphasis on the economic benefits and costs.

7.1 Introduction

In the Cheshire Basin and UK in general, relatively little work has been undertaken on heat exchangers for district heating schemes. Heat exchangers are vital to any geothermal scheme as they ensure that the extracted heat is useable, supplying the demand directly. Low-enthalpy or low-temperature geothermal schemes usually exploit resources under 100 °C, and heat is transferred through a heat exchanger which then feeds a district heat network. A heat exchanger operates by transferring heat between two fluids over a given surface area and prevents corrosion and scaling caused by the geothermal fluid in the heat network (Björnsson, 1999). Not all the heat can be transferred and, as such, the input temperature into the district heat network must be evaluated. It is also important to calculate the outlet temperature of the geothermal fluid to assess further use or disposal options. In geothermal fed district heat networks, counter-flow plate heat exchangers are most commonly used as they have been proven to be the most effective and can offer the highest economic benefits in comparison to other (e.g., shell and tube) (Chuanshan and Jun, 1999; Ağra et al., 2015). The model by Dagdas (2007) was used in this chapter for the counter-current flow plate heat exchanger, whilst the model for co-current flow plate heat exchangers is based on that of Bradley (2010). Counter-current flow heat exchangers transfer heat between two fluids passing in opposite directions, whilst co-current flow heat exchangers pass heat between two fluids travelling in the same direction (Fig. 7.1). An initial comparison between counter- and co-current flow heat

exchangers was undertaken to highlight the significant difference in output temperature and effectiveness.

Schematic of different heat exchangers
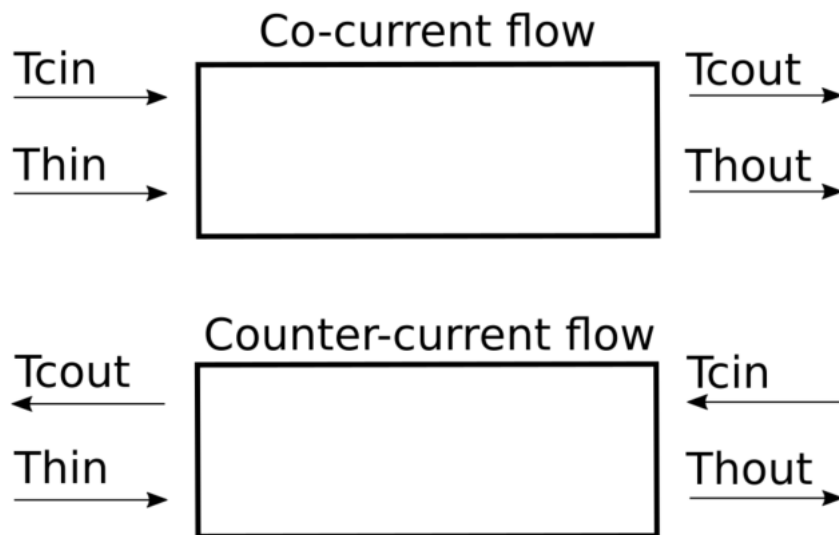
Figure 7.1: *Schematic of co-current flow and counter-current flow regimes for different heat exchanger configurations. Tc is the temperature of the circulatory fluid and Th is for the geothermal fluid. The addition of 'out' and 'in' refer to the inlet or outlet temperatures.*

The useable energy after the fluids have passed through the heat exchanger is an important parameter when determining whether a deep geothermal scheme can match demand, including operation at both peak and low demand periods. It is also useful to understand whether the savings in using a potentially cheaper source (geothermal) in comparison to typical fossil-fuel boiler schemes is worthwhile. Analysis will also help to determine optimal conditions of the surface area for a heat exchanger. In this chapter the focus was on normal configuration extraction only boreholes (e.g., Fig. 1.3a, 4.1a, 5.1b and 6.1a) (and to some extent standing column wells) where the outlet temperature and volumetric flow rate is high enough to meet the heat demand fed by a district heat network. Deep borehole heat exchangers have not been considered as it is likely they will require the fluid to

be passed through a heat pump or be heated further by an additional energy source in order to be used for the heat network. They also operate in a closed system where the fluid does not have the risk of corrosion as the circulating fluid can be predetermined.

7.2 Method of modelling heat exchangers

7.2.1 Thermal analysis of heat exchanger

7.2.1.1 Counter-current flow heat exchangers

Counter-current flow heat exchangers transfer heat between two fluids travelling in opposite directions, with one fluid being the hot geothermal fluid (T_h) and the other a clean circulating fluid (T_c) (Fig. 7.1). The output temperature of the geothermal fluid can be calculated from the input temperatures into the heat exchanger (Dagdas, 2007):

$$T_{hout} = T_{hin} - (T_{hin} - T_{cin}).\frac{(1-e^D)}{((C_h/C_c)-e^D)} \hspace{3cm} 7.1$$

where T is the temperature, C is the thermal capacity and D is calculated as $D = U.A\left(\frac{1}{C_h} - \frac{1}{C_c}\right)$. The thermal capacity can be calculated as $C = m.C_p$, where m is the mass flow rate and C_p is the specific heat capacity. The subscripts in and out represent the inlet or outlet into the heat exchanger, whilst subscripts h and c relate to the hot (geothermal) fluid and cold (clean circulating) fluid used in the district heat network. U is the heat transfer coefficient and A is the heat transfer area. The model also assumes that the mass flow rate for the circulatory fluid is higher than that of the geothermal fluid.

The temperature of the circulatory cold fluid can be calculated by assuming that the heat transfer rate of the geothermal fluid is known and determined from (Dagdas, 2007):

$$C_h.(T_{hin} - T_{hout}) = C_c.(T_{cin} - T_{cout}) \hspace{3cm} 7.2$$

The effectiveness (ε) can be calculated as $\varepsilon = \frac{(1-e^D)}{((C_h/C_c)-e^D)}$ and is expressed as a value

between 0 and 1, where 0 is ineffective and 1 is 100 % effective.

7.2.1.2 Co-current flow heat exchangers

Co-current flow heat exchangers involve the transfer of heat between two fluids travelling in

the same direction (Fig. 7.1) and were modelled using the equation from Bradley (2010):

$$T_{hout} = T_{cin} + \frac{(T_{hin}-T_{cin})}{(1+(C_c/C_h))\left(1-e^{-\frac{U.A}{C_c}}\right)} \qquad 7.3$$

where the effectiveness can be calculated from:

$$\varepsilon = (C_h/C_c).\left(1 - \frac{1}{(1+(C_c/C_h))\left(1-e^{-\frac{U.A}{C_c}}\right)}\right) \qquad 7.4$$

Typically, counter-current flow heat exchangers are used for heat networks due to their higher

efficiencies (Chuanshan and Jun, 1999; Ağra et al., 2015), however, co-current flow heat exchangers

were also modelled for comparison.

7.2.2 Economic modelling of a geothermal heat exchanger's performance for the Cheshire Basin

deep geothermal scheme

The heat exchanger is usually the most significant cost in a district heat network scheme

(assuming the geothermal well has already been drilled). A cost comparison can be made between

installing a heat exchanger for a geothermal fed heat network, and a conventional fossil fuelled

boiler fed heat network. The total savings of using the former can be calculated using the model from

Dagdas (2007).

The annual investment cost of a heat exchanger (C_a) can be calculated as:

$$C_a = I_c.A.CRF \qquad\qquad 7.5$$

where the capital recovery factor of investment (CRF) can be calculated as:

$$CRF = \frac{(1+i)^n.i}{(1+i)^n-1} \qquad\qquad 7.6$$

i is the interest rate and n is the lifetime of the heat exchanger. The net profit (NK) supplying a district heating scheme with geothermal fluid rather than utilising a conventional fossil fuelled boiler can be calculated from:

$$NK = ASM - C_a \qquad\qquad 7.7$$

The annual saved money (ASM) can be calculated for a conventional fossil fuel district heating system as:

$$ASM = Q.H.\frac{3600}{H_u.\eta}.F \qquad\qquad 7.8$$

where Q is the heat rate, H is the hours of plant operation, H_u is the lower heating value of fuel, η is the efficiency of the boiler and F is the cost of fuel.

7.3 Results of heat exchanger analysis

Dagdas (2007) defined optimum configurations for a case study in Turkey where a specific input temperature for a geothermal fluid was used (76 °C). In this study, a range of geothermal fluid input temperatures were used that were representative of the modelled and published temperatures for the Cheshire Basin (Crewe area). Current published estimates of the temperature of the base Permian rocks in the Crewe area range between 67 °C and 86 °C (Downing and Gray, 1986; Plant et al., 1999; Busby, 2011b). The lower end is similar to that of using the thermal gradient from un-corrected bottom-hole temperatures, whilst the higher limit is that from using the newly corrected

thermal gradient (Busby, 2014). As such, the two end-member scenarios for published temperature were used to compare different heat exchanger configurations in order to find the most efficient surface area of the heat exchanger and determine the maximum net profit.

The modelled production temperatures which are within the cut-offs defined in chapter 5 were between 73.55 °C and 89.85 °C. Additional modelling was undertaken to reflect these alternate geothermal fluid input temperatures, whilst reduced flow rates were also explored to extend the analysis to other UK schemes and for scalability within the Cheshire Basin.

7.3.1 Comparison of co-current and counter-current flow heat exchangers

The initial analysis focused on which heat exchanger would be most effective; as such, the minimum and maximum temperature range from literature highlighted above was used with fixed parameters, only altering the heat transfer area (parameters listed in Table 7.1). The inlet temperature of the circulating fluid was fixed at 30 °C as this is considered the typical rejection temperature for the UK (Downing and Gray, 1986). The initial circulation flow rate in the heat exchanger was set at 80 kg/s and the input geothermal fluid flow rate was 40 kg/s. The high geothermal fluid flow rate of 40 kg/s was chosen to test the potential for higher capacity production as analysis in chapter 5 showed multiple wells would be required to meet the demand of all phases of the heat network. The heat transfer coefficient was set at 4,000 W/m^2 °C. This is within the typical range of heat transfer coefficients in literature for geothermal district heating systems which is between 2,900 and 5,100 W/m^2 °C (e.g., Zhu and Zhang; 2004; Dagdas, 2007); however, it is a slightly reduced value as it is assumed some fouling (scaling) will occur in the heat exchanger, thus reducing the performance (Zarrouk et al., 2014). The heat transfer area was altered to establish the optimal configurations for both the co-current and counter-current flow heat exchangers. Initial evaluation of the Cheshire Basin has estimated that the input and output temperatures to the heat exchanger of

clean circulating fluid must have a greater difference than 25 °C to optimise efficiency and use of the

heat (Arup, 2018b).

Parameter	Value
Flow rate of geothermal fluid (m_h)	80 kg/s
Flow rate of circulating fluid (m_c)	40 kg/s
Inlet temperature of geothermal fluid (T_{hin})	67 °C (min) and 86 °C (max) [1,2,3]
Inlet temperature of circulating fluid (T_{cin})	30 °C [1]
Return temperature of circulating fluid (T_{cout})	48.5 °C (min) and 58 °C (max)
Specific heat capacity of water (C_p)	4200 J / kg K
Heat transfer coefficient (U)	4000 W/m^2 °C [4,5]
Boiler efficiency (η)	0.85 [6,7]
Cost of heat exchanger per unit area (I_c)	50 £/m^2
Lower heating value of fuel (H_u)	43000 kJ/kg [8]
Fuel cost (F)	0.49 £ per litre
Interest rate (i)	0.01 [9]
Lifetime (n)	25 years

Table 7.1: *Table of properties used in the simulations. Parameters explained in section 7.3.1 and 7.3.2. [1]*

Downing and Gray, 1986, [2] Plant et al., 1999, [3] Busby, 2011b, [4] Zhu and Zhang; 2004, [5] Dagdas, 2007, [6]

Teke et al., 2010, [7] Ağra, 2011, [8] Annamalai and Puri, 2006, [9] BOE, 2019.

Overall, the results highlight the poorer performance of co-current flow configuration (Figs. 7.2 and 7.3). More specifically;

High input temperature of geothermal fluid models

When analysing the higher geothermal fluid input temperature, counter-flow heat exchangers showed an exponential decrease in geothermal fluid output temperature with increasing transfer area until it reached the circulating fluid input temperature of 30 °C. The circulating fluid increases in temperature and becomes asymptotic to ~58 °C, which is the maximum output temperature of the clean circulatory fluid (Fig. 7.2a). This shows that the counter-current flow exchanger is working efficiently with most of the heat transferring to the circulatory fluid with larger surface areas. The outlet temperature for co-current flow heat exchangers for both the geothermal fluid and circulated water were asymptotic to ~49 °C (9 °C less than the counter-current flow heat exchanger) as the surface area increases (7.2b). The effectiveness of the co-current flow heat exchanger was poor in comparison and was always less than 0.34 (Fig. 7.2c). This shows not all the energy was transferred from the geothermal fluid to the circulatory fluid. From the modelled results, it is clear that counter-current flow heat exchangers are more suited for a district heating scheme in this case, which is consistent with findings in literature (Chuanshan and Jun, 1999; Ağra et al., 2015).
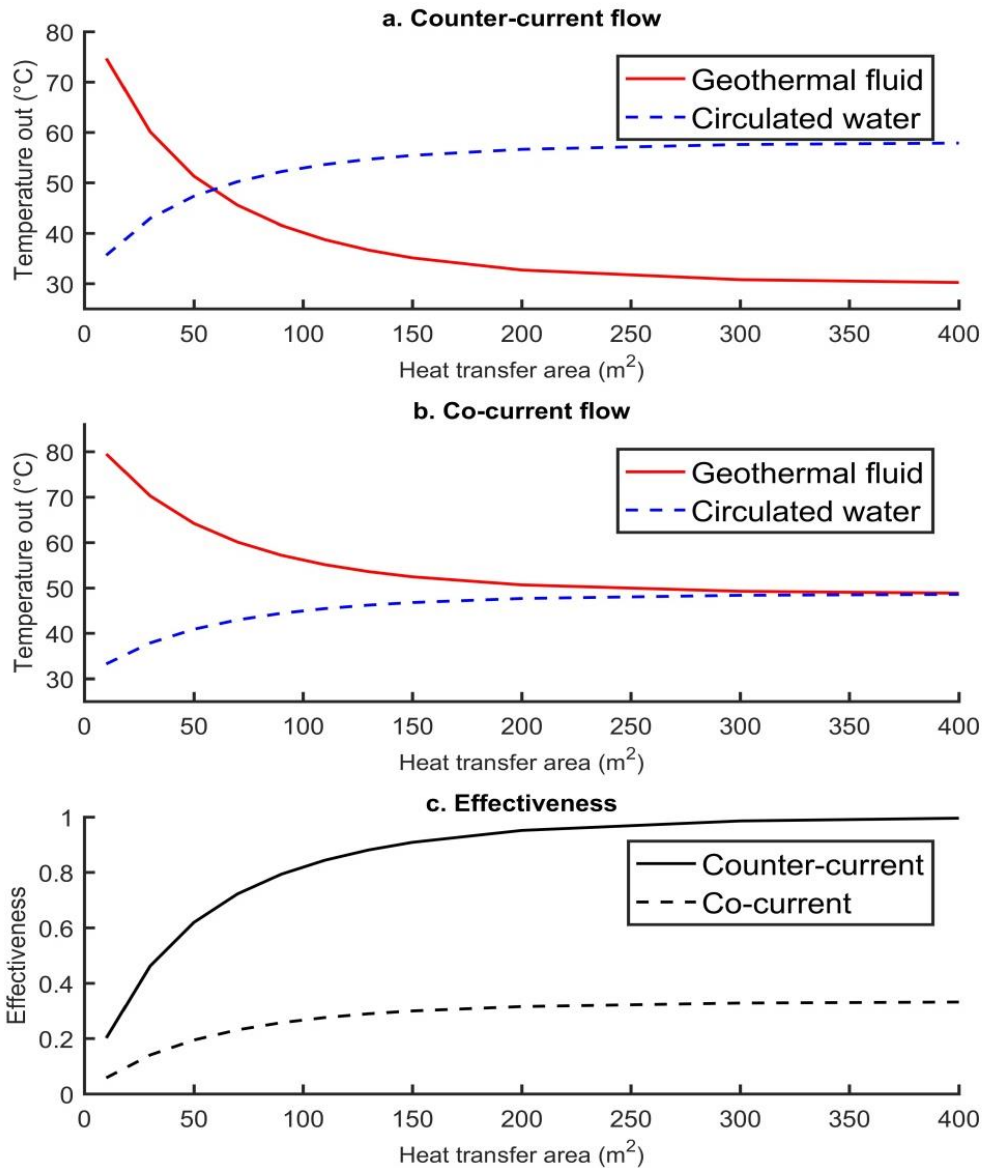
Figure 7.2: *Comparison of output temperatures for (a) counter-current and (b) co-current flows in heat exchangers across a range of surface areas, with their respective efficiencies (c). The input temperature for the geothermal fluid was 86 °C.*

Low input temperature models

For lower input temperatures (67°C), the heat exchanger efficiency was identical to that of the higher input temperature models, but the maximum output temperatures of the circulating fluid were far less at 42.3 °C and 48.4 °C for both co-current and counter-current flow respectively (Fig.

7.3). This is to be expected as the temperature of the geothermal fluid is closer to the input temperature of the circulating fluid.
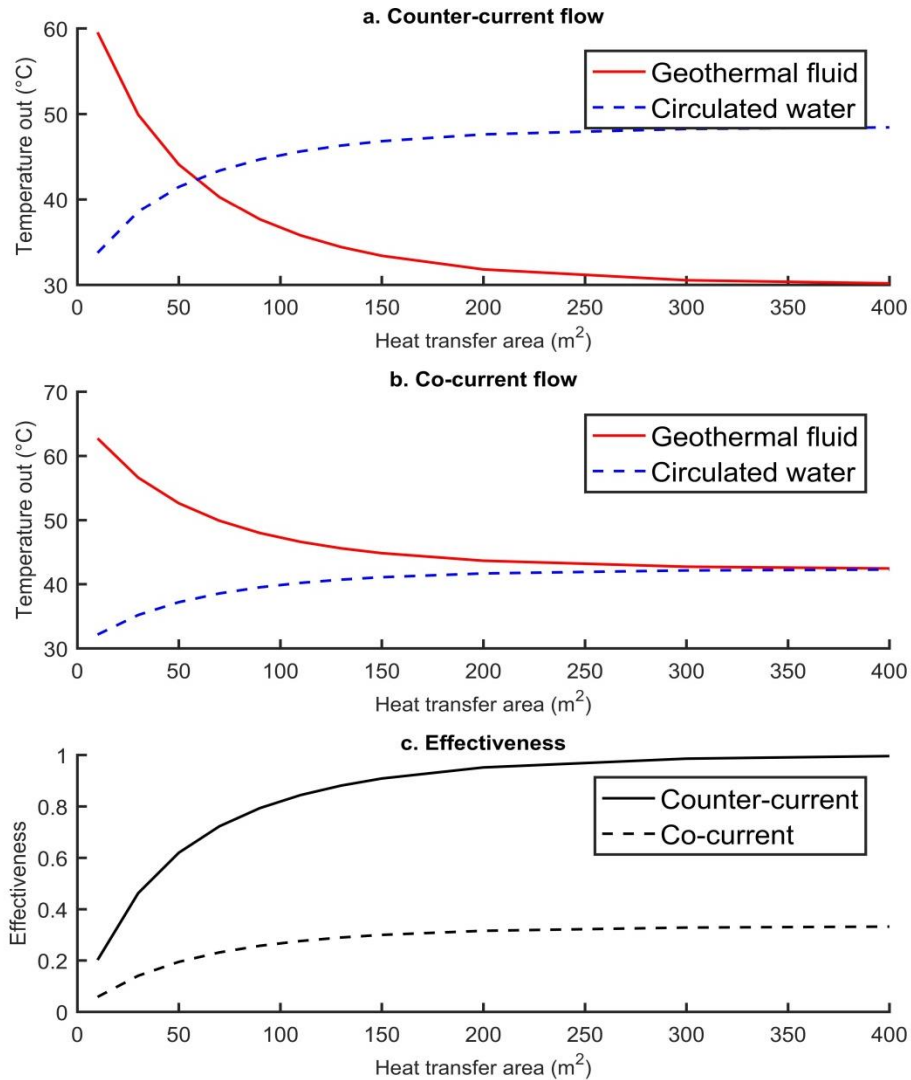
Figure 7.3: *Comparison of output temperatures for (a) counter-current and (b) co-current flows in heat exchangers across a range of surface areas, with their respective efficiencies (c). The input temperature for the geothermal fluid was 67 °C.*

7.3.2 Economic analysis of varying heat transfer area for counter-current flow heat exchangers

The economic performance of the geothermal fed district heat network with heat exchanger installation can be determined in comparison to its fossil fuelled counterpart. Fossil fuelled systems typically use a boiler and in this study its efficiency was set at 0.85 (Teke et al., 2010; Ağra, 2011), and

it was assumed the fuel source was heating oil (similar to diesel), which is typically used in small-scale UK domestic and commercial applications. The lower heating value was set at 43,000 kJ/kg (Annamalai and Puri, 2006) and the cost was 0.49 £/litre (as of April 2019) (values listed in Table 7.1). Heat exchanger prices were modelled at current market rates, whilst interest rates were modelled at the current and historical Bank of England interest rates (BOE, 2019). Both parameters were increased to show the reduction in annual savings. The cost analysis was based on that of a counter-current flow heat exchanger due to the higher efficiency identified in section 7.3.1.
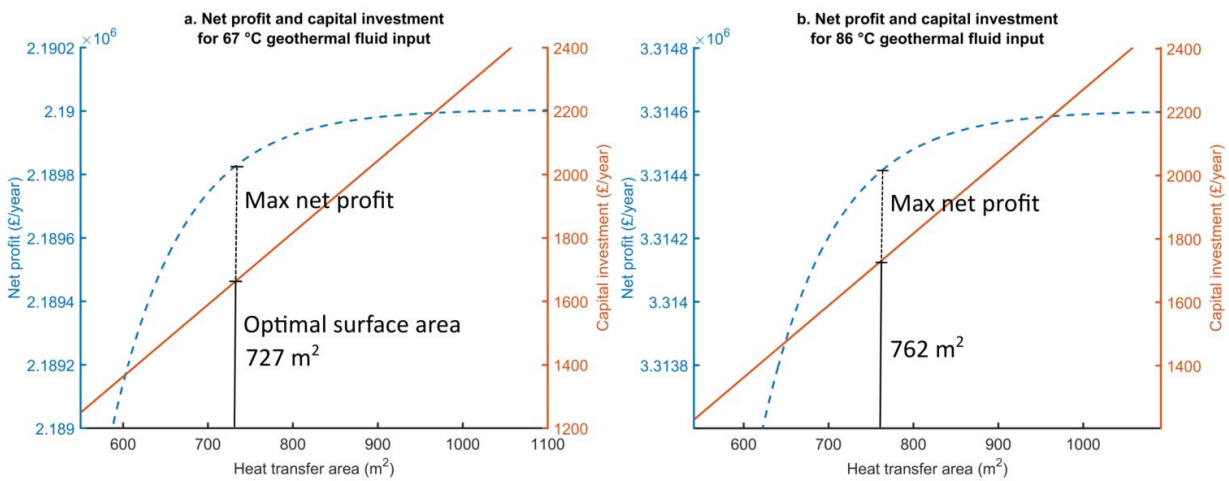
Figure 7.4: *Varying net profit and capital investment versus heat transfer area for different input geothermal temperatures (a) 67 °C and (b) 86 °C. The optimal surface area is the maximum difference between these two values.*

The maximum net profit increased as a consequence of the reduction in cost per m² of the heat exchanger, with a similar trend found with higher interest rates. For the minimum geothermal fluid input temperature value (67 °C), the optimal surface area of the heat exchanger was found to be 727 m² for a scheme with an interest rate of 0.01 and a low cost value of the heat exchanger of £50 per m² (Fig. 7.4a and 7.5 a). The optimal surface area was determined as the point net profit would be highest (Fig. 7.4a) and was £2.1858 million per year. For the higher cost heat exchanger of £400 per m², the optimal surface area reduced to 553 m² and net profit reduced to £2.1784 million

per year (Table 7.2, Fig. 7.5a). Similarly, higher interest rates (0.1) resulted in an optimal surface area of 594 m^2 and net profit of £2.1825 million per year (Table 7.2, Fig. 7.5b).
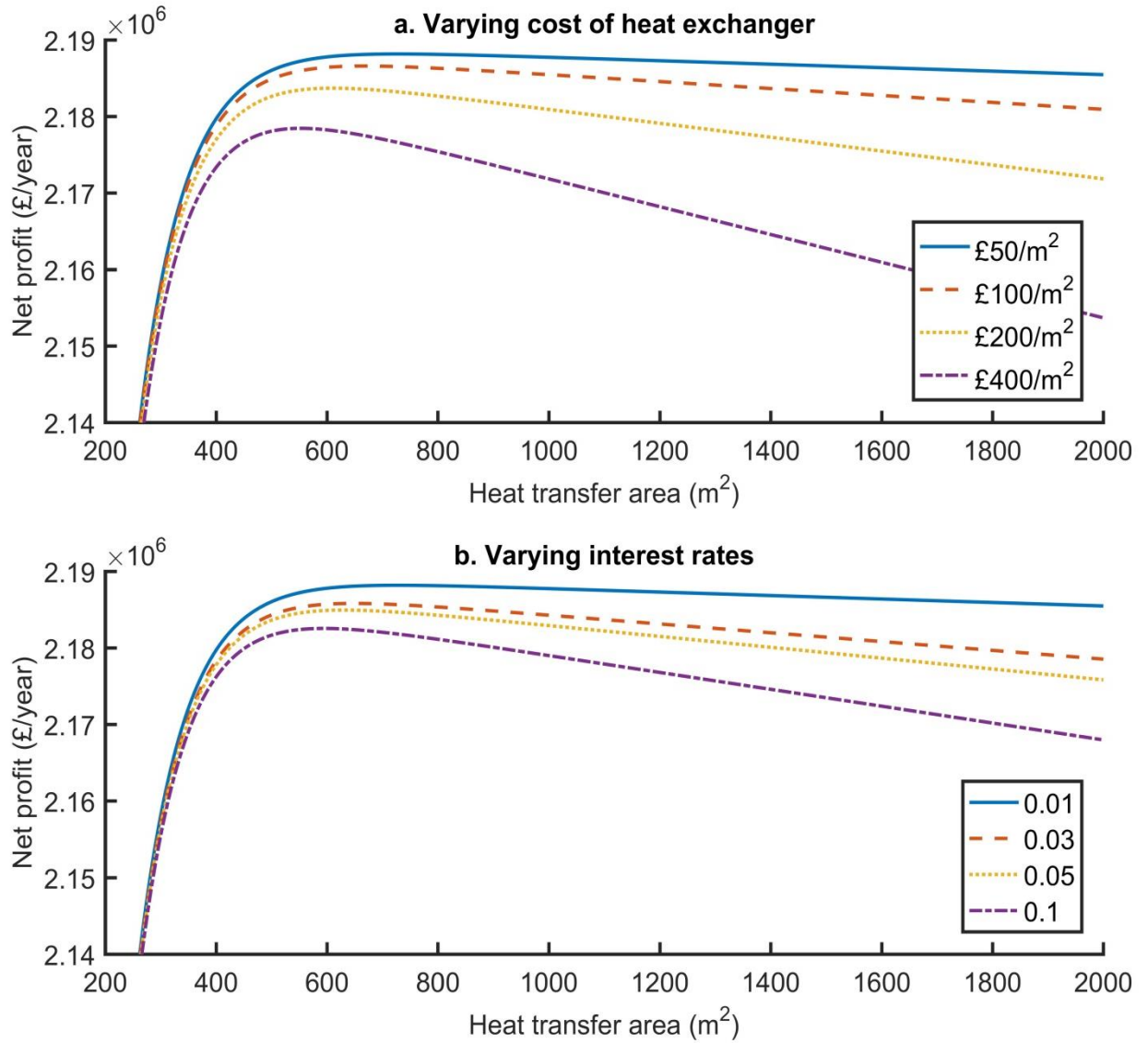
Figure 7.5: *Varying net profit versus heat transfer area for different heat exchanger costs (a) and interest rates (b). The input temperature of the geothermal fluid was 67 °C and the clean circulating fluid 30 °C.*

Heat exchanger (£/m^2)	Optimum heat transfer area (m^2)
50	727
100	669
200	611
400	553
Interest rate (i)	Optimum heat transfer area (m^2)
0.01	727
0.03	649
0.05	631
0.1	594

Table 7.2: *Optimal area compared to increasing heat exchanger cost and interest rates for an input temperature of 67 °C (of the geothermal fluid).*

A higher input temperature (86 °C) for the geothermal fluid into the heat exchanger results in far higher net profits per year. An interest rate of 0.01 and cost of £50 m^2 gives a net profit of £3.3127 million per year and an optimal surface area of 762 m^2 (Fig. 7.4b). Similar to the trend of the lower input geothermal fluid temperature's results, the optimal surface area and net profit reduced with increasing interest rates and cost per m^2 of the heat exchanger. The highest heat exchanger cost (£400 / m^2) resulted in a net profit of £3.3024 million per year and an optimal area of 587 m^2 (Table 7.3, Fig. 7.6a), whilst an interest rate of 0.1 gives a net profit of £3.3067 million per year and an optimal surface area of 629 m^2 (Table 7.3, Fig. 7.6b).

Optimal surface areas under the lowest heat exchanger costs and interest rates resulted in the output temperatures for the geothermal fluid being 30.0032 °C for both high and low temperature input scenarios. The output temperature of the circulatory fluid was 48.5 °C and 58 °C for the 67 °C and 86 °C input temperature of the geothermal fluids, respectively. As would be

224

expected, increasing the geothermal fluid input temperature results in greater circulating water output temperatures (Fig. 7.7) and higher net profits (Figs. 7.7 and 7.8). The optimal surface area also increased with higher temperature geothermal fluids.

Heat exchanger cost per m^2 (£/m^2)	Optimum heat transfer area (m^2)
50	762
100	704
200	645
400	587
Interest rate (i)	Optimum heat transfer area (m^2)
0.01	762
0.03	684
0.05	666
0.1	629

Table 7.3: *Optimal area compared to increasing heat exchanger cost and interest rates for an input*

temperature of 86 °C (of the geothermal fluid).
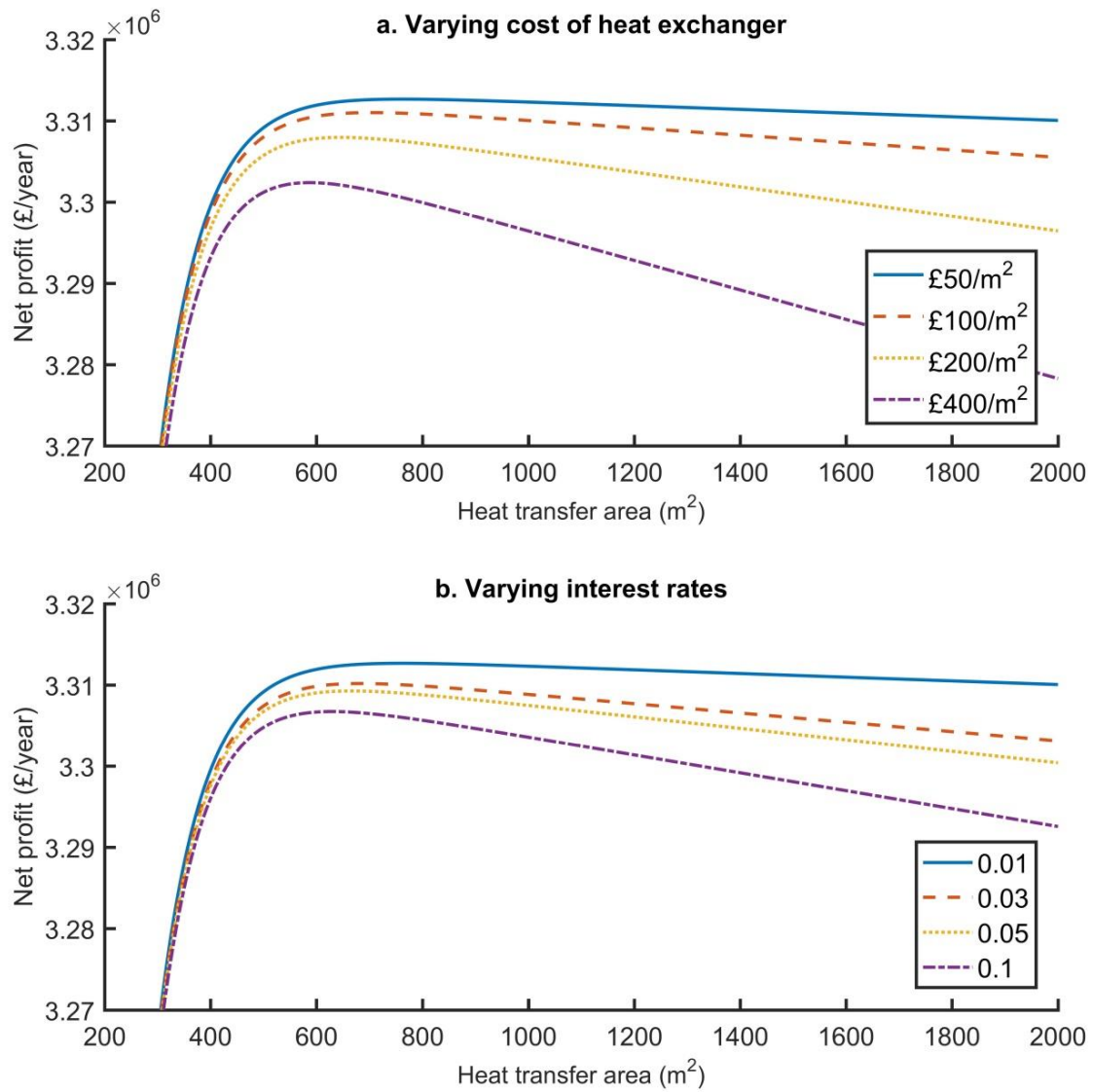
Figure 7.6: *Varying net profit versus heat transfer area for different heat exchanger costs (a) and interest rates*

(b). The input temperature of the geothermal fluid was 86 °C and the circulating fluid 30 °C.
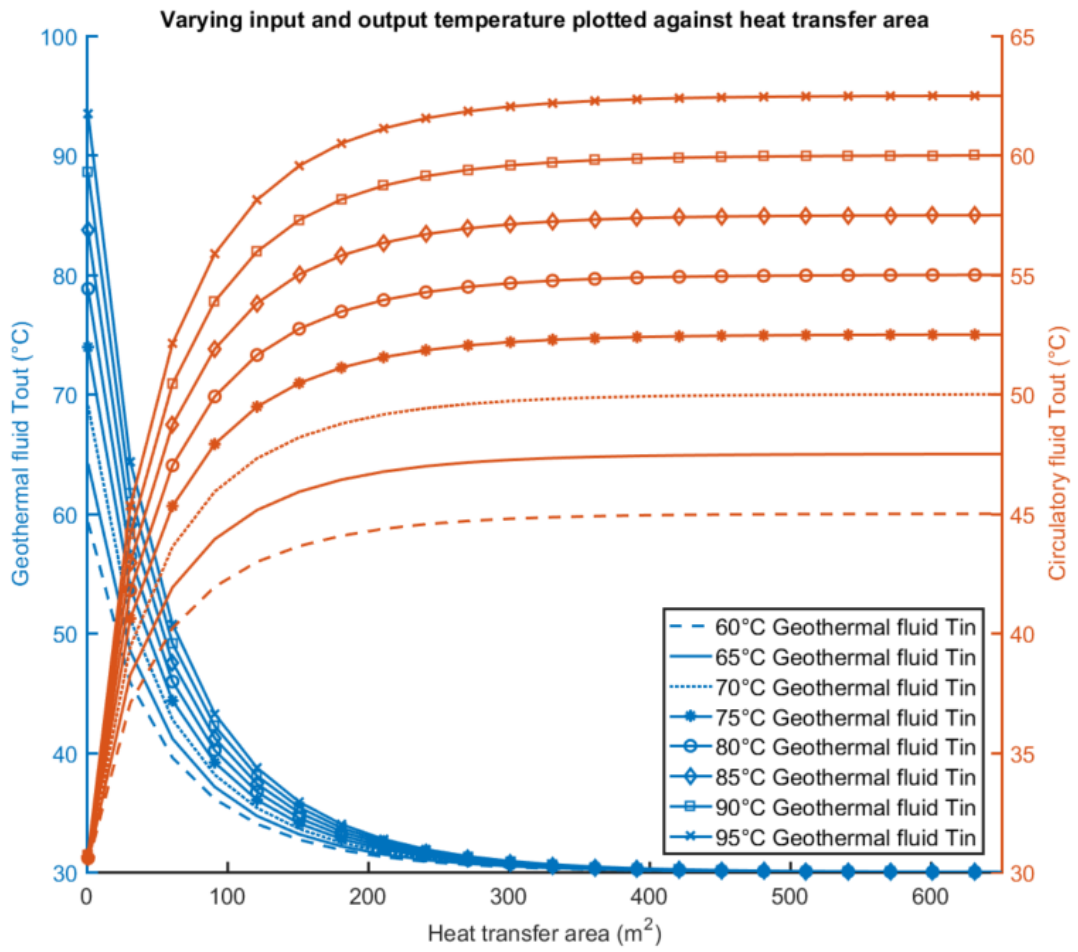
Figure 7.7 *Change in geothermal fluid and circulating fluid output temperatures for different heat exchanger transfer areas across the 60-95 °C input geothermal fluid temperature range.*
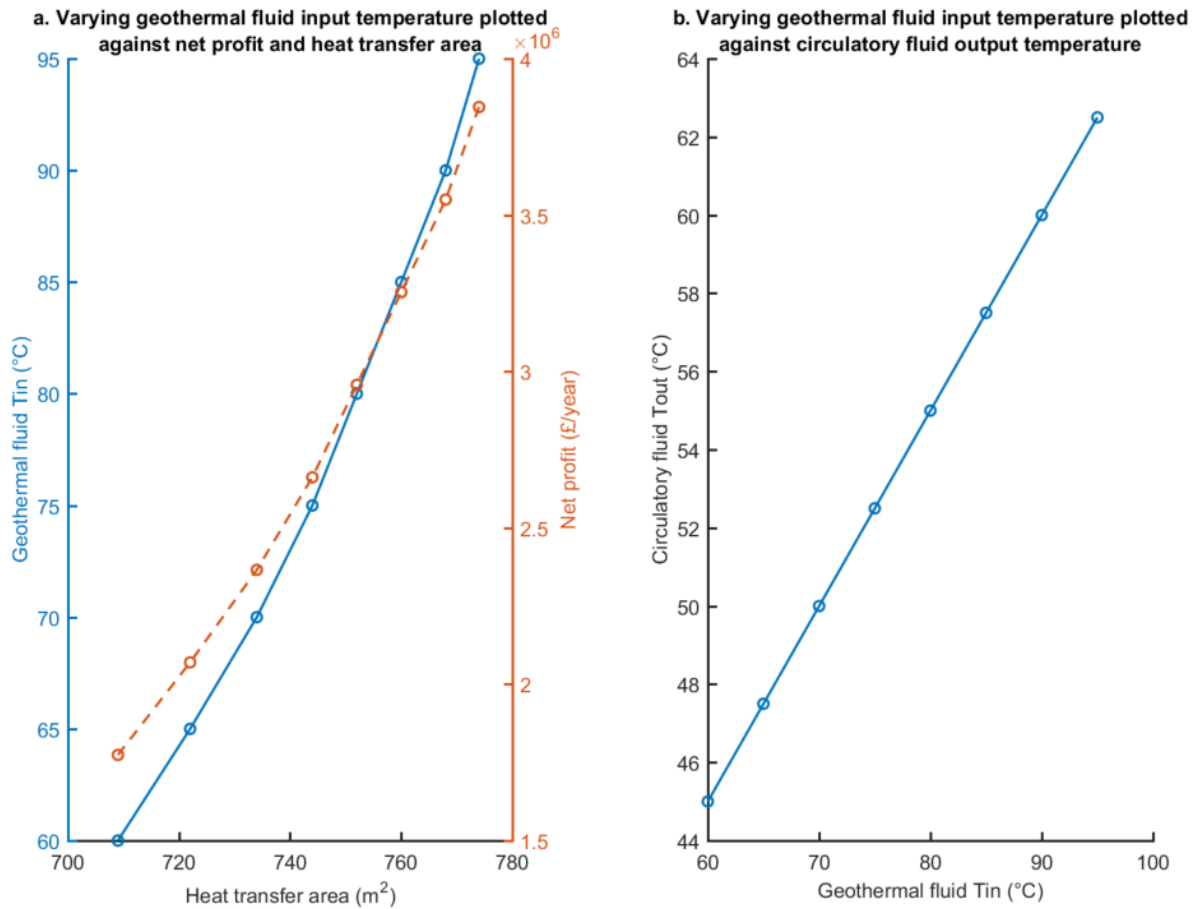
Figure 7.8: *(a) Variation in net profit and optimal transfer area as a consequence of changes in input temperature of the geothermal fluid. (b) Variation in output of circulating fluid in comparison to the geothermal fluid input temperature.*

7.3.3 Energy supply and demand for the Cheshire Basin in the Crewe area

Energy demand in the whole Crewe area has initially been estimated at 35 MW (Routledge et al., 2014), whilst the current town plans for phase 1 of the district heat network in the town centre have an estimated demand of between 1.6 and 0.04 MW (peak and low demand) (Arup, 2018b). To meet the peak demand for the town centre (phase 1) the temperature of the geothermal fluid must exceed 70 °C for the lowest production flow rate of 10 l/s (Fig. 7.9). All other scenarios (i.e., higher flow rates and production temperatures) produce enough energy to supply the lower demand estimates. If a higher energy demand is to be met either multiple producing wells or an additional

energy source for the heat network will be needed. The output temperature of the circulating fluid in the heat network also significantly decreased with respect to the input geothermal fluid temperature, which may make it too cool to be used. Hotter circulating fluids can be attained by reducing the flow rate proportionally to the geothermal fluid. The coolest and slowest flow rates also have a low net profit. These are, therefore, unlikely to be economic when the operating costs of the geothermal well and heat network are included.
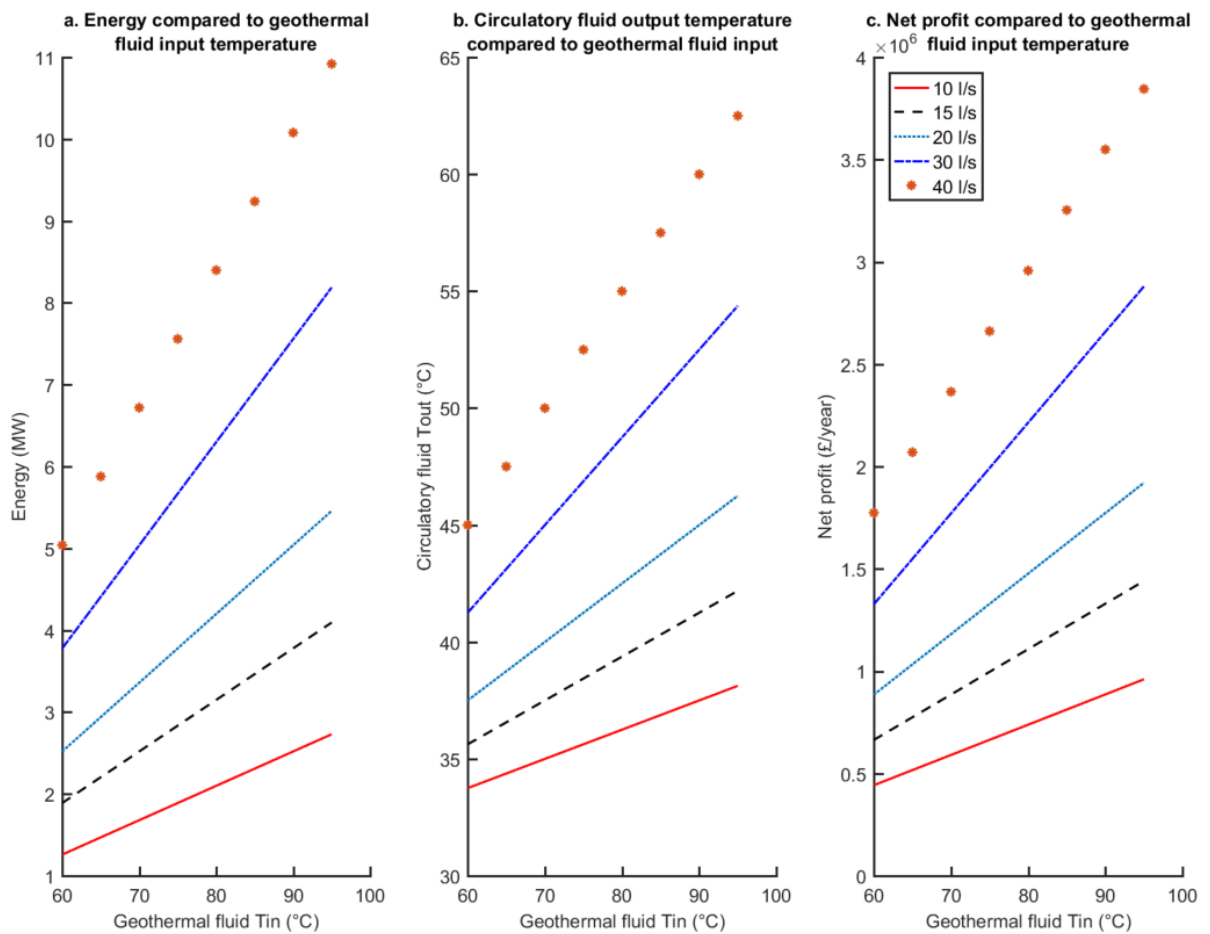
Figure 7.9: *Variation in energy (a), circulatory fluid output temperature (b) and net profit (c) with changes in geothermal fluid flow rate.*

7.4 Discussion: additional costs to consider

Drilling deep geothermal wells is costly and can be the greatest expense for a district heating scheme based on geothermal supply. The cost of drilling a well can be calculated according to (Lukawski et al., 2014):

$$Well\ cost = 1.72\ \times 10^{-7} \times (MD)^2 + 2.3\ \times 10^{-3} \times MD - 0.62 \qquad\qquad 7.9$$

where MD is depth of the well in metres. The equation gives the well cost in millions of dollars which is converted to pounds using a factor of 0.77.

The cost of drilling a single well in the Cheshire Basin would be in the region of £5.7 million, assuming the reservoir is located at a depth of 2,800 m and fluid is only extracted in a screened interval to 2,870 m. For the worst case scenario (67 °C input temperature of the geothermal fluid and high heat exchanger cost of £400 m^2) the savings of switching to a geothermal run district heat network would be £2.1784 million per year. The payback time for a single well scheme would therefore be ~2.6 years. The minimum total savings including the cost of a geothermal well would be £48.76 million (assuming a lifetime of 25 years). If the highest amount of savings can be made (86 °C input temperature of the geothermal fluid and a low heat exchanger cost of £50 m^2) then the payback time will be under two years. The savings over a 25 year lifetime will be £77.2 million.

There will be additional waste water disposal costs when developing the geothermal resource with a single well. To evaluate the likely cost of waste water disposal, relevant examples of active and passive schemes from the mining industry have been used where they are relevant for the treatment of deep, brine-rich formation waters (Westaway, 2018).

For active treatments, a capital expenditure of £4.25 million and £1.65 million was required for two mine water discharge treatment schemes; a copper mine in Cornwall (Knight Piesold and partners, 1998) and a lead mine in Cumbria (Bailey et al., 2016). They had operating costs of £0.3 and

£0.8 per cubic metre, respectively. Passive treatments are less costly (Westaway, 2018) and examples from Europe have shown capital expenditure of £0.43 million and an operating cost of £0.17 per cubic metre for a Uranium mine (Kunze & Küchler, 2003; Küchler et al., 2005). Assuming an annual operating period of 8 months, and a production rate of 40 l/s, the minimum annual operating cost for active treatment will be ~£250,000 and ~£140,000 for passive treatment. The total cost for a 25-year operating period (including capital expenditure) for each scenario would be £7,900,000 and £3,930,000 for active and passive treatments, respectively. This highlights that passive treatments are far cheaper to use; however, it only makes a minor saving to the overall budget in comparison to the cost of drilling two wells in a doublet style scheme. By extracting, treating and disposing the water at the surface (as would be needed for a single well) rather than re-injecting it into the reservoir also removes the benefit and operational sustainability of pressure maintenance in the reservoir. It is worth noting that the cost estimates provided are not case-specific to the nature of the fluids extracted from Mesozoic basins of the UK (i.e., the Cheshire Basin) and the true cost of waste water disposal could be different from that described above.

Summary

A feasibility study has been undertaken for the use of heat exchangers as part of a geothermal district heating scheme for the Cheshire Basin, highlighting that counter-flow heat exchangers can give significant savings when compared to fossil fuels over the lifetime of a heat exchanger (i.e., 25 years). This is even when the initial cost of drilling a single well is included. Waste water disposal would, however, need to be factored in and can be extremely costly.

Based on modelled production temperatures and literature, the most efficient surface area of the heat exchanger was found to be 727 m^2 and 762 m^2 for geothermal fluid input temperatures of 67 °C and 86 °C. This results in total savings of £48.76 million and £77.2 million, respectively. Using an input temperature of 30 °C for the circulatory fluid, the output temperature of the circulating fluid

for the lower and higher input geothermal temperatures were 48.5 °C and 58 °C. This would be the likely range of achievable system temperatures that a district heating system could operate under.

Building on this, for a deep geothermal energy scheme in the Cheshire basin, under the best case scenario (95 °C geothermal fluid temperature and 40 l/s flow rate) a single well system could produce 10.92 MW of energy. If coupled to the district heating scheme in Crewe town centre the initial capital expenditure would be £5.7 million (neglecting initial waste water disposal costs) and the operating costs would be £~140,000 per annum (passive disposal of waste water). However, by using a geothermal fed district heat network, rather than a conventional fossil fuelled network, savings of £3.845 million per annum could be made.

For the worst case scenario (60 °C geothermal fluid temperature and 10 l/s) a single well scheme could produce 1.26 MW. The capital expenditure would be identical to that of optimal conditions, whilst the operating cost for active waste water treatment would be £~250,000 per annum. The total saving per annum by using a geothermal fed heat network would be £0.443 million. In this scenario the geothermal scheme would not recover the initial capital expenditure over the 25-year lifetime.

This study has also determined that any single well scheme, when used in conjunction with a heat exchanger must have flow rates and production temperatures in excess of 10 l/s and 70 °C respectively to be viable to meet the Crewe energy demand for phase 1 of the heat network (1.6 MW). An initial review of the costs of passive and active methods for waste water treatment at surface level indicate that a 'two well' or doublet scheme may be a preferred option, due to near equivalent overall costs and the added benefit of pressure maintenance in the aquifer with re-injected water.

CHAPTER 8 – IMPACTS AND LIMITATIONS OF GEOTHERMAL RESOURCES EXPLOITATION USING SINGLE WELL METHODS

This chapter evaluates the findings in this thesis and discusses the impacts and limitations that may influence geothermal development within the Cheshire Basin.

8.1 Introduction

In this study, deep single well geothermal models of different configurations have shown that low-enthalpy resources can be exploited from the Cheshire Basin for direct heat use. This is significant for the Crewe area as the models can be used to match supply to demand, whilst financial modelling indicated that this carbon-neutral resource could make significant cost savings in comparison to fossil fuel fed district heat networks. Novel, low-risk single well strategies were also modelled which have wider implications as they can be used in almost any geological scenario in the UK for low heat demand schemes and small scale heat networks.

Although the models highlight (from a technical point of view) that single well schemes can produce heat, there are other considerations which may impact on the development of deep geothermal energy in the Cheshire Basin. These include, but are not limited to; waste water treatment and disposal, public perception and the protection of the resource.

8.2 Impacts on the exploitation of geothermal resources in the Wessex and Cheshire Basins

Multiple studies in the UK have identified that a significant deep geothermal resource is contained in low-enthalpy Mesozoic sedimentary basins (Downing and Gray, 1986a,b; Rollin et al., 1995; Busby, 2014), with few studies considering the exploitation of the resource due to both a high geological and financial risk (Hirst et al., 2015). In this thesis, a modelling study was undertaken with the aim of bridging the gap of resource development in both the Wessex and Cheshire Basins. Although geothermal resource estimations can give an indication of the total

energy available in the basin, the single well modelling studies in this thesis allow the total producible energy from a development well to be matched to demand.

Furthermore, resource estimations did not consider the key geological and engineering parameters, such as hydraulic conductivity or intricate details of the wellbore, leaving much of the operational performance of geothermal schemes in the UK unquantified. These limitations formed the initial focus of the PhD – i.e., to build, design and test a model that could simulate transient solutions for a range of energy extraction methods. Validation and testing of the model highlighted its benefits by providing high modelling accuracy in comparison to analytical solutions and a maximum spatial discretisation error for a range of meshes was <1 %. The model also closely matched case study solutions with computational time on a standard computer constrained to less than 3 hours.

The Wessex Basin models: Initial modelling (Barker, 1981; Downing et al., 1984) and further observation of water levels (Barker et al., 2000) led to the conclusion that the Marchwood Well in the Wessex Basin could not be used sustainably for the development of geothermal energy. This provided a driver to investigate the performance of alternative configurations as a hypothetical re-purposing of the Marchwood Well (i.e., using deep coaxial borehole heat exchangers and standing column wells). The results indicated that low-moderate heat loads could be attained from both borehole heat exchangers and standing column wells; however, neither could match the energy supply of extraction only wells under long term performance. Although the current status of the Marchwood Well is unknown (i.e., is it plugged or still used for monitoring), it could be converted to a deep borehole heat exchanger or standing column well. This is a significant finding, as it shows that a previously unsuitable exploration well could be used for geothermal operation to contribute to the growing heat network (Barker et al., 2000).

The Cheshire Basin parametric analysis: Although considerable research has been undertaken on the Cheshire Basin to quantify the geothermal resources (Rollin et al., 1995) and geological characteristics (e.g., Downing and Gray, 1986), no deep geothermal development has been undertaken. The geological characterisation of aquifers has indicated the rocks storing the heat in place have high-quality hydrological properties. However, few deep borehole penetrations have been drilled in the Cheshire Basin leaving a high uncertainty in the geology and aquifer quality at depth in the Crewe area. As such, a modelling study was undertaken which focused on the performance of a single extraction well where it was assumed that the initial exploration borehole would be converted to a development well, saving costs and reducing financial risk.

In contrast to the resource estimation and geological characterisation of the basal Permian sandstones in the literature (which indicate a significant geothermal resource with the potential to be developed) the modelling study highlighted important geological factors that impact well performance – i.e., the hydraulic conductivity and initial thermal gradient. The tolerance for variance in hydraulic conductivity was low and values less than 0.05 m/day almost instantly created a rapid drawdown in the wellbore in excess of 500 m during production. Therefore, the potentially tight aquifers at depth could be difficult to exploit. Poor initial aquifer temperature and hydraulic conductivities could, however, be mitigated using engineering solutions (such as, reduced flow rate and increasing the well screen length), increasing well performance and reducing geological uncertainty. Although this offers encouraging results for geothermal development by reducing the risks associated with poor geological conditions, the mitigation methods are likely to have negative financial connotations, such as increasing the capital expenditure and reducing the amount of energy to sell.

The sensitivity analysis of single extraction well performance in the Cheshire Basin also showed some wider implications in that the key geological and engineering risks of single well schemes are different to doublet schemes. In doublet schemes, production temperature and drawdown in the wellbore both influence performance. However, in single well schemes, drawdown in the well is the most significant obstacle to development as transient changes in temperature are minimal. Other studies suggest that for doublet schemes the most important parameters are the thermal conductivity, salinity, porosity, pore fluid salinity, initial aquifer temperature and production rate (Saeid et al., 2013, 2015; Aliyu and Chen, 2017). In comparison, the models show that the key parameters in single well schemes are hydraulic conductivity, initial thermal gradient, production rate, length and position of the well screen. Modelling of the single well scheme also highlighted that a significant amount of waste water would be produced over 25 years and some consideration would be required over the feasibility of disposal methods (Sect. 8.3.1).

8.3 Implication of novel single well exploitation methods

In the UK there is a reluctance to invest in deep geothermal schemes due to the high geological risk and lack of infrastructure to meet the demand. Two new innovative methods of energy extraction have been proposed (deep borehole heat exchangers and standing column wells) (Law et al., 2015; Collins and Law 2017), with Westaway (2018) highlighting the need for an accurate model to predict well performance. The geological risk lies with uncertainty of physical properties at depth and these new methods aim to minimise the impact of local geological variations (chapter 5). Modelling of the Wessex and Cheshire Basins indicated that both methods could meet a small proportion of the demand; however, they would likely need an additional energy source to meet the remaining demand. The implication of this is that either an

array of boreholes would be required to supply a district heat network or that either method is more suited to smaller domestic or commercial developments.

In contrast to the findings of Law et al. (2015), who suggested standing column wells could be used in almost any geological setting, the modelling of the Wessex Basin highlighted that consideration must be given to the hydraulic interactions in the aquifer, which could reach a maximum distance of nearly 2 km radially around the well screen over a well's lifetime. The use of deep borehole heat exchangers, however, would have minimal risk as thermal interactions between the borehole and subsurface are constrained to within a hundred metres of the borehole. This, and the closed-loop system design, mean that deep borehole heat exchangers can be deployed almost anywhere in the UK. It is hoped that the models developed in this study, could be used to accelerate the up-take of deep geothermal resource exploitation across the UK. It is also worth noting that infrastructure for such heating schemes would still need to be implemented or built into new commercial developments if targeting a small scaled system (i.e., block of flats).

Aquifer thermal energy storage schemes were also considered through the modelling of a single well scheme. In comparison to shallower schemes arrangements, relatively low recovery factors could be obtained (maximum ~50 %) which has a significant implication for energy storage schemes through this type of approach. The study highlighted the significant heat losses occurring in the wellbore with the outcome that deep aquifers are likely to yield poor recovery factors. It also demonstrated that substantial quantities of waste water would need storing and the cost/practicality of this is likely to be unfeasible.

8.4 Limitations to geothermal development

8.4.1 Waste water treatment and disposal within the Cheshire Basin

For extraction only single wells, the produced geothermal fluid must be treated prior to disposal as it is likely to be saline due to the dissolution of salt from aquifers and contain various contaminants including dissolved metallic ions and radionuclides (Westaway, 2018). Financial modelling in chapter 7 speculated that the cost of waste water treatment and disposal could reduce the economic performance of a single geothermal well, such that a two well (or doublet) scheme may be a preferred option.

The issue of waste water is problematic and at present, the options include: water treatment then disposal at surface level, disposal to the sea and/or re-injection underground. Currently, the only deep geothermal scheme in the UK at Southampton discharges brine cooled to 28 °C into the sea (Energie-Cités, 2001). If the geothermal fluid has a higher salinity than the seawater, or traces of contaminants, a passive treatment will be required prior to discharge (Robinson et al., 2016). Mesozoic basins in the UK are located proximal to the coast, with the Cheshire, Wessex, Rathlin, Larne and East England Basins all situated near to the sea. In some cases, such as the Cheshire Basin, the demand and greatest resource is located in-land, which would require transportation to the coast for disposal into the East Irish Sea. This is unlikely to be feasible or cost effective.

Many deep geothermal schemes rely on re-injection schemes via doublets (two well systems) to dispose of the produced brine; not only does this solve the issue of waste water disposal but also has the added benefit of maintaining reservoir pressure. Although there are many benefits to doublet schemes they do require a larger initial capital expenditure, which may not be available in the UK due to high geological and financial risk. This results in a limited numer of investors being willing to provide the initial capital investment. Alternative re-injection

options are available: 1) Disposal by re-injection via an alternative well into shallower aquifers, 2) Disposal of brine as fluid used in the hydraulic fracturing of shale and 3) Disposal of fluid through the same well (as modelled in chapters 4 and 6).

Re-injection of the brine into shallower aquifers in the Cheshire Basin may be a suitable unique alternative due to the thick sequence of Permo-Triassic sandstones (as recorded at the Prees-1 and Knutsford boreholes of 1,623 m TVDSS and 1,921 m TVDSS, respectively (UKOGL, 2019)). Upper Triassic aquifers retain high porosities and hydraulic conductivities (up to 30 % and 10 m / day (Allen et al., 1997)) which are capable of supporting high infiltration rates. Rejecting fluid to the subsurface via a shallow well (or direct infiltration from ground level where the geology permits) would account for the waste water. However, it would also increase the initial capital expenditure and operating costs.

Locally to Crewe, few wells have been drilled to depths that reach the Helsby Formation, which is the most proximal aquifer to the surface. The closest is the Burford-1 Well drilled ~10 km west from Crewe town centre. The Burford-1 Well was targeting a Triassic faulted trap during petroleum exploration. It was found to be dry due to an absence of source rocks or poor charging of the reservoir due to ineffective migration of hydrocarbons (Mikkelsen and Floodpage, 1997). The data shows there to be a high-quality, ~360 m thick sandstone succession (UKOGL, 2019) with the Triassic sandstones likely to extend to a far greater depth. It is likely that the geology and depth of any potential aquifers to re-inject fluid underlying Crewe is of similar depths (844 m below ground level) (UKOGL, 2019). Unfortunately, due to plugging and abandonment of the Burford-1 well, it cannot be used for disposal. It is also worth noting that the Helsby Sandstone Formation is a key aquifer in the UK, and an additional cost for the treatment of chemicals and desalination of the water prior to re-injection would be required. As a result, the additional costs of drilling a shallow

re-injection well and providing wastewater treatment prior to disposal would potentially increase prices to that of a doublet system.

Shale gas exploration is growing in the Northwest UK and it could prove a useful solution to the issue of waste water disposal. During shale gas operations, hydraulic fracturing is required to artificially enhance the hydraulic conductivity and simulate gas migration. Hydraulic fracturing works by injecting fluid and sand at high pressures, which, in turn, causes fractures and increased porosity/permeability in the rock for hydrocarbons to be extracted from. Initially a high amount of water may be required, but the longer-term demand is difficult to ascertain. Nevertheless, any stimulation is unlikely to require a constant supply of injected water and would be limited geographically (i.e., to locations where both the hydraulic stimulations of shale and geothermal extraction are proximal). Fractured wells in America have found to require between 1.5 and 16 million gallons of water (AGI, 2020). In the Cheshire Basin, under base case conditions (15 l/s flow rate) this would mean between ~10 and 102 fractured wells would be required to dispose all the fluid, respectively.

Disposal of fluid in the same well, via circulation, will reduce drawdown in the reservoir due to low extraction rates (if any), and able to produce relatively high heat loads for short periods. However, there are problems with this method which include a reduction in production temperature and heat load after a few days of constant exploitation, as shown in the standing column well and coaxial borehole heat exchanger models (chapters 4 and 6). Any further analysis should, therefore, focus on modelling both the financial and technical possibilities of alternate waste water disposal strategies.

8.4.2 Barriers to geothermal development: public perception and seismicity

Although the technical and economic analysis of deep, single well geothermal schemes confirms their potential and viability for delivering a renewable energy source, several barriers and

risks remain. Public perception is important for any geothermal development and schemes where fluid is re-circulated in the subsurface may cause earthquakes due to the reactivation of natural (or induced) faults. Recent seismic events associated with hydraulic fracturing have occurred in crystalline basement in locations such as Soultz-sous Forêts, France (e.g. Charléty et al. 2007) and Switzerland (e.g. Häring et al., 2008; Deichmann and Giardini, 2009; Diehl et al. 2017). Seismicity caused by geothermal operations is usually assumed to only occur in enhanced geothermal systems. However, this is not the case in the North Alpine Foreland Basin, an area considered to have low seismic hazard, where a series of 130 seismic events were identified ranging from 0.8 - 2.4 magnitude (Megies and Wasserman, 2014). The negative connotations associated to geothermal, and similarly hydrocarbon fracking, have significantly impacted public perception, leading to the public believing that 'geological activity induces underground harm' (Dowd et al. 2011; Stewart and Lewis, 2017). Recent geothermal developments in the UK, such as the Jubilee pools and the United Downs project, appear to be more accepted than shale gas exploration sites, however, with strict UK legislation and limits on induced seismicity, any sort of seismic event associated with a new deep, geothermal development scheme could easily change this public perception.

8.4.3 Resource protection and incentives for deep geothermal development

Currently, several additional key issues to geological uncertainty prevent geothermal exploration and development; these include a lack of protection over resources, government insurance against well failures and incentives to use renewable resources. The Crewe area is located in the Weaver and Dane area, regulated for water abstraction by the Environmental Agency (2013). To extract water, a license for extraction rates exceeding 20 m^3/day (or 0.2 l/s) is needed, as is a groundwater investigation consent and a discharge permit (if to the surface) (Environmental Agency, 2013; GOV, 2019). Any license granted by the water authority does not guarantee that water will be available (e.g., if the well is dry, or geology does not permit extraction) and is only available for 12 or 24 years. Interestingly, brine water abstraction that exceeds a salt content of 100,000 mg/l (or 0.1

ppm/10^6) can be abstracted without a license from 'brine fields'. Analysis from wells to the north and south of Crewe (Knutsford and Prees-1, respectively) indicate salt contents ranging from 0.02 to 0.08 ppm/10^6, whilst additional modelling in the centre of the basin highlights salt from the Mercia Mudstone Group could enhance this (Plant et al. 1999). As such, if the salinity concentration is as high as predicted then no water abstraction license is required. Additionally, there are no measures to protect the 'heat in place' (GOV, 2019) and therefore, developments utilising a doublet scheme, standing column well or borehole heat exchanger will be protected for the water resource, but not for thermal drawdown / breakthrough. Due to the lack of licensing schemes (similar to those used in the oil industry) there is a higher degree of investment risk, with no protection against other developers drilling proximal to any proven resource. Although licensing has been proposed it has not yet been put into practice (Fraser, 2013), leaving no protection of the geothermal resource.

Investment could be incentivised by government schemes such as feed-in tariffs, direct financial support and well insurance (Haraldsson, 2014). Feed-in tariffs provide a guaranteed price for the energy produced, direct financial support involves government investment to de-risk the resource and well insurance can cover drilling failure or resource decline over 25 years, similar to that in France (Rybach, 2010).

CHAPTER 9 - CONCLUSIONS AND RECOMENDATIONS

9.1 Principal conclusions from this study

In this thesis, a numerical model was designed to simulate different single well configurations, incorporating all aspects of a deep low-enthalpy geothermal system in a sedimentary basin, including the reservoir, borehole and confining beds. Further analysis has also been undertaken on the input and output temperatures of the geothermal and circulatory fluids used in heat exchangers typical of that needed for the district heating scheme in the Crewe area.

Preliminary analysis in chapter 4 validated and tested the model against analytical and case study scenarios, giving confidence in the model. Further work was undertaken investigating the application of various single well configurations to the Marchwood Well, Wessex Bain, Southampton. This highlighted that although conventional (extraction only) wells can produce far more energy without encountering thermal drawdown, they are largely influenced by geology which can result in significant drawdown in head in the wellbore. Deep borehole heat exchangers and standing column wells were proven to produce a lower heat load in comparison to extraction wells, but have the benefit of being a lower risk strategy for deep geothermal projects in the UK. When using optimal parameters and, after the rapid initial thermal drawdown in the first few days of modelling, deep borehole heat exchangers were shown to be able to produce a heat load of 100 kW, whilst outlet temperatures in standing column wells were modelled to give a heat load exceeding 300 kW.

The main focus of the study was the Cheshire Basin which is anticipated to hold 23 % (75×10^{18} J) of the estimated geothermal resource in the UK (Rollin et al., 1995). A sensitivity analysis was undertaken modelling various geological and engineering parameters of a standard configuration extraction only single well in the Crewe area (chapter 5). The results indicated that the key geological parameters were hydraulic conductivity and the thermal gradient. The key engineering

parameters were the length and position of the well screen, and production rate. Although it is difficult to mitigate against thermal gradient (i.e., initial reservoir temperature), it is possible to mitigate against poor hydraulic conductivities by altering the engineering parameters. By increasing the length of the well screen it was shown that low hydraulic conductivities (0.01 m/day) could produce fluid sustainably for the lifetime of the development (25 years). The energy produced from the base case (best estimate of the real geological conditions used in the sensitivity analysis in section 5.4.1) would be able to meet all of the initial demand for energy in the core scheme (i.e., phase 1 of district heat network development in Crewe town centre with a demand of <1.6 MW), however, would only be able to meet 35 % of demand over the lifetime of the entire district heat network scheme.

The study also concluded that the drilling of slim-boreholes only have a minor influence on production temperature and drawdown in comparison to regular boreholes. If any initial slim-borehole drilling and exploration is undertaken in the basin, it may facilitate the conversion of these wells to development wells to save costs. Additionally, it has been shown thermal dispersion only had a minor effect on the spatial and temporal variations in temperature change for single well schemes.

Although the initial analysis on standard configuration single wells in the Cheshire Basin is positive, the disposal of waste water and uncertainty in the geology at depth remains a concern. Further modelling analysis focused on methods where minimal (if any) waste water is disposed and where the geological uncertainty would present less of an issue. Standing column wells, coaxial borehole heat exchangers and seasonal injection-extraction (aquifer thermal energy storage) schemes were all modelled (chapter 6).

The latter injection-extraction scheme involved seasonal variations in extraction (in the winter) and injection (in the summer) via the same well (i.e., a seasonal aquifer thermal energy

storage scheme). Longer injection periods resulted in greater recovery factors in short simulations, with the recovery factor increasing from 22.9 % to 29.8 % for 2 and 6 months injection, respectively. The recovery factors of all annual variations were observed to increase with time due to an overall warming of the system. The maximum recovery factors observed were ~50 % and it was evident heat losses in the wellbore had a major impact on recovery factors with losses in temperature of up to 7 °C observed between the wellbore and surface.

Analysis of both the borehole heat exchanger and standing column well gave positive results with both being able to provide a heat load in excess of the demand for the initial core scheme/phase 1 of the district heat network (<1.6 MW) in Crewe town centre. Models of both the borehole heat exchanger and standing column wells were able to produce heat loads of nearly 3.7 MW at high flow rates in the first few hours, prior to subsequent rapid cooling of the fluid and reduced heat loads. Continual operation of the borehole heat exchanger over a 30 day period indicated a heat load of 200 – 300 kW should be achievable. Although this is a small contribution to the energy supply, results from the standing column well scenario were far more encouraging, offering a heat load at the end of the 30 day simulation period of between 684 kW to 1.725 MW. It is also worth noting that increasing the bleed flow only had a significant impact on the system and increasing performance in comparison to BHEs.

The final part of this study investigated the economics and effectiveness of heat exchangers. As expected, counter-current flow heat exchangers were far more effective than co-current flow. Low flow rates (< 10 l/s) with temperatures in excess of 70 °C can meet the energy demand for the core scheme/phase 1 of the district heat network (<1.6 MW), however, production rates exceeding this are needed to meet the highest forecasted energy demand. The economic analysis indicated switching from fossil fuels to geothermal energy would offer savings of between 48.76 million and £77.2 million for geothermal fluid temperatures of 67 °C and 86 °C.

9.2 Recommendations for future work

- **Ground truthing analysis.** Deep geothermal energy development in the Cheshire Basin may strongly depend on the acquisition of data from depth (i.e., from an exploration well). This would allow the true conditions to be modelled, allowing future well performance to be forecasted more accurately.

- **Financial modelling of a doublet scheme and various single well schemes modelled in this thesis.** Analysis of the net profit from a geothermal fed district heat network showed significant savings could be made, but there could be additional costs from waste water disposal which could make a doublet scheme have a higher net profit. As such, a detailed financial model of both operating costs and capital expenditure could provide a better informed comparison. By coupling the financial modelling with borehole operational performance (using the numerical model developed in this thesis) the recovery of energy can be used to determine the most profitable scheme.

- **Consider a hydro-thermal model that also incorporates solute transport for the Cheshire Basin and analyse varying salt concentrations in the system.** It has been suggested that higher concentrations of salt (and thus higher density) could be constrained to the centre of the Cheshire Basin (Plant et al., 1999). This could lead to density driven groundwater flow being prominent at depth, whilst also having an effect on heat transfer within the system. Any new models would, therefore, have to incorporate the temperature-dependent buoyancy effects (such as in chapter 6) and solute transport caused by high salt concentrations.

- **Investigate a scenario where the Manchester Marl Formation is not present and all Permo-Triassic sandstones are in hydraulic continuity.** In literature, the extent of the Manchester Marl Formation is poorly constrained with old estimations suggesting it thins to the south of Crewe (Downing and Gray, 1986). A modelling scenario which simulates a gross thickness of aquifers, and their respective heterogeneities, could alter the results and is likely to reduce the drawdown in the well.

- **Test the modelling approach for borehole heat exchangers and standing column wells in other basins across the UK.** Further analysis should be undertaken to test the performance of these novel methods of energy extraction. Different geological scenarios, such as an active groundwater flow, could increase performance (as it has been shown to in shallow modelling studies).

- **Add further detail into the numerical model.** The numerical models could be improved by incorporating the true geometry of the subsurface and by improving the physical description of the governing equations. The former could be achieved by altering the modelling approach by using the finite-volume or finite-element techniques, whilst the latter could be achieved by modelling the deformation of the rock under fluid withdrawal (i.e., porosity changes) and modelling chemical and solute transport.

LIST OF REFERENCES

Ackerer, P., Younes, A., Oswald, S.E., Kinzelbach, W., 2000. On modelling of density driven flow. *IAHS PUBLICATION*, 377-384.

Abdoh, A., Cowan, D., Pilkington, M., 1990. 3D gravity Inversion of the Cheshire Basin. Geophys. Prospect. 38, 999–1011. doi:10.1111/j.1365-2478.1990.tb01887.x

Adams, J.J., Bachu, S., 2002. Equations of state for basin geofluids: algorithm review and intercomparison for brines. Geofluids, 2: 257–271. doi:10.1046/j.1468-8123.2002.00041.x

Adams, C.A., Gluyas, J.G. and Mathias, S.A., 2010. Application of hydrogeological parameters for evaluating the thermal resource potential of deep groundwater systems, BHS Third International Conference : Role of hydrology in managing consequences of a changing global environment. Newcastle upon Tyne, 19-23 July 2010.

Afshari, S., Mandle, R., Liu, Q., Li, S.G., 2003. A Method for Predicting Drawdown at the Radius of a Pumping Well for Large Complex Systems.

Ağra, Ö., 2011. Sizing and selection of heat exchanger at defined saving–investment ratio. Applied Thermal Engineering, 31(5), 727-734. https://doi.org/10.1016/j.applthermaleng.2010.10.013

Ağra, Ö., Erdem, H.H., Demir, H., Atayılmaz, Ş.Ö. and Teke, İ., 2015. Heat capacity ratio and the best type of heat exchanger for geothermal water providing maximum heat transfer. Energy, 90, 1563-1568. https://doi.org/10.1016/j.energy.2015.06.107

AGI, 2020. How much water does the typical hydraulically fractured well require? Last accessed on August 2020. https://www.americangeosciences.org/critical-issues/faq/how-much-water-does-typical-hydraulically-fractured-well-require

Akbar, A.M., Arnold, M.D., Harvey, A.H., 1974. Numerical simulation of individual wells in a field simulation model. *Society of Petroleum Engineers Journal*, 14(04), 315-320. doi: 10.2118/4073-PA

Al-Khoury R., 2011. Computational modeling of shallow geothermal systems. CRC press.

Al-Khoury, R., Bonnier, P.G., Brinkgreve, B.J., 2005. Efficient finite element for- mulation for geothermal heating systems. Part I: steady state. *International Journal for Numerical Methods in Engineering* 63, 988–1013. doi:10.1002/nme.1313

Al-Khoury, R., Bonnier, P.G., 2006. Efficient finite element formulation for geothermal heating systems. Part II: transient. *International Journal for Numerical Methods in Engineering* 67, 725–745. doi:10.1002/nme.1662

Al-Khoury. R., Kolbel, T., Schramedei, R., 2010. Efficient numerical modeling of borehole heat exchangers. *Computer and Geosciences* 36 (10), 1301–1315. doi:10.1016/j.cageo.2009.12.010

Aliyu, M.D., Chen, H.P., 2017. Sensitivity analysis of deep geothermal reservoir: Effect of reservoir parameters on production temperature. Energy, 129, 101-113. doi:10.1016/j.energy.2017.04.091

Allan, M.L., 1997. Thermal conductivity of cementitious grouts for geothermal heat pumps. BNL, 65, 129. doi:10.2172/573177

Allen, D.J., Barker, J.A., Downing, R.A., 1983. The Production Test and Resource Assessment of the Southhampton (Western Esplanade) Geothermal Well. Institute of Geological Sciences.

Allen, D.J., Gale, I.N., Price, M., 1985. Evaluation of the permo-triassic sandstones of the UK as geothermal aquifers. Hydrogeology in the Service of Man. Memoirs of the 18th Congress of the International Association of Hydrogeologists, Cambridge. 12-22.

Allen, D.J., Brewerton, L.J., Coleby, L.M., Gibbs, B.R., Lewis, M.A., MacDonald, A.M., Wagstaff, S.J., Williams, A.T., 1997. The physical properties of major aquifers in England and Wales.

Ambrose, K., Hough, E., Smith, N.J.P., Warrington, G., 2014. Lithostratigraphy of the Sherwood Sandstone Group of England, Wales and south-west Scotland. Br. Geol. Surv. Res. Rep.

Anderson, M.P., Woessner, W.W., 1992. Applied groundwater modeling: simulation of flow and advective transport. Academic press. New York. ISBN-13: 978-0-12-059485-6

Anderson, M.P., 2005. Heat as a ground water tracer. *Groundwater*, *43*(6), 951-968.

Anderson, M.P., Woessner, W.W. Hunt, R.J., 2015. *Applied groundwater modeling: simulation of flow and advective transport*. Academic press.

Andrews, I.J., 2013. The Carboniferous Bowland Shale gas study: geology and resource estimation. British Geological Survey for Department of Energy and Climate Change, London, UK.

Annamalai, K., Puri, I. K., 2006. *Combustion science and engineering*. CRC press.

Arthurton, R.S., Wadge, A.J., 1981. Geology of the country around Penrith (Vol. 24). Institute of Geological Sciences, Natural Environment Research Council.

Arup, 2013. Cheshire East Energy Planning: Review of Geothermal Potential in Cheshire East. Cheshire East Council. 1-19.

Arup, 2018a. Website last accessed August 2020. https://www.arup.com/news-and-events/jubilee-pool-geothermal-drilling-begins

Arup, 2018b. Technical feasibility report – Crewe Town Centre Heat Network.

Atkins, 2013. Deep Geothermal Review Study. Final Report for the Department of Energy & Climate Change (DECC).

Axelsson, G., Stefánsson, V., Björnsson, G., Liu, J., 2005, April. Sustainable management of geothermal resources and utilization for 100–300 years. In Proceedings World Geothermal Congress (Vol. 8).

Bailey, M.T., Gandy, C.J., Jarvis, A.P., 2016. Reducing life-cycle costs of passive mine water treatment by recovery of metals from treatment wastes. In Mining Meets Water–Conflicts and Solutions. Proceedings of the International Mine Water Association Symposium. 1255-1262.

Barker, J.A., 1981. A multilayered aquifer model for the Marchwood pumping test. Report of the Institute of Geological Sciences. Report number: WD/ST/81/14.

Barker, J.A., Downing, R.A., Gray, D.A., Findlay, J., Kellaway, G.A., Parker, R.H., Rollin, K.E., 2000. Hydrogeothermal studies in the United Kingdom. *Quarterly Journal of Engineering Geology and Hydrogeology*, 33(1), 41-58. doi.:10.1144/qjegh.33.1.41

Barker, R.D., Tellam, J.H., 2006. Fluid Flow and Solute Movement in Sandstones: The Onshore UK Permo-Triassic Red Bed Sequence. Geological Society of London.

Barrash, W., Dougherty, M.E., 1997. Modeling axially symmetric and nonsymmetric flow to a well with MODFLOW, and application to Goddard2 well test, Boise, Idaho. *Groundwater*, 35(4), pp.602-611.

Batzle, M., Wang, Z., 1992. Seismic properties of pore fluids. Geophysics 57 (11), 1396–1408. doi: 10.1190/1.1443207

BBC, 2019. Website last accessed on June 2019. https://www.bbc.co.uk/news/uk-england-cornwall-48064582

Bear, J., 1972. Dynamics of Fluids in Porous Media, 764, Elsevier, N.Y.

Bear, J., Cheng, A.H.D., 2010. Modeling groundwater flow and contaminant transport (Vol. 23). Springer Science & Business Media.

Beaudry, G., Pasquier, P., Marcotte, D., 2018. Hydrogeothermal characterization and modelling of a standing column well experimental installation. In conference proceedings: International Ground Source Heat Pump Association. doi:10.22488/okstate.18.000009

BGS, 2011. Temperature and thermal properties. A report by the British Geological Survey. BGS Report No: GR_999999/1

BGS, 2019. Website last accessed July 2019. http://www.bgs.ac.uk/lexicon/lexicon.cfm?pub=PNG

Bijeljic, B., Muggeridge, A.H., Blunt, M.J., 2004. Pore-scale modeling of longitudinal dispersion. *Water Resources Research*, 40(11). doi:10.1029/2004WR003567.

Björnsson, O.B., 1999. Geothermal district heating. In International Workshop on Direct Use of Geothermal Energy, Chamber of Commerce and Industry of Slovenia, Ljubliana, Slovenia. https://geothermalcommunities.eu/assets/elearning/5.16.1999-Geothermal-District-Heating.pdf

Blöcher, M.G., Zimmermann, G., Moeck, I., Brandt, W., Hassanzadegan, A., Magri, F., 2010. 3D numerical modeling of hydrothermal processes during the lifetime of a deep geothermal reservoir. *Geofluids*, 10(3), 406-421. doi:10.1111/j.1468-8123.2010.00284.x

Bloomfield, J.P., Moreau, M.F., Newell, A.J., 2006. Characterization of permeability distributions in six lithofacies from the Helsby and Wilmslow sandstone formations of the Cheshire Basin, UK. Geol. Soc. Lond. Spec. Publ. 263, 83–101. doi:10.1144/GSL.SP.2006.263.01.04

BOE, 2019. Website last accessed on October 2019. https://www.bankofengland.co.uk/

Bofang, Z., 2019. The Finite Element Method: Fundamentals and Applications in Civil, Hydraulic, Mechanical and Aeronautical Engineering. doi:10.1002/9781119107323

Boonstra, J., 1992. Aquifer tests with partially penetrating wells: theory and practice. *J. Hydrol.*, 137: 165-179.doi:10.1016/0022-1694(92)90054-Y

Boussinesq, J., 1903. Théorie Analytique de la Chaleur, vol. 2. Gauthier-Villars, Paris

Bradley, J.C., 2010. Counterflow, crossflow and cocurrent flow heat transfer in heat exchangers: analytical solution based on transfer units. Heat and mass transfer, 46(4), 381-394. doi:10.1007/s00231-010-0579-5

Brenchley, P.J., 2006. The Geology of England and Wales. Geological Society of London.

Brons, F., Marting, V.E., 1961. The effect of restricted fluid entry on well productivity. *Journal of Petroleum Technology*, *13*(02),172-174.

Burgess, W.G., Burley, A.J., Downing, R.A., Edmunds, W.M., Price, M., 1981. The Marchwood geothermal borehole-a preliminary assessment of the resource. Report of the Institute of Geological Sciences.

Burley, A.J., Smith, I.F., Lee, M.K., Burgess, W.G., Edmunds, W.M., Arthur, M.J., Bennett, J.R.P., Carruthers, R.M., Downing, R.A., Houghton, M.T., 1980. Preliminary Assessment of the Geothermal Potential of the United Kingdom, in: Strub, A.S., Ungemach, P. (Eds.), Advances in European Geothermal Research. Springer Netherlands, 99–108.

Busby, J.P., 2010. Geothermal prospects in the United Kingdom. Presented at the World Geothermal Congress 2010, Bali, Indonesia.

Busby, J., Kingdon, A., Williams, J., 2011a. The measured shallow temperature field in Britain. *Quarterly Journal of Engineering Geology and Hydrogeology*, *44*(3), 373-387. doi:10.1144/1470-9236/10-049

Busby, J., 2011b. UK data for geothermal resource assessments. Presentation. Website last accessed

on June 2019. http://egec.info/wpcontent/uploads/2011/09/UK-deep-geothermal-

resources_JBusby.pdf

Busby, J., 2014. Geothermal energy in sedimentary basins in the UK. Hydrogeology journal,

22(1),129-141. doi:10.1007/s10040-013-1054-4

Butler, J., 1990. A review of the tectonic history of the Shropshire area. Geol. Soc. 9, 20–34.

Cacace, M., Kaiser, B.O., Lewerenz, B., Scheck-Wenderoth, M., 2010. Geothermal energy in

sedimentary basins: what we can learn from regional numerical models. *Chemie der Erde-*

Geochemistry, 70, 33-46. doi:10.1016/j.chemer.2010.05.017

Campbell, S.A., Mielke, P., Götz, A.E., 2016a. Geothermal energy from the Main Karoo Basin? New

insights from borehole KWV-1 (Eastern Cape, South Africa). *Geothermal Energy*, 4(1), 9.

doi:10.1186/s40517-016-0051-y

Campbell, S.A., Lenhardt, N., Dippenaar, M.A., Götz, A.E., 2016b. Geothermal energy from the Main

Karoo Basin (South Africa): an outcrop analogue study of Permian sandstone reservoir

formations. *Energy Procedia*, 97, 186-193. doi:10.1016/j.egypro.2016.10.050

Carslaw, H.S., Jaeger, J.C., 1959. Conduction of Heat in Solids, 2nd edition. Oxford: Clarendon

Press.

Cattaneo, L., Comunian, A., de Filippis, G., Giudici, M., Vassena, C., 2015. Modeling groundwater flow

in heterogeneous porous media with YAGMod. *Computation*, 4(1), 2.

doi:10.3390/computation4010002

Causon, D.M., Mingham, C.G., 2010. *Introductory finite difference methods for PDEs*. Bookboon.

Chadwick, R.A., 1997, Fault analysis of the Cheshire Basin, NW England: Geological Society, London, Special Publications, v. 124, no. 1, 297-313

Chapra, S.C., Canale, R.P., 2010. *Numerical methods for engineers*. Boston: McGraw-Hill Higher Education.

Charléty, J., Cuenot, N., Dorbath, L., Dorbath, C., Haessler, H., Frogneux, M., 2007. Large earthquakes during hydraulic stimulations at the geothermal site of Soultz-sous-Forêts. *International Journal of Rock Mechanics and Mining Sciences*, *44*(8), 1091-1105.

Chen, Z., Zhang, Y., 2009. Well flow models for various numerical methods. *International Journal of Numerical Analysis & Modeling*, 6(3), 375-388.

Cho, J.H., Nam, Y., Kim, H.C., 2016. Performance and feasibility study of a Standing Column Well (SCW) system using a deep geothermal well. Energies, 9(2), 108. doi:10.3390/en9020108

Chow, P., Cross, M., Pericleous, K., 1996. A natural extension of the conventional finite volume method into polygonal unstructured meshes for CFD application. *Applied Mathematical Modelling*, *20*(2), 170-183.

Chuanshan, D., Jun, L., 1999. Optimum design and running of PHEs in geothermal district heating. Heat Transfer Eng, 20(4) 52–61. https://doi.org/10.1080/014576399271295

Clauser, C., 2006. Geothermal energy. *Landolt-Börnstein, group VIII: advanced materials and technologies*, *3*, 493-604.

Cocks, L.R.M., Woodcock, N.H., Rickards, R.B., Temple, J.T., Lane, P.D., 1984. The Llandovery Series of the type area. Bulletin of the British Museum, Natural History, Vol. 38, 131–182

Cocks, L.R.M., 1989. The Geology of South Shropshire. Proceedings of the Geologists' Association, 100(4), 505-519.

Collins, M.A., Law, R., 2017. The development and deployment of deep geothermal single well (DGSW) technology in the United Kingdom. *European Geologist Journal*, *43*, 63-68.

Colter, V. S, Ebburn, J, 1978. The petrography and reservoir properties of some Triassic sandstones from the Northern Irish Sea Basin. Geol Soc Vol. 135, 5762.

Cope, J.C.W., Ingham, J.K., Rawson, P.F., 1992. Atlas of palaeogeography and lithofacies. Memoir of the Geological Society of London, No. 13

Courant, R., Friedrichs, K., Lewy, H., 1928. Über die partiellen Differenzengleichungen der mathematischen Physik. *Mathematische annalen*, 100(1), 32-74.

Cox, B.M., Sumbler, M.G., Ivimey-Cook, H.C., 1999. A formational framework for the Lower Jurassic of England and Wales (onshore area). British Geological Survey Research Report, RR/99/0

Crooijmans, R. A., Willems, C. J. L., Nick, H., Bruhn, D. F., 2016. The influence of facies heterogeneity on the doublet performance in low-enthalpy geothermal sedimentary reservoirs. *Geothermics*, 64, 209-219. doi:10.1016/j.geothermics.2016.06.004

Dagdas, A., 2007. Heat exchanger optimization for geothermal district heating systems: A fuel saving approach. Renewable Energy, 32(6), 1020-1032. https://doi.org/10.1016/j.renene.2006.03.008

De Marsily, G., 1986. *Quantitative hydrogeology*. Paris School of Mines, Fontainebleau.

Dehghan, M., 2004. Numerical solution of the three-dimensional advection–diffusion equation. *Applied Mathematics and Computation*, 150(1), 5-19. doi:10.1016/S0096-3003(03)00193-0

Deichmann, N., D. Giardini (2009), Earthquakes induced by the stimulation of an enhanced geothermal system below Basel (Switzerland), Seismol. Res. Lett., 80(5), 784–798, doi:10.1785/gssrl.80.5.784

Dewey, J., Mange, M., 1999. Petrography of Ordovician and Silurian sediments in the western Irish Caledonides: tracers of a short-lived Ordovician continent-arc collision orogeny and the evolution of the Laurentian Appalachian-Caledonian margin. Geol. Soc. Lond. Spec. Publ. 164, 55–107. doi:10.1144/GSL.SP.1999.164.01.05

Dickinson, E.J., Ekström, H., Fontes, E., 2014. COMSOL Multiphysics®: Finite element software for electrochemical analysis. A mini-review. Electrochemistry communications, 40, 71-74.

Diehl, T., Kraft, T., Kissling, E., Wiemer, S., 2017. The induced earthquake sequence related to the St. Gallen deep geothermal project (Switzerland): Fault reactivation and fluid interactions imaged by microseismicity. *Journal of Geophysical Research: Solid Earth*, *122*(9), 7272-7290.

Diersch, H.J.G., 2013. FEFLOW: finite element modeling of flow, mass and heat transport in porous and fractured media. Springer Science & Business Media

Diersch, H. J.G., Bauer, D., Heidemann, W., Rühaak, W., Schätzl, P., 2011a. Finite element modeling of borehole heat exchanger systems. Part 1. Fundamentals. Computers & Geosciences, 37(8), 1122–1135. doi:10.1016/j.cageo.2010.08.003

Diersch, H. J.G., Bauer, D., Heidemann, W., Rühaak, W., Schätzl, P., 2011b. Finite element modeling of borehole heat exchanger systems. Part 2. Numerical simulation. Computers & Geosciences, 37(8), 1136–1147. doi:10.1016/j.cageo.2010.08.002

Dijkshoorn, L., Speer, S., Pechnig, R., 2013. Measurements and design calculations for a deep coaxial borehole heat exchanger in Aachen, Germany. International Journal of Geophysics, 2013.

Dineley, D.L., 1960. Shropshire Geology: an outline of the tectonic history. Field Studies Council.

DiPippo, R., 2012. Geothermal Power Plants: Principles, Applications, Case Studies and Environmental Impact, 3rd ed. Ph.D. Chancellor Professor Emeritus University of Massachusetts Dartmouth North Dartmouth, Massachusetts.

Dogru, A. H., 2010. Equivalent Wellblock Radius for Partially Perforated Vertical Wells—Part1: Anisotropic Reservoirs with Uniform Grids. *SPE Journal*, 15(04), 1-28. doi: 10.2118/137051-PA

Dowd, A.M., Boughen, N., Ashworth, P., Carr-Cornish, S., 2011. Geothermal technology in Australia: Investigating social acceptance. *Energy policy*, *39*(10), 6301-6307.

Downing, R. A., Allen, D. J., Barker, J. A., Burgess, W. G., Gray, D. A., Price, M., Smith, I. F., 1984. Geothermal exploration at Southampton in the UK: a case study of a low enthalpy resource. *Energy exploration & exploitation*, 2(4), 327-342.

Downing, R.A., Gray, D.A., 1986a. Geothermal resources of the United Kingdom. J. Geol. Soc. 143, 499–507. doi:10.1144/gsjgs.143.3.0499

Downing, R.A., Gray, D.A., 1986b. Geothermal Energy The potential in the United Kingdom. BGS, National Environment Research Council.

Dunham, K.C., 1974. Geothermal energy for the United Kingdom geological aspects. Report of the Institute of Geological Sciences. (Unpublished).

El-Kadi, A. I., Ling, G., 1993. The Courant and Peclet number criteria for the numerical solution of the Richards equation. *Water Resources Research*, 29(10), 3485-3494. doi:10.1029/93WR00929

Elders, W. A., Friðleifsson, G. Ó., Albertsson, A., 2014. Drilling into magma and the implications of the Iceland Deep Drilling Project (IDDP) for high-temperature geothermal systems worldwide. *Geothermics*, 49, 111-118. doi:10.1016/j.geothermics.2013.05.001

Energie-Cités, 2001. Geothermal Enegry District heating scheme Southampton (United Kingdom). Case study prepared with the City of Southampton. https://geothermalcommunities.eu/assets/elearning/5.13.SOUTH_EN.PDF

Environmental Agency, 2013. Weaver and Dane abstraction licensing strategy. Report. https://assets.publishing.service.gov.uk/government/uploads/system/uploads/attachment_data/file/319959/lit_7884_52dcff.pdf

Eppelbaum, L., Kutasov, I., Pilchin, A., 2014. Thermal properties of rocks and density of fluids. *Applied geothermics*, 99-149. Springer, Berlin, Heidelberg. doi:10.1007/978-3-642-34023-9_2

ETB, 2017. The Engineering Toolbox, website accessed on 06/03/2017 [WWW Document]. URL. https://www.engineeringtoolbox.com/

Evans, W.B., 1970. The Triassic salt deposits of north-western England. Q. J. Geol. Soc. 126, 103–123. doi:10.1144/gsjgs.126.1.0103

Evans, D.J., Rees, J.G., Holloway, S., 1993. The Permian to Jurassic stratigraphy and structural evolution of the central Cheshire Basin. J. Geol. Soc. 150, 857–870. doi:10.1144/gsjgs.150.5.0857

Fang, L., Diao, N., Shao, Z., Zhu, K., Fang, Z., 2018. A computationally efficient numerical model for heat transfer simulation of deep borehole heat exchangers. Energy and Buildings, 167, 79-88.

Feili, H.R., Akar, N., Lotfizadeh, H., Bairampour, M., Nasiri, S., 2013. Risk analysis of geothermal power plants using Failure Modes and Effects Analysis (FMEA) technique. Energy Convers. Manag., The III. International Conference on Nuclear and Renewable Energy Resources NURER2012 72, 69–76. doi:10.1016/j.enconman.2012.10.027

Fitches, W.R., Campbell, S.D.G., 1987. Tectonic evolution of the Bala Lineament in the Welsh Basin. Geol. J. 22, 131–153. doi:10.1002/gj.3350220513

Fletcher, C.A.J., 1988.Computational Techniques for Fluid Dynamics, vol. 1, 387. Springer, New York.

doi:10.1007/978-3-642-58229-5

Ford, W., 2014. *Numerical linear algebra with applications: Using MATLAB*. Academic Press.

Fraser, S., 2013. Report proposals for improving regulatory framework for geothermal electricity –

Appendix 1. GEOELEC. http://www.geoelec.eu/wp-content/uploads/2011/09/D4.1-A.1-Overview-of-

National-Rules-of-Licencing.pdf

Geiser, J., 2008. Iterative operator-splitting methods with higher-order time integration methods and

applications for parabolic partial differential equations. Journal of Computational and Applied

Mathematics, 217(1), 227-242. doi.10.1016/j.cam.2007.06.028

Gibson, W., 1901. Upper Coal Measures of the Midlands. 57, 251 – 266.

Glennie, K.W., 1995. Permian and Triassic rifting in northwest Europe. Geol. Soc. Lond. Spec. Publ. 91,

1–5. doi:10.1144/GSL.SP.1995.091.01.01

Gluyas, J.G., Adams, C.A., Busby, J.P., Craig, J., Hirst, C., Manning, D.A.C., McCay, A., Narayan, N.S.,

Robinson, H.L., Watson, S.M. and Westaway, R., 2018. Keeping warm: A review of deep geothermal

potential of the UK. *Proceedings of the Institution of Mechanical Engineers, Part A: Journal of Power

and Energy*, *232*(1), pp.115-126.

Google Maps., 2018. Map of the Crewe area. Retrieved from

[https://www.google.com/maps/@53.097487,-2.4541898,14z] on the 1/11/2018.

GOV, 2019. Website accessed on 2/7/2019: https://www.gov.uk/guidance/deep-geothermal-energy-

regulation

Gray, J., Harvey, T., 2006. Potential exploration opportunities E. Irish sea.

Griffiths, D.F., 1986. Finite Element Methods for Time Dependent Problems. In *Astrophysical Radiation Hydrodynamics,* 327-357. Springer, Dordrecht.

Griffiths, K.J., Shand, P., Ingram J., 2003. Baseline Report Series: 8. The Permo-Triassic Sandstones of Manchester and East Cheshire British Geological Survey Commissioned Report No. CR/03/265N.

Gringarten, A., 1978. Reservoir lifetime and heat recovery factor in geothermal aquifers used for urban heating. *Pure and applied geophysics*, 117(1-2): 297-308

Guo, W., Langevin, C.D., 2002. *User's guide to SEAWAT; a computer program for simulation of three-dimensional variable-density ground-water flow* (No. 06-A7).

Halford, K. J., Hansen, R. T., 2002. User Guide for the Drawdown-Limited, Multi-Node Well (MNW) Package for the U.S. Geological Survey's Modular Three-Dimensional Finite Difference Ground-Water Flow Model, Versions MODFLOW-96 and MODFLOW-2000 (Vol. 2, No. 293). Us Department of the Interior, US Geological Survey.

Hampson, G.J., Elliott, T., Davies, S.J., 1997. The application of sequence stratigraphy to Upper Carboniferous fluvio-deltaic strata of the onshore UK and Ireland: implications for the southern North Sea. Journal of the Geological Society, 154(4), 719-733.

Hantush, M. S., 1961. Drawdown around a partially-penetrating well. *J. Hydraul. Div., Proc. ASCE*, 87(HY4): 83-98.

Hantush, M. S., 1962. Aquifer tests on partially penetrating wells, American Society of Civil Engineers. Trans. Vol 127. Part 1, 284-308.

Haraldsson, I.G., 2014. Government incentives and international support for geothermal project development. United Nations University Geothermal Training Programme Orkustofnun, Grensasvegi

9, 108 Reykjavik Iceland https://geothermalcommunities.eu/assets/elearning/10.8.UNU-GTP-SC-18-37.pdf

Häring, M.O., Schanz, U., Ladner, F., Dyer, B.C., 2008. Characterisation of the Basel 1 enhanced geothermal system, Geothermics, 37(5), 469–495, doi:10.1016/j.geothermics.2008.06.002.

Harvey, T., Gray, J., 2013. The Hydrocarbon Prospectivity of Britains onshore basins. Promote UK 2014. DECC report. https://www.ogauthority.co.uk/media/1695/uk_onshore_2013.pdf

Haslam, S. R., 2013. Informing the practice of ground heat exchanger design through numerical simulations (Master's thesis, University of Waterloo).

Hindmarsh, A.C., Gresho, P.M., Griffiths, D.F., 1984. The stability of explicit Euler time-integration for certain finite difference approximations of the multi-dimensional advection–diffusion equation. *International journal for numerical methods in fluids*, 4(9), 853-897. doi:10.1002/fld.1650040905

Hirst, C., M, Gluyas, J., G, Adams, C, A, Mathias, S., A, Bains, S., Styles, P., 2015. UK Low Enthalpy Geothermal Resources: the Cheshire Basin. Proc. World Geotherm. Congr. 2015.

Hirt, C. W., 1968. Heuristic stability theory for finite-difference equations. *Journal of Computational Physics*, 2(4), 339-355. doi:10.1016/0021-9991(68)90041-7

Hirst, C., M, 2017. The Geothermal Potential of Low Enthalpy Deep Sedimentary Basins in the UK, Durham theses, Durham University.

Hobbs, P., Hallam, J.R., Forster, A., Entwisle, D., Jones, L.D., Cripps, A.C., Northmore, K.J., Self, S., Meakin, J.L., 2002. Engineering geology of British rocks and soils: Mudstones of the Mercia Mudstone Group. British Geological Survey. Howard, A S, Warrington, G, Ambrose K, Rees, J G, 2008. A formational framework for the Mercia Mudstone Group (Triassic) of England and Wales. Br. Geol. Surv. Res. Rep.

Holmberg, H., Acuña, J., Næss, E., Sønju, O. K., 2016. Thermal evaluation of coaxial deep borehole heat exchangers. Renewable energy, 97, pp.65-76.

Hopmans, J.W., Šimunek, J., Bristow, K.L., 2002. Indirect estimation of soil thermal properties and water flux using heat pulse probe measurements: Geometry and dispersion effects. *Water Resources Research*, *38*(1), 7-1.

Howells, M. F., 2007. British regional geology: Wales. Keyworth, Nottingham: British Geological Survey.

Huddlestone - Holmes, C., Hayward, J., 2011. The potential of geothermal energy. CSIRO.

Hughes, R.A., 2003. Permian and Triassic rocks of the Appleby district (part of Sheet 30, England and Wales). Br. Geol. Surv. Res. Rep. RR0201 21pp.

Huisman, L., 1972. Ground water recovery. Winchester Press, New York, 131.

Hull, E., 1864. The geology of the country around Oldham, including Manchester and its suburbs. Memoir of the Geological Survey of Great Britain, Sheet 88SW.

Hutton, D.H.W., Murphy, F.C., 1987. The Silurian of the Southern Uplands and Ireland as a successor basin to the end-Ordovician closure of Iapetus. J. Geol. Soc. 144, 765–772. doi:10.1144/gsjgs.144.5.0765

Huyakorn, P.S., Pinder, G.F., 1983. Computational Methods in Subsurface Flow, Academic Press, 473 .

Jackson, T., 2012. Geothermal potential in Great Britain and Northern Ireland. SKM, London

Jones, O.T., 1925. The Geology of the Llandovery District: Part 1.The Southern Area. Quarterly Journal of The Geological Society. 81. 10.1144/GSL.JGS.1925.081.01-04.15.

Jones, O. T., 1949. The geology of the Llandovery district. Part II: the northern area. Quarterly Journal of the Geological Society of London 105, 43–64

Jubilee pool, 2019. Website last accessed on June 2019. https://www.jubileepool.co.uk/geothermal-share-offer

Kajishima, T., Taira, K., 2017. Finite-Difference Discretization of the Advection-Diffusion Equation. In: Computational Fluid Dynamics. Springer, Cham. doi:10.1007/978-3-319-45304-0_2

Kappelmeyer, O., Hänel, R., 1974. Geothermics with special reference to application. 238. Gebtider Bomtrlger, Berlin-Stuttgart.

Kinniburgh, D.G., Newell, A.J., Davies, J., Smedley, P.L., Milodowski, A.E., Ingram, J.A., Merrin, P.D., 2006. The arsenic concentration in groundwater from the Abbey Arms Wood observation borehole, Delamere, Cheshire, UK.

Knight Piesold and partners, 1998. Wheal Jane Minewater Project: Consultancy Studies 1996–1999. Appraisal and Selection of Long Term Treatment Option. Knight Piesold Ltd, Ashford, Kent

Knox, R.W., Burgess, W.G., Wilson, K.S., Bath, A.H., 1984. Diagenetic influences on reservoir properties of the Sherwood Sandstone (Triassic) in the Marchwood geothermal borehole, Southampton, England. Clay Miner. 19, 441–456.

Kolditz, O., Ratke, R., Diersch, H.J., Zielke, W., 1998. Coupled groundwater flow and transport: 1. Verification of variable density flow and transport models. Adv Water Resour. 21:27–46.

Konikow, L.F., Hornberger, G.Z., Halford, K.J., Hanson, R.T., 2009. Revised multi-node well (MNW2) package for MODFLOW ground-water flow model: U.S. Geological Survey Techniques and Methods 6–A30, 67.

Kozeny, J., 1933. Theorie und berechnung der brunnen: Wasserkraft und Wasserwirtschaft, v. 28.

Küchler, A., Kiessig, G., Kunze, C., 2005. Passive biological treatment systems of mine waters at WISMUT sites. In: Proceedings, 9th International Congress on Mine Water & the Environment, Oviedo, Spain, 361–368.

Kunze, C., Küchler, A., 2003. Passive biological treatment systems of mine waters at WISMUT sites. In: Proceedings, 8th International Congress on Mine Water & the Environment, Johannesburg, South Africa, 187–199.

Law, R., 2010. *Geothermal systems in the Chalk of the south east of England: methods of predicting thermal transport in a fractured aquifer.* PhD thesis. University of Birmingham.

Law, R., 2014. Deep Geothermal Heat Production – Single Well Trial. In: Renewable Heating & Renewable Cooling; Ground Source Heat Pump Association 5th Technical Seminar, De Montfort University, Leicester, 16 November 2014, 8. Retrieved from http://www.gshp.org.uk/DeMontfort/ GeothermalEngineeringLtd.pdf [last accessed 20 February 2019].

Law, R., Bridgland, D., Nicholson, D., Chendorain, M., 2015. Heat extraction from deep single wells. In: Proceedings World Geothermal Congress 2015, 19–25 April 2015, Melbourne, Australia. https://pangea.stanford.edu/ERE/db/ WGC/papers/WGC/2015/28002.pdf

Lapidus, L., Amundson, N. R., 1952. Mathematics of adsorption in beds. VI. The effect of longitudinal diffusion in ion exchange and chromatographic columns. *The Journal of Physical Chemistry*, 56(8), 984-988. doi:10.1021/j150500a014

LDA design, 2011. Cheshire East Climate Change & Sustainable Energy Planning Research: Technical Report.

Le Brun, M., Hamm, V., Lopez, S., Ungemach, P., Antics, M., Ausseur, J. Y., Cordier, E., Giuglaris, E., Goblet, P., Lalos, P., 2011. Hydraulic and thermal impact modelling at the scale of the geothermal heating doublet in the Paris Basin, France. *In 36th Stanford Geothermal Workshop*. 403-416.

Leonard, B.P., 1980. Note on the von Neumann stability of the explicit FTCS convective diffusion equation. Applied Mathematical Modelling, 4(5), 401-402.

LeVeque, R.J., 2007. Finite difference methods for ordinary and partial differential equations: steady-state and time-dependent problems (Vol. 98). Siam. doi:10.1137/1.9780898717839

Leveridge, B., Hartley, A, J., 2006. The Variscan Orogeny: the development and deformation of Devonian/Carboniferous basins in SW England and South Wales, in: The Geology of England and Wales/edited by PJ Brenchley and PF Rawson. London: Geological Society of London, 225–255.

Lipnikov, K., Shashkov, M., Svyatskiy, D., Vassilevski, Y., 2007. Monotone finite volume schemes for diffusion equations on unstructured triangular and shape-regular polygonal meshes. *Journal of Computational Physics*, *227*(1), 492-512.

Liu, J., Wang, F., Cai, W., Wang, Z., Wei, Q., Deng, J., 2019. Numerical study on the effects of design parameters on the heat transfer performance of coaxial deep borehole heat exchanger. Int J Energy Res.;1–16. https://doi.org/10.1002/er.435716LIUET AL.

Lovelock, P.E.R., 1977. Aquifer properties of PermoTriassic sandstones in the United Kingdom. Geol Surv. 56.

Lukawski, M.Z., Anderson, B.J., Augustine, C., Capuano Jr, L.E., Beckers, K.F., Livesay, B., Tester, J.W., 2014. Cost analysis of oil, gas, and geothermal well drilling. Journal of Petroleum Science and Engineering, 118, 1-14. https://doi.org/10.1016/j.petrol.2014.03.012

Lund, J.W., Freeston, D.H., Boyd, T.L., 2005. World-Wide Direct Uses of Geothermal Energy 2005. Proc. World Geotherm. Congr. 2005 Antalya Turk. 24–29.

Lund, J.W., Freeston, D.H., Boyd, T.L., 2011. Direct utilization of geothermal energy 2010 worldwide review. Geothermics, 40(3),159-180.

Lund, J.W. and Boyd, T.L., 2016. Direct utilization of geothermal energy 2015 worldwide review. *Geothermics*, *60*, pp.66-93.

Macchi, L.C., 1981. Sedimentology of the Penrith Sandstone and brockrams (Permo-Triassic) of Cumbria, north-west England. Unpublished PhD thesis, University of Hull.

Major, M., Poulsen, S.E., Balling, N., 2018. A numerical investigation of combined heat storage and extraction in deep geothermal reservoirs. *Geothermal Energy*, 6(1). doi:10.1186/s40517-018-0089-0

Manning, D. a. C., Younger, P.L., Smith, F.W., Jones, J.M., Dufton, D.J., Diskin, S., 2007. A deep geothermal exploration well at Eastgate, Weardale, UK: a novel exploration concept for low-enthalpy resources. J. Geol. Soc. 164, 371–382. doi:10.1144/0016-76492006-015

Mazumder, S., 2017. Comparative Assessment of the Finite Difference, Finite Element, and Finite Volume Methods for a Benchmark One-Dimensional Steady-State Heat Conduction Problem. *Journal of Heat Transfer*, *139*(7).

McCann, T., 2008. The Geology of Central Europe: Precambrian and palaeozoic. Geological Society of London.

McClay, Norton, M.G., Coney, P., Davis, G.H., 1986. Collapse of the Caledonian orogen and the Old Red Sandstone. Nature 323, 147–149. doi:10.1038/323147a0

McDermott, C.I., Randriamanjatosoa, A.R., Tenzer, H., Kolditz, O., 2006. Simulation of heat extraction from crystalline rocks: the influence of coupled processes on differential reservoir cooling. *Geothermics*, *35*(3), 321-344.

McKerrow, W.S., Niocaill, C.M., Dewey, J.F., 2000. The Caledonian Orogeny redefined. J. Geol. Soc. 157, 1149–1154. doi:10.1144/jgs.157.6.1149

McKeown, C., Haszeldine, R.S., Couples, G.D., 1999. Mathematical modelling of groundwater flow at Sellafield, UK. *Engineering Geology*, 52(3), 231-250. doi:10.1016/S0013-7952(99)00008-3

Meadows, N.S., Beach, A., 1993. Structural and climatic controls on facies distribution in a mixed fluvial and aeolian reservoir: the Triassic Sherwood Sandstone in the Irish Sea. *Geological Society, London, Special Publications*, *73*(1), 247-264.

Megies, T., Wassermann, J., 2014. Microseismicity observed at a non-pressure-stimulated geothermal power plant. *Geothermics*, *52*, 36-49.

Mendum, J.R., 2012. Late Caledonian (Scandian) and Proto-Variscan (Acadian) orogenic events in Scotland. J. Open Univ. Geol. Soc. 33, 37–51.

Mikkelsen, P.W., Floodpage, J.B., 1997. The hydrocarbon potential of the Cheshire Basin. Geol. Soc. Lond. Spec. Publ. 124, 161–183. doi:10.1144/GSL.SP.1997.124.01.10

Moukalled, F., Mangani, L., Darwish, M., 2016. The finite volume method in computational fluid dynamics. *An advanced introduction with OpenFoam® and Matlab®. New York: Springer.*

Molina-Giraldo, N., Bayer, P., Blum, P., Cirpka, O.A., 2011. Propagation of seasonal temperature signals into an aquifer upon bank infiltration. Groundwater, 49(4), 491-502. doi:10.1111/j.1745-6584.2010.00745.x

Molina-Giraldo, N., Bayer, P., Blum, P., 2011. Evaluating the influence of thermal dispersion on temperature plumes from geothermal systems using analytical solutions. International Journal of Thermal Sciences, 50(7), 1223-1231.

Morel, C.R.G., van Reeuwijk, M., Graf, T., 2015. Systematic investigation of non-Boussinesq effects in variable-density groundwater flow simulations. *Journal of contaminant hydrology*, *183*, 82-98. doi:10.1016/j.jconhyd.2015.10.004

Mottaghy, D., Pechnig, R., Vogt, C., 2011. The geothermal project Den Haag: 3D numerical models for temperature prediction and reservoir simulation. *Geothermics*, 40(3), 199-210. doi:10.1016/j.geothermics.2011.07.001

Mountney, N.P., Thompson, D.B., 2002. Stratigraphic evolution and preservation of aeolian dune and damp/wet interdune strata: an example from the Triassic Helsby Sandstone Formation, Cheshire Basin, UK. Sedimentology 49, 805–833. doi:10.1046/j.1365-3091.2002.00472.x

Muffler, P., Cataldi, R., 1978. Methods for regional assessment of geothermal resources. *Geothermics*. 7, 53-89.

Muskat, M., Wyckoff, R.D., 1946. The flow of homogeneous fluids through porous media. *International series in physics*. J. W. Edwards, In., Ann Arbor, Mich., xix, 763 p. pp.

Nabi, M., Al-Khoury, R., 2012a. An efficient finite volume model for shallow geothermal systems. Part I: Model formulation. *Computers & Geosciences*, 49, 290-296. doi:10.1016/j.cageo.2012.03.019

Nabi, M., Al-Khoury, R., 2012b. An efficient finite volume model for shallow geothermal systems—Part II: Verification, validation and grid convergence. *Computers & Geosciences*, 49, 297-307. doi: 10.1016/j.cageo.2012.03.023

Naylor, H., Turner, P., Vaughan, D.J., Boyce, A.J., Fallick, A.E., 1989. Genetic studies of red bed mineralization in the Triassic of the Cheshire Basin, northwest England. J. Geol. Soc. 146, 685–699. doi:10.1144/gsjgs.146.4.0685

Ng, B., 2011. *Numerical modelling of multiple standing column wells applied to geothermal heating and cooling in UK buildings* (Doctoral dissertation, Northumbria University).

Nguyen, A., Pasquier, P., Marcotte, D., 2015. Influence of groundwater flow in fractured aquifers on standing column wells performance. Geothermics, 58, 39-48. doi:10.1016/j.geothermics.2015.08.005

NHP, 2017. The national heat map website, website accessed on 06/03/2017 [WWW Document]. URL. [nationalheatmap.cse.org.uk].

Nick, H. M., Schotting, R., Gutierrez-Neri, M., Johannsen, K., 2009. Modeling transverse dispersion and variable density flow in porous media. *Transport in porous media*, 78(1), 11-35. doi:10.1007/s11242-008-9277-x

Nield, D. A., Bejan A., 1992. Convection in a Porous Media, 408, Springer-Verlag, New York.

Oberbeck, A., 1879. Über dieWärmeleitung der Flüssigkeiten bei Berücksichtigung der Strömungen infolge von Temperaturdifferenzen. Annalen der Physik und Chemie 7, 271–292

Ogata, A., Banks, R. B., 1961. A solution of the differential equation of longitudinal dispersion in porous media, US Geological Survey, Professional Paper 411-A.

Oude Essink, G., 1998. MOC3D adapted to simulate 3D density-dependent groundwater flow. In *Proceedings of the MODFLOW'98 Conference,* 291-303.

Ovo, 2019. Website last accessed on July 2020. https://www.ovoenergy.com/guides/energy-guides/how-much-heating-energy-do-you-use.html

Ozbek, H., Phillips, S.L., 1979. Thermal Conductivity of Aqueous NaCl Solutions from 20Č to 330Č. Department of Energy, Lawrence Berkeley Laboratory.

O'Sullivan, M.J., O'Sullivan, J.P., 2016. Reservoir modeling and simulation for geothermal resource characterization and evaluation. In Geothermal Power Generation (pp. 165-199). Woodhead Publishing.

Paksoy, H.O., Andersson, O., Abaci, S., Evliya, H., Turgut, B., 2000. Heating and cooling of a hospital using solar energy coupled with seasonal thermal energy storage in an aquifer. *Renewable energy*, *19*(1-2), 117-122.

Pang, G., Chen, W. and Sze, K.Y., 2016. A comparative study of finite element and finite difference methods for two-dimensional space-fractional advection-dispersion equation. *Advances in Applied Mathematics and Mechanics*, *8*(1), pp.166-186.

Pasquali, R., O'Neill, N., Reay, D., Waugh, T., 2010. The geothermal potential of Northern Ireland. Proc. World Geotherm. Congr. 2010 Bali Indones.

Pasquier, P., Nguyen, A., Eppner, F., Marcotte, D., Baudron, P., 2016. Standing column wells. In: Advances in Ground-Source Heat Pump Systems (pp. 269–294). Elsevier. doi:10.1016/B978-0-08-100311-4.00010-8.

Patankar, S.V., 1980. Numerical Heat Transfer and Fluid Flow. Washington, DC: Hemisphere Publishing Corporation.

Peace, G.R., Besly, B.M., 1997. End-Carboniferous fold-thrust structures, Oxfordshire, UK: implications for the structural evolution of the late Variscan foreland of south-central England. J. Geol. Soc. 154, 225–237. doi:10.1144/gsjgs.154.2.0225

Peaceman, D. W., 1978. Interpretation of Well-Block Pressures in Numerical Reservoir Simulation. SPE J. 18 (3): 183-194; Trans., AIME, 265. SPE-6893-PA. doi:10.2118/6893-PA.

Pearson, S.C., 2012. Modeling the effects of direct use on the Tauranga low-temperature geothermal system, New Zealand. In Proceedings: 34th Workshop on Geothermal Reservoir Engineering, Stanford University, Stanford, California.

Pinder, G. F., Gray, W. G., 1977. "Finite Element Simulation in Surface and Subsurface Hydrology." Academic Press, New York.

Plant, J.A., Jones, D.G., Haslam, H.W. eds., 1999. *The Cheshire Basin: basin evolution, fluid movement and mineral resources in a Permo-Triassic rift setting*. British Geological Survey.

Poulsen, S. E., Balling, N., Nielsen, S. B., 2015. A parametric study of the thermal recharge of low enthalpy geothermal reservoirs. *Geothermics*, 53, 464-478. doi:10.1016/j.geothermics.2014.08.003

Powell, J.H., Chisholm, J., I., Bridge, D., McC, Rees, J.G., Glover, B.W., Besly, B.M., 2000. Stratigraphical framework for Westphalian to Early Permian red-bed successions of the Pennine Basin British. Geol. Surv. Res. Rep.

Praprotnik, M., Sterk, M., Trobec, R., 2004. Inhomogeneous Heat-Conduction Problems solved by a new explicit finite difference scheme. International Journal of Pure and Applied Mathematics. Volume. 13. 275-291.

Price, M., Allen, D. J., 1984. The use of pumping tests to evaluate a geothermal reservoir-the Triassic sandstones at Marchwood, Southampton. Proceedings of the Institution of Civil Engineers, 76(3), 697-711.

Prickett, T. A., 1967. Designing pumped well characteristics into electric analog models. *Groundwater*, 5(4), 38-46. doi:10.1111/j.1745-6584.1967.tb01625.x

Prickett, T. A., Lonnquist, C. G., 1971. Selected digital computer techniques for groundwater resource evaluation. Bulletin (Illinois State Water Survey) no. 55.

Puppala, H., Jha, S. K., 2018. Identification of prospective significance levels for potential geothermal fields of India. Renewable Energy, 127, 960-973.

Rapp, B.E., 2016. *Microfluidics: Modeling, Mechanics and Mathematics*. William Andrew.

Rast, N., Crimes, T.P., 1969. Caledonian orogenic episodes in the British Isles and North-Western France and their tectonic and chronological interpretation. Tectonophysics 7, 277–307. doi:10.1016/0040-1951(69)90075-4

Rau, G.C., Andersen, M.S. and Acworth, R.I., 2012. Experimental investigation of the thermal dispersivity term and its significance in the heat transport equation for flow in sediments. Water Resources Research, 48(3).

Rayner, D.H., 1981. Stratigraphy of the British Isles. CUP Archive.

Rees, S.J., Spitler, J.D., Deng, Z., Orio, C.D., Johnson, C.N., 2004. A Study of Geothermal Heat Pump and Standing Column Well Performance. ASHRAE Transactions, 110(1).

Remson, I., Hornberger, G. M., Molz, F. J., 1971. Numerical Methods in Subsurface Hydrology. New York Wiley-Interscience, 389 pp.

Richardson, L.F., 1911. The approximate arithmetical solution by finite differences of physical problems involving differential equations, with an application to the stresses in a masonry dam. Philosophical Transactions of the Royal Society of London. Series A, Containing Papers of a Mathematical or Physical Character, 210, 307-357.

Richardson, L. F., Gaunt, J. A., 1927. The deferred approach to the limit. Part I. Single lattice. Part II. Interpenetrating lattices. Philosophical Transactions of the Royal Society of London. Series A, containing papers of a mathematical or physical character, 226, 299-361.

Ringrose, P.S., 2017. Principles of sustainability and physics as a basis for the low-carbon energy transition. *Petroleum Geoscience*, 23, 287-297. doi:10.1144/petgeo2016-060

Rippon, J.H., Ellison, R.A., Gayer, R.A., 2006. A review of joints (cleats) in British Carboniferous coals: indicators of palaeostress orientation. *Proceedings of the Yorkshire Geological Society*, *56*(1), pp.15-30.

Roache, P.J., 1994. Perspective: a method for uniform reporting of grid refinement studies. Transactions-American Society of Mechanical Engineers Journal of Fluids Engineering, 116, 405-405. doi:10.1115/1.2910291

Robinson, R.A.J., Townsend, P., Steen, P., Barron, H., Abesser, C.A., Muschamp, H., McGrat, I., Todd, I., 2016. Geothermal Energy Challenge Fund: the Guardbridge Geothermal Technology Project. 105 pp.

Rollin, K.E., 1995. A simple heat-flow quality function and appraisal of heat-flow measurements and heat-flow estimates from the UK Geothermal Catalogue. Tectonophysics, 244(1), pp.185-196.

Rollin, K.E., Kirby, G.A., Rowley, W.J., Buckley, D.K., 1995. Atlas of Geothermal Resources in Europe: UK Revision. Technical Report WK/95/07, British Geological Survey, Keyworth.

Rosen, M.A., Koohi-Fayegh, S., 2017. Geothermal Energy: Sustainable Heating and Cooling Using the Ground. John Wiley & Sons.

Routledge, K., Williams, J., Lehdonvirta, H., Kuivala, J-P., Fagerstrom, O., 2014. Heat Network Mapping for Leighton West. A report prepared for Cheshire East Council. Report number: 298-692.

Rowley, E., White, N., 1998. Inverse modelling of extension and denudation in the East Irish Sea and surrounding areas. Earth Planet. Sci. Lett. 161, 57–71. doi:10.1016/S0012-821X(98)00137-X

Roy, C.J., 2003. Grid convergence error analysis for mixed-order numerical schemes. AIAA journal, 41(4), 595-604.

Roy, C.J., 2005. Review of code and solution verification procedures for computational simulation. *Journal of Computational Physics*, 205(1), 131-156. doi:10.1016/j.jcp.2004.10.036

Roy, C.J., 2010. Review of discretization error estimators in scientific computing. 48th AIAA Aerospace Sciences Meeting Including the New Horizons Forum and Aerospace Exposition, Aerospace Sciences Meetings. doi:10.2514/6.2010-126

Rubio-Maya, C., Díaz, V.A., Martínez, E.P., Belman-Flores, J.M., 2015. Cascade utilization of low and medium enthalpy geothermal resources– A review. *Renewable and Sustainable Energy Reviews*, *52*, 689-716

Ruffell, A., Shelton, R., 1999. The control of sedimentary facies by climate during phases of crustal extension: examples from the Triassic of onshore and offshore England and Northern Ireland. J. Geol. Soc. 156, 779–789. doi:10.1144/gsjgs.156.4.0779

Rühaak, W., Guadagnini, A., Geiger, S., Bär, K., Gu, Y., Aretz, A., Homuth, S., Sass, I., 2015. Upscaling thermal conductivities of sedimentary formations for geothermal exploration. *Geothermics*, *58*, 49-61.

Rushton, K.R., 2003. Groundwater hydrology: conceptual and computational models. John Wiley & Sons.

Rybach, L., 2010: Legal and regulatory environment favorable for geothermal development investors. Proceedings World Geothermal Congress 2010, Bali, Indonesia, 7 pp. Website: http://www.geothermal-energy.org/pdf/IGAstandard/WGC/2010/0303.pdf

Sachse, A., Rink, K., He, W., Kolditz, O., 2015. OpenGeoSys-Tutorial: computational hydrology I: groundwater flow modeling. Springer.

Saeid, S., 2015. Experimental and Numerical Study of Heat Flow under Low-Enthalpy Hydrothermal Conditions.

Saeid, S., Al-Khoury, R., Barends, F., 2013. An efficient computational model for deep low-enthalpy geothermal systems. *Computers & Geosciences*, 51, 400-409. doi:10.1016/j.cageo.2012.08.019

Saeid, S., Al-Khoury, R., Nick, H. M., Hicks, M. A., 2015. A prototype design model for deep low-enthalpy hydrothermal systems. *Renewable Energy* 77, 408–422. doi:10.1016/j.renene.2014.12.018

Sanmiguel-Rojas, E., Ortega-Casanova, J., del Pino, C., Fernandez-Feria R 2005. A Cartesian grid finite-difference method for 2D incompressible viscous flows in irregular geometries. *Journal of Computational Physics*, 204(1), pp.302-318. doi:10.1016/j.jcp.2004.10.010

Schout, G., Drijver, B., Gutierrez-Neri, M., Schotting, R., 2013. Analysis of recovery efficiency in high-temperature aquifer thermal energy storage: a Rayleigh-based method. Hydrogeology Journal, 22(1), 281–291. doi:10.1007/s10040-013-1050-8

Smith, G.D., 1985. Numerical solution of partial differential equations: finite difference methods. Oxford university press.

Smith, N.T., 1998. The Carboniferous to Mesozoic structural and stratigraphic evolution of the Cheshire basin. PhD.

Smith, N.T., 1999. Variscan inversion within the Cheshire Basin, England: carboniferous evolution north of the Variscan Front. Tectonophysics 309, 211–225. doi:10.1016/S0040-1951(99)00140-7

Smith, N.J.P., Kirby, G.A., Pharaoh, T.C. 2005. Structure and evolution of the south-west Pennine Basin and adjacent area. Subsurface Memoir of the British Geological Survey.

Soper, N.J., Woodcock, N.H., 2003. The lost Lower Old Red Sandstone of England and Wales: a record of post-Iapetan flexure or Early Devonian transtension? Geol. Mag. 140, 627–647. doi:10.1017/S0016756803008380

Spiegelman, M., 2000. Myths and methods in modeling. Columbia University Course Lecture Notes.

Spitler, J.D., Rees, S.J., Deng, Z., Chiasson, A., Orio, C.D., Johnson C, 2002. R&D Studies Applied to Standing Column Well Design (No. ASHRAE 1119-RP).

Sternberg, Y. M., 1973. Efficiency of Partially Penetrating Wells. *Ground Water*., Vol. 11, No. 3. doi: 10.1111/j.1745-6584.1973.tb02967.x

Stewart, I.S., Lewis, D., 2017. Communicating contested geoscience to the public: Moving from 'matters of fact'to 'matters of concern'. *Earth-Science Reviews*, *174*, pp.122-133.

Teke, I., Ağra, Ö., Atayılmaz, Ş.Ö., Demir, H., 2010. Determining the best type of heat exchangers for heat recovery. Applied Thermal Engineering, 30(6-7), pp.577-583. doi:10.1016/j.applthermaleng.2009.10.021

Theis, C.V., 1935. The relation between the lowering of the Piezometric surface and the rate and duration of discharge of a well using ground-water storage. *Eos, Transactions American Geophysical Union*, *16*(2), 519-524.

Thiem, G., 1906. Hydrologische Methoden. Gebhardt, Leipzig.

Thompson, D.B, 1969. Dome shaped aeolian dunes in the Frodsham Member of the so-called Keuper Sandstone Formation [Scythian–?Anisan: Triassic] at Frodsham, Cheshire (England). Sed Geol 3, 263–289.

Thompson, D.B., 1970. The stratigraphy of the so-called Keuper Sandstone Formation (Scythian–?Anisian) in the Permo–Triassic Cheshire Basin. Q. J. Geol. Soc. 126, 151–181. doi:10.1144/gsjgs.126.1.0151

Thomas, L.P., Holliday, D.W., 1982. Southampton No. 1 (Western Esplanade) Geothermal Well: Geological Well Completion Report. Report of the Deep Geology Unit, Institute of Geological Sciences No. 82.

Todd, D.K., Mays, L.W., 2005. Groundwater hydrology edition. Welly Inte.

Trescott, P.C., Pinder, G.F., Larson, S.P., 1976. Finite-difference model for aquifer simulation in two dimensions with results of numerical experiments. US Government Printing Office.

Turcotte, D.L., Schubert, G., 2014. Geodynamics. Cambridge University Press.

Turkel, E., 1986. Accuracy of schemes with nonuniform meshes for compressible fluid flows. *Applied Numerical Mathematics*, 2(6), 529-550. doi:10.1016/0168-9274(86)90006-1

UKOGL, 2019. Website last accessed on January 2019. https://ukogl.org.uk/map/?e=-282393,7032566,-262519,7043630&l=1431655429,81,0&f=14,136,-267870,7038088&b=3&sm=true

Van Genuchten, M. T., Alves, W. J., 1982. Analytical solutions of the one-dimensional convective-dispersive solute transport equation (No. 157268). United States Department of Agriculture, Economic Research Service.

Voss, C. I., Provost, A. M., 2003. SUTRA a model for saturated - unsaturated variable-density groundwater flow with solute or energy transport. In: U.S. Geological Survey Water-ResourcesInvestigationsReport02-4231,250.

Vosteen, H.D., Schellschmidt, R., 2003. Influence of temperature on thermal conductivity, thermal capacity and thermal diffusivity for different types of rock. Phys. Chem. Earth Parts ABC, Heat Flow and the Structure of the Lithosphere 28, 499–509. doi:10.1016/S1474-7065(03)00069-X

Wang, Z., Wang, F., Liu, J., Ma, Z., Han, E., Song, M., 2017. Field test and numerical investigation on the heat transfer characteristics and optimal design of the heat exchangers of a deep borehole ground source heat pump system. Energy Conversion and Management, 153, pp.603-615.

Waples, D.W., Waples, J.S., 2004. A review and evaluation of specific heat capacities of rocks, minerals, and subsurface fluids. Part 1: Minerals and nonporous rocks. Natural resources research, 13(2), 97-122 doi:10.1023/B:NARR.0000032647.41046.e7

Waters, C.N., Davies, S.J., 2006. Carboniferous : extensional basins, advancing deltas and coal swamps, in: Brenchley, P.J., Rawson, P.F. (Eds.), In: The Geology of England and Wales / Edited by P.J. Brenchley and P.F. Rawson. London : Geological Society of London. Geological Society of London, London, England, 173–223.

Wang, H.F., Anderson, M.P., 1982. Introduction to Groundwater Modeling: Finite Difference and Finite Element Methods. Academic Press, San Diego, CA, 237 p.

Waters, C.N., Waters, R.A., Barclay, W.J. and Davies, J.R., 2009. A lithostratigraphical framework for the Carboniferous successions of southern Great Britain (Onshore). British Geological Survey.

Waugh, B., 1970. Petrology, provenance and silica diagenesis of the Penrith sandstone (lower Permian) of northwest England. Journal of Sedimentary Research, 40(4), 1226-1240.

Wen-mei, W.H., 2011. *GPU Computing Gems Jade Edition*. Elsevier.

Westaway, R., 2018. Deep Geothermal Single Well heat production: critical appraisal under UK conditions. Quarterly Journal of Engineering Geology and Hydrogeology, 51(4), 424-449. doi:10.1144/qjegh2017-029

Williams, G.D., Eaton, G.P., 1993. Stratigraphic and structural analysis of the Late Palaeozoic–Mesozoic of NE Wales and Liverpool Bay: implications for hydrocarbon prospectivity. J. Geol. Soc. 150, 489–499. doi:10.1144/gsjgs.150.3.0489

Wilson, A.A., 1993. The Mercia Mudstone Group (Trias) of the Cheshire Basin. Proc. Yorks. Geol. Polytech. Soc. 49, 171–188. doi:10.1144/pygs.49.3.171

Woodcock, N.H., Strachan, R.A., 2009. Geological History of Britain and Ireland. John Wiley & Sons.

Younger, P.L., Gluyas, J.G., Stephens, W.E., 2012. Development of deep geothermal energy resources in the UK. *Proceedings of the Institution of Civil Engineers-Energy*, *165*(1), 19-32.

Younger, P. L., Feliks, M. E. J., Westaway, R., McCay, A. T., Harley, T. L., Elliott, T., Stove, G. D. C., Ellis, J., Watston, S., Waring, A. J., 2015, Renewing the Exploration Approach for MidEnthalpy Geothermal Systems: Examples from Northern England and Scotland, Proceedings of the World Geothermal Congress, Melbourne, Australia, 19-25 April, 2015.

Zarrouk, S.J., Woodhurst, B.C., Morris, C., 2014. Silica scaling in geothermal heat exchangers and its impact on pressure drop and performance: Wairakei binary plant, New Zealand. *Geothermics*, *51*, 445-459.

Zeghici, R.M., Essink, G.H.O., Hartog, N., Sommer, W., 2015. Integrated assessment of variable density–viscosity groundwater flow for a high temperature mono-well aquifer thermal energy

storage (HT-ATES) system in a geothermal reservoir. *Geothermics*, *55*, 58-68.

doi:10.1016/j.geothermics.2014.12.006

Zhou, P., 1993. Finite Difference Method. In: Numerical Analysis of Electromagnetic Fields. Electric

Energy Systems and Engineering Series. Springer, Berlin, Heidelberg

Zhu, J., Zhang, W., 2004. Optimization design of plate heat exchangers (PHE) for geothermal district

heating systems. *Geothermics*, *33*(3), 337-347.

Zimmerman, W.B., 2006. Multiphysics modeling with finite element methods (Vol. 18). World

Scientific Publishing Company.